THE UNIVERSITY
of EDINBURGH

Hydrogen Storage in Depleted Gas Fields: Capacity and Performance

Jonathan Scafidi

THE UNIVERSITY *of* EDINBURGH

Thesis submitted for the degree of

Doctor of Philosophy

The University of Edinburgh

School of Geosciences

December 2021

Declaration

I declare that this thesis has been composed solely by myself and that it has not been submitted, in whole or in part, in any previous application for a degree. Except where stated otherwise by reference or acknowledgment, the work presented is entirely my own.

Jonathan Scafidi

December 2021

Abstract

The Paris Agreement to limit anthropogenic warming to 1.5 °C above pre-industrial levels requires rapid reduction of greenhouse gas emissions. The UK has a large natural gas demand which varies massively across the year, with peaks in winter up to five times as high as the lows in summer. Decarbonising this system will require an emissions-free alternative to natural gas coupled with large-scale seasonal storage. Hydrogen can be used as an alternative to natural gas as it releases no CO_2 when burned. Hydrogen can also be used to store renewable electricity during times of surplus, as well as buffering hydrogen production from natural gas coupled with CCS. The aim of this thesis is to investigate the potential for seasonal storage of hydrogen in depleted gas fields with a focus on the UK. There are three main parts to this thesis: a regional capacity estimate for the UK continental shelf; a reservoir engineering, geological modelling, and hydrogen storage simulation study of an onshore gas field; and the development of an open-source tool for the accurate estimation of the flow rates and cushion gas requirements of gas storage sites.

A high-level assessment of gas fields on the UK continental shelf for hydrogen storage potential was undertaken, alongside calculations of the seasonal storage requirement for the 100% replacement of natural gas demand in the UK with hydrogen. UK natural gas demand over the past five years has exceeded was 800 TWh with peak daily demand in winter reaching almost 5 TWh/day compared to summer lows of 1 to 1.5 TWh/day. Using monthly demand data an estimate of 150 TWh of seasonal hydrogen storage is required to replace seasonal variations in natural gas production. A method is determined to screen gas fields and saline aquifers for suitability, however it is found that the estimates for saline aquifers are extremely low confidence due to a lack of data. Gas fields are able to hold 13,800 TWh of hydrogen and assuming a cushion gas requirement of 50%, this gives a value of 6900 TWh working gas capacity for hydrogen across 95 gas fields. Of these 85% are in the Southern North Sea which could utilise existing infrastructure and large offshore wind developments to develop large-scale offshore hydrogen production.

As depleted gas fields still contain some natural gas, there is a need to investigate the effects of storing hydrogen in such a field. The Cousland gas field, a small, 0.9 billion cubic feet (BCF) gas field in Scotland was selected for a simulation study. The

field had previously been earmarked for town gas storage in the 1960s and so a reservoir engineering study was performed using well testing and production data from the 1930s to 1960s. From this study, a geological model was developed and history matched against the results of the reservoir engineering study and production data. Three one-well, 20 year hydrogen storage scenarios at different pressures were then simulated. Hydrogen was injected for 2 years, allowed to settle for 2 years, then 14 storage cycles of injection, storage, extraction, and empty were completed before a final depletion of the cushion gas over 1 year. The initial volume injected into the reservoir had little effect on the hydrogen recovery factor, storage capacity, well flow rates, produced gas composition, and pressure response. The extracted hydrogen showed less contamination with natural gas over time and the results show that the mixed zone between the hydrogen and natural gas was pushed further from the well with each subsequent storage cycle. The field has a capacity of close to 1000 tonnes of hydrogen with recovery factors higher than 90%. The natural gas in the reservoir behaved as a cushion gas, and hydrogen purity could be controlled through injection strategies.

Cushion gas requirements for gas storage sites are important for both deliverability and economics, and, outside of reservoir simulation studies, cushion gas requirements are generally assumed. The final chapter of this thesis describes an open-source program designed to improve these assumptions. The programs uses basic reservoir parameters (original reservoir pressure, average permeability, average porosity, formation thickness, depth, gas initially in place, and reservoir temperature) for volumetric gas fields to calculate the working and cushion gas volumes, expected flow rates, and well performance. The program uses an open-source fluid property database (CoolProp) to model the properties of both methane and hydrogen. LIT (laminar-inertial-turbulent) and pseudopressure equations are used to solve the generalized radial-flow diffusivity equation which allows the program to be used on reservoirs of all pressures. Bottom hole flowing pressure is computed using the average temperature and compressibility method. As the program is open-source the code can be downloaded and adjusted according to need. The program is validated using data from four real gas storage sites. The results from these four sites are used to compare hydrogen and methane gas storage performance and finds that similar levels of performance can be achieved in terms of energy deliverability with hydrogen showing significantly lower cushion gas requirements than methane, particularly for the higher pressure, larger fields. The

results suggest that cushion gas requirements and deliverability are not entirely dependent on reservoir properties but can be changed significantly by adjusting the number of wells and well diameter. A simple economics model shows that this has implications for the optimal number of wells drilled in a storage site.

Lay Summary

Burning fossil fuels produces greenhouse gases such as carbon dioxide, which warm the Earth's atmosphere by trapping more of the Sun's heat. This is causing the climate to change, with disastrous consequences. In 2015, 191 countries plus the European Union signed what is now known as the Paris Agreement to limit the warming to 1.5 degrees Celsius above the average temperature between 1850 and 1900.

Currently, the UK burns a lot of natural gas both to produce electricity, and to heat people's homes. During the winter, five times more gas is needed for heating than in the summer. To meet this demand, the UK imports or extracts more natural gas from gas fields. This reliance on natural gas is not compatible with the UK's commitment to the Paris Agreement and so a replacement fuel source is needed.

Hydrogen is one possible alternative as it releases no carbon dioxide when burned, and can be used to produce electricity and provide heat. Hydrogen can be produced either from water and electricity, or from natural gas and heat. From an economics perspective, it is best to produce hydrogen from these processes at one constant rate throughout the year, but this results in a mismatch between production and demand. In the summer there would be a surplus to demand and in the winter there would be a deficit. Luckily, hydrogen can be stored in vast quantities, deep underground in porous rocks like those found in gas fields and extracted again when it is needed. This storage allows the mismatch between production and demand to be balanced out across the year.

This thesis looks at how much hydrogen storage the UK will need to replace the current natural gas demand, and how much hydrogen can be stored in gas fields which have been emptied of natural gas. It also takes a more detailed look at one particular gas field by building a computer model and simulating the storage of hydrogen in the summer and the extraction again during the winter. Finally, it will describe a computer program that calculates how quickly the hydrogen can be produced from a storage site, which has implications for the amount of hydrogen that can be effectively stored.

The first chapter is a review of all the relevant science relating to storing hydrogen in porous rocks and the contribution this thesis will make. The second chapter looks at the amount of hydrogen storage the UK would need if it were to replace all the

natural gas with hydrogen, and found that it would need to be able to store the equivalent of 20% of the total gas demand for one year. There is much more potential storage than this: 46 times the required storage can be found in old gas fields in the North Sea and East Irish Sea. Other rocks were investigated for storage, but because not enough is known about them, the estimates are not very reliable. The gas fields identified for hydrogen storage are all located very close to large offshore wind farms which could be used to make hydrogen from water, with storage in the gas fields.

To store hydrogen in an old gas field, it is compressed and then injected through a well. When the hydrogen is needed again, it is extracted through the same well. The rate at which the hydrogen can be extracted depends on the pressure in the field. The more hydrogen is stored in the field, the higher the pressure and the faster the hydrogen can flow out of the field again. However, to keep the pressure high enough to get the hydrogen out at a reasonable rate, there needs to be some gas in the field at all times. This is called cushion gas and the third and fourth chapters investigate whether natural gas left in an old gas field can be used for this purpose. The third chapter describes the building of a computer model of a real gas field in Scotland, called the Cousland field, and the fourth chapter describes simulating the injection and extraction of hydrogen from the model. The results suggest that the natural gas can be used as a cushion gas, and that around 1000 tonnes of hydrogen could be stored in the Cousland field without significant mixing.

As some hydrogen storage sites may not have any natural gas left in them to use, they will need a different approach. Hydrogen is expensive and so determining the amount of cushion gas required is very important when planning new storage sites. The fifth chapter of this thesis describes the building and testing of a computer program that can calculate the amount of cushion gas a field might need. The program was tested against real data from real gas storage sites and found to be very accurate. It also showed that the amount cushion gas needed in a storage site can be adjusted by changing the number of wells. By only using free, open-source software this program can be used by anyone for free and will be a useful tool for researchers without access to expensive computer programs.

The final chapter of this thesis summarises all of the key findings, and there are some appendices at the end which contain extra data, computer codes, and a paper published form the results.

Acknowledgements

First and foremost I'd like to thank my principal supervisor Mark Wilkinson at the University of Edinburgh for guiding me along the PhD process. Through countless conversations both in the office and in the field, you have taught me to see things in an entirely different way, and this has translated not only into my work but also my way of thinking. I'd also like to thank the rest of my supervisory team at the University of Edinburgh. Stuart Gilfillan has always been available for a chat, giving me fresh perspective on problems and driving me to publish my first paper. Stuart Haszeldine is a fountain of knowledge on all things and has given me valuable insights and introductions into the world between science and industry. Niklas Heinemann got me performing my own simulation studies and with his help and guidance this aspect took over most of my PhD. To all of you, thank you – I am a better scientist for it.

Thanks to NERC and Hydrenor for funding the project with a special mention for the E3DTP. A particular thanks goes to Laurent Schirrer and Isabelle Vervoort at Hydrenor for taking a massive chance on funding my project through the NPIF and CASE partnerships, working with me and introducing me to the oil and gas (and music) industry in Aberdeen. I can now call myself a reservoir engineer thanks to you, and working on real projects has given me vital experience to kick start my career. I still hope one day to witness Claude's Funky Taxi in person. Chris Banks at Schlumberger gave much of his valuable time to answer my questions, fix software licences, and learn how to build a proper reservoir model as well as many interesting discussions on the energy transition. Tim Tubby of TT Earth Science helped me to understand the basics of poroperm modelling and found me the one document I'd been missing on Cousland production data. Mike Hall at the University of Edinburgh used his incredible talents to transform my crumbly rock samples into beautiful thin sections. A huge thanks goes to the GeoEnergy group for the discussions, presentations, knowledge sharing, and feedback.

My time as a PhD was made infinitely better by my colleagues in the Grant Attic. Amy Shore: always there for a stroll and some good wildlife (special mention to the swangoose), and Hannah Rogers for keeping me sane in the best booth, Sophie Butcher for making Gradmin an actual word, and to the rest of the GradSchool Committee, Andy Twelves and Berta Ramiro Sanchez – I'm so proud of what we achieved and have you all to thank for it, as well as Alex Jackson for his help getting

us vehicles. A huge thanks to everyone in the Grant Institute and University administration for looking after my needs after the operation, with particular thanks to Stephanie Robin. Massive thanks to Ross Taylor and Justin MacNeil in IT, without whom I would not have had the software or a laptop to run it on. To everyone I spent time with on fieldwork, especially Mikael Attal, Simon Mudd, Andy Hein, Laura Quick, Emma Graf, and the Great Cowboy in the Sky: it has been unforgettable.

No thanks goes to the pandemic. But there was one silver lining – the Geology department at the University of Oslo adopted me and gave me a place to work for over a year. Thanks to Anja Sundal and Catherine Braathen for making that happen. Huge thanks to the Oslo PhD/Post-doc community for the beers, camping, and delicious dinners. Might find that meteorite one day… To the Mekkitude: you guys have made me feel so welcome and at home in Norway under the strange circumstances. Thank you all and I promise I will talk about something other than my code not working from now on.

To my Family, Fiona and Oscar. You've been there from day one and your support has made all of this possible. From letting me have all those issues of Techno-Quest, and bringing me on crazy road trips, it's all in here somewhere. And I know you've both been dying to read this, so enjoy!

Finally, to my darling Juliane for putting up with my stress, listening to me try to explain concepts and practice presentations, for building me back up after the operation, and for reading my first drafts. You are my rock and I love you. I promise I will start running again now.

Thank you all.

Table of contents

Contents

List of tables

Chapter 1 Literature Review

"The country will be covered with rows of metallic windmills working electric motors which in their turn supply current at a very high voltage to great electric mains. At suitable distances, there will be great power stations where during windy weather the surplus power will be used for the electrolytic decomposition of water into oxygen and hydrogen." – J. B. S. Haldane (1924)

J. B. S. Haldane's predictions for the 23rd century may well be realised much sooner. As the international community pushes forward with climate mitigation strategies, there is an increasing focus on decarbonising the heating and transport sectors. This can be achieved through the production and storage of hydrogen which has led to a large increase in the amount of research concerning hydrogen as an energy source over the past two decades (Figure 1) and is the focus of this thesis.

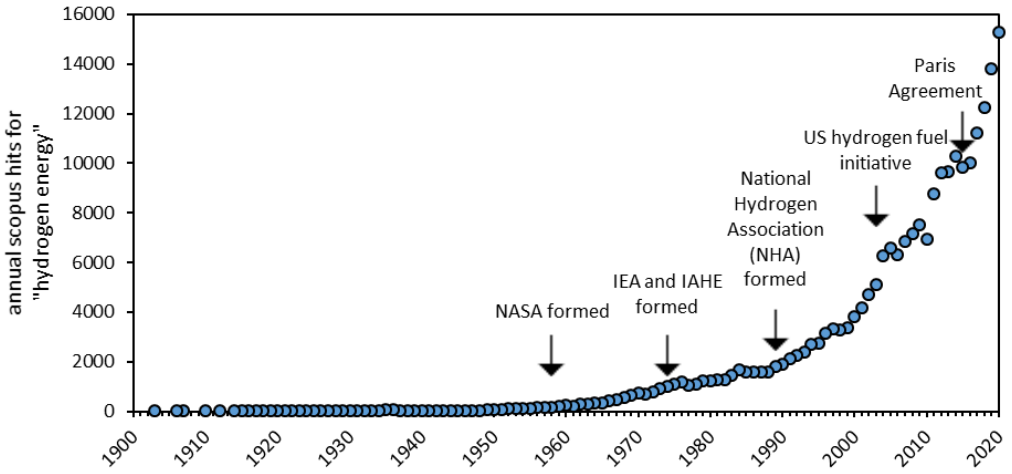

Figure 1: Search results for "hydrogen energy" on Scopus on 15/07/2021 from 1903 to 2020, with some key associations and events labelled. NASA = The National Aeronautics and Space Administration, IEA = International Energy Agency, IAHE = International Association of Hydrogen Energy. Significant increases in research output in hydrogen energy can be seen in the 1960s – 1980s, the late 1990s-2000s, and from 2015 onwards.

The UK has made a legal commitment to reducing greenhouse gas emissions by 80% relative to 1990 levels by 2050 by signing the Paris Agreement (UNFCCC 2015). Under the Climate Change Act 2008 (The UK government 2008), the Climate Change Committee (the CCC) was formed which advises the government on emissions targets, their progress in achieving these, and adaptation options.

In 2016 the Climate Change Committee recommended a 57% reduction target for all emissions from 1990 levels by 2030 in the fifth carbon budget (Climate Change Committee 2016) and increased this to 68% in the sixth carbon budget with a 78% reduction for all emissions from 1990 levels by 2035, and a 100% reduction from 1990 levels by 2050 (Climate Change Committee 2020).

Greenhouse gas emissions from heating of business, public, and residential sectors accounted for 34% of the total emitted by the UK in 2016 (Department for Business Energy & Industrial Strategy 2018a) and the transport sector accounted for a further 26% in 2016 (Department for Business Energy & Industrial Strategy 2018a). The majority of these emissions are CO_2, produced by the combustion of hydrocarbon fuels such as natural gas, petrol, and diesel. These fuels could feasibly be replaced with hydrogen, which on combustion produces no CO_2, only H_2O. Hence, hydrogen has the potential to play a vital role in decarbonising these sectors and could make an important contribution to the UK's legal commitment to reducing greenhouse gas emissions by 80% relative to 1990 levels by 2050 as per the Paris Agreement (UNFCCC 2015).

1.1 Hydrogen for electricity decarbonisation

Increasing the proportion of renewable energy sources (RES) such as wind and solar in the UK energy mix has helped to decarbonise electricity production in the UK. However, RES rely on intermittent energy sources such as wind and solar to produce electricity, raising issues of grid stability and energy security, which will only increase with an increasing proportion of RES (Albadi and El-Saadany 2010; Katzenstein and Apt 2012; Ren *et al.* 2018; Liebensteiner and Wrienz 2019). Energy storage provides a means to level out the disparity between production and demand associated with RES. However, current technologies such as battery or pumped hydro storage can help to alleviate daily fluctuations (Landinger *et al.* 2014), but they lack the ability to store the large quantities required over seasonal timescales and allow its rapid release in times of need.

Energy demand is lower during the summer than during the winter, so excess production of energy relative to demand is more likely in the summer. The opposite is true in the winter where demand is more likely to exceed production and so there is an energy supply deficit. This concept is illustrated schematically in Figure 2. Producing and storing hydrogen during times of excess energy supply then using it to make up the shortfall during times of energy supply deficit could be more efficient

than curtailing production and result in lower residual peak loads (Michalski *et al.* 2017). If hydrogen production over the long term is in excess of demand, then it could be used for other purposes than grid balancing, such as heating, transport, industry, or sold to the export market.

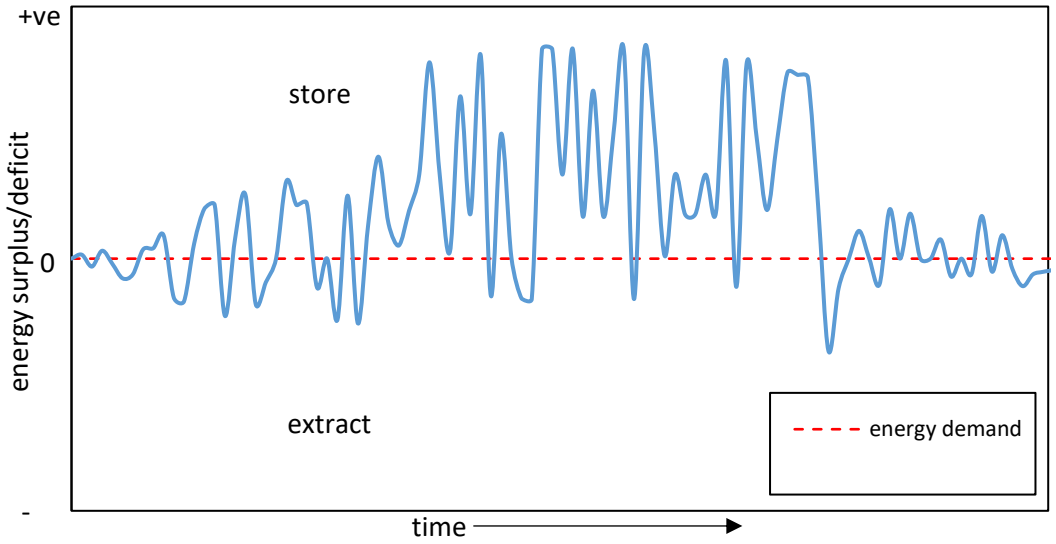

Figure 2: Schematic diagram made by author showing the energy supply deficit of a renewable energy source (solid blue line)The dashed red line is the energy demand which by definition has a deficit of zero. Where the renewable energy source is producing more than required by demand, the energy supply deficit is positive and where it is producing less than demand the energy supply deficit is negative. In terms of balancing the energy supply deficit, energy produced above the demand line can be used to generate hydrogen and store it (marked store on the figure) to be extracted and converted back to electricity when the energy supply deficit is negative (marked extract).

1.2 Hydrogen for heat decarbonisation

23 million homes are connected to the gas grid in the UK with domestic heating and hot water accounting for 20% of the UK's greenhouse gas emissions (Climate Change Committee 2016). The Climate Change Committee (CCC) has recommended a reduction of heating and hot water emissions by 20% below 1990 levels by 2030 in order to meet UK climate targets (Climate Change Committee 2016). Annual total UK gas demand over the past decade is in the region of 800 TWh and highly seasonal with winter demand (4-5 TWh per day) up to five times as high as summer (1-2 TWh per day) (Ofgem 2020a). Some of this seasonal difference is addressed by increasing imports from Norwegian gas fields and other parts of the world, and some of it is addressed using storage in both depleted gas fields and salt caverns (Ofgem 2020a, b).

There is considerable emphasis on the potential for decarbonisation of the UK natural gas supply by replacing it with hydrogen from low carbon sources such as steam methane reformation (SMR) with carbon capture and storage (CCS) (Northern Gas Networks 2016; Isaac 2019). In order to produce this hydrogen, natural gas will need to be extracted and reformed, a process which requires less reformers if they operate at consistently higher load factors and are coupled with large-scale storage capacity (Energy Research Partnership 2016). This concept is shown in Figure 3 where the hydrogen production rate is constant and overproducing during the summer and storing it for use in the winter, when the hydrogen production rate is lower than demand.

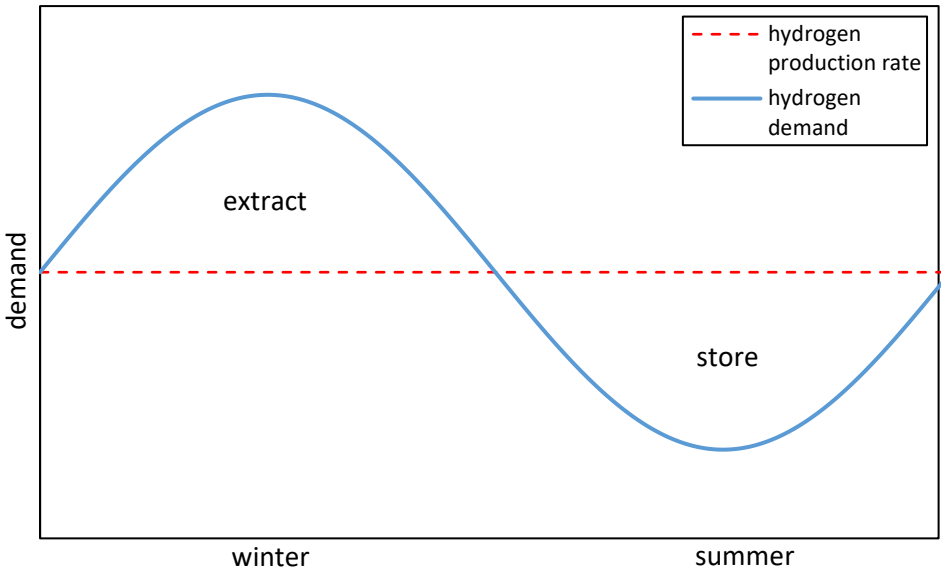

Figure 3: Schematic figure showing demand (blue solid line) and hydrogen production rate (dashed red line) over one year. Where the demand exceeds production in winter, hydrogen is extracted from storage (marked extract) and where production exceeds demand in summer, hydrogen is stored (marked store).

1.3 Estimates of inter-seasonal storage requirements

The exact amount of inter-seasonal hydrogen storage required to replace natural gas demand with hydrogen is highly dependent on future gas demand for heating, industry, and transport. Emerging technologies such as heat pumps and electric vehicles are likely to play a significant role in decarbonising the UK energy system, which will reduce future gas demand alongside energy efficiency improvements such as building renovation. There have been several estimates of storage requirements which are detailed in this section.

Led by utility network provider Northern Gas Networks, H21 Leeds City Gate investigated the feasibility and requirements of a 100% hydrogen gas network conversion in the city of Leeds, UK (Sadler *et al.* 2016). The project found that a 100% hydrogen network was both technically and economically possible using steam methane reformation coupled with carbon capture and storage (CCS). They estimated that the city would require 1.025 GW of hydrogen production from steam methane reformers, an inter-seasonal storage capacity of 40 times the maximum average daily demand using seven 400,000 m^3 salt caverns in the Humber region for this purpose (Sadler *et al.* 2016). The study gives a figure of 700,000 MWh (0.7 TWh) of inter-seasonal hydrogen storage to satisfy a peak annual demand of 6.4 TWh (Sadler *et al.* 2016). The figures from the study are given in Table 1.

The H21 North of England study, also led by Northern Gas Networks, built on the H21 Leeds City Gate project to look at the conversion of the entire North of England to a 100% hydrogen gas network (Northern Gas Networks 2018). They determined that this would require 12.15 GW of hydrogen production via steam methane reformation with associated CCS, along with 8.052 TWh of inter-seasonal storage capacity in ninety 400,000 m^3 salt caverns (Northern Gas Networks 2018). They also looked at the possibility of using less storage and increasing the hydrogen production capacity which gave figures of 16.99 GW of hydrogen production capacity with 2.164 TWh of inter-seasonal storage (Northern Gas Networks 2018). The figures from the study are given in Table 1 and an overview of the proposed system is shown in Figure 4.

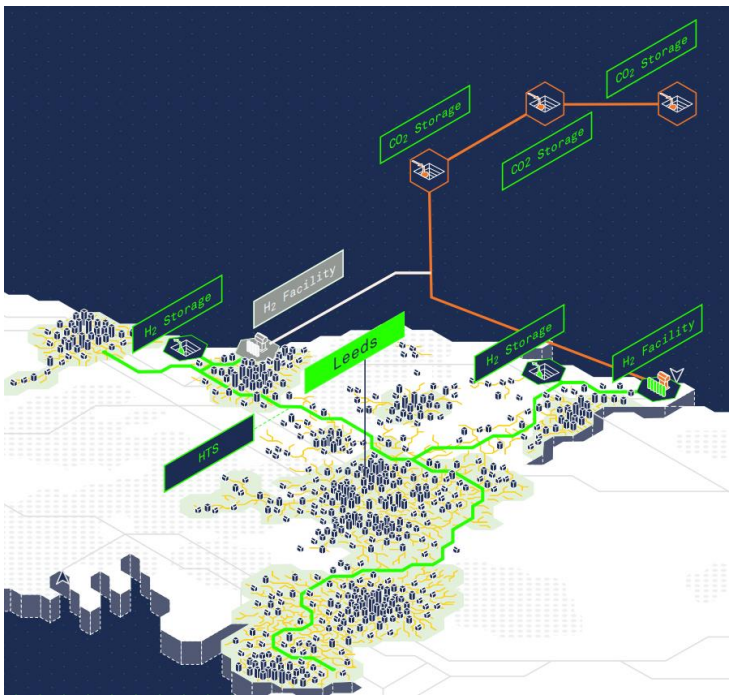

Figure 4: Overview of the proposed H21 North of England energy system showing the city of Leeds, CO_2 storage in the North Sea, onshore hydrogen storage and the hydrogen transmissions system (green lines marked HTS). Image from Northern Gas Networks (2018).

The Energy Research Partnership investigated the potential for decarbonising the UK domestic heat demand of 424 TWh using hydrogen (Energy Research Partnership 2016). Hydrogen produced by steam methane reformation with CCS is considered in the study with a focus on the amount of production capacity required to meet demand with differing levels of storage capacity. The study finds that by increasing the load factor of the steam methane reformers and coupling them with large-scale storage, the steam methane reformation capacity is reduced. The figures from the study are given in Table 1.

An applied UK case study from the University of Edinburgh looking at mapping storage capacity on the UK continental shelf in depleted gas fields along with regional domestic heating demands determined that 77.9 TWh of inter-seasonal hydrogen storage capacity is required to supply a demand of 309 TWh (Mouli-Castillo *et al.* 2021). The figures from the study are given in Table 1.

All the estimates of storage capacity, demand, and production capacity have been plotted in Figure 5. Figure 5 A shows a general trend of higher demand requiring higher inter-seasonal storage capacity, however the trend is also influenced by the production capacity which is shown in Figure 5 B (note: production capacity was not

considered in the University of Edinburgh study (Mouli-Castillo *et al.* 2021)).

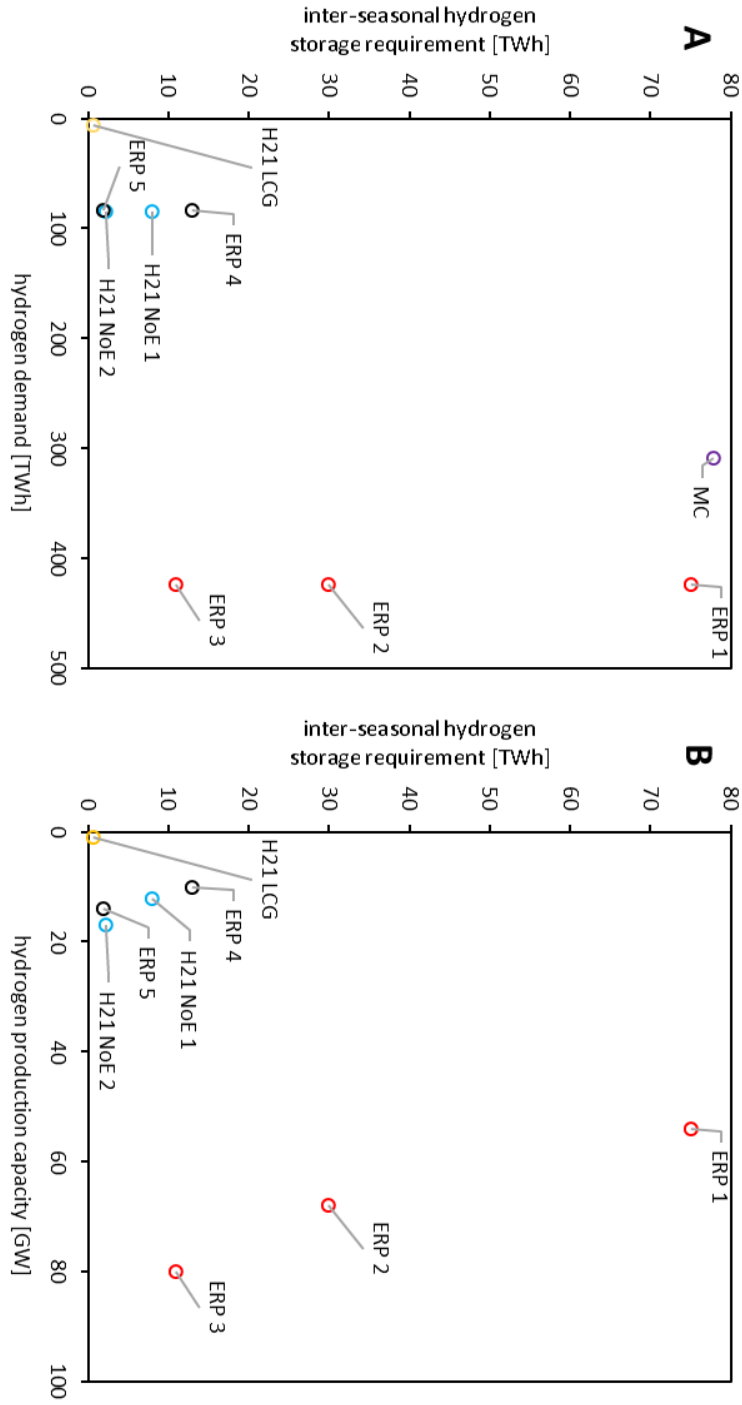

Figure 5: (Details of abbreviations used on both graphs are given in Table 1) A - plot of inter-seasonal hydrogen storage requirement vs. annual hydrogen demand; B - plot of inter-seasonal hydrogen storage requirement vs hydrogen production capacity. There is a general trend in graph A that with higher hydrogen demand, there is need for higher inter-seasonal storage capacities although this is also affected by the hydrogen production capacity shown in graph B. The trend in B can be seen most clearly between ERP 1 – 3 data points with higher storage capacities allowing for lower hydrogen production capacities. Points which share the same colour in both A and B have the same level of hydrogen demand.

Looking at the data points that are grouped by hydrogen demand (Points which share the same colour in both A and B have the same level of hydrogen demand), the trend is clear that increased inter-seasonal storage capacity leads to a lower production capacity requirement. This trend is clearest with points ERP 1, ERP 2,

and ERP 3. ERP 1 has the most storage and least production capacity of the three and ERP 3 has the least storage and most production capacity of the three.

Table 1: Hydrogen demand, inter-seasonal storage requirements, and hydrogen production capacity data for the four projects detailed in this section. The column graph legend gives the abbreviations used in Figure 5. ERP = Energy Research Partnership, SMR = steam methane reformer. Data from (Energy Research Partnership 2016; Northern Gas Networks 2018; Mouli-Castillo *et al.* 2021)*.*

Project	**graph legend**	**demand [TWh]**	**storage [TWh]**	**production capacity [GW]**
H21 Leeds City Gate	H21 LCG	6.4	0.7	1.025
H21 North of England high storage	H21 NoE 1	85	8.052	12.15
H21 North of England low storage	H21 NoE 2	85	2.164	16.99
Mouli-Castillo et al. 2021	MC	309	77.9	
ERP: SMR run continuously (>90% load factor)	ERP 1	424	75	54
ERP: SMR at 1.4 x average demand (~70% load factor)	ERP 2	424	30	68
ERP: SMR meets peaks (~60% load factor)	ERP 3	424	11	80
ERP: SMR run continuously	ERP 4	84	13	10
ERP: SMR meets peaks (~60% load factor)	ERP 5	84	2	14

1.4 Storing hydrogen in porous rocks

Gas has been successfully stored underground since 1915 in Welland Country, Ontario, Canada when the National Fuel Gas Company converted a depleted gas field for storage (Allen 1985). By the end of 2016 424 billion cubic metres (bcm) of storage across 672 underground storage facilities existed worldwide, accounting for 12% of world gas consumption (Cornot-Gandolphe 2017). There is a general consensus that hydrogen storage in porous rocks is technically feasible (Foh *et al.* 1979; Amid *et al.* 2016; Heinemann *et al.* 2021a).

1.4.1 Porous rock storage site concepts

The required elements of a porous rock storage reservoir are similar to those for a petroleum system. A reservoir rock with suitable porosity and permeability is required, along with a seal or caprock to prevent upward migration of gas. A three dimensional trap is also required to prevent dissipation of gas beyond the reaches of the wells. Traps are either structural, where folds and/or faults have deformed the reservoir rock in such a way as to prevent upward migration of fluids, or they are stratigraphic where changes in depositional environment have formed a barrier to upward migration such as pinch-outs or unconformities. A suitable trap volume is also required otherwise the injected gas will fill the structure and escape beyond retrieval via spill points. Figure 6 shows a schematic diagram of the key features of a porous rock gas storage site. Storage sites can be either in an aquifer in which case the pore space is initially filled with water, or in a depleted gas field in which case the pore space is initially filled with gas.

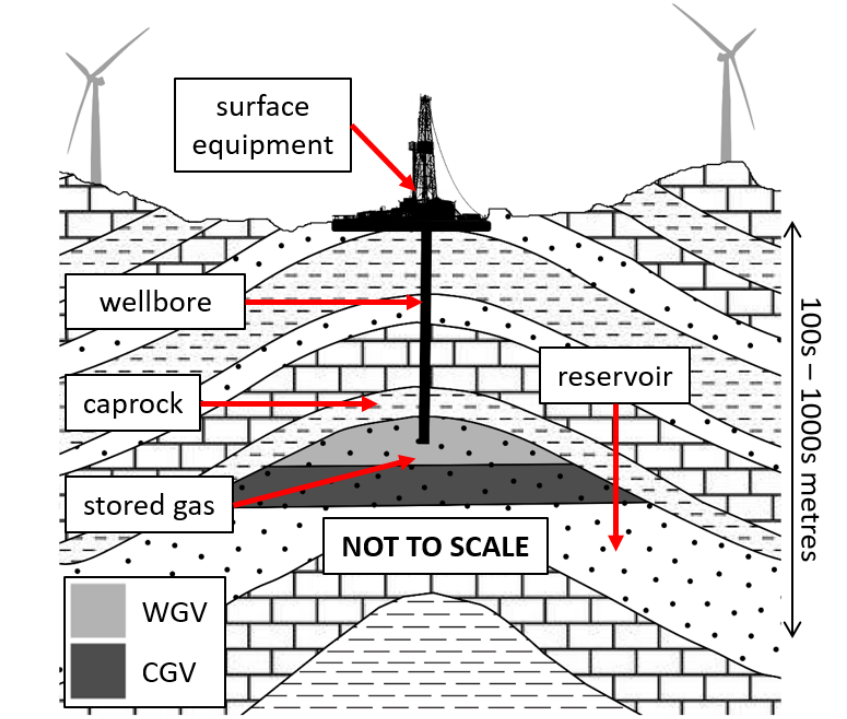

Figure 6: A shematic diagram showing the key features of an underground gas storage site. The gas is injected through the wellbore into the reservoir where it fills the pore space and displaces any existing fluids. The gas is buoyant in the subsurface but is prevented from escaping to the surface by the impermeable caprock. WGV = working gas volume, the volume of gas that can be injected and recovered without the reservoir pressure dropping too low for economic flow rates to be acheived. CGV = cushion gas volume, the volume of gas that must be left in the reservoir during operation to keep the pressure high enough for economic flow rates (aka pressure support). NOT TO SCALE. Modified from (Heinemann *et al.* 2018a).

At the pore-scale of an aquifer storage reservoir, the pores are initially saturated with water. As gas is injected, the water is pushed out of the pores, reducing the water saturation towards the irreducible water saturation which is the maximum water saturation a formation can retain without producing water. Any water below this saturation is held in place by capillary forces. In the case of a gas-water system the grains are water wet meaning that they retain a thin film of water on their surface. When the gas is produced again, the water refills the pores however some gas may be trapped in pores in the reservoir. This gas is called the residual gas saturation. These concepts are shown schematically in Figure 7.

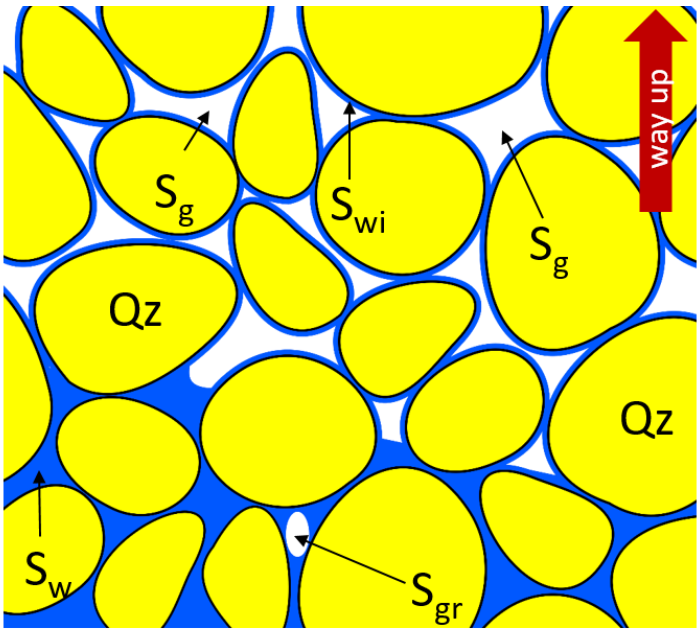

Figure 7: Pore-scale view of a gas storage reservoir (field of view approximately 10 mm. S_w = water saturation, S_{gr} = residual gas saturation, Qz = quartz grain, Swi = irreducible water saturation, S_g = gas saturation. As gas is injected into the reservoir, water is pushed out of the pores until it reaches the irreducible water saturation. When gas is produced again the water refills the pores however some gas may be trapped in the pores and this is called the residual gas saturation.

1.4.2 Physical behaviour

Hydrogen is the most abundant element in the universe and the third most abundant on the Earth's surface (Korte *et al.* 2016). Hydrogen is a much smaller molecule than methane with a higher diffusivity index. It is also lighter, meaning that it is more likely to find and escape through pathways in caprocks, well casings etc. Lateral spreading may also be an issue (Liebscher *et al.* 2016), with increased risk of viscous fingering where injection strategies are not properly managed (Hagemann *et al.* 2016).

The energy density of hydrogen is just 30% that of methane and 0.24% that of gasoline (Simbeck 2004). At certain reservoir conditions this may be higher e.g. the Rough gas storage facility where it is estimated at 42% with an overall deliverability of ca. 40% that of natural gas (Amid *et al.* 2016). Compression to high density liquid is inefficient and requires extremely low temperatures of only a few tens of kelvin (Simbeck 2004). A comparison of the energy density of different fuels is given in Table 2.

Table 2: Energy density in kJ/m^3. of different fuels at different pressure conditions (Lanz 2001). Dashes show where data is missing fom the orginal table.

Fuel	1 atm, 15 °C	204 atm, 15 °C	680.5 atm, 15 °C	liquid
hydrogen	10050	1825000	4500000	8491000
methane	32560	6860300	-	561500
propane	86670	-	-	23488800

Mixing with any existing cushion gas in the reservoir is likely to be minimal when injection strategies are well managed (Feldmann *et al.* 2016). This has implications for the usage of depleted gas fields, with residual gas acting as a cushion. This would save using hydrogen as a cushion and reduce costs.

Experimental work on hydrogen (Yekta *et al.* 2018) shows that due to a low variation of hydrogen viscosity at different pressure/temperature ranges it is likely that relative permeability will be similar under different reservoir conditions, and higher than that of methane. The results of the study were obtained for Triassic sandstones with 19% porosity and 44 mD (millidarcys) permeability (Yekta *et al.* 2018). Figure 8 shows a comparison of density, viscosity, energy density, and energy density ratio for methane and hydrogen at 100°C, from 0 to 200 Megapascals (MPa) made using data from the NIST Chemistry Webbook (Lemmon *et al.* 2021).

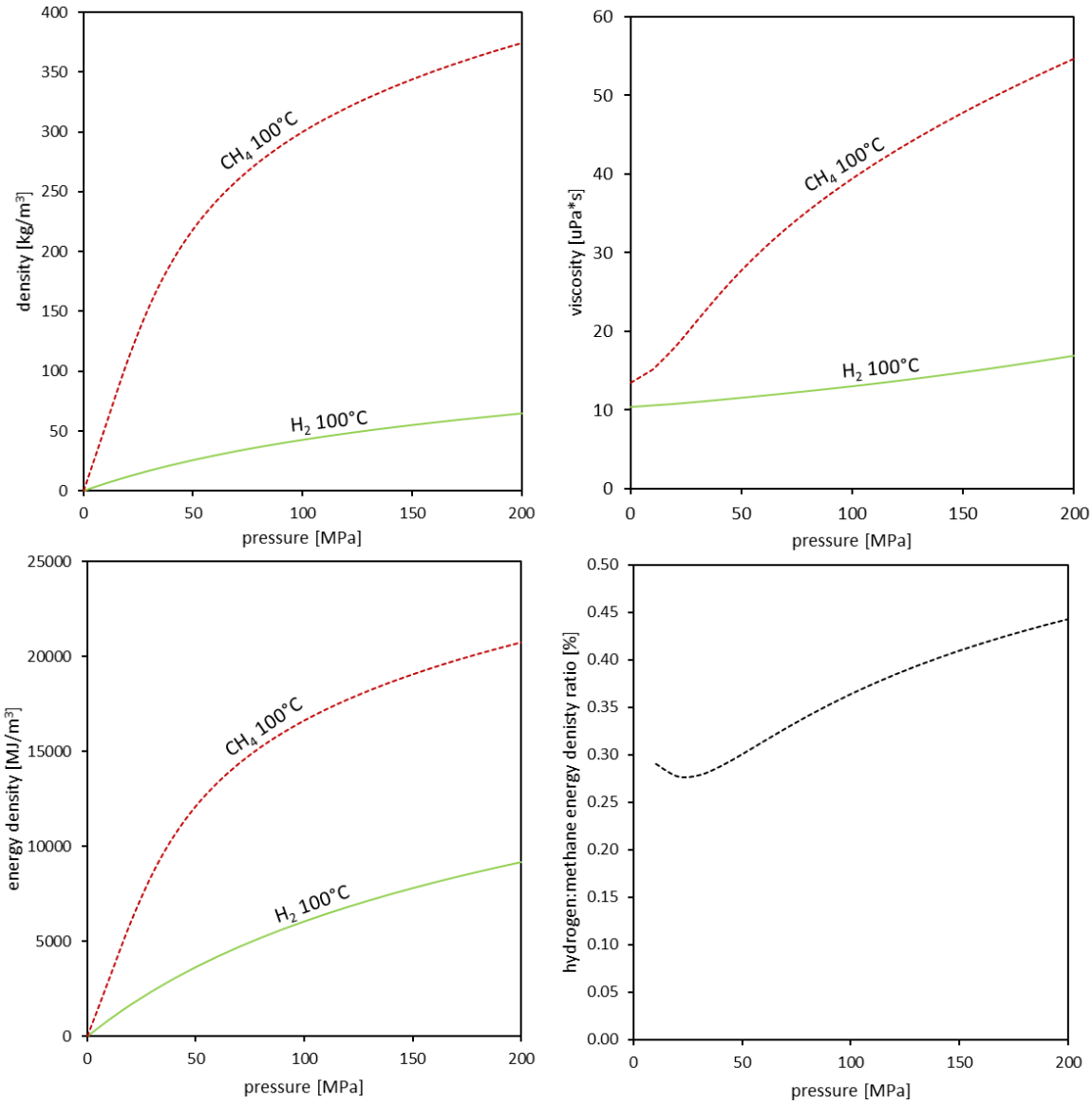

Figure 8: Plots showing density, viscosity, energy density, and energy density ratio vs pressure for hydrogen and methane at 100°C. Methane shows significantly higher densities, viscosities, and energy densities at 100°C and the pressures shown. Hydrogen has between 0.28 and 0.45 times the energy density of methane at 100°C and the pressures shown indicating that storage sites will need to be in the region of 2-3 times larger than those used for methane. Data from (Lemmon *et al.* 2021).

Methane is up to nine times denser, with viscosities reaching nearly five times those of hydrogen, and an energy density that is 2-3 times higher than that of hydrogen (Figure 8). This suggests that 2-3 times more space will be needed to store the equivalent (in energy terms) amount of hydrogen when compared to methane. However the low viscosity variation of hydrogen might lead to much higher relative permeabilities than for methane and so a higher volume of hydrogen compared to methane could be stored in the same volume of rock which might offset some of the

difference in energy density between the two. A higher relative permeability also means that the rate at which hydrogen can be produced from a reservoir could be higher than for methane which will also offset some of the issues associated with its lower energy density, closing the gap somewhat in energy delivery rates from storage sites.

1.4.3 Chemical behaviour and biological influence

The presence of other gases in the reservoir could lead to problems. A major one identified in the reservoir at Lobodice is the Sabatier reaction where CO_2 and H_2 are converted to CH_4 (Panfilov 2010; Panfilov *et al.* 2016). Under reservoir conditions this reaction is unlikely to occur spontaneously but methanogenic bacteria that live in the subsurface can cause the reaction, leading to a drop in reservoir pressure as one mole of gas is produced from every two. Amid et al. (Amid *et al.* 2016) suggested that this would be limited by the amount of CO_2 present in the reservoir and was only likely to be an issue for the first few injection/extraction cycles.

Iron(III) reduction, sulfate reduction, and acetogenesis are other reactions that could occur with iron(III) reduction being most likely as the bacteria that cause it are able to out-compete the organisms involved in the other reactions (Hagemann *et al.* 2016). Methanogenic archaea, acetogenic archaea, sulfate-reducing bacteria, and iron-reducing bacteria have all been identified as potentially problematic microorganisms (Hagemann *et al.* 2016). However, careful site selection that takes into account the optimum conditions for microbial growth could minimise any biological problems (Thaysen *et al.* 2021).

1.5 Real-world experience with hydrogen storage

The following sections describe real gas storage projects that stored either pure hydrogen or gases with a significant proportion of hydrogen in either porous rock or salt cavern storage sites.

1.5.1 Town gas storage projects

Town gas, also known as coal gas, is generated from the gasification of coal to produce a flammable mixture of gases. The composition is 45-50% H_2, 2-25% CH_4, 8-12% CO_2, 7-12% CO, 6-10% N_2 (Buzek *et al.* 1994). The high hydrogen content is of interest here. Town gas storage sites give an indication of some of the potential issues with hydrogen storage in porous rock formations as its behaviour in the subsurface has been studied, in particular the chemical and biological reactions that can lead to methane generation and a loss of pressure in the reservoir as a result.

1.5.1.1 Lobodice, Czech Republic

In the late 1960s (Buzek *et al.* 1994), town gas with a composition of 55% H_2, 20% CH_4 and 20% CO_2 + CO (Panfilov 2010) was injected into heterogeneous sands and gravels (Kopal *et al.* 2016; Liebscher *et al.* 2016) at a depth of 430 m (Panfilov 2016) near the village of Lobodice in what is now the Czech Republic. Figure 9 shows a geological model of the field (Kopal *et al.* 2016). Upon retrieval, 5 to 7 months later, the gas had a composition of 37% H_2, 40% CH_4 and 12% CO_2 + CO (Panfilov 2010).

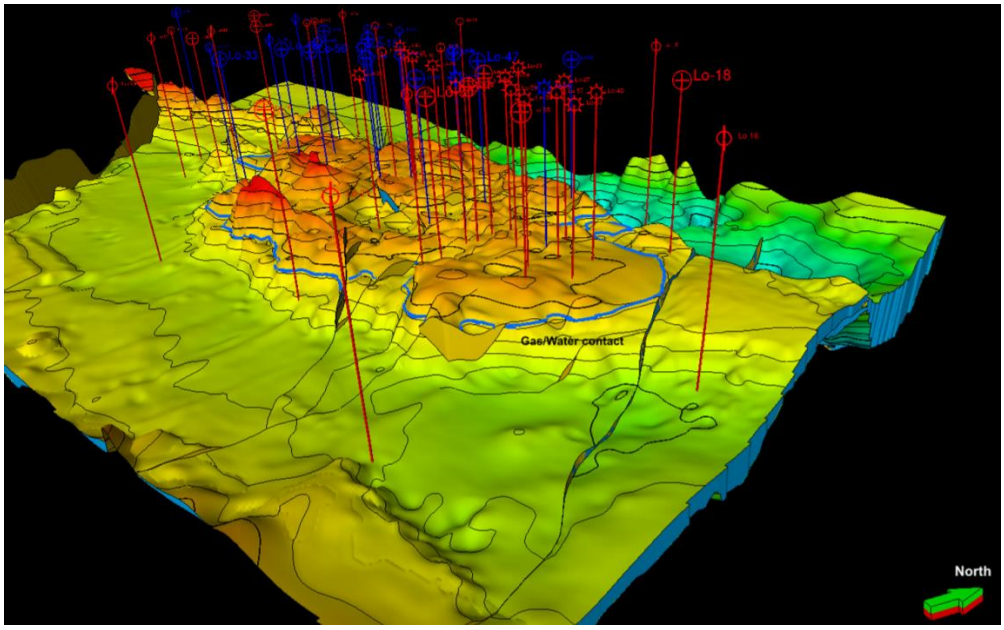

Figure 9: geological model of the town gas storage reservoir at Lobodice. Red wells penetrate the reservoir itself and blue wells do not. From Kopal, Cizek and Milička, (2016).

Volume losses of 10 - 20% were measured in this reservoir which led to significant pressure losses (Šmigáň *et al.* 1990) which resulted in lost revenue and usability in some gas appliances designed for higher H_2 concentrations (Buzek *et al.* 1994). A combination of bacterial action, chemical catalyst reactions, and suspected cap rock leakage were identified as the major culprits for the observed volume loss (Šmigáň *et al.* 1990).

Buzek *et al.* (1994) also proposed an explanation for the separation of gases in the underground storage facility: differential diffusivity coefficients between the different gas components of the town-gas could lead to observed H_2-rich and CH_4-rich zones. Further work by Panfilov (Panfilov 2010) suggested that the process is a dynamic one with patterns of standing waves in the reservoir which fit the Turing model. This can be explained by changing bacteria colony structures over time. However, later

work by Amid et al (Amid *et al.* 2016) suggests that losses to bacterial action could be limited to 3% or less by careful management of the CO_2 content of the reservoir as this is the reaction limiting nutrient.

1.5.1.2 Ketzin, Germany

Town gas was stored at Ketzin, 40 km west of Berlin in sandstone units at a depth of 630 to 650 m (Martens *et al.* 2013) from the 1960s to the 1970s. The Ketzin storage site was subsequently converted to natural gas storage until 2000, when it was repurposed as a CO_2 storage test site, which has now been plugged and abandoned (Martens *et al.* 2013). The Ketzin storage site recorded losses of around 200 mcm (million cubic metres) from 1964 to 1985 (Evans and West 2008). After investigation the tightness and integrity of wells and cap rock were proven. Corrosion of underground installations, and changes in gas composition and reservoir permeability were also observed (Evans and West 2008). Increases in CO_2, H_2, and CH_4 were detected alongside a decrease in CO. These compositional changes could not be explained by simple microbial degradation of hydrogen and carbon dioxide as they were for Lobodice, however chemical and microbial processes were determined to have caused the losses (Evans and West 2008).

1.5.1.3 Beynes, Ile de France, France

This saline aquifer was used to store 330 mcm of town gas between 1957 and 1974. The town gas contained up to 50% hydrogen but unfortunately losses from the store were not measured (Carden and Paterson 1979). In 1975 another reservoir was added to bring capacity up to 1185 mcm (Storengy France 2018). Remaining town gas in the original reservoir made up most of the cushion gas requirement (CGR) and minimal mixing occurred during subsequent operation (Foh *et al.* 1979).

1.5.2 Depleted field and aquifer hydrogen storage projects

1.5.2.1 Yakshunovskoe (Якшуновское), The Russian Federation

The Yakshunovskoe gas storage facility was created in the late 1960s to store natural gas (Gazprom 2018) in an aquifer at pressures up to 12 MPa with a storage capacity of 268 mcm (VNIPITRANSGAZ 2013). It was located 150km southwest of Moscow near the town of Kaluga and during the late 1980s to mid-1990s hydrogen and methane was injected and recovered during field tests (Basniev *et al.* 2010). Results of these tests are shown in Figure 10, but it is not clear exactly what these results show. The text in the paper states that the figure shows: "…the dependence between pressure and time for methane and hydrogen while injection and

producing, calculated in Gubkin Russian State University of Oil and Gas." - Basniev, Roman J Omelchenko, *et al.*, (2010).

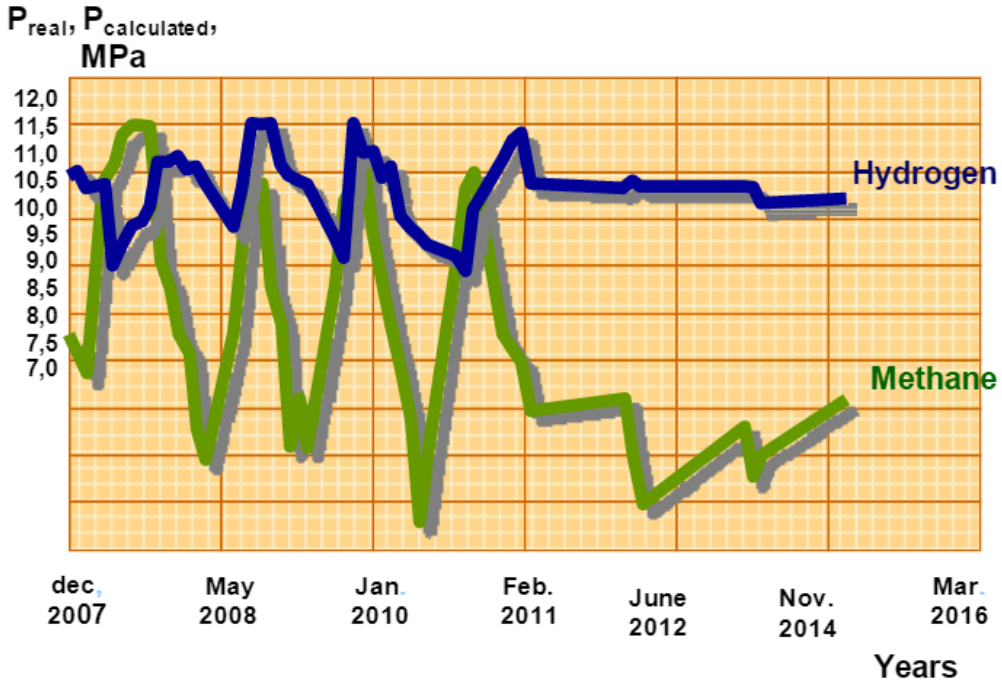

Figure 10: Results of hydrogen and methane injection and recovery in the Yakshunovskoe gas storage field, The Russian Federation. From Basniev, Roman J Omelchenko, et al., (2010) which describes the figure as : "…the dependence between pressure and time for methane and hydrogen while injection and producing, calculated in Gubkin Russian State University of Oil and Gas."

1.5.2.2 Hychico, Patagonia, Argentina

The Hychico project takes power generated from the Diadmea Wind Park (with a capacity of 6.3 MW) and has used it to electrolyse water to produce oxygen and hydrogen since 2008 (Aprea and Bolcich 2020). In 2010, the project undertook studies to store a hydrogen/natural gas mix (up to a concentration of 10% hydrogen at 10 bar) in a nearby depleted gas field on the Golfo de San Jorge basin at a depth of 815 metres (Pérez *et al.* 2016).

A field test was implemented in order to test the tightness of the reservoir, changes in composition and the behaviour of hydrogen in the subsurface and methane generation in the subsurface was observed (Strobel *et al.* 2020). As a result a methanation project is now underway where hydrogen and carbon dioxide will be injected into the reservoir with the aim of biological methanogenesis taking place and producing methane (Pérez *et al.* 2016). Initial lab results indicate that there are favourable conditions for methanogensis in the reservoir (Strobel *et al.* 2020).

1.5.2.3 Underground Sun Storage 2030, Austria

This project has gone through several different stages since it began in 2013, all of them have been headed by RAG Austria AG.

The following paragraph describes the findings of the field test part of the Underground Sun Storage project which ended in 2017, as detailed in the final report (RAG Austria AG *et al.* 2017). Initially a 10% hydrogen/90% natural gas mix was injected into the Lehen field (a depleted gas reservoir) near the city of Vöcklabruck, Austria. The field tests monitored leakage pathways in the well completions and found that there were no integrity issues. A total of 1.22 million Nm^3 of gas mixture containing 115,444 Nm^3 of hydrogen was injected into the Lehen field over a period of 3 months. There followed a four month shut-in phase after which 1.24 million Nm^3 of gas was produced from the reservoir with a total of 94,549 Nm^3 of hydrogen recovered. This is around 82% of the hydrogen injected. Other components such as carbon dioxide, nitrogen, and ethane were also found in the produced gas. It was concluded that the remaining hydrogen had diffused into the cushion gas and that a saturation gradient between the injected gas and the cushion gas in the reservoir had developed, and that around 3% was converted through bacterial action. Because a closed system will always move towards equilibrium, this was expected during the project.

The following paragraph describes the Underground Sun Conversion project which is ongoing at the same field site as the preceding Underground Sun Storage project. A gas blend of hydrogen and carbon dioxide in a 4:1 ratio will be injected into the reservoir and shut-in. Biological methanogenesis should occur and with methane produced from the well after a certain amount of time (Biegger *et al.* 2018). Pressure, temperature, and gas composition will be monitored, and a future two well system is also planned with an end date of 2021 (Strobel *et al.* 2020), however this may have been delayed due to the pandemic.

1.5.3 Salt cavern hydrogen storage projects

Salt caverns are used for lower volume but higher deliverability gas storage than depleted gas fields and aquifers. The caverns themselves are created by a process called solution mining (Plaat 2009). Fresh water is injected into an underground salt structure such as a dome or thick salt sequence. This dissolves the salt and the resulting brine can be extracted to the surface leaving a large cavity behind. The

shape of the cavern is controlled during this process by using two leaching strings, one to inject the water and one to remove the brine. Adjusting the positions of these relative to each other, along with circulation rates gives control over the shape of the cavern. A nitrogen or diesel blanket is used to prevent the roof of the cavern from being dissolved during the process. After several months to years the salt cavern is ready for gas storage. The processes and different types of salt caverns are shown in Figure 11.

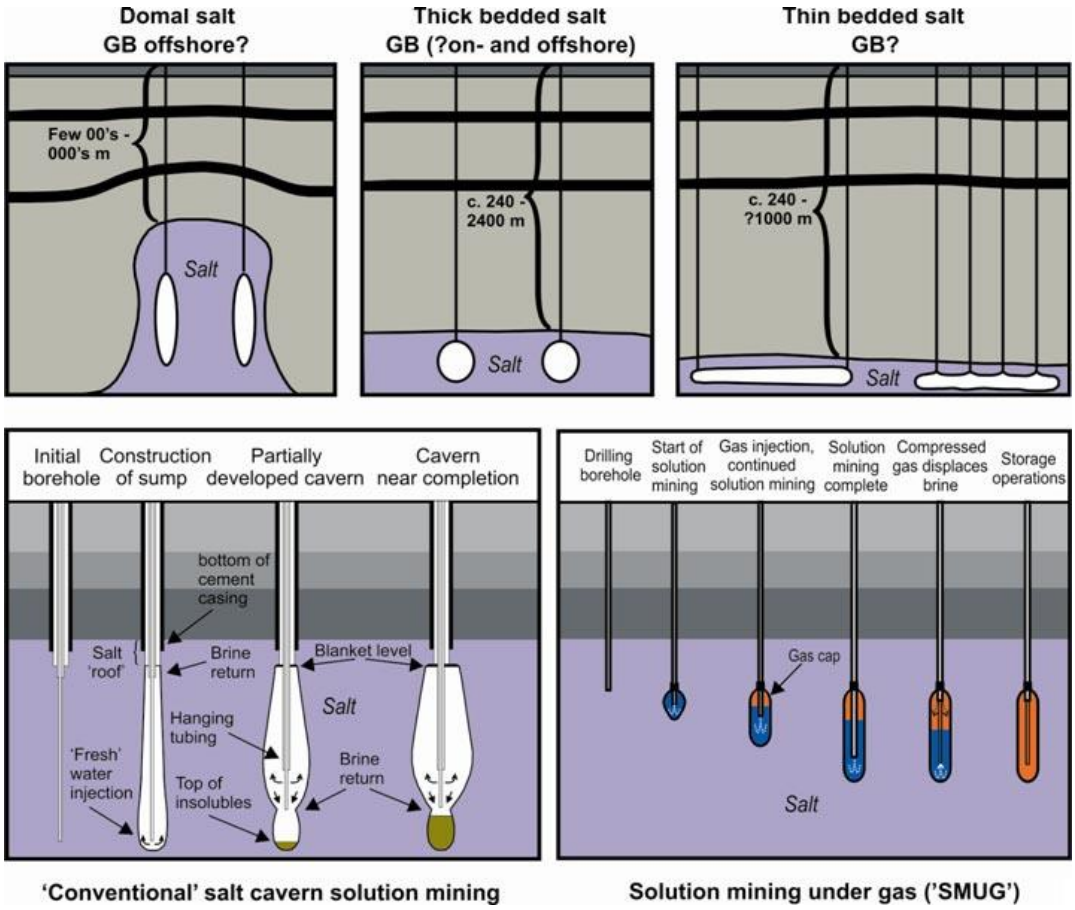

Figure 11: Schematic diagram to illustrate different types of solution mined salt caverns in different forms of halite beds, the conventional solution mining process, and the solution mining under gas (SMUG) process. From Evans et al. (2008).

Salt is the ideal medium for gas storage as it is self-healing with low leakage potential (Chen *et al.* 2013). However, the same fluidity that allows fractures to self-heal can also lead to a process called salt creep which can result in subsidence if the pressure is not high enough in the reservoir. Salt creep can lead to a decrease in volume of the reservoir so a proportion of gas is used for pressure maintenance (Plaat 2009). This is called the cushion gas requirement (CGR) and is usually around one third of the cavern storage volume (Le Fevre 2013). Despite salt being

self-healing under certain conditions it can also behave in a brittle manner (Senseny *et al.* 1992), and interbedded salt storage caverns can form complex leakage pathways as discovered in some Chinese storage facilities (Yu and Liu 2015). Proper understanding of stresses within the cavern are vital to prevent catastrophic failure from occurring (Khaledi *et al.* 2016).

1.5.3.1 Teesside, Yorkshire, UK

Imperial Chemical Industries (since taken over by SABIC) has stored 95% pure hydrogen within three elliptical salt caverns between 350 and 450 metres depth, at a pressure of 45 bar, with a volume of approximately 70,000 m^3 each in Teesside since 1972 (Beutel and Black 2004; Evans and West 2008; Hévin 2019). Pressure is maintained through brine injection which means that no cushion gas is required (Liebscher *et al.* 2016).

1.5.3.2 Spindletop, Texas, USA

This salt cavern storage site is run by Air Liquide, has a total volume of >580,000 m^3, and has been in operation since 2014 (Hévin 2019).

1.5.3.3 Clemens Dome, Texas, USA

This salt cavern storage site is run by Conoco Philips, has a volume of 580,000 m^3, an operating pressure range of 70-135 bar, and has been in operation since 1983 (Hévin 2019). The depth of the salt cavern is approximately 800 metres (Caglayan *et al.* 2020).

1.5.3.4 Moss Bluff, Texas, USA

This salt cavern storage site is run by Praxair, has a volume of 566,000 m^3, an operating pressure range of 55-152 bar, and has been in operation since 2007 (Hévin 2019). The depth of the salt cavern is approximately 800 metres (Caglayan *et al.* 2020).

1.5.3.5 Kiel, Germany

Town gas was stored with a 62% hydrogen content in a salt cavern with a volume of 32,000 m^3 at a pressure of between 80 and 100 bar (Liebscher *et al.* 2016). It has operated since 1971, was leached out of impure Permian age halite deposits at a depth of 1305-1400 metres which caused many issues initially with volume loss due to the high amount of insoluble in the halite (British Geological Survey 2008)

1.6 Field-scale numerical simulation of hydrogen storage in porous rocks

Reservoir simulation is a tool used to answer questions about the behaviour, production potential, risk, and economics of a reservoir and has taken place since the 1950s when computations of radial gas flow were first carried out (Watts 1997). Since then it has become an increasingly powerful tool used to address an ever increasing number of questions about the movement of fluids into, within and out of various kinds of reservoirs. In recent years questions relating to the behaviour of reservoirs filled with hydrogen have come into focus as a way to replace natural gas in energy systems. Most simulation studies focus on a particular reservoir as the questions they are designed to address are specific to those areas/reservoirs. However, there are also generalized studies investigating the effects of changing reservoir parameters or to test new methods of simulating multiphase systems (Pfeiffer *et al.* 2016; Heinemann *et al.* 2021b).

The first hydrogen reservoir simulation studies were based on real reservoirs and found that one of the most important factors was the extent of mixing within the reservoir between hydrogen and injected cushion gases such as nitrogen, which led to the production of contaminated hydrogen (Pfeiffer and Bauer 2015; Feldmann *et al.* 2016). Both Pfeiffer and Bauer (2015) and Feldmann *et al.* (2016) found that once the injected hydrogen was recovered, the average contamination was in the region of 15-20 mol%. This level of contamination was also seen in later studies (Luboń and Tarkowski 2020; Lysyy *et al.* 2021) and all the studies found that this contamination was highest during the first withdrawal cycle and decreased with subsequent cycles. An example of this effect from *Feldmann et al. (2016)* is shown in Figure 12.

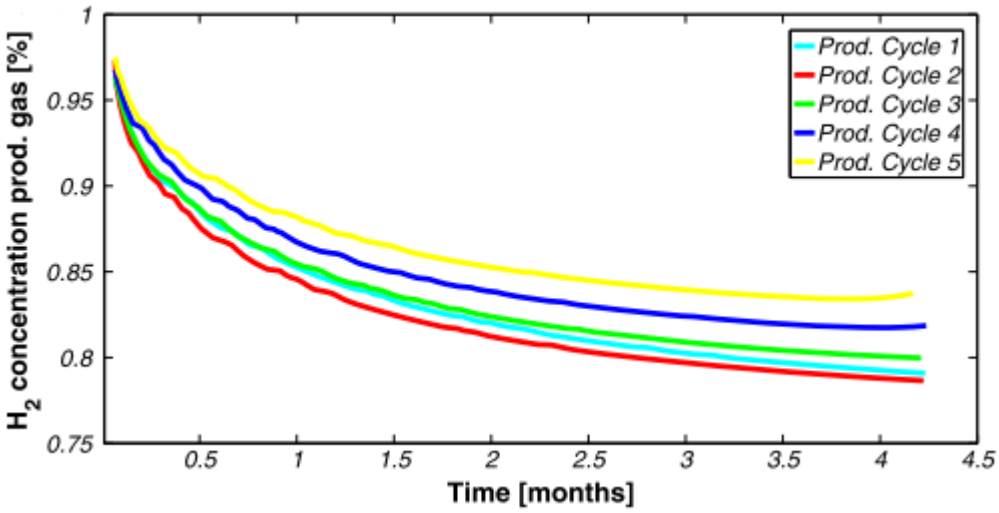

Figure 12: Hydrogen concentration vs time for each of the five production cycles. After production cycle 1, the concentrations of hydrogen in the produced gas increases with each subsequent cycle. From Feldmann et al. (2016).

One of the studies investigated the effects of storing hydrogen in different parts of the Norne oil and gas field in the Norwegain North Sea (Lysyy *et al.* 2021). Hydrogen storage in the gas, oil, and water legs were investigated and it was found that contamination of gas in the oil and gas legs was similar, however storage in the water zone resulted in the highest losses of injected hydrogen due to gravity effects. It is worth noting that this study investigated the injection of formation gases as cushion gas, hence gas contamination in the water leg of the reservoir.

The placement of wells close to the crest of a structure was also determined to be a key factor in achieving higher purity of recovered hydrogen as gravity effects lead to the migration of buoyant hydrogen towards the shallower parts of the reservoir (Sainz-Garcia *et al.* 2017; Lysyy *et al.* 2021). Placing wells higher on the structure also reduces the effects of water upconing where the gas-water contact reaches the well and water is produced with gas remaining in the reservoir (Sainz-Garcia *et al.* 2017; Luboń and Tarkowski 2020; Heinemann *et al.* 2021b; Lysyy *et al.* 2021).

Interestingly, none of the simulation studies mentioned in this review found evidence of viscous fingering which was expected to be an issue in hydrogen storages leading to the loss of hydrogen beyond the spill point of the storage structure (Paterson 1983). This lack of viscous fingering in the models is likely to be a result of the grid resolution in the models being too coarse and the fact that it is a computationally expensive phenomenon to model (Mostaghimi *et al.* 2016).

Well flow rates have not been the main focus of any study and generally the flow rates have been constrained by bottom hole pressures with simulators left to calculate the flow rates themselves. A dedicated reservoir simulation study on flow rates and the effect of the number of wells on hydrogen storage performance is yet to be published. Furthermore, a history-matched model of a volumetric (or sometimes called closed) gas reservoir is yet to be performed, although the model of the Norne oil and gas field has been history-matched (Lysyy *et al.* 2021). Finally, a key missing element in the hydrogen storage simulation literature is a comparison between hydrogen and natural gas or methane storage. This is important as depleted natural gas fields are the best candidates for hydrogen storage and will have a wealth of data on their behaviour when filled with natural gas. Understanding the differences between natural gas and hydrogen will determine the key elements to consider when deciding on the number of wells required to achieve the required deliverability for the storage site. A summary of the key findings of the hydrogen storage simulation literature can be found in Table 3.

1.6.1 Technical details of the hydrogen storage simulation literature

This section is a summary of the technical details and main conclusions of the simulation literature and is written in addition to the previous discussion to serve as a useful resource for those studying and/or performing hydrogen storage simulations who are interested in the technical details.

Pfeiffer and Bauer (2015) define a hydrogen usage scenario in the German state of Schleswig-Holstein with a demand period of one week, and a demand of 0.82 million GJ. This scenario required 120 million standard cubic metres of hydrogen at surface conditions to be delivered over one week. A hypothetical open storage structure based on a real anticlinal structure in Schleswig-Holstein was modelled with five wells completed over the full 12 to 13 metre thickness of the formation. Eclipse 300 was used for the simulation. Fluid densities and viscosities were calculated using a generalized version of the Peng-Robinson equation of state (Peng and Robinson 1976). Nitrogen was used as a cushion gas in this study and hydrogen injected later with a total of four storage cycles simulated. The key finding was that mixing occurred between the nitrogen and as a result the produced gas had an average fraction of only 52% hydrogen after the first cycle. This increased in subsequent cycles to reach 85% by the final cycle. The study also found that the hypothetical

structure could deliver slightly more than 20% of the energy requirement for the area that they defined.

The Feldmann et al. (2016) study was part of the H2STORE research project (Helmholtz Centre Potsdam 2015) and simulated hydrogen storage in a depleted gas reservoir. The reservoir was charged with hydrogen for 5 years, followed by 5 years of seasonal cyclic storage operations in order to predict injection and production rates, pressure response, and compositional changes in the produced gas. The simulation was implemented in DuMU^x using the DUNE toolbox (Flemisch *et al.* 2011) with program adjustments to allow importing of a grid from Petrel (Schlumberger 2019). The modelled storage site is a part of one of the largest onshore gas fields in Europe however it is not explicitly named in the paper. The model has dimensions of 800 by 1200 metres and a gross thickness of 50 metres. Four separate sandstone layers are modelled with tight clay layers separating them and a closed no-flow boundary at the edges of the model. The global porosity and permeability averages of the sandstone layers is 13.08% and 22.40 mD respectively with a 90% gas saturation above the gas-water contact. The composition of the gas in the reservoir is 90% mol nitrogen and 20% mol methane. Injection and production were constrained by average reservoir pressures of 400 and 300 bar respectively with 400 bar represent the original reservoir pressure. A peak of 271 million Sm^3 was stored, allowing 107.7 million Sm^3 to be extracted over a period of 4 months, enough for 43,500 average German households. The average composition of the extracted gas contained 82 mol% hydrogen in the first cycle and increased to 85.2 mol% in the last cycle, see Figure 12.

Pfeiffer, Graupner and Bauer (2016) presented an approach for coupling OpenGeoSys and ECLIPSE (Graupner *et al.* 2011) in order to deal with multiphase-multicomponent systems while accounting for thermal effects (such as the Joule-Thomson effect), geochemical feedback on fluid flow, and mass transport. A series of benchmarks are used to determine the relative errors of the approach and then a hydrogen storage scenario is used to demonstrate the coupled simulator approach. A simple 2D sloped aquifer model with a constant pressure boundary condition was used to simulate a ten cycle hydrogen storage schedule with an initial hydrogen saturation of 0.7. Each cycle consisted of injecting hydrogen at 300,000 sm^3/day for 30 days and then production at a rate of 900,000 sm^3/day for 10 days. The borehole temperature was set to be constant so that temperature changes due to the Joule-

Thomson effect could be observed. The temperature increased during injection due to the negative Joule-Thomson coefficient of hydrogen, with heat spreading via advection and conduction.

Sainz-Garcia et al. (2017) investigated the feasibility of storing hydrogen produced by wind powered electrolysis in northern Spain in a semi-open saline aquifer in the Castilla-León. The study simulated three annual injection/production cycles in COMSOL Multiphysics (COMSOL Inc 2016). It found a maximum hydrogen recovery factor of 78% and a global energy efficiency of 30%. Other key findings were that water upconing was a significant risk but it could be minimised through the use of shallow extraction wells in a steeply dipping structure. The aquifer model was of the Utrillas formation in the San Pedro dome, with a depth of 500 metres, a porosity of 0.2, and a permeability of 1×10^{-13} m^2 (101 mD). An initial 7492 tons of hydrogen was injected as cushion gas over one year at a rate of approximately 0.24 kg s^{-1} (230,000 sm^3 d^{-1}). During the three years of storage cycles the hydrogen is injected between October and May, and extracted between June and September. Storage cycle injection rates were 0.345 kg s^{-1} (335,000 sm^3 d^{-1}). The study found that no viscous fingering occurred during the simulation and that in total the storage site could provide 15% of the electricity needs of the city of Burgos between June and September when electricity production from wind power is below the level of demand.

Pfeiffer, Beyer and Bauer (2017) furthers the work done in Pfeiffer and Bauer (2015b) using the same geological model (open saline aquifer) with 5 wells implemented in ECLIPSE 300 (Schlumberger 2014). 25 different realizations with differing permeability properties were simulated in three stages: nitrogen cushion gas injected for 710 days at a target rate of 55,625 Sm^3/day/well. Hydrogen was then injected for 210 days at a rate of 155,000 Sm^3/day/well. Following this are six storage cycles which consist of 1 week producing at 1,000,000 Sm^3/day/well followed with a one day shut-in period. The key findings were that the hydrogen fraction in the produced gas reduces during the production phase, resulting in the power output of the well decreasing during the production cycle. The overall amount of hydrogen produced increases with each subsequent storage cycle along with the hydrogen fraction in the produced gas (see Figure 13). Increased power could be achieved with more wells and injecting more hydrogen as the structure was not filled to spill point in this study. The pressure response of the reservoir was significant,

with an increase of around 3 bars observed at a distance of 5 km from the wells. This suggests that monitoring of storage sites at a distance may be possible.

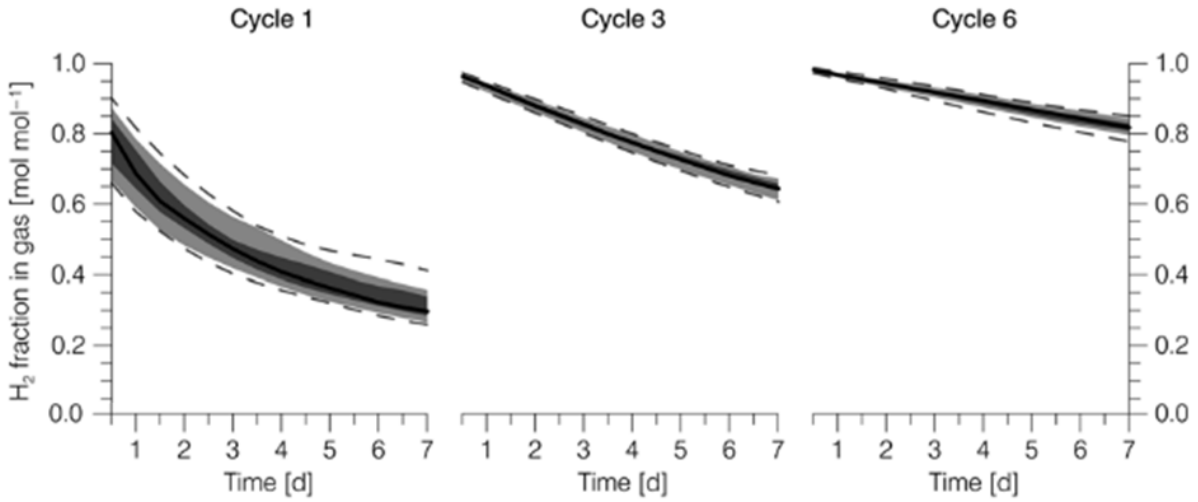

Figure 13: hydrogen fraction in produced gas vs time in days for cycles 1, 3, and 6. The solid black line depicts the median of all realizations, the dark grey shaded area is the interval spanning between the 25th and 75th percentiles, and the light grey shaded area is the interval spanning between the 5th and 95th percentiles. The dashed lines indicate the absolute minimum and maximum values. Adapted from Pfeiffer, Beyer and Bauer (2017).

Luboń and Tarkowski (2020) used the PetraSim TOUGH2 simulator (Pruess *et al.* 1999) to investigate hydrogen storage in the Suliszewo structure, a deep, open aquifer in Poland at a depth to crest of 1293 metres. Ten layers were modelled with porosities ranging from 7.63% to 27.80% and permeabilities ranging from 8.77 mD to 3669.65 mD. One well was modelled for both injection and withdrawal. The reservoir was charged with hydrogen without exceeding the fracture pressure over different periods of time between 6 and 36 months. Subsequently, four storage cycles were simulated with 6 months withdrawal and 6 months injection each. Only 25% of the injected hydrogen was recovered after the first cycle but subsequent cycles showed recovery factors of 88-89%. Water upconing was identified as a significant issue severely limiting hydrogen recovery when it occurred. However, viscous fingering was not observed during the simulation.

Lysyy, Fernø and Ersland (2021) investigated hydrogen storage in the Norne offshore depleted oil and gas field in Norway using ECLIPSE E100 (Schlumberger 2014) and a publicly available history-matched simulation model of the Norne field (Equinor 2013). Two wells were used and three storage zones were investigated in each well in the gas, oil, and water zones. The schedule included four annual storage cycles and one prolonged withdrawal period after. The study sought to

identify the ideal storage candidates within the field while assessing the hydrogen deliverability, the nature of the cushion gas, its composition, and the effect of structural geometries. The main conclusions of the study were that the gas zone gave the highest recovery factor of 87% and the water zone the lowest at 49%. Delivery of 400 million Sm^3 for each 5 month withdrawal period was achieved. More than 84% of the injected hydrogen remained underground as cushion gas when injecting pure hydrogen, with the use of formation gas as cushion gas the recovery factor was improved. Gravity segregation effects were observed when injecting a 30% hydrogen – 70% formation gas mixture. A summary of the key findings of the hydrogen storage simulation literature can be found in Table 3.

Table 3: Summary of key literature on hydrogen storage simulation

Storage type	Cushion gas	Software	Key findings	Reference
Aquifer - hypothetical open storage structure based on a real anticlinal structure in Schleswig-Holstein	nitrogen	Eclipse 300	Mixing occurred between the nitrogen and hydrogen with increased hydrogen purity with each subsequent production cycle	Pfeiffer and Bauer (2015)
Aquifer - simple 2D model	hydrogen	OpenGeoSys and ECLIPSE	Temperature increased during injection due to negative Joule-Thomson coefficient of hydrogen, with heat spreading via advection and conduction.	Pfeiffer *et al.* (2016)
Depleted gas reservoir - based on real, unnamed field	natural gas	DuMU^x - DUNE toolbox	Mixing occurred between residual gas and hydrogen with increased hydrogen purity with each subsequent production cycle	Feldmann *et al.* (2016)
Aquifer - semi-open saline aquifer in the Castilla-León	hydrogen	COMSOL Multiphysics	Maximum hydrogen recovery factor of 78% and a global energy efficiency of 30%. Upconing is a significant risk	Sainz-Garcia *et al.* (2017)
Aquifer - hypothetical open storage structure based on a real anticlinal structure in Schleswig-Holstein	nitrogen	Eclipse 300	As per Pfeiffer and Bauer (2015) plus increased power could be achieved with more wells and injecting more hydrogen	Pfeiffer *et al.* (2017)

Aquifer - Suliszewo structure: a deep, open aquifer in Poland	hydrogen	PetraSim TOUGH2 simulator	Only 25% hydrogen recovery factor after first cycle. Subsequent cycles showed recovery factors of 88-89%. Water upconing severely limits hydrogen recovery.	Luboń and Tarkowski (2020)
Depleted oil and gas reservoir - Norne field (Norwegian continental shelf)	hydrogen/formation gas	ECLIPSE E100	Gas zone gave highest recovery factors, and water zone gave lowest. Recovery factor improved when using formation gas as cushion gas.	Lysyy *et al.* (2021)
Aquifer - hypothetical 3D anticline reservoir model	hydrogen	GEM	Cushion gas requirements depend strongly on reservoir depth, shape of the trap, and permeability.	Heinemann *et al.* (2021)

1.7 Hydrogen well performance

The performance of individual hydrogen wells is poorly understood for porous rock storage sites, however, the extensive research and experience of predicting the performance of natural gas wells can be drawn upon. There is currently one study of hydrogen well performance which is a report from TNO on large-scale energy systems (Groenenberg *et al.* 2020) which uses the methods of a study which investigated natural gas storage (Juez-Larré *et al.* 2016). The methods used are standard practice in the oil and gas industry and are known as inflow/outflow performance. Inflow refers to flow into the well from the reservoir, and outflow refers to flow out of the well to the surface. The equations in use for predicting natural gas flow are based on those used to predict oil flow which were first empirically derived by Vogel in 1968 based on computer simulations (Vogel 1968). In order to adapt these equations for gas however, a way of accounting for changes in viscosity and compressibility with pressure is needed. The calculation of pseudopressure normalizes pressure for viscosity and compressibility and allows the solution of Darcy and non-Darcy flow equations (Al-Hussainy *et al.* 1966a).

The TNO study investigated the injection and production rates of hydrogen wells using a database of gas fields in the Netherlands. They determined cushion gas requirements and compared the hydrogen wells to methane wells. The main conclusion was that the lower density and viscosity of hydrogen compared to methane led to higher flow rates which compensated for its lower energy density

leading to energy flow rates from wells of 0.7 to 0.8 times that of methane. The study did not explicitly model different numbers of wells for each field, but stated that the method could be used to estimate the number of wells required. The methods were developed in open-source code however the code itself has not been made open-source. Therefore, there exists a gap for a study that investigates the effects of well numbers on flow rates and cushion gas requirements, as well as one that provides a published, open-access code that can benefit the wider research community.

1.8 Conclusions

This literature review has found that hydrogen is an important tool for the decarbonisation of the UK energy system that has been seriously considered in several key UK projects, the most notable of which being the H21 and Energy Research Partnership projects. It has also been determined that subsurface hydrogen storage capacity can reduce the amount of hydrogen production capacity required to meet future demand, especially on seasonal timescales. However, the required storage capacity for replacing the entire UK gas demand with hydrogen has not yet been determined, and will be addressed by the first aim of this thesis. No full UK study on the capacity of depleted gas fields and saline aquifers on the UK continental shelf for the storage of hydrogen has been completed and will be addressed by the second aim of this thesis.

The storage of hydrogen has been successfully achieved at commercial scales in salt caverns in both the UK and the USA, and hydrogen rich gas has been successfully stored in the form of town gas in porous rocks at several sites across Europe over several decades. Several projects in Russia, Argentina, and Austria have experimented with injecting pure hydrogen and other mixtures as well. From the literature on these sites, there appears to be no insurmountable technical hurdles that would prevent the storage of pure hydrogen in porous rocks. Work on numerical simulation of hydrogen storage at the field scale has been published several times in the literature over the past six years and conclusions seem to be similar in that water upconing is the main issue in terms of hydrogen recovery. All the studies also show that where another gas is used for a cushion gas, it is expected that the purity of recovered hydrogen will increase with each subsequent storage cycle. However, all of these studies look at large-scale storage sites, equivalent to medium sized natural gas fields or field scale natural gas storage sites.

There is likely to be a need for much smaller sites when real hydrogen storage is attempted in order to test the technology and because of the expected phase-in of hydrogen into the natural gas grid. The history matching and simulation of such a storage site will be addressed by the third and fourth aims of this thesis.

There is a lack of basic reservoir engineering work and the implications of hydrogen on well performance in the literature. There exists only one study and it does not provide the code behind the methodology. This lack of an open-access code for the investigation of hydrogen well performance will be addressed by the fifth aim of this thesis.

1.9 Aims & objectives of this thesis

This thesis has five key aims that will tackle the critical issues surrounding capacity estimates for hydrogen storage in porous rocks ranging in scale from the entire UK continental shelf, to an individual field, and down to single wells. The thesis will work down from the highest capacity estimates, or theoretical capacities, to the technical capacity of a single field or well.

The first aim of this thesis will be to determine the seasonal hydrogen storage requirement for the total UK gas demand if it was replaced 100% with hydrogen. In order to achieve this, sufficiently detailed data on UK gas demand at a monthly scale will be collected. It will then be analysed to establish the scale of seasonal fluctuations in demand in order to determine the amount of seasonal storage required.

The second aim of the thesis is to provide a robust figure for the amount of hydrogen that could reasonably be stored in porous rock formations on the UK continental shelf (UKCS). This will include oil & gas fields, along with saline aquifer formations. This will be done by screening and filtering data previously used in determining CO_2 storage capacities on the UKCS, and calculating the static storage capacity for hydrogen in each site using pressure-volume-temperature (PVT) equations.

The third aim of the thesis is to select and model a suitable small-scale storage site in the UK and determine the static volume available for hydrogen storage. This will be achieved by acquiring and cleaning publicly available data on a small onshore gas field and using the data to model reservoir properties and structure in Petrel (Schlumberger 2019).

The fourth aim of the thesis is to simulate hydrogen storage in the modelled reservoir in order to determine the dynamic hydrogen storage capacity and whether natural gas can be used as cushion gas. This will be achieved through a detailed analysis of pressure and production data using reservoir engineering techniques in order to history match the model through repeated simulations of historical gas production. Once history matching is completed, several hydrogen storage scenarios will be designed and performed and the results analysed.

The fifth aim of the thesis is to investigate the well performance of hydrogen storage sites. This will be achieved by developing a program that incorporates inflow and outflow performance equations and generates their respective curves in order to determine the maximum achievable flow rates for hydrogen wells. The program will also be developed in such a way that it can be used for any gas or gas mixture, so a comparison with methane or natural gas will be possible.

Chapter 2 A quantitative assessment of the hydrogen storage capacity of the UK continental shelf

The work presented in this chapter has been published as:

Scafidi, J., Wilkinson, M., Gilfillan, S.M.V., Heinemann, N. and Haszeldine, R.S. 2021. A quantitative assessment of the hydrogen storage capacity of the UK continental shelf. *International Journal of Hydrogen Energy*, **46**, 8629–8639, https://doi.org/10.1016/j.ijhydene.2020.12.106.

The text in the following chapter is adapted from this paper, with the published paper given in Appendix 1.

2.1 Introduction

In 2018, fossil fuels accounted for 85% of global primary energy demand (*Primary Energy - BP Statistical Review of World Energy 2019* | *68th edition*, 2019), resulting in the release of 33.1 billion tons of carbon dioxide into the atmosphere (IEA, 2019). The Paris agreement, reached in December 2015 by 196 members of the United Nations Framework Convention on Climate Change (UNFCCC), aims to keep the increase in global average temperature to well below 2 °C above pre-industrial levels (preferably less than 1.5 °C) in order to substantially reduce the risks and effects of climate change (UNFCCC 2015). Meeting these targets requires rapid decarbonisation of power generation, heating, industry, and transport.

Success in decarbonising the UK electricity sector has led to increased deployment of renewable energy sources such as wind and solar. Whilst this increase in renewable energy sources will reduce CO_2 emissions intensity, economic security of supply and grid balancing issues associated with variations in wind, solar and water energy production are likely to increase (Albadi and El-Saadany 2010; Katzenstein and Apt 2012; Ren *et al.* 2018; Liebensteiner and Wrienz 2019).

Decarbonising heating has proven to be more challenging. The UK relies heavily on natural gas for heating with 23 million homes connected to the existing gas grid out of around 28 million in total (Climate Change Committee 2016). Heating and hot water in buildings alone accounts for 20% of the UK's total greenhouse gas emissions (Climate Change Committee, 2016). The CCC (Committee on Climate Change) recommended a reduction in these specific emissions of 20% below 1990 levels by 2030 (Climate Change Committee, 2016) and a target of 57% reduction for all emissions from 1990 levels by 2030 (Climate Change Committee, 2015).

A major challenge is replacing the seasonal flexibility of the natural gas supply with a low carbon alternative that can match the peak winter demand. Currently production rates from UK gas fields, along with imports from Norway, are increased in the winter to match peak demand and satisfy 70% of UK gas demand (Ofgem, 2020a). The seasonal difference in gas demand between summer and winter is between 45 and 75 TWh (calculated from Ofgem data (Ofgem, 2020a), 2009-2018).

The key to solving issues of intermittency is the coupling of low carbon energy sources with large-scale energy storage systems capable of storing several TWh across seasonal timescales (Crotogino, Schneider and Evans, 2018). Large-scale natural gas (CH_4) storage is a proven technology where subsurface stores are filled during periods of low demand (i.e. summer) and emptied during high demand periods in winter.

Large-scale hydrogen production coupled with storage in geological structures is a technically feasible method for seasonal energy balancing (Foh *et al.* 1979; Stone *et al.* 2009; Crotogino *et al.* 2018) and could play an important role in enabling a low carbon energy system. However, this requires a decarbonised source of hydrogen either through steam methane reforming of natural gas combined with carbon capture and storage, or electrolysis using low carbon energy sources, with both sources being the subject of investigation on the UK continental shelf(Babarit *et al.* 2018; Alcalde *et al.* 2019; Caine *et al.* 2019; Cranfield University *et al.* 2019; Progressive Energy 2019; Dawood *et al.* 2020; Element Energy 2020).

With 8.4 GW of existing offshore wind capacity in the UK and a government commitment of increasing that figure to 40 GW by 2030 (Prime Minister's Office, 2019), large-scale production and storage of hydrogen on the UK continental shelf could provide inter-seasonal balancing of renewable energy production while making use of existing oil and gas infrastructure. A capcity of 40 GW of offshore wind with a load factor of 60% and an electrolyser efficiency of 70% could produce 147.17 TWh of hydrogen per year. Supplying the whole UK gas demand of 877.51 TWh (BEIS, 2020b) would require around six times this amount of offshore wind. Steam methane reformation of natural gas is therefore the more likely source for hydrogen to replace natural gas, but hydrogen production via electrolysis could still play an important role in balancing renewable electricity generation.

2.2 Underground hydrogen storage

Similar to natural gas, hydrogen can be stored in subsurface salt caverns, providing energy densities around 100 times greater than compressed air energy storage (Hart *et al.*, 2015). Hydrogen storage in salt caverns has been implemented commercially for industrial feedstock in three caverns at Teesside (UK) since the 1970s (Evans and Holloway, 2009) and in two at the US Gulf Coast since the 1980s (Panfilov, 2016). Salt cavern natural gas storage is important for short term energy demand fluctuations as they allow multiple injection and withdrawal cycles per year. However, salt caverns currently contribute only 20% of the total worldwide gas storage capacity (Cornot-Gandolphe, 2018) and their availability is limited to areas with thick subsurface salt deposits.

Hydrogen can also be stored in the pore space within a geological structure, displacing formation waters or, in the case of depleted gas fields, residual gases, which offers a geographically more independent and flexible solution for large-scale hydrogen storage (Zivar, Kumar and Foroozesh, 2020). Leakage is prevented by the presence of a caprock with a high capillary entry pressure above the reservoir and a trap structure will prevent the hydrogen from migrating laterally to guarantee its reproduction (Heinemann *et al.*, 2018). To date, pure hydrogen has not been stored in porous rocks, however, hydrogen-rich town gas (typically ~50% by volume) has been stored in porous rocks in Germany, France, and the Czech Republic (Kruck *et al.*, 2013).

As of 2018 there are 46 billion cubic metres (bcm) of natural gas storage in 75 saline aquifer storage sites and 334 bcm in 492 depleted hydrocarbon fields worldwide (Cornot-Gandolphe, 2018). Whilst no commercial projects currently store hydrogen in porous rocks, no physical or chemical barriers have been identified that could not be addressed using the knowledge gained from decades of experience in underground natural gas storage, and it was concluded early on that the physical and chemical challenges associated with hydrogen storage were manageable (Carden and Paterson, 1979; Foh *et al.*, 1979; Stone, Veldhuis and Richardson, 2009). Several modelling studies have investigated the cyclic injection and storage of hydrogen in geological formations using standard industry software and no major technical obstacles have been reported (Pfeiffer and Bauer, 2015; Sainz-Garcia *et al.*, 2017; Luboń and Tarkowski, 2020).

Recent work compared the possibility of hydrogen storage with natural gas storage at the Rough Gas Storage Facility (Amid, Mignard and Wilkinson, 2016), which at 3.3 bcm was the UK's largest porous rock gas store until it ceased to operate as a storage site in 2017. The hydrogen storage capacity (in terms of energy) was found to be approximately one third that of natural gas, due to its lower energy density (Hassanpouryouzband *et al.*, 2020). The same study found that losses through dissolution and bacterial action would be negligible (Amid, Mignard and Wilkinson, 2016).

Replacement of natural gas in the UK gas grid will require large-scale storage and, to date, no large-scale quantitative assessment of the potential hydrogen storage capacity available in subsurface porous rock has been undertaken. Here, we estimate the hydrogen storage capacity of the porous rocks on the UK continental shelf using a database originally compiled for geological CO_2 storage. The methodology outlined here is directly applicable to other national databases for carbon storage where they exist, paving the way for the compilation of robust hydrogen storage capacities for other large sedimentary basins. Furthermore we also calculate the proximity to storage sites to existing and planned offshore wind developments on the UK continental shelf which could provide a source of low carbon hydrogen in the future and may require large-scale energy storage.

2.3 Hydrogen storage capacity requirements for the UK

2.3.1 Replacement of existing storage

The current total natural gas storage capacity for the UK is 16.56 TWh (BEIS, 2020a), which is equivalent to 6.89 days' average supply based on 2019 UK gas demand of 877.51 TWh (BEIS, 2020b). This is spread across 1.50 billion cubic metres (bcm) of underground gas storage (Ofgem, 2020b), 0.37 bcm of which is in porous rocks at Humbly Grove and Hatfield Moor (National Grid, 2018) which equates to a porous rock working gas capacity of 2.34 TWh for natural gas (Horseman *et al.*, 2008). If the UK moves to a 100% hydrogen gas network, only one third of the energy can be stored in these porous rock sites, equivalent to 0.78 TWh (assuming a similar cushion gas requirement as per a study on the Rough Gas Storage Facility study (Amid, Mignard and Wilkinson, 2016)) due to the lower energy density of hydrogen (Amid, Mignard and Wilkinson, 2016). This would require an extra 1.56 TWh of working gas capacity to be found.

Further to additional porous rock storage capacity, the natural gas that is stored within the gas network itself, known as linepack, also needs to be considered. The energy density of hydrogen at linepack pressures can be four times lower than that of natural gas (Haeseldonckx and D'haeseleer, 2007), so replacement of natural gas with hydrogen would, in the worst case, result in four times less energy stored in the linepack. Currently the UK national transmissions system and local gas grids contain 4.88 TWh at their maximum and 3.84 TWh at their minimum, with an average of 4.41 TWh (Wilson and Rowley, 2019). Assuming that energy needs to be accessible for grid functionality then a further 2.88 to 3.66 TWh of working gas capacity will be required.

This means that replacing natural gas with hydrogen in the UK grid will require 4.44 to 5.22 TWh of additional working gas capacity to compensate for hydrogen's lower energy density.

2.3.2 Estimates of Inter-seasonal storage requirements

2.3.2.1 Estimates from demand

The H21 Leeds City Gate project produced by utility network provider Northern Gas Networks, focused on the provision of heat through a 100% hydrogen gas network for the Yorkshire city of Leeds in northern England, UK (Northern Gas Networks, 2016). This was based on converting the existing natural gas network of the city entirely to hydrogen. The study calculated that the conversion of the city's natural gas network to hydrogen would require 40 days of maximum average daily demand for inter-seasonal storage (Northern Gas Networks, 2016). Extrapolating this 40 day storage requirement to a national level using the maximum 3 hourly change in the gas network as peak demand of 251 GWh (Wilson and Rowley, 2019) (from data between January 2013 and March 2018) results in a maximum daily demand of 2.0 TWh which translates to a storage requirement of 80.3 TWh.

Using the same assumption of a 40 day requirement but using a peak demand figure of 170 GW calculated from household user data (Watson, Lomas and Buswell, 2019) (collected between May 2009 and July 2010) gives a maximum daily demand of 4.1 TWh. Multiplying this maximum daily demand by the 40 day requirement equates to a storage requirement of 163.2 TWh. Finally, using the 2018 UK gas demand of 881 TWh (BEIS, 2018), 40 days of seasonal storage would equal 96.5 TWh.

2.3.2.2 Estimates from supply

Over 70% of UK gas demand is supplied by gas fields located within the UK continental shelf (UKCS) and Norway, with storage, LNG (liquefied natural gas) and pipeline imports making up the balance (Ofgem, 2020a). Figure 14 shows the UK gas demand and supply source between October 2009 and October 2018 (data from Ofgem (Ofgem, 2020a)).

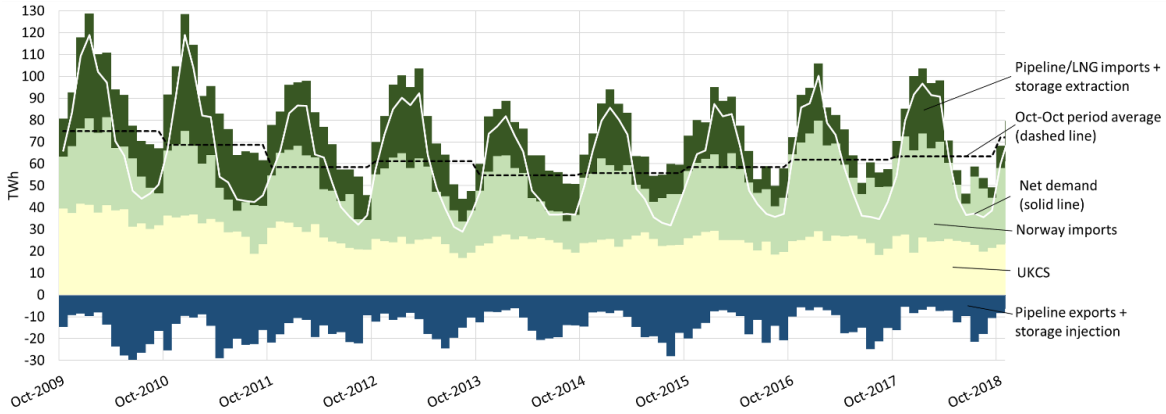

Figure 14: UK gas demand and supply source from October 2009 to October 2018 made using data from Ofgem *(Ofgem, 2020a)*. Gas supplied from the UK continental shelf (UKCS) and Norway respectively makes up over 70% of demand. Negative values indicate injection into storage and pipeline exports. The dashed line is the yearly average from October to October, and the white line is the net demand.

Negative values indicate exports and injection into storage. Over the past decade, seasonal variations in demand are increasingly accommodated by imports from Norway and other pipelines from Europe due to a reduction in supplies from the UKCS and LNG imports.

We have calculated the average monthly demand for each 12 month period from October to September in order to capture the full range of seasonal change in gas

demand. The difference from this average for each month is shown in Figure 15.

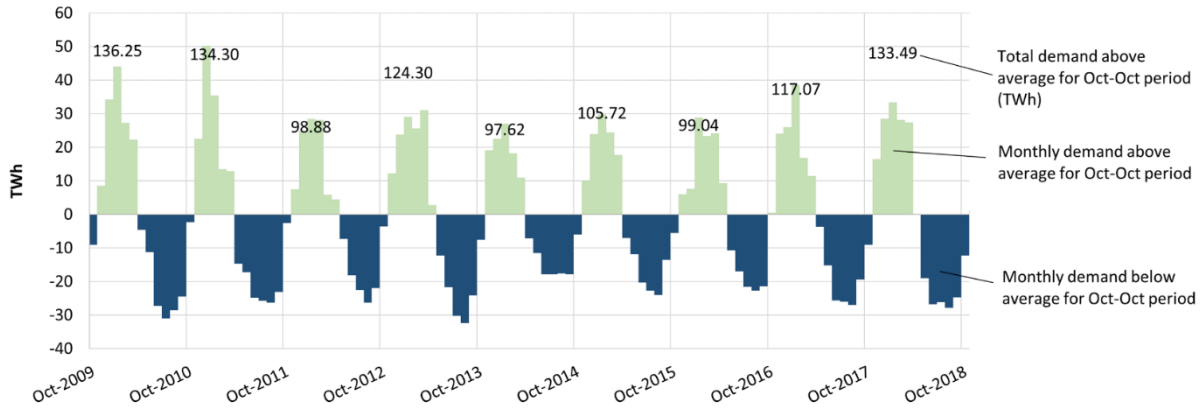

Figure 15: UK gas demand difference from yearly October to October average (see dashed line on Figure 14). Positive values are supply above average and negative values are supply below average. This graph quantifies the seasonal changes in gas demand over each October-October period. The difference between winter peaks and summer lows are 45 to 75 TWh depending on the year.

In the winter period of 2017/18 total demand above the period average was 133.49 TWh. Assuming a constant hydrogen production rate of 63.35 TWh per month (the October 2017 to October 2018 average monthly demand as shown by the dashed line in Figure 14) and no imports then the 133.49 TWh figure would be indicative of the level of working gas capacity required for seasonal storage of hydrogen. However, it is worth noting that this figure represents a maximum required working gas capacity as hydrogen production via steam methane reformation (SMR) could still utilise the seasonal variations in production rates of natural gas fields by building more capacity (Energy Research Partnership, 2016).

The Energy Research Partnership (ERP), a UK public-private partnership seeking to guide and accelerate innovation in the energy sector through enhancing dialogue and collaboration, investigated the potential role of hydrogen in the UK energy system (Energy Research Partnership, 2016). This work found that if the full UK domestic heat and industrial demand of 424 TWh for the year 2013 was switched to hydrogen produced by SMR, as little as 54 GW of installed SMR capacity could be used (run continuously at a >90% load factor with 1 month downtime per year) if combined with 75 TWh of storage capacity (it is assumed that this figure is working gas capacity) (Energy Research Partnership, 2016). Assuming the relationship between storage capacity and gas demand is linear, then the 2018 UK gas demand of 881 TWh (BEIS, 2018) would require around double this amount of working gas capacity, ~150 TWh . This is consistent with the 133.5 TWh figure calculated previously from the 2008 to 2018 Ofgem data (Ofgem, 2020a).

2.4 Methods and Data

2.4.1 The CO_2 Stored database

The CO_2 Stored database was developed by the UK Storage Appraisal Project, a consortium of Universities and the British Geological Survey (BGS), funded by the Energy Technologies Institute and published in 2012. It was developed to ascertain the geological storage capacity of the UK continental shelf for CO_2, and was maintained by the Crown Estate and BGS between 2013 and 2018 (Bentham *et al.*, 2014). It is now maintained and developed solely by the BGS.

The database includes saline aquifers (porous rock formations saturated with saline, non-potable water), depleted and active hydrocarbon fields, and consists of some 574 entries. Information contained in the database includes porosity and permeability, areal extent, thickness, pore volume, pressure regime, location, and type of storage site. Entries are classified as either having identified structures/traps or not, and being open or closed pressure systems. Storage volumes in the database were calculated using Monte Carlo analysis and are provided in tonnes of CO_2. However, calculations in this study are given in TWh to allow comparison between hydrogen and natural gas. P50 values (meaning that 50% of volumes exceed the P50 estimate and hence 50% of volumes are less than the P50 volume) for formation pore volumes in the CO_2 Stored database were used in this study and therefore all hydrogen storage capacities are also P50 values.

2.4.2 Methodology

The method used to calculate the hydrogen storage capacity of the UK continental shelf from the database comprised of three stages:

1) Filtering: The database was filtered for depth, reservoir quality, type (oil fields, gas fields, aquifers), along with removal of inappropriate entries.

2) Aquifer efficiency calculations: The calculation of storage efficiency to estimate usable pore volumes within saline aquifers with and without identified structures.

3) Hydrogen capacity calculation: Conversion of the available pore volume for hydrogen storage into hydrogen energy equivalent.

The stages were coded in “R” programming language (R Core Team, 2019) and run using the CO_2 Stored database as input. The code used is available in the supplementary information Appendix 2.

2.4.2.1 Stage One: Filtering

2.4.2. Site selection

Sites containing oil or gas condensates were considered unsuitable due to the potential for contamination of stored hydrogen. These were removed and only gas fields and saline aquifers were considered, bringing the total number of entries in the database down to 470.

Saline aquifers are far less well understood than hydrocarbon fields due their size and lack of discovered commercially exploitable hydrocarbon fields. However, they can contain traps that may be suitable for hydrogen storage. Whilst some of these traps have been studied during oil and gas exploration, there are likely to be many undiscovered or undocumented traps not present in the CO_2 Stored database, which relies heavily on hydrocarbon industry data. Hence, we deem saline aquifers to be suitable for hydrogen storage and include them in the hydrogen storage capacity estimate.

2.4.2. Reservoir quality filtering of saline aquifers

Gas fields are deemed to be highly suitable for hydrogen storage as they have trapped and stored buoyant natural gas for geological periods of time. Therefore, gas fields were not filtered for depth and other reservoir properties due to their proven ability to store gas over long time scales.

Saline aquifers were filtered for a minimum permeability of 100 mD and porosity of 10% based on CO_2 storage parameters (Raza *et al.*, 2016). However, hydrogen is a much smaller molecule and based on recent work on helium (Kilgallon *et al.*, 2018), it may be diverted into disconnected and dead-end pores not accessed by larger molecules. This means that lower porosities and permeabilities than those required for CO_2 storage may be acceptable, but further investigation is needed to verify this. Porous rock natural gas storage sites in the UK show average permeabilities of less than 100 mD. The Rough gas storage facility in the UKCS has well average permeabilities ranging between 2 mD – 184 mD (Stuart, 1991), the average core permeabilities for the two wells at the UK Hatfield Moors gas storage facility are 38.4 and 248 mD (Ward, Chan and Ramsay, 2003), and the average permeability for the UK Humbly Grove gas storage facility is only 20 mD in the storage formation (Great Oolite Group) (Gluyas *et al.*, 2020). However, we apply the precautionary principle and filtering for reservoir quality reduced the number of entries to 325.

2.4.2. Depth filtering of saline aquifers

The saline aquifers were then filtered for depth, using a minimum value of 200 m TVDSS based on accepted compressed air storage guidance (Allen *et al.*, 1983). As hydrogen requires more work to compress than CO_2 or natural gas, having a shallow minimum depth would save on compression costs. This reduced the number of entries in the database considered in this study to 317.

A maximum depth filter of 2500 m TVDSS was applied to the mean depth of saline aquifers. This depth was chosen as porosity in sandstone reservoirs typically declines to less than 10% below these depths (Ehrenberg and Nadeau, 2005), meaning a lack of available effective pore space for storage. Despite there being producing gas reservoirs at greater depths, 2500 m is also the maximum depth cited for best practice in CO_2 storage (Chadwick *et al.*, 2008) and so is also used in this study. This brought the number of entries considered down to 202.

2.4.2. Duplicate entries and missing data

Some sites were duplicated as result of subdivision of larger units. For example, the Bunter sandstone which has entries for the full extent, zones, and closures. The full extent and zones were filtered out as the closures had been identified as separate entries in the database. This brought the number of entries considered down to 191.

Not all entries in the CO_2 Stored database were complete, with some missing key data required for the hydrogen capacity calculation. These were filtered out bringing the number of entries in the database considered down to 177.

2.4.2.2 Stage Two: Efficiency Calculations for Saline Aquifers

After the filtering stage, 82 saline aquifers remained. Of these 12 have no identified structures or traps. In order to store hydrogen in a porous rock formation we assume that, as with natural gas storage, a trap (a physical shape to the rock layers) is required to contain injected hydrogen within the areal extent that allows production wells to recover it. As there are no identified traps in these 12 saline aquifers we must estimate the likely pore volume of unidentified traps within them. Based on a method recently developed for compressed air energy storage (Mouli-Castillo, 2018) we determined that there were very low storage capacities in these saline aquifers. Combining this with the low confidence of location, and lack of data we do not consider these saline aquifers further. More details on these calculations and their results are provided for interest in appendix 1.

2.4.2. Estimating useable pore volumes in saline aquifers with identified structures and/or traps

A storage efficiency of 1% was applied to the 70 saline aquifers with identified structures and traps based on the conservative estimate of the proportion of pore volume available for CO_2 storage in the CO_2 Stored database (Bentham *et al.*, 2014). This assumption was required as no information on trap geometries and their suitability for seasonal gas storage exists in the CO_2 Stored database.

2.4.2.3 Stage Three: Hydrogen Capacity Estimation

For depleted gas fields and saline aquifers, the estimated reservoir pore volumes were converted into hydrogen energy equivalent in TWh, allowing direct comparison to estimated energy storage requirements.

Pore volumes were converted to equivalent hydrogen volumes at STP using equation 1 adapted from the Rough Gas Storage Facility study (Amid, Mignard and Wilkinson, 2016).

$$(1)\ V_{H\ (STP)} = \frac{V_{H2}(1-S_{wi})P}{ZP_0}\frac{T_0}{T}$$

Where $V_{H\ (STP)}$ is the volume of hydrogen at STP, V_{H2} is the volume of pore space suitable for hydrogen storage, S_{wi} is the irreducible water saturation (defined as the lowest water saturation that can be achieved by displacing the water with oil or gas and given in the CO_2 Stored database as 0.423), P_0 is pressure at STP, P is reservoir pressure (assumed to be hydrostatic pressure as reservoir pressures are not given in the CO_2 Stored database), T_0 is temperature at STP, T is reservoir temperature, and Z is the compressibility factor of hydrogen which was linked to the temperature and pressure of the reservoir using an equation of state (Lemmon, Huber and Leachman, 2008). The irreducible water saturation in the CO_2 Stored database was used as a conservative estimate. We are currently aware of only one laboratory measurement of hydrogen-water relative permeability in sandstone from Yekta et al. (Yekta *et al.*, 2018) which gives a value of ~0.13. The calculation was also run using this value to see what effect it had on the hydrogen storage capacity. Equation 1 was also subject to a sensitivity analysis to determine the influence of each variable.

Only a proportion of the total volume calculated using equation 1 comprises the working gas capacity (WGC) i.e. the gas that could be economically stored and removed each cycle. The gas required to keep reservoir pressure at a suitable level

to allow efficient production of stored gas is called the cushion gas requirement (CGR). We assumed a cushion gas requirement of 50% based on the Rough Gas Storage Facility study (Amid, Mignard and Wilkinson, 2016). Hydrogen volume was converted using density at STP to calculate mass using the Nobel-Abel equation of state (Johnston, 2005) (equation 2).

$$(2)\ \rho = P/\left(RT + bP\right)$$

Where ρ is density, P is pressure, R is the gas constant (4160 J/kg K for hydrogen (Bolton, 2006)), T is temperature, and b is the co-volume (15.84 cm^3/mol for hydrogen (San Marchi and Somerday, 2008) and is defined as the volume of the molecules at rest (the volume of the molecules in motion is higher). Mass was converted to energy using the higher heating value (HHV) for hydrogen (39.41 kWh/kg (HyWeb, 2007)) to allow a comparison to energy demand in the UK.

2.4.2.4 Offshore wind development proximity calculation

After filtering and volumetric calculations were completed, the remaining gas field and saline aquifer data were tabulated and loaded into QGIS v3.4 geographical information software (QGIS Development Team, 2020). Crown estate offshore wind installation data (Crown Estate Scotland, 2018; The Crown Estate, 2018) was also loaded into the GIS software and a nearest neighbour analysis was performed to calculate how close each of the remaining gas fields and saline aquifers were to existing or planned offshore wind installations. For the locations of saline aquifers without identified structures the geographic centres given in the CO_2 Stored database were used.

2.5 Results

Using the methods outlined and the irreducible water saturation of 0.423 given in the CO_2 Stored database, 95 depleted gas fields and 82 saline aquifers were identified as suitable for hydrogen storage. Using an available pore space of 62.9 billion cubic metres, a total working gas capacity of 9100 TWh energy equivalent of hydrogen was calculated. A full list of sites and calculated capacities is available in the supplementary information, appendix 1 section 8.1.4.

Gas fields account for 6,900 TWh of working gas capacity, saline aquifers with identified structures account for 2,100 TWh of working gas capacity, and saline aquifers with no identified structures account for 70 TWh of working gas capacity (see Table 4). Calculated figures are given to 2 significant figures for gas fields and

saline aquifers with identified structures, and 1 significant figure for saline aquifers with no identified structures based on the differing uncertainties associated with them. Table 4 also shows the capacity estimates where S_{wi} = 0.13 (from Yekta et al (Yekta *et al.*, 2018)), an increase of 51% (see section on sensitivity analysis below).

Table 4: filtering parameters, final number of entries from the CO_2 Stored database post-filtering, and storage capacities by site type and S_{wi} value used. Storage capacities given to 2 significant figures.

	Depth	**Porosity & Permeability**	**No. of entries**	**Working gas capacity (TWh) S_{wi}=0.423**	**Working gas capacity (TWh) S_{wi}=0.13**
Gas fields	n/a	n/a	95	6,900	10,000
Saline aquifer with identified structure	>200m <2500m	≥10% ≥100mD	70	2,100	3,200
Saline aquifer with no identified structure	>200m <2500m	≥10% ≥100mD	12	70	100
Total			177	9,100	14,000

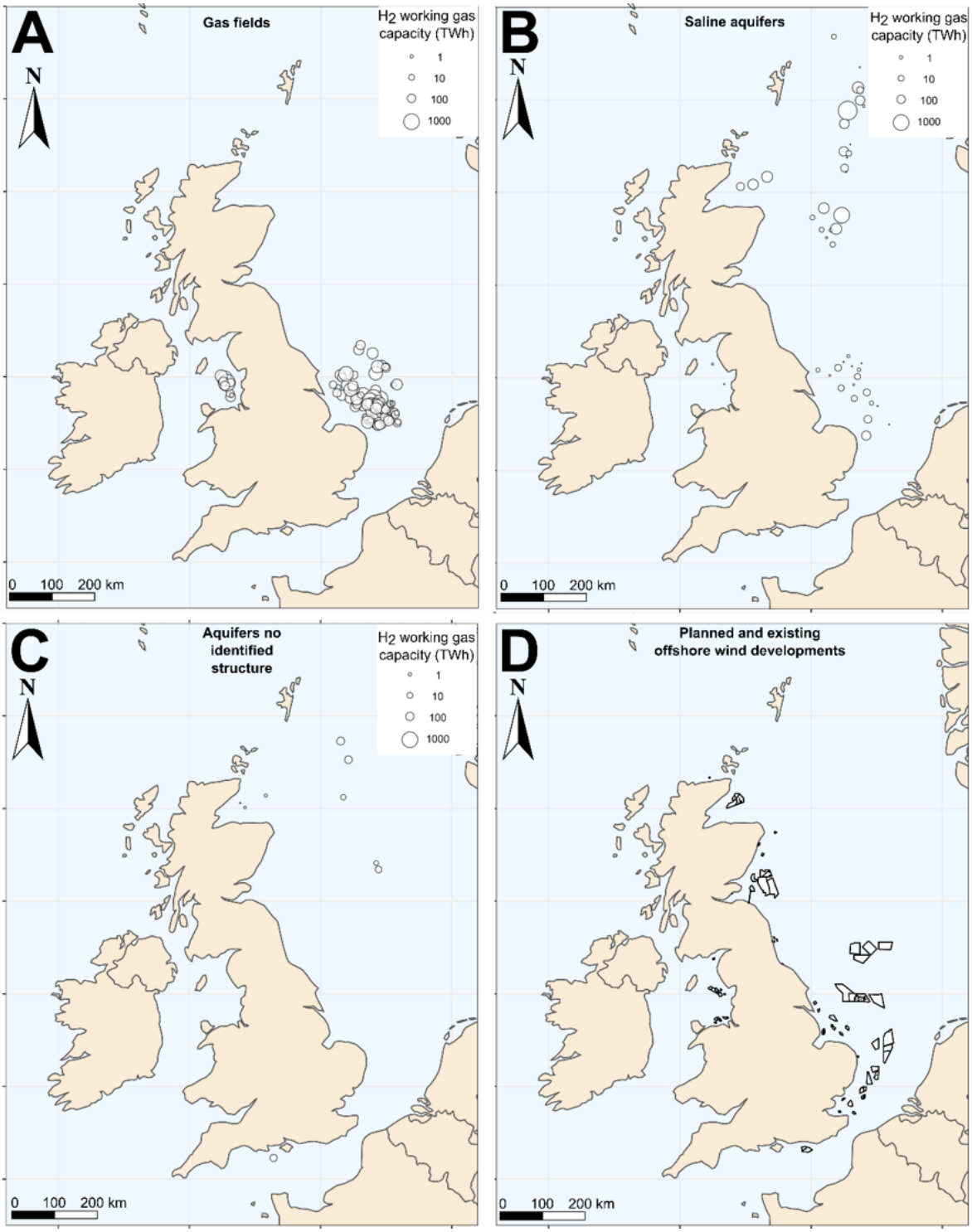

Figure 16: Location and relative sizes of different storage types and offshore wind on the UK continental shelf. A = Gas fields; B = Saline Aquifers with Identified Structures; C = Aquifers with no identified structures; D = location of existing and planned offshore wind developments. The majority of storage exists in the gas fields of the Southern North Sea, in close proximity to the majority of offshore wind developments. Figure generated in R using gplot2 (Wickham, 2016).

Figure 16 shows the location of all identified hydrogen storage sites and the location of active, under construction, and planned offshore wind developments.

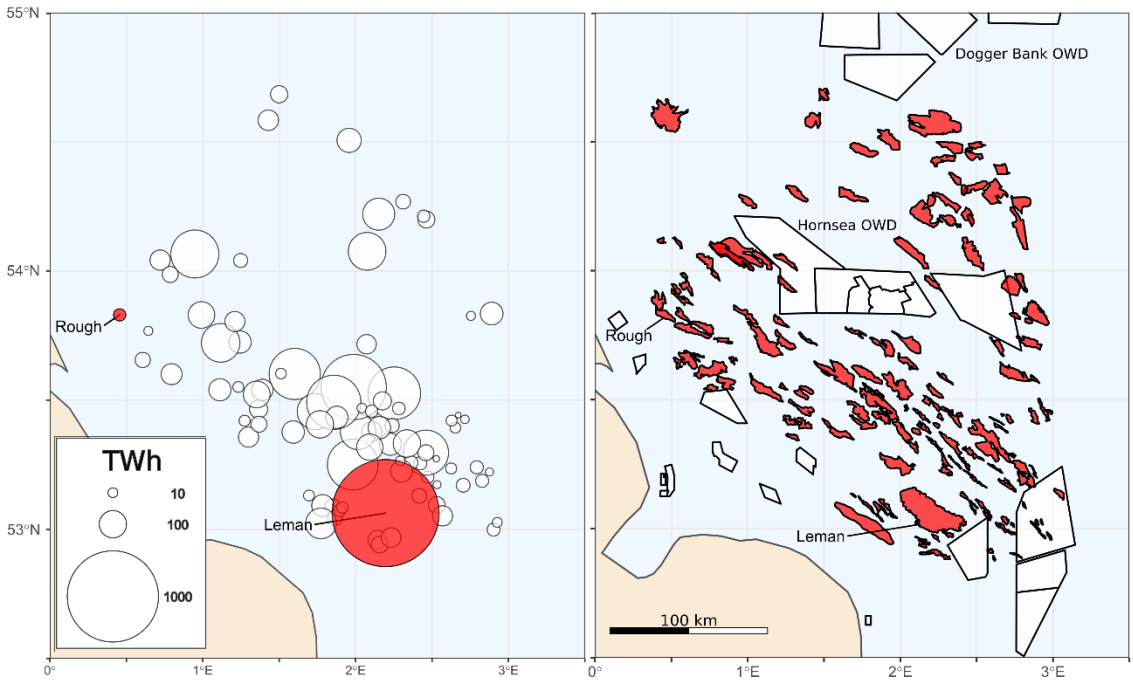

Figure 17: Detailed view of the Southern North Sea gas fields. Left panel shows gas fields and their relative storage capacities in TWh. Right panel shows the locations of the gas fields relative to planned and visiting offshore wind developments (OWD). The Rough (12 TWh) and Leman (1200 TWh) gas fields are highlighted in both panels.

Twenty-nine of the gas fields are 10 km or less from wind developments with the maximum distance being 46 km. Twenty-one of the saline aquifer storage sites with identified structures are 10 km or less from wind developments, with twenty-two sites at a distance of 100 km or greater, with the maximum distance being 186 km. Four of the saline aquifer storage sites with no identified structures are 10 km or less from wind developments with seven sites at a distance of 100 km or greater with the maximum distance being 189 km. As the distances for saline aquifers with no identified structures are measured from centroids rather than identified sites these hold little meaning.

85% of identified gas field storage capacity is located in the Southern North Sea (SNS) and the remaining 15% is located in the East Irish Sea (EIS). Figure 17 shows the Southern North Sea gas fields and offshore wind developments. The Rough gas field (previously Rough gas storage facility) mentioned earlier is highlighted along with the largest gas field, Leman.

The majority of storage sites have a capacity between 1 and 100 TWh. Size distribution of storage sites by type and geographic area is given in Figure 18.

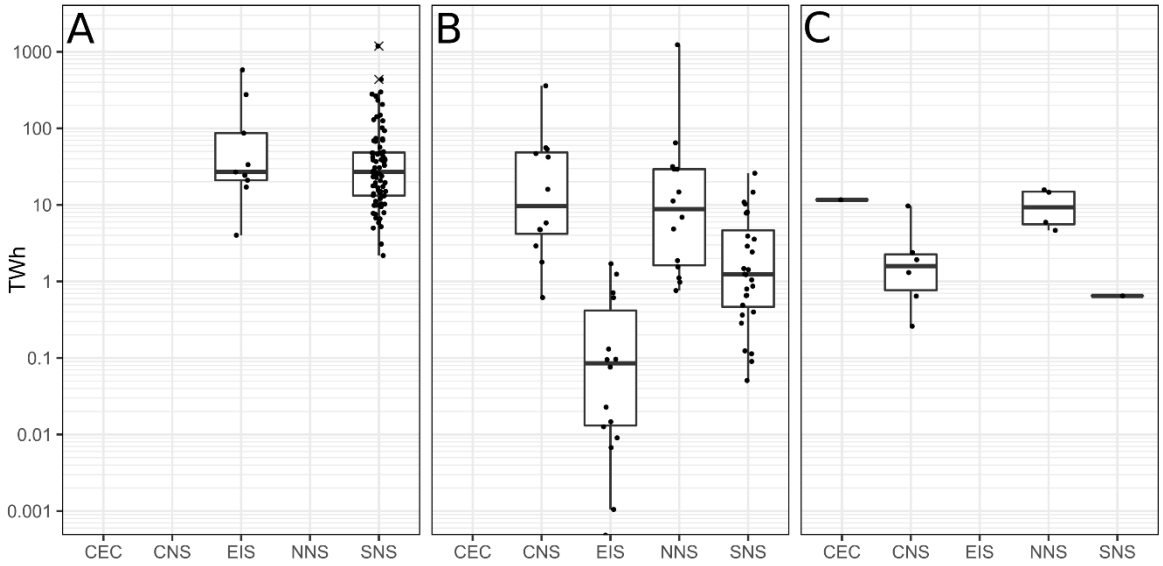

Figure 18: Boxplot diagram showing storage site size distribution by geographic region. A = Gas fields; B = Saline aquifers with identified structures; C = Saline aquifers with no identified structures. White boxes extend to the 25th and 75th percentiles, bold horizontal lines within boxes represent the median value, whiskers extend 1.5 times the distance between the first and third quartiles, crosses represent outliers and black points represent data points. CEC = Central English Channel; CNS = Central North Sea; EIS = East Irish Sea Basin; NNS = Northern North Sea; SNS = Southern North Sea. The SNS gas fields provide the largest number and diversity of site sizes.

2.6 Sensitivity analysis and factors affecting hydrogen storage capacity estimates

A base case scenario was created from average values in the CO_2 Stored database (with an arbitrary 1 bcm pore volume), along with high and low values for each variable based on extremes. This data is shown in Figure 19 as a tornado plot, with the base case values shown in the middle of each bar and the extreme values on

the ends (labelled high and low).

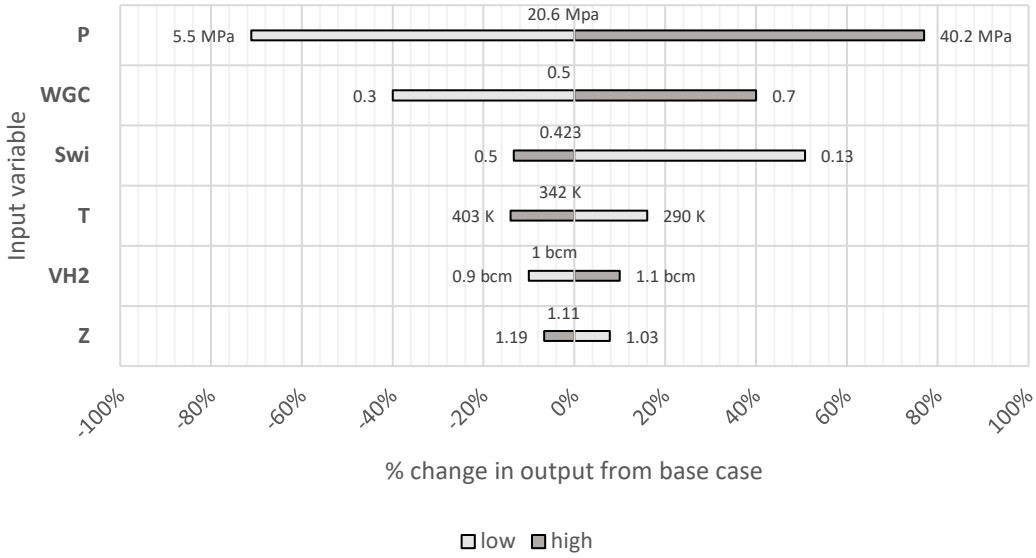

Figure 19: Tornado plot showing the base, high and low for variables in equation 1 and their effect on the output (hydrogen storage capacity). Uncertainty in P, WGC, and Swi have the biggest potential to change the storage capacity estimate P = reservoir pressure; WGC = the working gas capacity fraction; Swi = the irreducible water saturation; T = reservoir temperature; VH2 = the volume of pore space suitable for hydrogen storage; and Z = the compressibility factor of hydrogen.

The variables that are least well known are the storage pressure (P), working gas capacity fraction (WGC), and irreducible water saturation (S_{wi}). All three will be site specific to some degree, affected by the geology of the storage site and in the case of WGC and pressure, economics of compression and storage. Irreducible water saturation is likely to be lower than the base case as evidenced by the work of Yekta et al (Yekta *et al.*, 2018). Z (compressibility factor) has relatively little effect as hydrogen compressibility does not change significantly across the temperature/pressure range encountered in the CO_2 Stored database.

A sensitivity analysis was performed to determine which of the variables in equation 1 had the biggest influence on working gas capacity estimates for hydrogen. Figure 20 shows the influence of each variable in equation 1 on the output (working gas capacity) as they are varied by ±10%. Compressibility (Z) has the biggest influence with a change of -1.006% in output with every increase of 1%, however as this is directly linked to temperature and pressure, it is ultimately these variables that result in changes in compressibility. Irreducible water saturation (S_{wi}) has the smallest

effect of -0.733% with every increase of 1%.

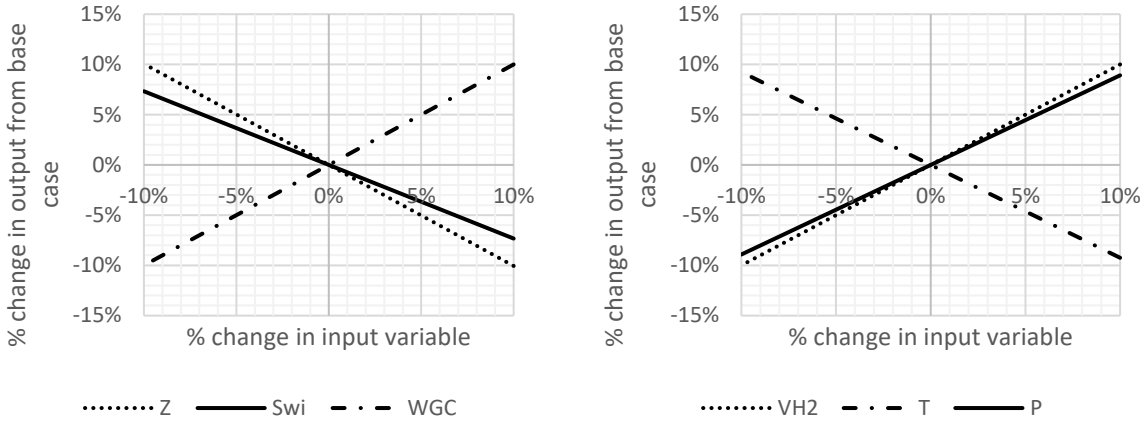

Figure 20: Sensitivity of variables in equation 1. All variables are positively correlated with changes in output except temperature, irreducible water saturation, and compressibility factor. P = reservoir pressure; WGC = the working gas capacity fraction; Swi = the irreducible water saturation; T = reservoir temperature; VH2 = the volume of pore space suitable for hydrogen storage; and Z = the compressibility factor of hydrogen.

2.7 Discussion

Our results show that there is a potential 6900 TWh of high confidence (P50) working gas capacity for hydrogen in gas fields in the Southern North Sea and East Irish Sea.

This is greater than any estimates of seasonal storage capacity requirements given earlier, the highest of which was ~150 TWh. The majority of this storage capacity is located in the Southern North Sea close to existing and planned large offshore wind developments which could be used to produce hydrogen that could be injected into seasonal energy stores in the future. Individual gas fields offer a range of storage capacities between <10 TWh to >1000 TWh. Offshore hydrogen production is currently being investigated along with energy hubs which combine hydrogen and electricity production from offshore wind with existing oil and gas infrastructure(Babarit *et al.* 2018; Alcalde *et al.* 2019; Caine *et al.* 2019; Cranfield University *et al.* 2019; Progressive Energy 2019; Element Energy 2020).

There is a potential 2200 TWh of working gas capacity for hydrogen in saline aquifers, however there are considerable hurdles to providing accurate estimations of hydrogen storage capacity in saline aquifers in the CO_2 Stored database. This is due to the amount of uncertainty in the size and location of useable pore space within suitable structures, especially in aquifers with no identified structures, making this a low confidence estimate.

Sensitivity analysis of equation 1 and the tornado plot in Figure 19 show that the ideal storage sites in terms of capacity of hydrogen stored would be low temperature reservoirs capable of containing high pressure while allowing for a relatively high working gas capacity fraction i.e. a higher working gas capacity would make a storage site more economically viable. Further refinement of ideal storage site parameters for site selection would need to take this into account.

As the relative permeability of hydrogen in water is not well defined it is unclear as to whether viscous fingering would dominate over capillary limited flow. As viscous fingering can be controlled to some degree by injection rate it is not unlikely that the low irreducible water saturations demonstrated by Yekta et al (Yekta *et al.*, 2018) could be achieved in real storage sites.

This high-level study sought to estimate total hydrogen storage capacity in the UK continental shelf. Further refinement would need to take into consideration the potential conflict with CO_2 storage sites, potential reactions between hydrogen and existing fluids in the gas fields such as natural gas, carbon dioxide, and hydrogen sulphide, and well integrity.

This methodology can also be applied to other carbon storage databases where they exist to provide an estimate of hydrogen storage capacity at a national level. Such databases currently exist in Australia (Carbon Storage Taskforce, 2010), Brazil (Ketzer *et al.*, 2015), China (Dahowski *et al.*, 2009), Europe (Vangkilde-Pedersen *et al.*, 2009), Norway (Norwegian Petroleum Directorate, 2011), and North America (NETL and US DOE, 2015).

2.8 Conclusions

This chapter presents a methodology to estimate hydrogen storage capacity in porous rocks at a national level using a carbon dioxide storage database for the UK. We find a P50 estimate of 6900 TWh of hydrogen storage capacity in the gas fields of the UK continental shelf and a lower confidence estimate of 2200 TWh in saline aquifers. These figures are an order of magnitude greater than all known estimates for the seasonal storage requirement for the UK. This methodology can be applied to other national carbon dioxide storage databases where they exist to provide a high-level quantified estimate of hydrogen storage potential.

Chapter 3 Geological model of Cousland

3.1 Introduction and aims

This chapter covers the building of a geological model of the Cousland gas field. The aim of building this model was to determine the pore volume of the gas-bearing part of the reservoir, determine the most important and least well understood variables involved in calculating the volume, and provide an estimate of the average properties of the reservoir. These properties will be refined in the next chapter through a reservoir engineering study and history matching during simulation.

The structure of this chapter will build a picture of how the model was built, starting with some historical and geological context of the Cousland gas field. A summary and discussion of the available data is included, this is split into both raw and interpreted data. After this, a workflow will be introduced and the steps involved will be explained along with decisions made at each stage. Finally, a sensitivity analysis of the calculated reservoir volume is performed and a discussion of the key assumptions, limitations, and uncertainties of the model takes place.

3.2 The history of the Cousland gas field

The Midland Valley of Scotland has long been known for oil seeps both at the surface, such as St. Catherine's well in Liberton, and in coal and oil shale mines (Falcon and Kent 1960; Bagnall 1979). The oil shale industry was born in the Midland Valley of Scotland and the piles of waste generated, called bings, are still visible as red, flat topped hills in the landscape today (Harvie and Hobbs 2013). Exploration for liquid oil was focussed on anticlines and the target was the oil shale formation. It was thought that igneous intrusions had destructively distilled the oil from the shale in a similar manner to the industrial process invented by James Young in the 19th Century (Lees *et al.* 1937).

After conversion of its naval fleet from coal to oil between 1912 and 1914, Britain was entirely dependent on imported oil during WWI and needed to safeguard its supply. Government intervention was required to develop a domestic oil industry. The Petroleum (Production) Act 1918 and Defence of the Realm Act 1918 paved the way for exploration, giving power to enter land for the purposes of drilling for oil (Lees *et al.* 1937; Hallett *et al.* 1985; Dean 2018). This led to the drilling of 11 test-

wells between 1918 and 1921 by S. Pearson & Son, Ltd. under government contract. Nine of these were in England and two in Scotland. The two in Scotland were drilled in 1919 at West Calder and D'Arcy. At West Calder the target oil shales were found to be of low quality, the target sandstones were largely absent and there were extensive volcanics (ash, intrusions etc.). The well at D'Arcy did encounter sands and also found oil and gas. However, with the war over, demand had declined and the D'Arcy well was abandoned in 1922.

The Petroleum Production Act 1934 stimulated further interest in the D'Arcy well and also to the north on the same structural trend at Cousland. The Anglo-American Oil Company developed the D'Arcy well in what became known as the Midlothian oil field and the D'Arcy Exploration Company (named after William Knox D'Arcy, mining entrepreneur and businessman who founded Anglo-Persian oil; confusingly, the D'Arcy well was named after the nearby D'Arcy farm) discovered gas at Cousland in 1937 in sandstone horizons in what was then known as the Calciferous sandstone measures (Hallett *et al.* 1985) and is now known as the Strathclyde group (Underhill *et al.* 2008). Four more wells were drilled around the Cousland structure before production was started by Sir Harold Smith, Chairman of the Gas Council (later to become British Gas) on 28th October 1957 (ITN 1957), with a further well drilled in 1959. The gas was sold to the Musselburgh Gas Works via a dedicated pipeline. Natural Gas from Cousland (Figure 21) was mixed with coal gas from the Musselburgh Gas Works and supplied local parish residents (Dean 2018; East Lothian Antiquarians and Field Naturalists Society 2018a). This picked up the shortfall from the closure of Prestonpans Gas Works in 1954 (East Lothian Antiquarians and Field Naturalists Society 2018b). Production continued for eight years until 1965, producing a total of around 330 million cubic feet (9.3 million m^3) of natural gas (Hallett *et al.* 1985) - this figure includes all horizons and testing: the main reservoir produced around 250 million cubic feet (7.1 million m^3). The Gas works was closed in 1966 (East Lothian Antiquarians and Field Naturalists Society 2018a) and the only remaining well at the Cousland field was plugged and abandoned in 1974 (Exploration Dept. Lasmo 1985).

Figure 21: Gas testing at Cousland (Fisher 1945) © *British Geological Survey.*

Geological setting

3.2.1 The Midland Valley of Scotland

The Midland Valley of Scotland (MVS) is a Late Palaeozoic sedimentary basin that trends WSW to ENE. It is bounded by the Highland Boundary Fault to the north and the Southern Upland fault to the south. The basic geology, structure, and location of the Cousland gas field is shown in Figure 22. It formed after the closure of the Iapetus Ocean during the Caledonian Orogeny. The basin itself extends west to Northern Ireland (Williams and Harper 1988) and east out into the Forth Approaches (Cartwright *et al.* 2001). Differential weathering of the resistant metamorphosed strata that outcrop to the north and south of both fault systems and the less resistant unmetamorphosed sediments within the basin has led to the development of the central lowland belt of Scotland.

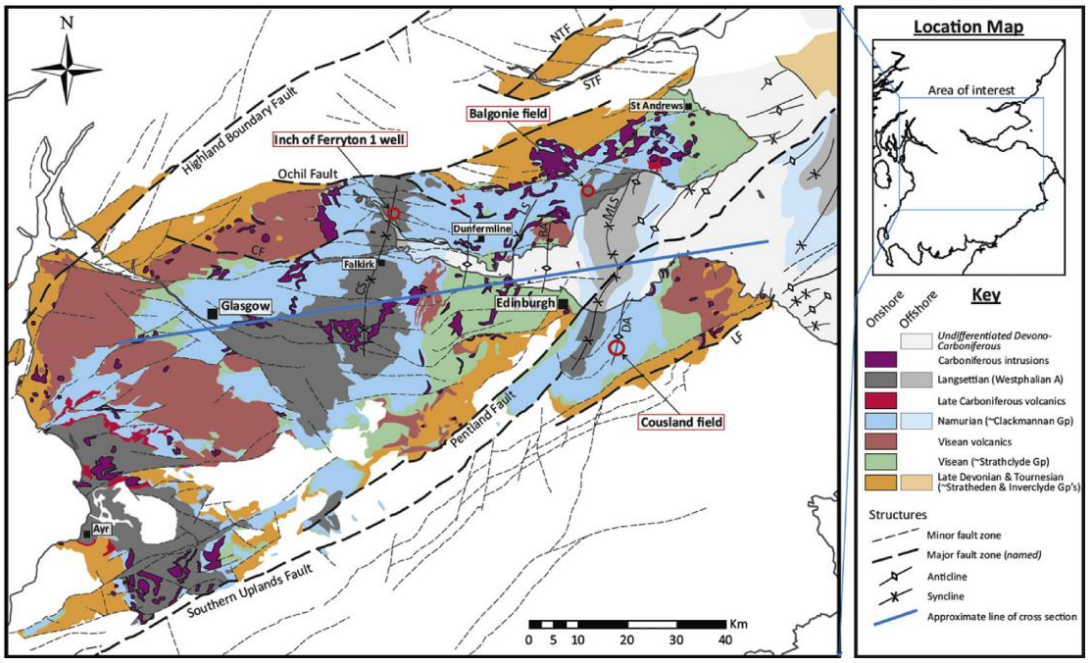

Figure 22: Location map and simplified geological map of the Midland Valley of Scotland from Heinemann *et al.* (2018b) *showing the location of the Cousland gas field. Faults, anticlines, and synclines are labelled as follows: CF, Campsie Fault; NTF, North Tay Fault; STF, South Tay Fault; LF, Lammermuir Fault; CS, Clackmannan Syncline; LS, Lochore Syncline; BA, Burntisland Anticline; MLS, Midlothian-Leven Syncline; DA, D'Arcy-Cousland Anticline where the Cousland gas field is located. The blue lines refers to the cross section in Fig. 5 of* Heinemann *et al.* (2018b)*. Originally compiled from BGS data.*

The eastern part of the Midland Valley of Scotland contains several north-northeast to south-southwest striking folds that cross the Firth of Forth. Namely the Clackmann, Midlothian, and Leven synclines which are separated by the Balmule, Burntisland, and D'Arcy-Cousland anticlines respectively. This period of folding was complete by the end of the Carboniferous as evidenced by later E-W striking Carboniferous/early Permian cross-cutting dykes, normal faults, and extensional fractures (Underhill *et al.* 2008). There is little evidence of subsequent major tectonic events as the east-west striking intrusions are relatively undeformed. The Carboniferous clastic sediments that fill the basin are derived from the mountains uplifted during the Caledonian Orogeny in what is now north-east Scotland, Norway, and East Greenland.

3.2.2 The Strathclyde group

The Coulsand gas field is found in the Strathclyde group which is Visean in age and is around 1.2 km thick in East Lothian and over 2.2 km thick in Fife (Monaghan 2014). In East Lothian it is characterised by cyclical sandstones, siltstones,

mudstones, and minor seatrock, coals, ironstones, limestones, and dolostones. The base consists of 560 metres of lavas, tuffs, and volcaniclastic rocks of the Arthur's seat and Garleton Hills volcanic formations. In Fife similar cyclical sediments exist along with thick (10s of metres) oil-shales. The volcanic members include the Kinghorn Volcanic formation and the Charles Hill Volcanic member. Certain limestones can be correlated between Fife and East Lothian including the Hurlet Limestone which marks the top of the Stratchclyde group.

3.2.3 Cousland stratigraphy

At Cousland the Lower Limestone Formation is identifiable at outcrop and was mined in the area for many years. The Burdiehouse limestone (or its equivalent) is thought to be identifiable at Cousland and across most of the Midland Valley of Scotland, which puts the producing reservoir at the Cousland gas field in either the Aberlady or Gullane formations (Figure 23). These sandstones, in what was known as the Calciferous Sandstone Measures when the gas field was being developed, cannot be correlated across any large distance (> 1km) with confidence. It is thought that these sands are lenticular in shape and laterally variable on a scale of 100s of metres. Evidence of this is found in the pressure data from Cousland well testing and production (which will be discussed in detail in the next chapter: *Compositional reservoir simulation of hydrogen storage in the Cousland gas field*; also see Illing (1961)), The Stewart 1 well (Exploration Dept. Lasmo 1985), and the Firth of Forth 1 well (Exploration Dept. Lasmo 1985; CONOCO (U.K.) Limited and ENTERPRISE OIL p.l.c. 1991), which suggest that the sands are sheet-like and not laterally extensive or verticaly connected.

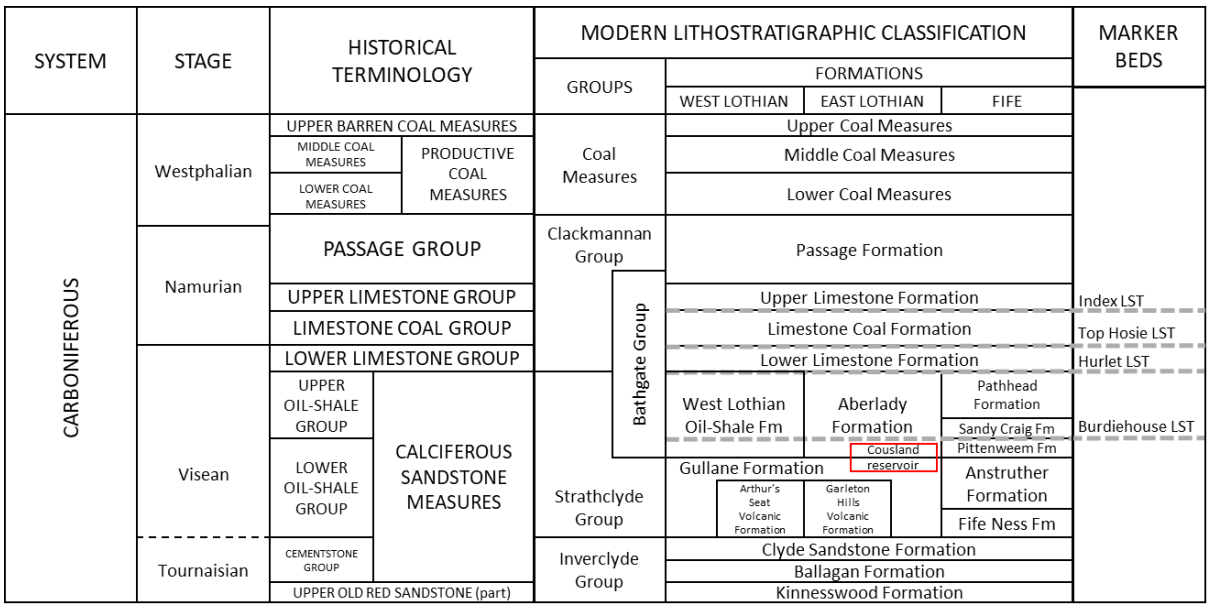

Figure 23: Stratigraphy of the Midland Valley Scotland with marker beds and the location of the Cousland gas reservoir highlighted in the red box in the East Lothian column, just below the Burdiehouse LST marker bed. After Underhill et al. (2008) and Heinemann et al. (2018).

Correlation of sands between wells in East Lothian and across the Firth of Forth is extremely difficult, however correlations at the formation level have been possible using marker beds such as the Burdiehouse limestone and certain shale formations (Monaghan 2014). Despite the lack of correlation of sands across the Firth of Forth, the coastal section between Coal Farm and Pittenweem in East Fife (the Pathhead, Sandy Craig, and Pittenweem formations) was considered a good analogue for the reservoir section in the Cousland gas field by the geologists working on the field due to the similarity in rock types in the upper sections (the Pathhead formation in Fife) and as crinoidal limestones compare well at both locations (Falcon 1938). However, the lower succession differs significantly in that it is dominantly sandy and gritty in the East Fife section and not so at Cousland (Falcon 1938).

3.2.4 Environment and sandbody connectivity

Studies on the Strathclyde group (previously the Oil Shale Formation, see Figure 23) of the Midland Valley (Greensmith 1961, 1962, 1965; Loftus and Greensmith 1988) suggest a depositional environment composed of intradistributary lagoonal tracts and channels at the western margin of a major delta system with sediments sourced from the north-east. This lead to the deposition of sandstones of varying reservoir quality, shales, limestones, dolostones, and coals, as seen in the

analogous coastal section between Coal Farm and Pittenweem in Fife, around 40 km to the northeast of Cousland (Falcon 1938).

Sedimentological studies performed on core material from the nearby Stewart 1 well (located in the Midlothian oil field to the South of Cousland) indicate a wave-dominated, delta-like depositional environment for the sands of the Oil Shale Formation which were reworked to a high degree in a shallow marine, nearshore environment and probably deposited in bodies parallel to the shoreline (Exploration Dept. Lasmo 1985). That study did not determine whether the sands were extensive or isolated bars, however it did determine that vertical connectivity was likely to be poor due to a relatively static shoreline that varied between sand and mud-dominated deposition phases.

This lack of vertical connectivity between the sands is confirmed by pressure test data from Cousland 1 (Adcock 1939; Martin 1974). The nature of the drop in pressure during production from Cousland 1 without any encroachment of water suggests that the gas occupied the same volume in the reservoir as production continued (Illing 1961). This is indicative of isolated sand bodies encased by impermeable shales rather than extensive sheets and was the basis for considering Cousland as a potential gas storage site in the 1960s (Illing 1961; Adcock 1969). It is for this reason that the edges of the geological model described in this chapter are treated as no-flow boundaries.

3.3 Hydrogen storage potential at Cousland

Here an initial estimate of the hydrogen storage capacity is given based on the assumption that the volume of produced gas from the Cousland field could be replaced with hydrogen. This estimate is for the purposes of benchmarking the more detailed caluclations described later. The storage volume is equivalent to the total gas produced from the field, 330×10^6 ft^3 of natural gas (Hallett *et al.* 1985), and assumes a 50% cushion gas requirement. This estimate shows that Cousland could store enough hydrogen to cover the gas requirements of around 1125 homes based on the following assumptions: an annual gas usage of 13,442 kwh per year per household in Scotland in 2016 (Department for Business Energy & Industrial Strategy 2018b), a storage volume of 330×10^6 ft^3 (9.3×10^6 Nm^3 (normal cubic metres)) which is equivalent to 100.8×10^6 kWh of natural gas, and hydrogen

having an energy density 30% that of natural gas at standard conditions (McCarty *et al.* 1981; Friend *et al.* 1989).

3.4 Data

3.4.1 Summary of available data

The Cousland gas field is relatively data rich, however most data exists in PDF scans of reports. These reports are typed, handwritten, and annotated in pen and pencil with some scans of very low quality, some examples of which are shown in Figure 24. As a result, they are not searchable and optical character recognition (OCR) software does not work either. Several weeks were spent extracting data from these reports and putting it into a digital format. These are available in Appendix 3. The raw data itself is available from two sources: the UK Onshore Geophysical Library (UKOGL) (UK Onshore Geophysical Library 2020) , and the National Geoscience Data Centre (NGDC) (British Geological Survey 2020b).

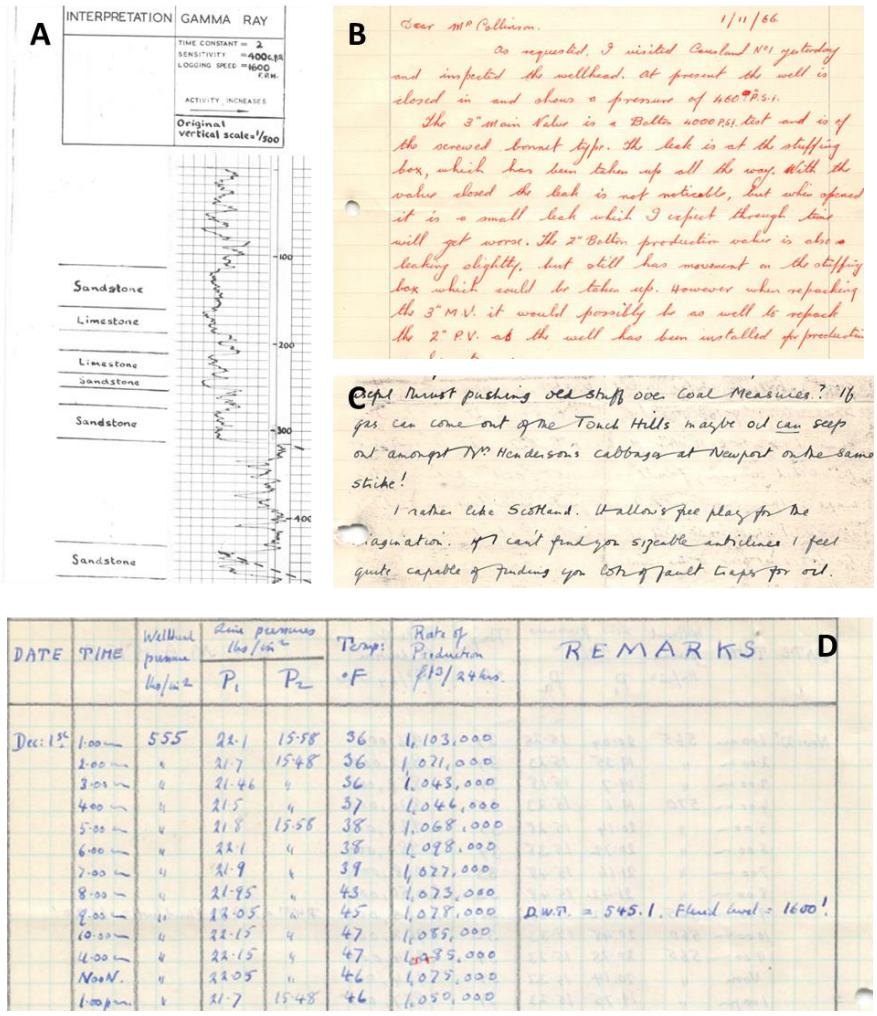

Figure 24: Examples of available data from the Cousland gas field. A: hand annotated gamma ray log with fading and no scale; B: handwritten correspondance relating to a leaking valve on the wellhead; C: hand written correspondence relating to oil seeps in Mrs Henderson's Cabbages; D: handwritten pressure and flow rate data.

The UKOGL is a map based graphic user interface that allows navigation to the area of interest and filtering of data types. Wells, seismic lines etc. can be selected and data viewed/downloaded directly. The NGDC is search based, entering keywords brings up data containing those keywords. In this work the search terms "Cousland", "Midlothian" and "Stewart 1" were used to find data from the Cousland-D'Arcy Anticline used in this study.

A summary of the available data is shown in Table 5, more detailed data description is available in Appendix 3. Note that it was intended to visit the BGS Core store and inspect the physical samples however due to the COVID-19 pandemic this has not been possible.

Table 5: Summary of available data for the Cousland gas field. *ghost well/undrilled prospect; [1]available at BGS core store (British Geological Survey 2020a); [2]available at UKOGL (UK Onshore Geophysical Library 2020); [3]available at NGDC (British Geological Survey 2020b); [4]extracted from Appendix C of (Monaghan 2014).

Well	Physical samples[1]	Core porosity and permeability[2,3]	Fluid analysis[2,3]	Well logs[2,3,4]	Production data[2]	Well test data[2,3]	Reports[2,3]
Cousland 1	x	x	x	x	x	x	x
Cousland 2	x	x	x				x
Cousland 3	x		x				x
Cousland 4		x	x				x
Cousland 5	x	x	x	x			x
Cousland 6	x	x	x	x			x
Cousland 7*							x
Stewart 1	x			x			x
D'Arcy 1							x
Cousland G1	x						x
Cousland G2	x						x
Cousland G3	x						x
Cousland G4							x
Cousland G5							x
Midlothian 1	x		x	x			x
Midlothian 2				x			x
Midlothian 3							x
Midlothian 4							x
Midlothian 5							x
Midlothian 6							x
Midlothian G1							

3.4.2 Core and Well log data

Core porosity and permeability data were extracted from petroleum engineering and geological reports for wells C1 to C6. The raw data including locations within the reports is in Appendix 3. Well log data was extracted from scanned well logs, images of well logs within reports, and from Appendix C of Monaghan (2014). Within the Cousland gas field, only wells C1, C5, and C6 had accessible well logs, and in all three cases only the gamma ray logs were digitised (C5 also had resistivity logs). Summary interpreted lithological logs were also available in the scanned reports.

3.4.3 Seismic data

There are 12 seismic lines shot in 1977 and 1892 across the Cousland-D'Arcy Anticline. These are of generally poor quality and interpretation of them is very uncertain. LASMO did attempt some interpretation of these lines in order to calculate a reservoir volume but the figure is highly uncertain and is not published in their relinquishment report (Exploration Dept. Lasmo 1985).

3.4.4 Well test data

Several deliverability and flow tests were performed on C1 between the late 1930s and mid 1950s. However the technology of the time combined with equipment breakdowns and human error means that most of this data is well below modern standards and as a result only one test and subsequent pressure buildup from 1956 is deemed as good enough to produce any meaningful results. This test was designed to find the absolute open flow potential (AOFP) of the well. There is no evidence in the available reports that a downhole pressure gauge was used which limits the effective analysis of these tests.

3.4.5 Production data

Production data can be found in an appendix of the Lasmo relinquishment report (Exploration Dept. Lasmo 1985) and provides monthly and cumulative production data along with what is assumed to be end of month well head pressure.

3.4.6 Surface maps

A relatively simplistic surface map of the base Lower Limestone formation drawn up after the drilling of Cousland 6 was created by the original geologists from shallow well data, structural contour mapping, and the deep well data. It is probably the most that can be confidently said about the subsurface structure although Lasmo provide a much more detailed version of the same surface which they interpreted from seismic (Exploration Dept. Lasmo 1985). However, as the seismic lines are of very poor quality and the Lasmo report states they are not considered reliable, the simpler surface map was used as a basis for the geological model in this work.

3.5 Geological model of the Cousland gas field – workflow

The model of the Cousland gas field was created in Petrel (Schlumberger 2019)using the workflow illustrated in Figure 25. This workflow will be discussed in detail, point by point below.

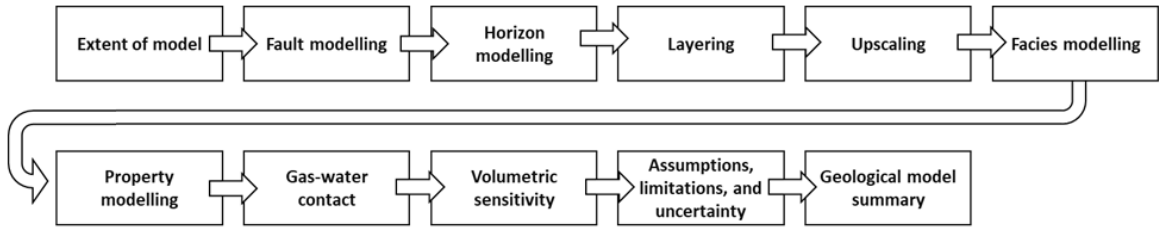

Figure 25: Workflow used to create model of Cousland gas field

3.6 Extent of the model

Testing in well C1 revealed several sandstone horizons that produced gas. These were named according to their depths in feet in the Cousland 1 well: 1188 sand, 1248 sand, 1582 sand and the 1720 sand. Upon testing, 1188 and 1248 produced 20,000 and 30,000 cubic feet of gas per day respectively (approx. 560 and 840 m^3/d). 1582 produced 3,000,000 cubic feet per day (approx. 84,000 m^3/d) and 1720 produced 6,000,000 cubic feet per day (approx. 168,000 m^3/d). However, production in the late 1950s and early 1960s was solely from the 1582 sand. Because of this, the only horizon modelled in this study was the 1582 sand which is 50 feet (15.2 metres) thick in well C1, 8 feet (2.4 metres) thick in well C2, and 67 feet (20.4 metres) thick in well C5. A small amount of oil was produced from the 1248 sand, however none from the 1582 sand and so oil was also not included in the model.

The lateral extent of the model was constrained by the area in which wells penetrated and it was also assumed that the fault (indicated from the drilling logs) between wells C1 and C6 was impermeable. This decision was based on pressure data whereby no changes were detected in well C6 during production from well C1, which suggests no pressure connection between the wells. As the gas water contact was just below the 1582 sand in well C1, none of the other wells penetrated the gas one of the 1582 sand, making this a closed, one well system (**Error! Reference s ource not found.**).

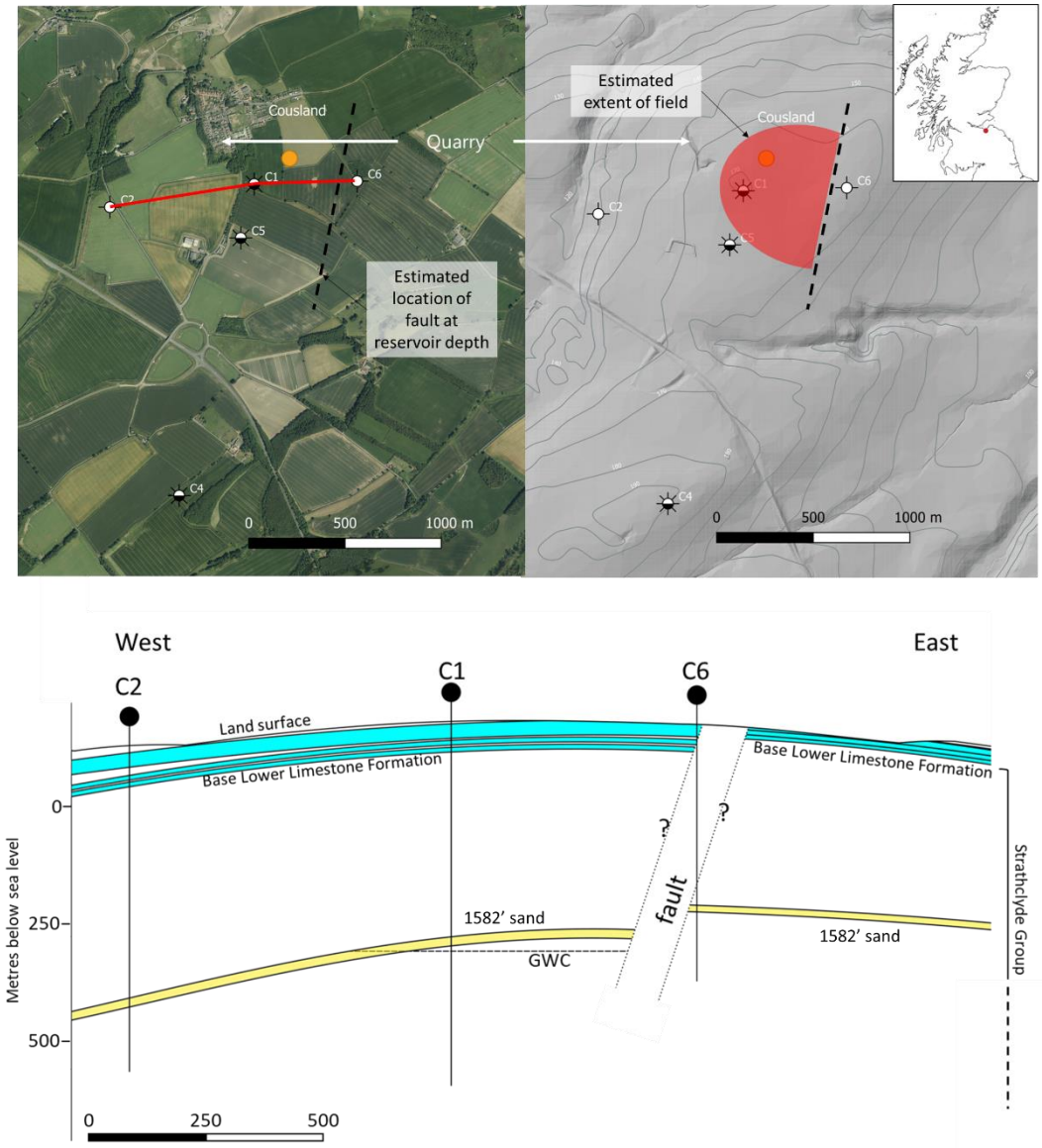

Figure 26: (a) sattelite map of Cousland site showing wells and shows. Orange circle is the suggested site of a gas storage well from the 1961 report (Illing 1961)*; (b) LIDAR image of the Cousland anticline with countours showing the surface expression of the anticline at Cousland along with an indication of the gas field extent. Dashed line represents the estimated location of the fault at reservoir depth. (c) cross section through the red line shown in (a) with the Lower Limestone formation and 1582' sand shown along with the likely location of the fault and the gas/water contact (GWC).*

3.7 Fault Modelling

A vertical fault was added between wells C1 and C6 as indicated on the surface map in **Error! Reference source not found.** and the depth map in **Error! Reference source not found.**. As the pressure data indicated no communication across this fault it will be treated as a no-flow boundary and become the edge of the model (Figure 28).

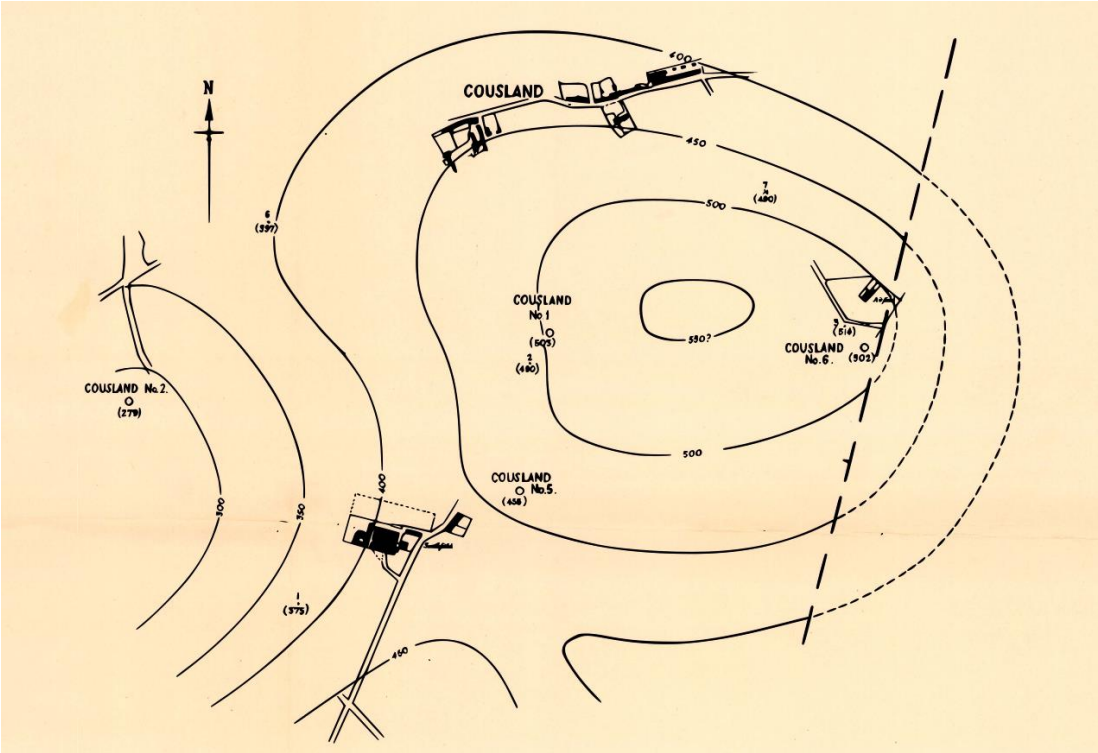

Figure 27: Depth map of the base of the Lower Limestone Group from the geological report for well Cousland 6 (BP 1960b) *showing the location of the fault at that depth along with the well locations, roads, and buildings. Contours are shown in feet above sea level.*

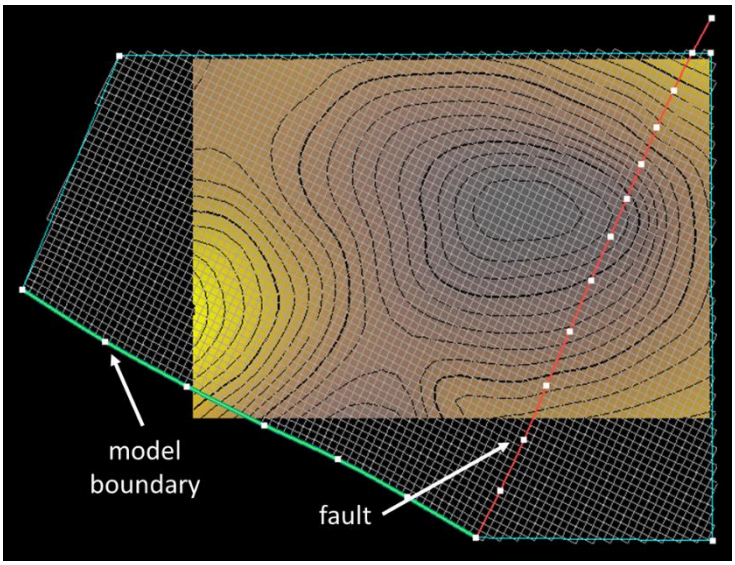

Figure 28: plan view of model showing location of fault (red line), model boundary, and digitised contour map for reference

3.8 Horizon modelling

3.8.1 Well correlation

There is relatively good correlation of sandstones between wells C1 and C5 however, the changing nature of the sand horizons over short distances made

correlations beyond these wells somewhat difficult and the presence of a fault between C1 and C6 also adds to the uncertainty. Thin limestone horizons were more easily identifiable from the lithology logs (BP 1960a, b) and using these allowed the sands to be better constrained. Using this combination of lithology and gamma ray logs allowed updated correlations between wells where possible. These were then cross checked against well tops determined by the original geologists working on the site. In this way, the 1582 sand was correlated between wells C1, C2, C5, and C6 as shown in Figure 29 (C2 had no gamma ray log and was based soley on the original lithology logs from the wellsite geologists (BP 1960a, b)).

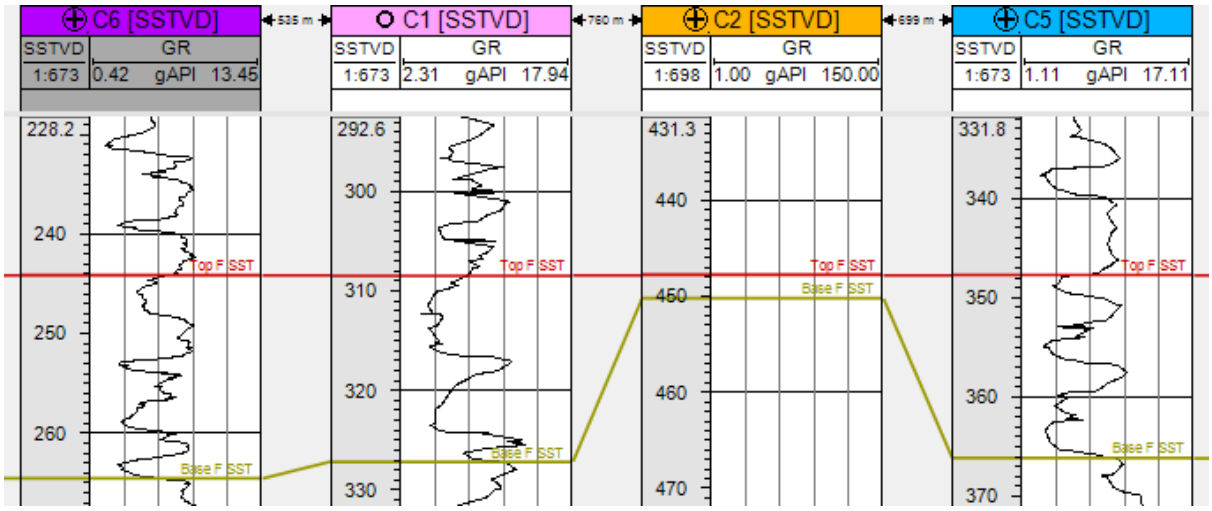

Figure 29: Correlation between wells flattened to the top of 1582 sandstone (named F SST in diagram). Scale is in metres TVDSS.

3.8.2 Surfaces

Once sands were identified and correlated between wells, the surface map of the base Lower Limestone Formation (**Error! Reference source not found.**) was used a s a template for the surfaces of the sands. To create a 3D surface from the 2D map, it was imported into Petrel and contours traced onto it. These were then assigned the depths given on the map to produce a 3D set of contours. These were then converted to a surface. To make surfaces lower down in the formation, a copy of this surface was made and, using the calculator, the depth of the copy was increased to the average depth of the sands. This was repeated for each major sand in the field. The surfaces were then converted to horizons which allowed them to be tied to the well tops, changing the shape of the surface to intercept the well tops as shown in Figure 30. The algorithm used was the convergent gridder (Schlumberger 2019), which uses control points (in this case the well tops) to iteratively converge on a

solution and is suitable for faulted horizons as is the case here. As a result, there will be more detail in areas with more data, and general trends will be followed in areas with less data. This process was then quality checked in the well section view window to make sure the surfaces and interpreted well tops matched.

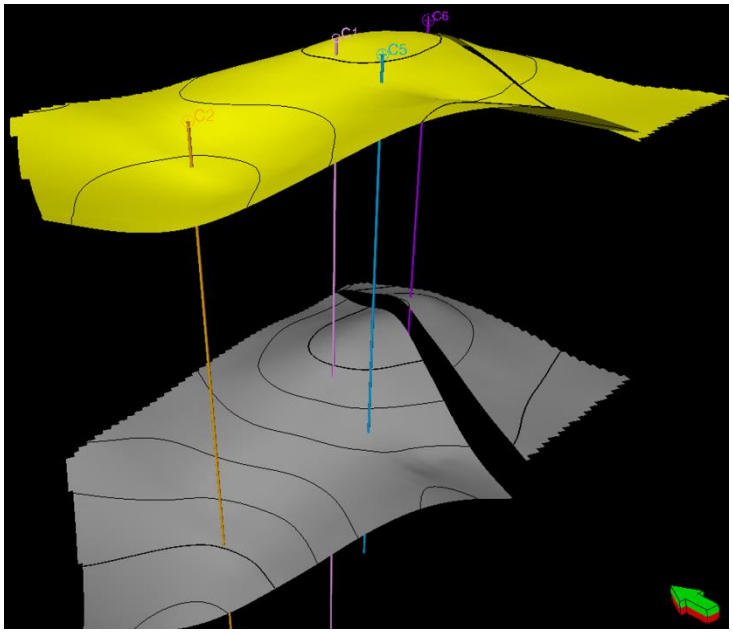

Figure 30: Horizons tied to well logs: the base lower limestone formation (yellow, at top) surface, and top 1582 sandstone surface (grey, at bottom) are shown. Wells C1 (pink, centre-left), C2 (orange, left), C5 (blue, centre right), and C6 (purple, right) are also shown and the fault is visible as the break in the surfaces.

3.9 Layering

A grid was created for the reservoir section with 119 × 86 × 70 cells in the x,y, and z directions respectively. This gives a resolution of 25 metres in the horizontal directions and 0.2 metres in the vertical direction. Vertical resolution is high in order to capture any potential mixing fronts between the natural gas and hydrogen during the simulation study, and also to allow for any upconing effects to be captured. This also allows the vertical heterogeneity of the sands to be captured.

3.10 Upscaling

The next step in the model build is to upscale the logs. Upscaling entails assigning values to cells in the 3D grid that are penetrated by well logs. The properties must be scaled up as each grid cell can only hold one value. These values at the wells can then be used to populate the cells between wells with values later during property modelling. It is essential during upscaling to ensure that the properties don't

differ so much from those at the well as to significantly change the behaviour and characteristics of the whole system. With the Cousland model, well logs were upscaled into 70 vertical blocks. Gamma ray logs were used to calculate V_{shale} (the proportion of shale in the rock) which in turn was used to calculate net-sand (the proportion of sand in the rock). Net-sand was upscaled to provide a binary choice between the two facies modelled: sand and shale. This was then used as a basis for property modelling.

3.10.1 Volume of shale (V_{shale})

Calculation of V_{shale} determines the proportion of shale in the formation by using the gamma ray response of a formation. This is possible because shale is usually more radioactive than sand or carbonate (Asquith and Krygowski 2004). The gamma ray index is calculated first as follows:

$$I_{GR} = \frac{GR_{log} - GR_{min}}{GR_{max} - GR_{min}}$$

Where I_{GR} is the gamma ray index, GR_{log} is the gamma ray reading of formation, GR_{min} is the minimum gamma ray reading (clean sand or carbonate), and GR_{max} is the maximum gamma ray reading (shale). A linear response is used for an initial estimation of V_{shale}:

$$V_{sh} = I_{GR}$$

There are also several non-linear empirical methods to determine V_{shale}, all of which return values with a lower proportion of shale than the linear equation. These, in order of decreasing shale volume, are as follows:

Larionov for Tertiary rocks Larionov (1969) $$V_{sh} = 0.083 \times (2^{3.7*I_{GR}} - 1)$$

Stieber (1970) $$V_{sh} = \frac{I_{GR}}{3 - 2 \times I_{GR}}$$

Clavier (1971) $$V_{sh} = 1.7 - [3.38 - (I_{GR} + 0.7)^2]^{\frac{1}{2}}$$

Larionov for older rocks (Larionov 1969) $$V_{sh} = 0.33 \times (2^{2*I_{GR}} - 1)$$

As there is no empirical method known to be suitable for the rocks of the Cousland field or region, the linear response was used. The V_{shale} is used to determine porosity and permeability which will be adjusted during history matching during reservoir simulation so a close approxiamtion is all that is needed at this stage. The different V_{shale} equations are shown graphically in Figure 31

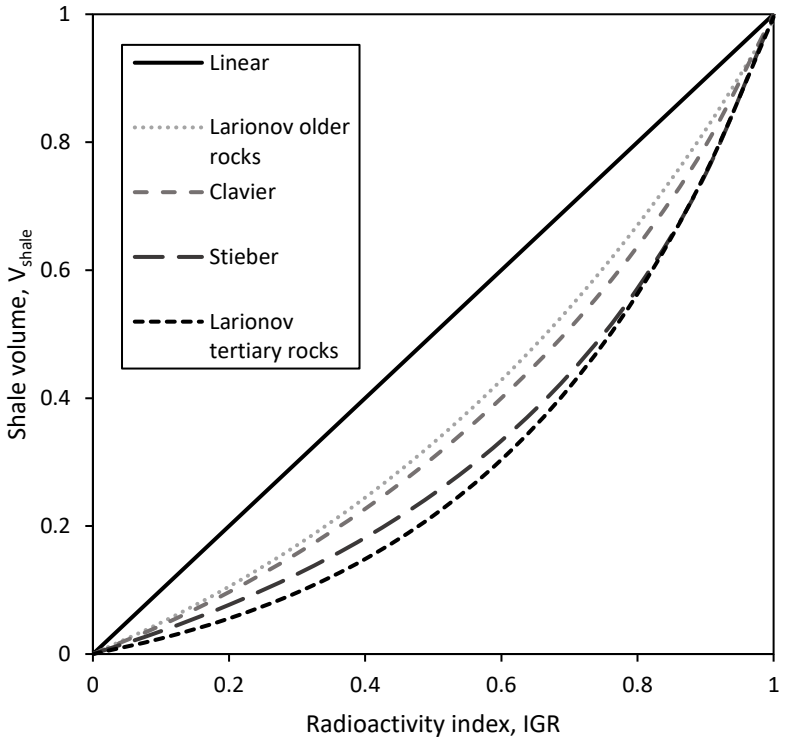

Figure 31 Different V_{shale} equations from the literature presented graphically as V_{shale} vs Radioactivity index. The linear equation ws used in this study as no known equations exist for the rocks of the Cousland field, and the property values calculated from v_{shale} will be adjusted later during history matching so a match at the level of the sands is all that is required.

3.10.2 Net-sand

Net-sand is a simple way to determine whether part of a formation is classified as sand or not. It is a cutoff using V_{shale} with anything below a certain value classified as sand. It can be adjusted based on known sands in the reservoir and is useful for determining net pay and correlating between wells as it provides a visualisation of sand thickness within the formation. It is also used during the porosity and permeability modelling. In the Cousland model, a net-sand cutoff value for V_{shale} of 0.4 (where V_{shale} values below 0.4 were considered to be sand) gave good correlation to lithological and gamma ray logs.

3.10.3 Upscaling V_{shale}

The V_{shale} log was initially upscaled using the arithmetic mean, however this produced a very poor fit with the gamma ray logs and lithology logs i.e. location of sands in the formation did not match the upscaled V_{shale} log. The upscaling was then repeated using the net-sand property as a bias. This bias prevented intermediate values from skewing the upscale values as illustrated in Figure 32.

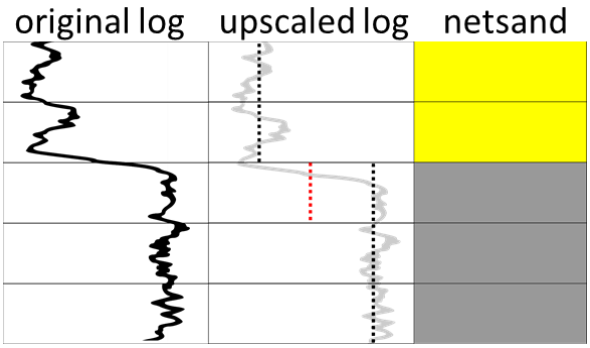

Figure 32: example of upscaling bias. Where the arithmetic mean is used during uspscaling intermediate values can skew the upscale values. This is illustrated by the red dashed line on the upscaled log, which gives an intermediate value between the sand and shale. Biasing the log to net-sand results in cleaner statistics, the biased value shown here as the black dashed line.

Upscaling resulted in a good match for clean sands in the gamma ray and lithology logs, but picked consistently higher values for shales when compared to the original V_{shale} log. This cannot be explained by use of net-sand as a bias during upscaling as

this has very little effect except at the boundaries between sands and shales. However, as this process is the precursor to property modelling in which all shales will be treated as no-flow units, this overestimation of V_{shale} in the upscaled cells within shales will have no effect. The key result is that there is a good match between the sands in the upscaled V_{shale} log compared to gamma ray and lithiology logs.

3.10.4 Upscaling net-sand

Net-sand was upscaled to the resolution required for gridding using the arithmetic mean and quality checked against the net-sand log to check that the proportions of sand and shale had not changed significantly (Figure 33). This shows two things: that the net pay of the reservoir horizon is around 70% and that the grid resolution is fine enough to capture the sands to within 1.2% of the well log values.

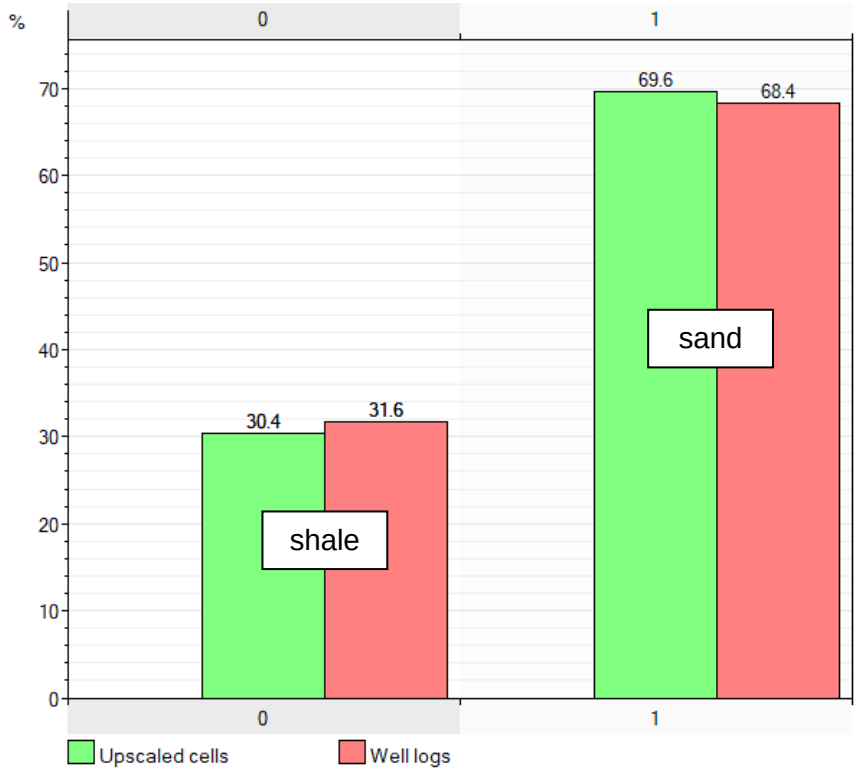

Figure 33: upscaled net-sand vs non-upsacled net-sand logs. 0 is equivalent to shale and 1 to sand. Upscaled cells are shown on the left of each pair in green and net-sand logs are shown on the right of each pair in red. The proportions shown are for the 1582 sand.

3.11 Facies modelling

As the well logs were of a relatively poor resolution (due to the extraction process from low quality scans of analogue originals) and no sedimentological data was available from the Cousland wells, a simple facies model was used. Units were classified as either sand or shale. Sand facies were subjected to property modelling for porosity and permeability and shale facies were designated as no-flow units.

3.12 Property modelling

The next stage is to model the porosity and permeability of the reservoir. Several approaches were attempted until a reasonable solution was found, details of which will be discussed later in this section. As the field had very little porosity and permeability data from cores and none from seismic data there is no way of

checking that the distribution of values is reasonable. However, the average porosity and permeability of the gas containing part of the reserovir can be checked later during the reservoir engineering study which uses PVT (pressure volume temperature) analysis combined with production data to determine the average porosity of the field and pressure testing data to find the average permeability of the field. Therefore these values will be adjusted as part of history matching and only need to be a reasonable approximation at this stage.

3.12.1 Porosity modelling

As there were only a small number of cores from the reservoir a porosity model based on other data needed to be established. Modeling of porosity consisted of two main methods with the second method used in the final model. The first was to establish a porosity depth trend from sonic calculated porosity data from the Stewart 1 well (approximately 3 km south form Cousland 1 on the Cousland-D'Arcy anticline) and create a porosity model based on that. The second was a simpler model in which porosity was calcualted from V_{shale} values assuming an inversely proportional relationship.

3.12.1.1 Porosity depth trend from Stewart 1 sonic log

After the Stewart 1 well log was digitized (see Appendix 4 for methods for digitizing images of well logs) the sonic and gamma ray logs were used to determine the porosity depth trend in the sands. There was no access to cores or core data for Stewart 1 in this study so this model could not be quality checked against real data other than the few core samples in the Cousland field.

3.12.1.2 Porosity from sonic log

To calculate porosity from the sonic log, the Wyllie time-average equation (Wyllie *et al.* 1956) was used

$$\phi = \frac{\Delta t - \Delta t_{ma}}{\Delta t_f - \Delta t_{ma}}$$

Where ϕ is the fractional porosity of the rock, Δt is the acoustic transit time (μsec/ft), Δt_{ma} is the acoustic transit time of rock matrix (μsec/ft), and Δt_f is the acoustic transit time of interstitial fluids (μsec/ft). As the sandstones were to be isolated using

the V_{shale} method described in the previous section, the acoustic transit time of the rock matrix used was that of consolidated sandstone, a value of 52.6 µsec/ft (Carmichael 1982), with any non-sand discounted from the analysis.

To find the acoustic transit time of interstitial fluids, water sample data was used to determine the salinity and a graph of transit time vs NaCl concentration was made using data from Carmichael (1982). The salinity of the water sample was then plotted on the graph and the transit time determined graphically. The only water

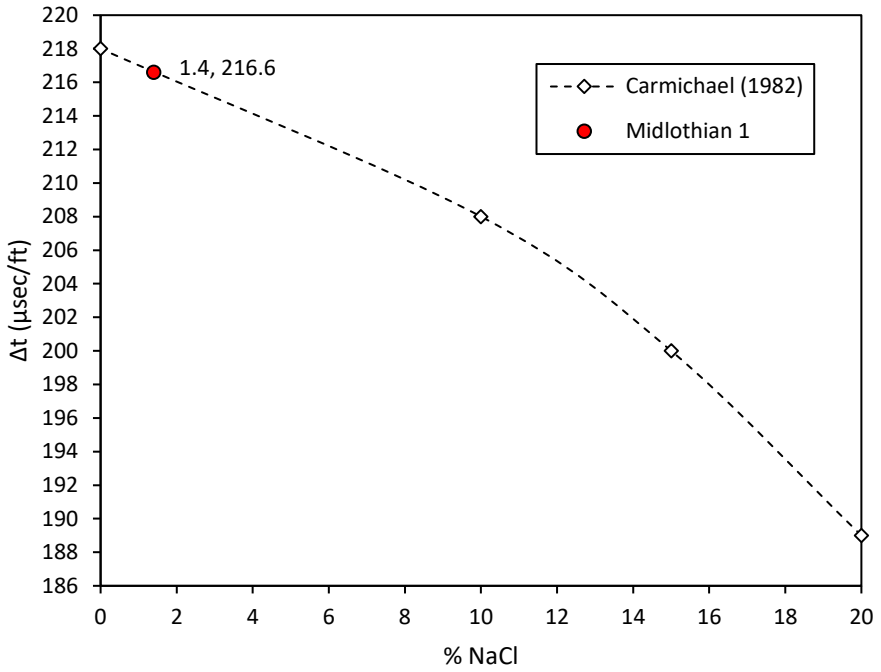

Figure 34: Transit times of interstitial fluids made using data from Carmichael (1982). This shows the NaCl concentration vs transit time with value from the Midlothian 1 well water sample plotted as a red filled circle. The Carmichael data is plotted as white diamonds with a dashed line.

sample data available was from the nearby (~100m) Midlothian 1 well which showed a salinity of 1.41% NaCl (Anglo-American Oil Company 1939).

The porosity was then calculated and plotted vs depth for the Stewart 1 well, with a V_{shale} cutoff of 0.4 to isolate the sands. The available core data for Cousland wells 1,2,4,5, and 6 were also plotted to quality check the data. Comparison of the sonic calculated porosity trend and the Cousland wells core data trend shows that the sonic porosity has higher values on average.

3.12.1.3 Porosity model method 1

As the sonic porosity and core porosity showed significant differences in the depth range of the reservoir interval, a new model using the depth trend from the core was used to determine porosity. This model was built in Excel (Microsoft Corporation 2016), and used the trend-line as a starting point before selecting a random number based on the inverse normal cumulative distribution of the core data, which resulted in a spread of values either side of the trendline as seen with the core data from the field (see Figure 35). This method was used as the distribution of core values was known and so the inverse normal cumulative distribution can be used to generate porosity values based on the probability of the distribution.

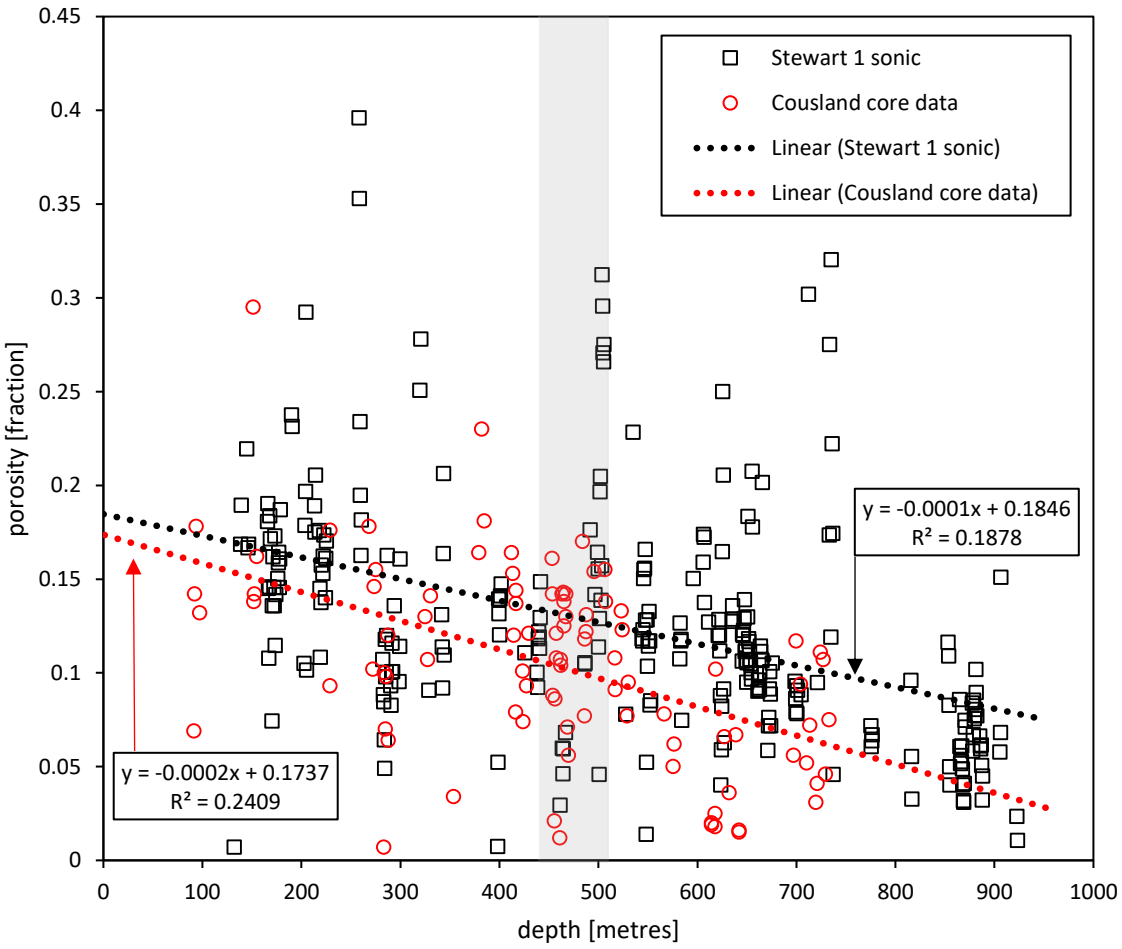

Figure 35: Stewart 1 sonic porosity (black squares and black dotted line) and Cousland field core porosity data (red circles and red dotted line) vs depth. Shaded interval is the depth of the 1582 reservoir interval.

However, some values ended up being negative and an increasingly large number of zero values were generated with increasing depth. To counter this, the minimum value of the core was added to all the generated values and if they still equalled or fell below zero a random number between the minimum and maximum was selected. However, a large number of zero values still occurred and so this model was discarded.

A porosity model was developed in Petrel (Schlumberger 2019) using a truncated normal distribution with the maximum, minimum, mean, and standard deviation obtained from the core data (Table 6 and Figure 36).

Table 6: parameters for Petrel porosity model

porosity		**permeability**	
n	93	n	131
Std. deviation	0.051529	Std. deviation	95.44396
Min	0.007	Min	0
Max	0.295	Max	451
Mean	0.104355	Mean	54.45878
Variance	0.002627	Variance	9040.01

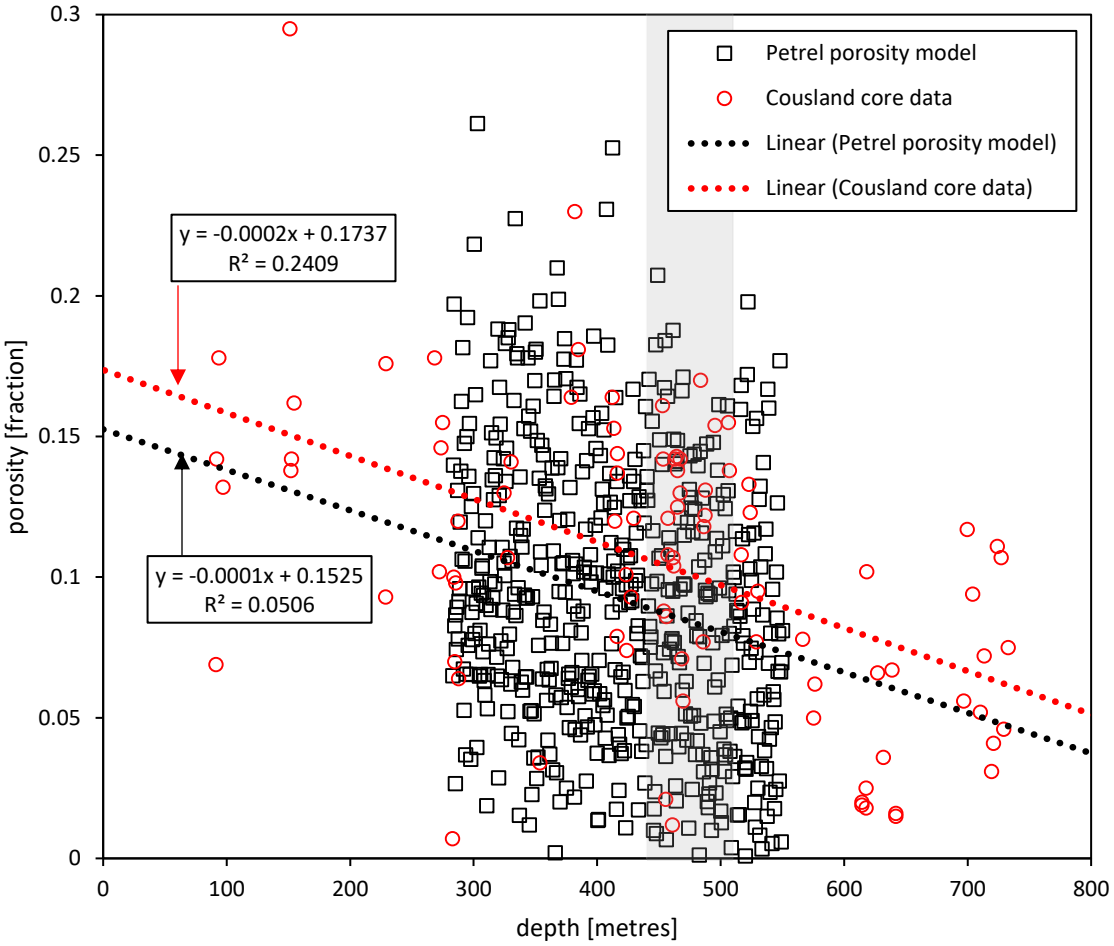

Figure 36: Petrel porosity model 1 (black squares and black dotted line) and Cousland field core porosity data (red circles and red dotted line) vs depth. Shaded interval is the depth of the 1582 reservoir interval.

This model under estimated porosity overall when compared to the core data. To remedy this, the model was adjusted by weighting it to V_{shale}. This gave higher porosities to cleaner sands. The effect was to increase the average porosity at depth which gave a better fit at the reservoir interval (Figure 37).

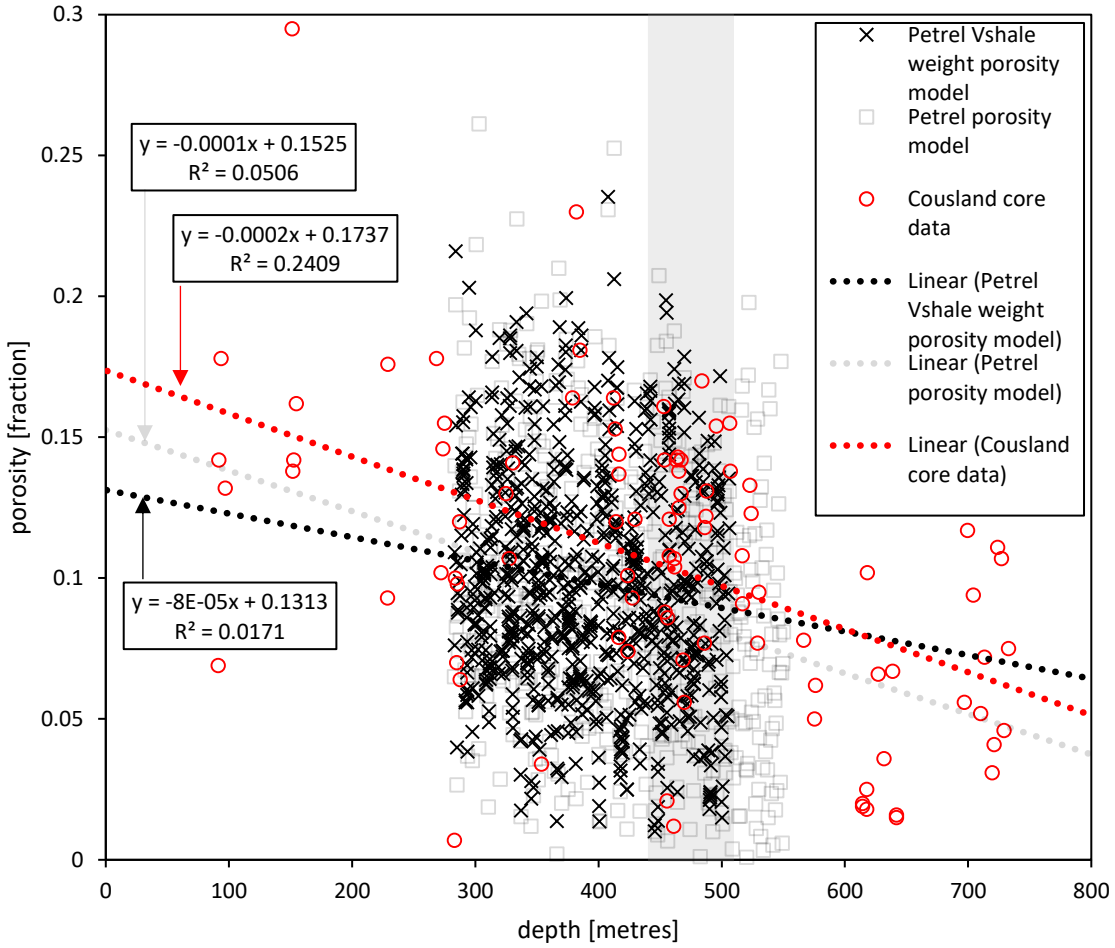

Figure 37: Petrel porosity model 2 (black crosses and black dotted line), Cousland field core porosity data (red circles and red dotted line), and Petrel porosity model 1 (grey squares and grey dotted line) vs depth. Shaded interval is the depth of the 1582 reservoir interval.

The main drawback with these models is that they do not capture a realistic porosity trend through individual sands. The random selection method leads to a relatively good fit in terms of porosity trends through the whole reservoir interval , but do not capture the expected porosity trends through individual sandbodies e.g. a channel sand. For this reason these porosity models were not used in the final geological model. A new model based on the V_{shale} value of sands was used instead.

3.12.1.4 Porosity model method 2

The V_{shale} values for depths where cores porosity data existed were plotted against core porosity. Of a total of 93 available core porosity data points, 43 had gamma ray logs at that depth and therefore were able to be plotted against V_{shale}. Four points were removed as outliers are not part of the trend (Figure 38).

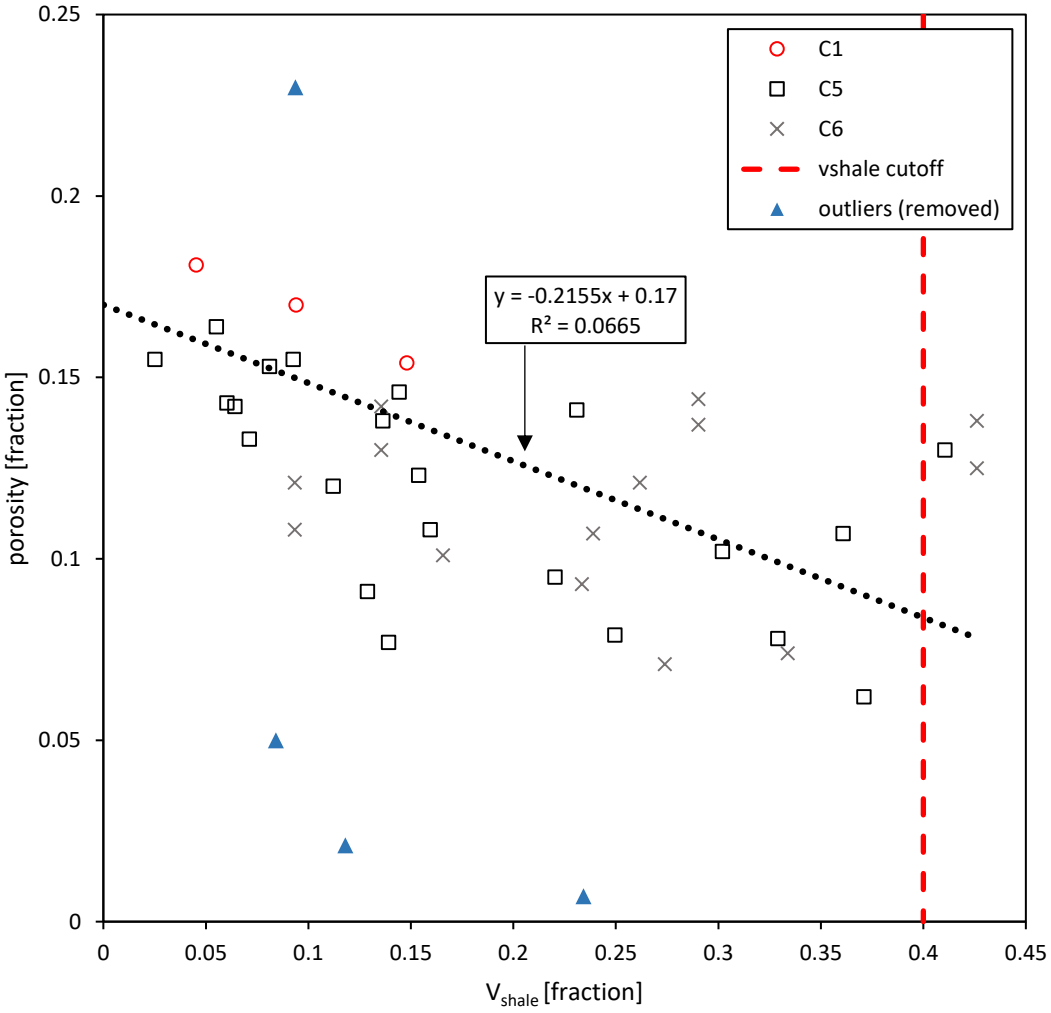

Figure 38: Core porosity for wells C1,C5, and C6 vs Vshale values. Outliers (blue triangles) were removed.

The model itself was linear and used the equation of the trendline through all the core data points where V_{shale} was less than 0.4. If V_{shale} was above 0.4 then a value of 0 was used (assumed no-flow unit). The linear model equation used is

$$\phi = -0.2155 \times V_{sh} + 0.17$$

This model gave reasonable values for porosity however there was significant spread in the data (Figure 39).

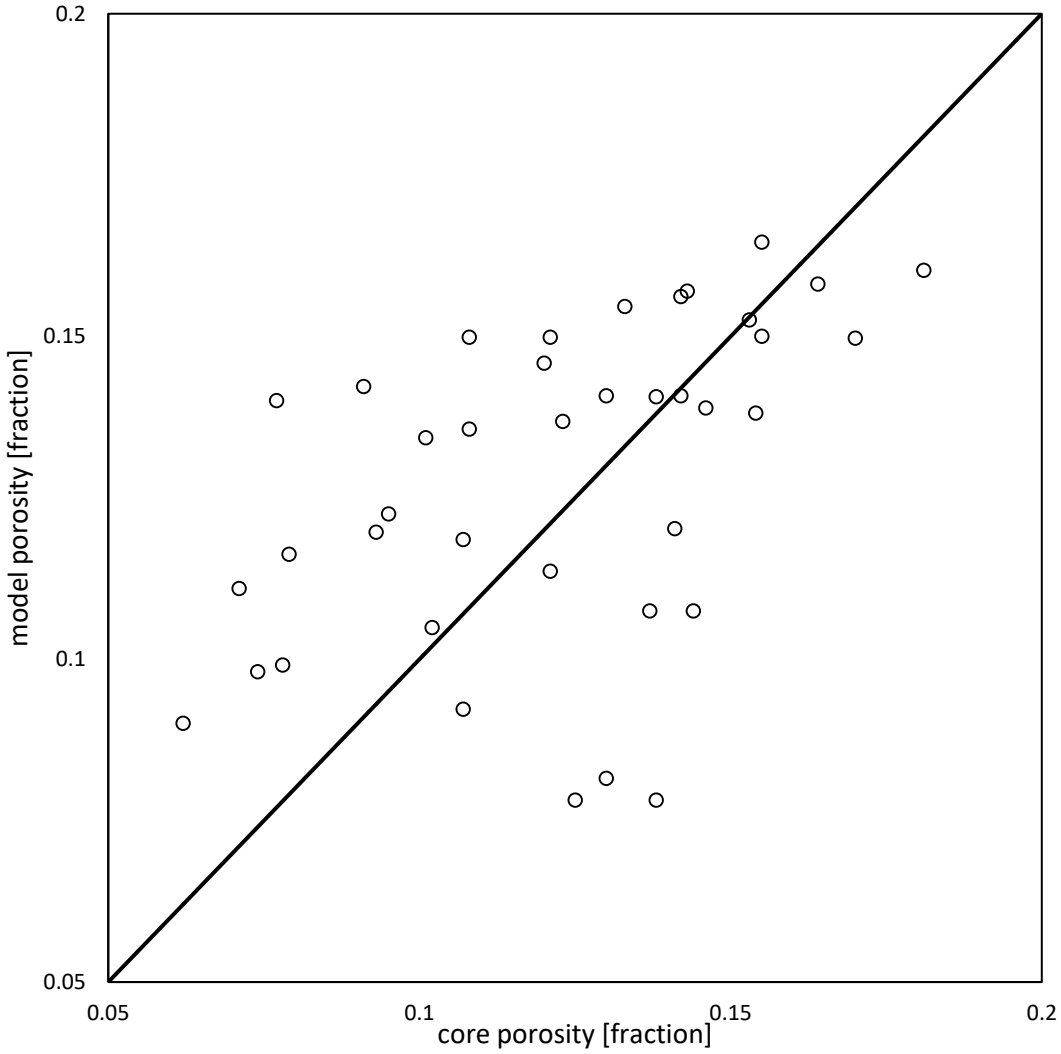

Figure 39: Model porosity vs core porosity. The bold line represents a perfect match between the two.

The cumulative frequency of porosity values was a better fit however (Figure 40). Given the low quality of the gamma ray (and therefore the V_{shale}) logs and the low number of core porosities available, it is not possible to greatly improve upon this model. As the core data is the best evidence of a trend within the Cousland field itself, this model was used in the final geological model. It is important to reiterate that these values will be adjusted anyway during history matching in the simulator.

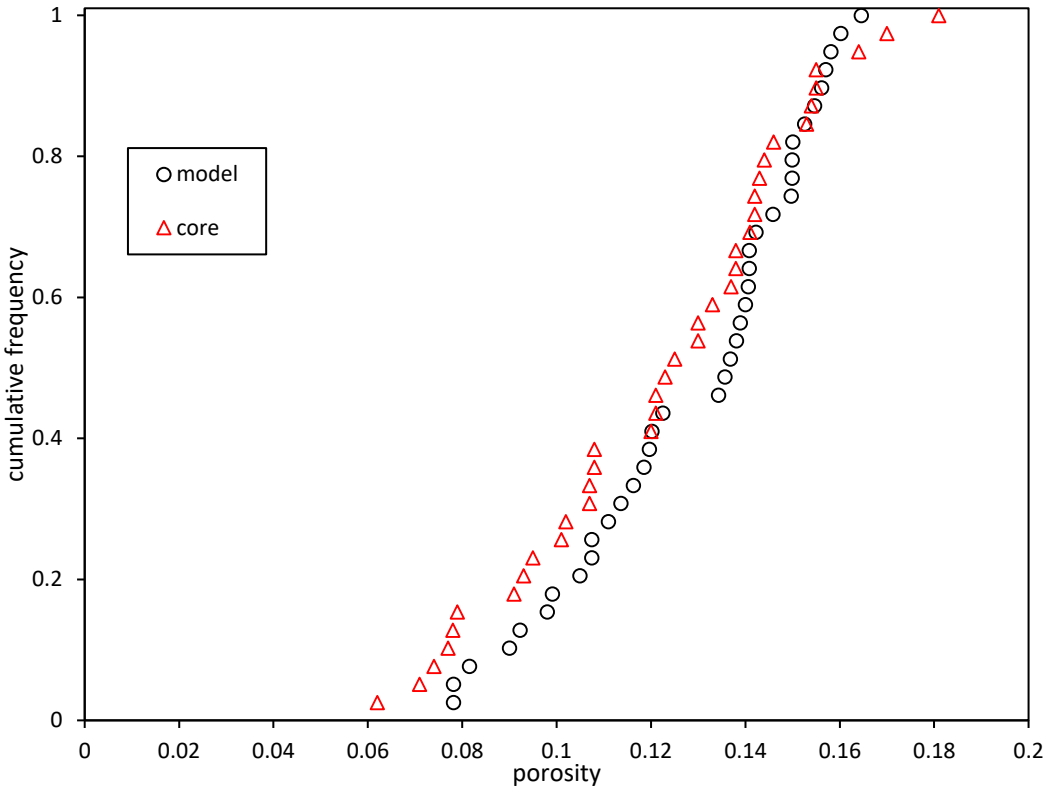

Figure 40: Cumulative frequency of porosity values for Cousland field cores and modelled porosity.

3.12.2 Permeability modelling

Initially a modification of porosity modelling method 1 was used to model permeability using all of the core poroperm data and the resulting trend line. However this approach of generating random values based on standard deviation from the mean was not generating reasonable values and tended to overestimate permeability when compared to the core data. A different approach, looking for porosity-permeability trends in individual wells and attempting to identify different facies using both stratigraphy and gamma ray log shapes was implemented.

3.12.2.1 Porosity-permeability trends in wells

Porosity-permeability data for cores are shown in Figure 41. One would generally expect permeability to be proportional to porosity and this is the case in wells C2, C4, and C5. However C1 shows inverse proportionality, which could be a result of there being so few data points or the presence of fractures. Well C5 showed the

strongest trend between porosity and permeability and was used as the permeability model.

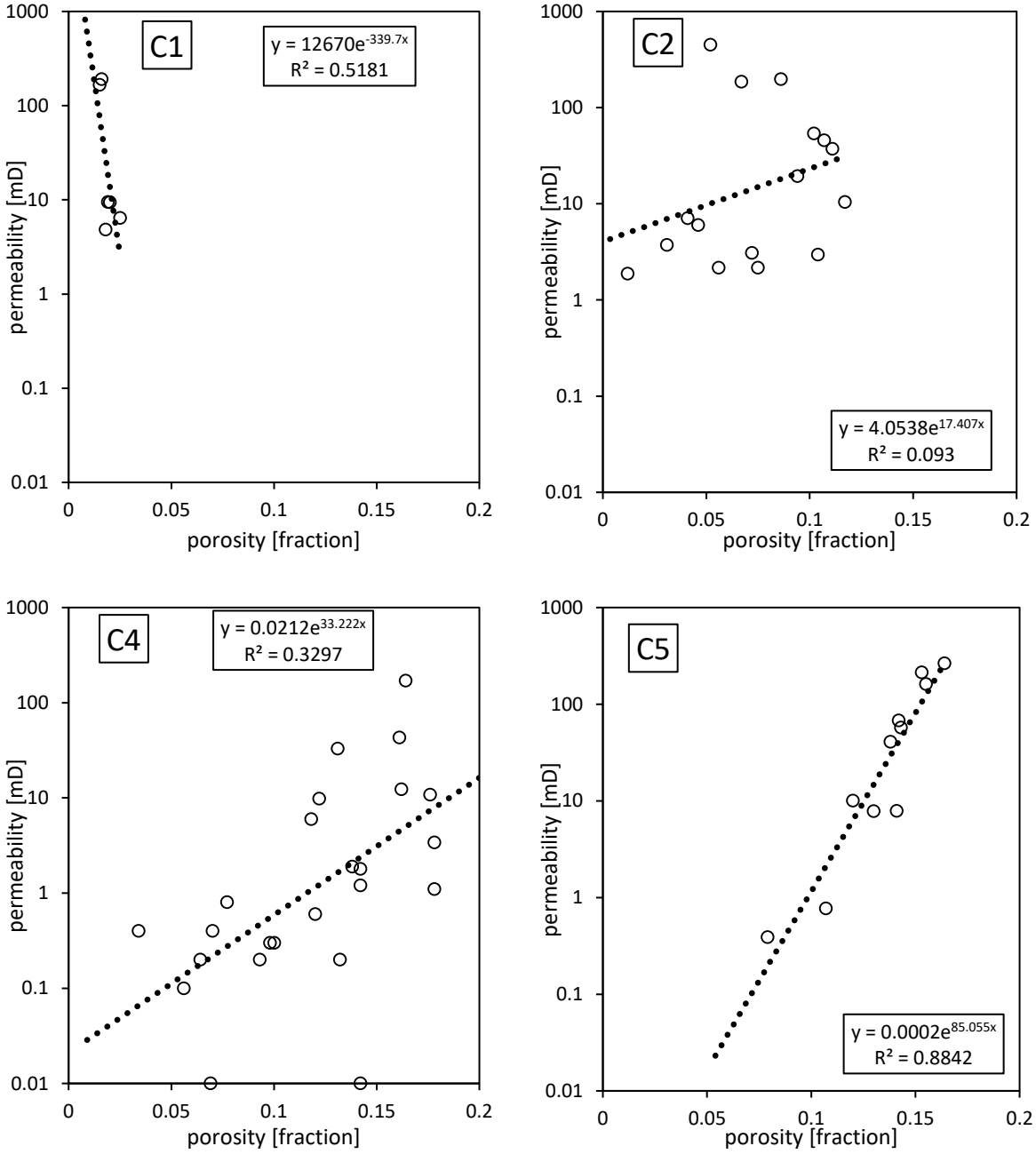

Figure 41: Permeability vs porosity plots for cores from wells C1, C2, C4, and C5 (all at the same scale to allow for comparison).

3.12.2.2 Permeability trends in different facies and sandstone horizons

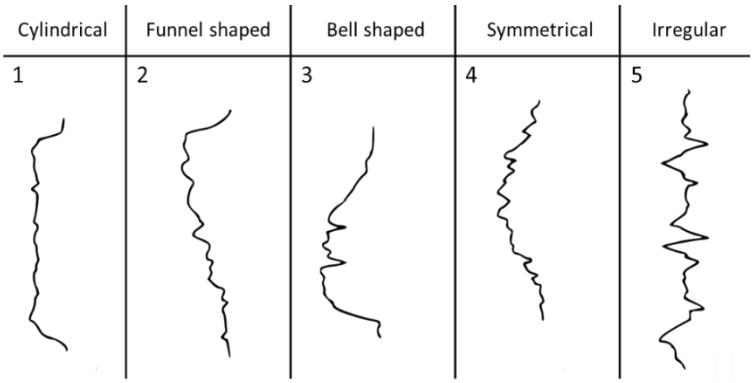

Figure 42: Idealized common gamma-ray log curve shapes. After Cant (1992). Number flags used in log shape interpretation.

Where core permeability and porosities existed at the same level as gamma ray logs, an interpretation of facies was attempted. Five different log shapes (Figure 42) were used as a basis for interpretation and labelled 1 to 5 (Figure 43). No discernible trends between facies and porosity/permeability were identified and no facies number 5 were identified. The same goes for trends in different sandstone horizons.

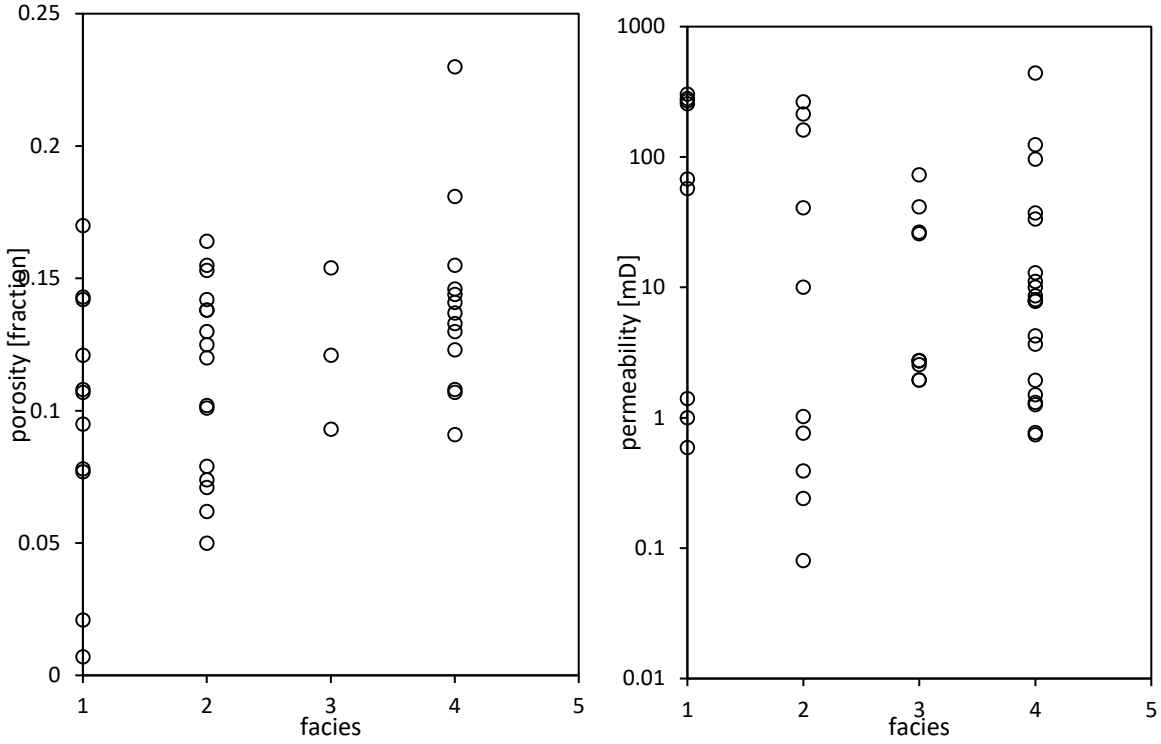

Figure 43: Porosity and permeability vs facies flags from log shape analysis (see Figure 42 for facies flag numbers). Facies number 5 is intentionally blank as none matching were found.

3.12.3 Property modelling between wells

The facies modelling included a north to south trend to represent the sandbodies (as per the section: Depositional Environment Interpretations), and due to a lack of data on facies only two were defined: either sand with a modelled permeability and porosity or shale which was treated as a no-flow unit. A truncated Gaussian simulation was used in Petrel to generate values within the field. These values will be adjusted later during history matching in the simulation study.

3.13 Gas-water contact

The gas water contact was added at 510.5 m TVD as per p.24 of production report 2 from C1 (Martin 1974). The GWC was placed here in the original report as well C2 which intercepts the reservoir interval down structure did not encounter gas and during testing it was determined that the water level was just below the reservoir interval in well C1 meaning that well C1 intercepted the gas containing part of the reservoir close to the edge of the gas bubble.

3.14 Volumetric sensitivity

Table 7: Variable used in volumetric sensitivity calculation. NtG is net:gross, φ is the porosity, Sw is the water saturation, Bg is the formation volume factor, rf is the recovery factor, and GWC TVDSS is the gas/water contact level.

variable	base	high	low
NtG [frac]	0.6	0.8	0.4
φ [frac]	0.1	0.2	0.1
Sw [frac]	0.5	0.6	0.2
Bg [frac]	0.021	0.015	0.025
rf [frac]	0.7	0.9	0.6
GWC TVDSS [m]	- 327.2	- 332.2	- 322.2

Volumetric calculations were carried out in Petrel (Schlumberger 2019) and a sensitivity analysis was performed. Variables for each case are shown in Table 7 **Error! Reference source not found.**and a tornado plot is shown in **Error! Reference source not found.**.

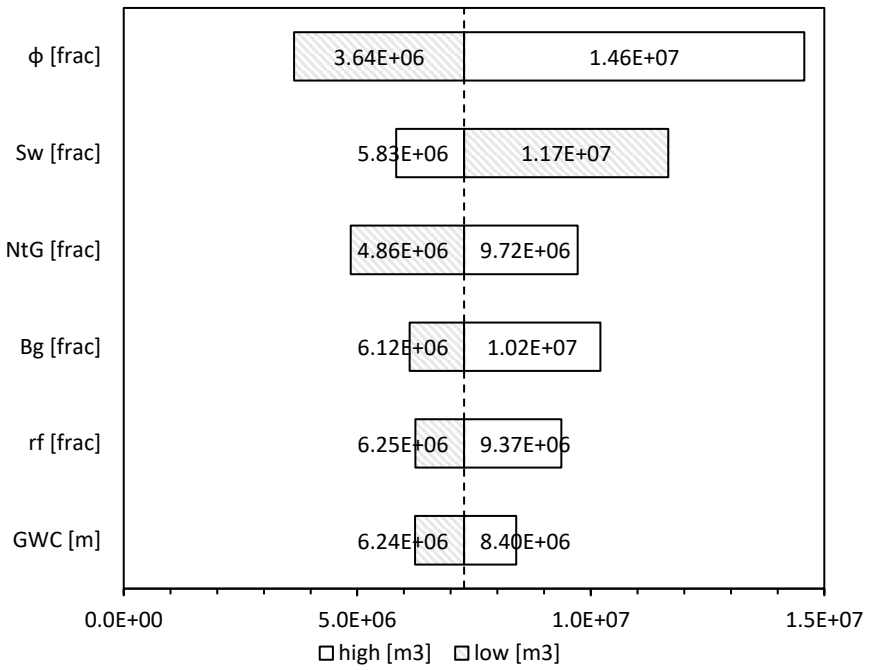

Figure 44: Tornado plot showing how high and low estimated variables change the amount of gas recoverable from the Cousland field from a base case scenario. φ is the porosity, Sw is the water saturation, Bg is the formation volume factor, NtG is net:gross, rf is the recovery factor, and GWC TVDSS is the gas/water contact level. Base case = 7.28E+06 m^3

3.15 Assumptions, limitations, and uncertainty

There is no pressure communication between different sand horizons and therefore gas cannot move between them. This is based on pressure test data from well C1 and a report on Cousland as a gas storage site (Illing 1961). Sand horizons are enclosed in impermeable shales and therefore act as closed reservoirs with no aquifer drive. There was no consensus at the time of development on whether or not the field showed aquifer drive and based on the pressure data and reports, it is not conclusive and so it is assumed that there is none. If there is any aquifer drive it is weak and only accounts for an increase of around 1 psi per year, therefore it will not significantly affect the results of a simulation study over the course of a 20 year simulation run. The edges of the model are no-flow boundaries, again based on pressure data and the report on gas storage at Cousland (Illing 1961). Non-sand layers within the model are treated as no-flow boundaries in order to reduce the number of cells in the model and keep the simulation time to a minimum. There is a lot of uncertainty in the geometry and thickness of sands in the Cousland field, however in terms of reservoir simulation, as it is a closed system and a relatively small reservoir, this should not have any significant effects on the overall results as the gas water boundary is not going to move significantly.

3.16 Geological model summary

The final geological model contains 716,380 cells and is shown visually in **Error! R eference source not found.**. With 119 × 86 × 70 cells in the I, J, and K directions respectively. The resolution is 25 metres in both the I and J directions and averages 0.23 metres in the K direction. This model was then exported to CMG builder ready for history matching and simulation.

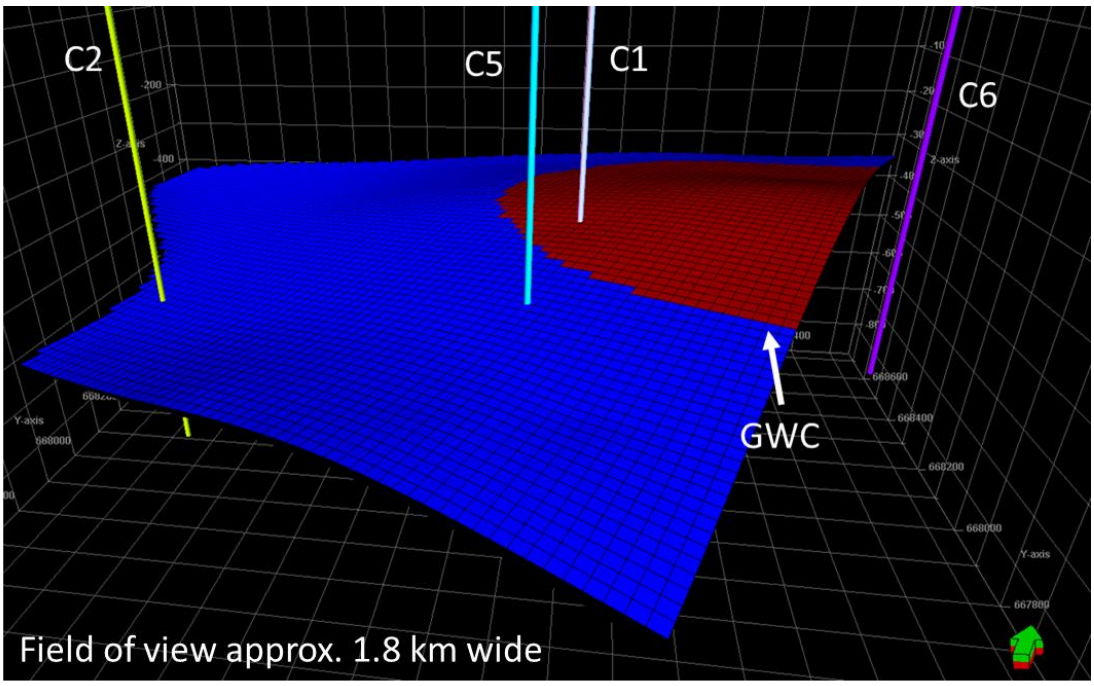

Figure 45: Final geological model showing wells C1, C2, C5, and C6. GWC = gas/water contact, gas zone is red, water zone is blue. Field of view is ~1.8 km. Background grid size is 100m x 100m x 100m, model grid size is 25m x 25m x ~0.2m.

Chapter 4 Compositional reservoir simulation of hydrogen storage in the Cousland gas field

4.1 Introduction and aims

This chapter presents the work behind simulating the injection and recovery of hydrogen into/from the geological model of the Cousland gas field built in the previous chapter. The structure of this chapter is as follows: first, it will describe the fluid model for both natural gas and hydrogen, reservoir engineering study, and history matching of the Cousland gas field. This will feed into the second section which will describe the design and justification for the hydrogen storage simulation schedule, and the results of the hydrogen storage schedule. Thirdly, there will be a discussion of the results. Equations are given in the original field units as per their references to avoid the need for conversion factors in the equations which make checking against the original references difficult, and also because the Cousland field data was given in field units. This allows for easy comparison with the orginal data without the need for conversion back and forth.

There are six key questions that the hydrogen storage simulation is designed to address:

1. How different will the composition of the produced gas be from the injected hydrogen i.e. what is the extent of mixing within the reservoir between the injected hydrogen and the remaining natural gas in the Cousland field?
2. Will the remaining natural gas in the Cousland field provide pressure support i.e. will it behave as cushion gas?
3. What is the hydrogen storage capacity (the average mass of hydrogen injected and produced per cycle) of the Cousland field?
4. Of the injected hydrogen, how much is recoverable i.e. what is the recovery factor?
5. What are the production and injection rates for the wells?
6. Does the pressure response have a significant effect on any of the aforementioned factors?

The reservoir engineering study was performed in Excel (Microsoft Corporation 2016) and the history matching and hydrogen storage simulation were performed in GEM compositional simulator (CMG 2019b).

The fluid model description is a key input for the reservoir engineering study, history matching, and hydrogen storage simulation. As a result it is discussed first and covers the gas composition, properties, and calculations done in WinProp Fluid Property Characterization Tool (CMG 2019c) to be utilised in GEM (CMG 2019b) in order to determine PVT properties and composition of gas mixtures both in the reservoir and produced from the well. This section also covers the fluid initialisation settings required by GEM prior to simulation runs and a description of how GEM calculates composition.

The reservoir engineering study begins with calculation of bottom hole pressure in the well from wellhead pressure. Next, production, flow test and backpressure test data from the Cousland field is analysed to determine the inflow performance and absolute open flow potential of the well, along with average reservoir properties and the extent of formation damage around the well (also known as skin). The results of this analysis are then used for history matching in which repeated simulations and adjustments to the reservoir model are performed until it closely reproduces the past behaviour of the real reservoir and well.

The hydrogen storage simulation schedule design is based on a real natural gas storage facility in the UK called Hatfield Moors (Ward *et al.* 2003). The similarities of this field to the the Cousland gas field along with the justification for basing the design of the hydrogen storage simulation schedule on data from Hatfield Moors will be discussed and the schedule will be defined.

After this the three different pressure scenarios for the hydrogen storage simulation will be presented. There will be three different pressure scenarios in order to perform a sensitivity analysis on the effect of pressure on the results. The results of the hydrogen storage simulation will then be presented and discussed in detail.

4.2 PVT modelling of Cousland natural gas and hydrogen using WinProp and GEM

To determine the phase behaviour of the gas and water in the reservoir and at surface conditions, pressure-volume-temperature (PVT) data for reservoir fluids must be characterised. This data can then be used to determine the following properties of a mixture with a known composition: number of phases, proportions of each phase, phase compositions, and phase properties (molecular weight, density, and viscosity).

The calculation of phase behaviour is made in one of the following two ways: a black-oil approach based on a simple interpolation of PVT properties as a function of pressure or a compositional approach which is based on a thermodynamically-consistent model such as a cubic equation of state (EOS). This study takes the compositional approach using the Peng-Robinson EOS (Peng and Robinson 1976) (which is suitable for both hydrogen, natural gas, and mixtures of the two (Qian *et al.* 2013)):

$$P = \frac{RT}{V_m - b} - \frac{a\alpha}{V_m^2 + 2bV_m - b^2}$$
$$a = \frac{0.45724R^2T_c^2}{P_c}$$
$$b = \frac{0.07780RT_c}{P_c}$$
$$\alpha = \left(1 + (0.37464 + 1.54226\omega - 0.26992\omega^2)(1 - T_r^{0.5})\right)^2$$
$$T_r = \frac{T}{T_c}$$

Where ω is the acentric factor for the species, P_c is the critical pressure, T_c is the critical temperature, V_m is the molar volume, and R is the ideal gas constant (8.314413J/mol-K).

PVT calculations were made in WinProp (CMG 2019c) – a fluid characterization tool that is used to perform calculations to determine PVT properties of pure and mixed composition fluids. GEM compositional simulator is a multiphase darcy flow simulator which takes the PVT properties generated in WinProp and fits these to the Peng-Robinson equation of state (EOS) (Peng and Robinson 1976) as a mixture of components. GEM then uses the fitted EOS to calculate the movement of phases and components in the reservoir model. The flow equations are discretized using the adaptive-implicit method in a variation of the approach of Collins et al. (Collins *et al.*

1992). A full description of the theoretical outline is provided in Appendix 6 - Theoretical outline of GEM compositional simulator flow equations.

4.3 Number of phases

At a given temperature and pressure, components are distributed between the solid, liquid, and gas phases in the reservoir. Each phase is a homogenous portion of a system that is bounded by a surface and is physically seperable from other phases. The Cousland field contains water and natural gas and so we would expect two phases: liquid and gas. At the temperatures and pressures encountered in the Cousland field, there is unlikely to be transferring of components between the two phases in the simulator given the gas composition. It is assumed that there is no mobile oil in the Cousland field as none was produced during testing/production and so there is no oil input in the simulation.

4.4 Proportions of each phase

Where two phases exist within a cell, a two-phase flash calculation determines the molar amounts of each phase and the phase compositions within a cell. The calculation uses the overall moles and molar composition to do this and WinProp requires the solution of two equations: an equilibrium equation and a material balance equation. The equilibrium equation is solved using the Quasi-Newton Successive Substitution (QNSS) method (Nghiem and Heidemann 1982) and the material balance is solved using a method for quick single-phase detection (Nghiem *et al.* 1983).

4.5 Components

4.5.1 Composition

Only one gas sample analysis was available from the production reservoir (referred to as the 1582 ft sand) in the Cousland field.Table 8 shows gas component analysis from the Cousland 1 well for various sandstone horizons with the reservoir interval (1582-1632 ft) highlighted and underlined. This gas was greater than 95% methane by volume, with ethane and nitrogen making up the remainder. The hydrogen composition for the storage phase of the simulation was assumed to be *100% hydrogen.*

Table 8: Gas samples composition by depth interval for the Cousland-1 well. C1 - C4 are hydrocarbon fractions given in volume%. N_2 is nitrogen fraction given in volume%. The highlighted and underlined row is the reservoir interval and gas composition used in this study.

Interval (MD) [feet]	C1	C2	C3	C4	N_2
1188-1279	95.85	2.30	1.24	0.60	-
1248-1279	90.75	3.10	3.50	2.65	-
1582-1632	95.85	2.60	-	-	1.55
1720-1800	94.00	2.90	0.60	-	2.59
2094-2122	87.90	3.85	1.05	0.65	6.53

4.5.2 Properties

WinProp requires certain properties to be given values in order to initialise the PVT calculations. These are already pre-filled in WinProp for all the components as they are common in oil and gas reservoirs. However hydrogen did not have values pre-filled and so values were taken from the literature. Table 9 shows the property values for all the components in the simulation and

Table 10: Definitions of terms from Table 9, values used for hydrogen and references for hydrogen values. Units are given in brackets where variables have units.

shows the properties values for hydrogen, along with a definition of the headings used in Table 9 and references for the hydrogen values taken from the literature. Not all properties are essential to run the simulation, those that are left blank for hydrogen are non-essential.

Table 9: Properties and input values used for WinProp PVT calculations. All values except those for hydrogen are pre-programmed into WinProp. For definitions of variables and references for hydrogen values see

Table 10: Definitions of terms from Table 9, values used for hydrogen and references for hydrogen values. Units are given in brackets where variables have units.

. Units are given in brackets where variables have units.

Component	**HC**	**P_c(atm)**	**T_c (K)**	**Acentric fact.**	**Mol. weight**	**Vol. Shift**	**V Shift Coef1**
H_2	0	12.759	32.976	-0.216	2.01594	Internal	-
N_2	0	33.5	126.2	0.04	28.013	-0.1927	0
CH_4	1	45.4	190.6	0.008	16.043	-0.1595	0
C_2H_6	1	48.2	305.4	0.098	30.07	-0.1134	0
	V Shift Tref (K)	**Z – Rackett**	**V_c (l/mol)**	**V_c (viscosity)**	**Omega A**	**Omega B**	**Beta Factor**
H_2	288.71	1.00E-16	0.0642	0.0642	-	-	1
N_2	288.71	0.2905	0.0895	0.0895	0.457235529	0.077796074	1
CH_4	288.71	0.2876	0.099	0.099	0.457235529	0.077796074	1
C_2H_6	288.71	0.2789	0.148	0.148	0.457235529	0.077796074	1
	SG	**T_b (K)**	**Parachor**	**Ref. Henry (atm)**	**V inf. (l/mol)**	**P ref. (atm)**	**Enth. Coeff. A**
H_2	0.0696	20.25	-	Default	-	-	-
N_2	0.809	77.4	41	Default	0	0	-0.65665
CH_4	0.3	111.7	77	Default	0	0	-2.83857
C_2H_6	0.356	184.5	108	Default	0	0	-0.01422
	Enth. Coeff. B	**Enth. Coeff. C**	**Enth. Coeff. D**	**Enth. Coeff. E**	**Enth. Coeff. F**	**Enth. Coeff. G**	**Heating Value (Btu/gmol)**
H_2	-	-	-	-	-	-	-
N_2	0.2541	-1.66E-05	1.53E-08	-3.10E-12	1.52E-16	0.048679	0
CH_4	0.53829	-0.000211409	3.39E-07	-1.16E-10	1.39E-14	-0.602869	844.2900105
C_2H_6	0.26461	-2.46E-05	2.91E-07	-1.28E-10	1.81E-14	0.083346	1478.460015

Table 10: Definitions of terms from Table 9, values used for hydrogen and references for hydrogen values. Units are given in brackets where variables have units.

Heading	**Parameter or property**	**Value [H_2]**	**Reference**
Component	Component name	H2	
HC	Hydrocarbon flag (=1 for hydrocarbons)	0	
Pc(atm)	Critical pressure in atm	12.759	(McCarty *et al.* 1981)
Tc (K)	Critical temperature in Kelvin	32.976	(McCarty *et al.* 1981)
Acentric fact.	Acentric factor	-0.216	(Poling 2001)
Mol. weight	Molecular weight	2.01594	(McCarty *et al.* 1981)
Vol. Shift	Volume shift (dimensionless)		
V Shift Coef1	Volume shift temperature coefficient (1/deg F or 1/deg C)		
V Shift Tref	Volume shift reference temperature (K)		
Z - Rackett	Rackett's compressibility factor		
Vc (l/mol)	Critical volume in l/mol	0.0642	(Poling 2001)
Vc (viscosity)	Critical volume in l/mol for viscosity calculations		
Omega A	Ωa EOS parameter		
Omega B	Ωb EOS parameter		
SG	Specific gravity (air = 1)	0.0696	(Energy Technology Training Center 2001)
Tb (K)	Normal boiling point in Kelvin	20.25	
Parachor	Parachor IFT parameter	34.141	eq. (58) in (Williams 2003)
Ref. Henry (atm)	Reference Henry's constant in atm		
V inf. (l/mol)	Molar volume at infinite dilution		
P ref. (atm)	Reference pressure for Henry's constant in atm		
Enth. Coeff. A	Ideal gas enthalpy coefficient A		
Enth. Coeff. B	Ideal gas enthalpy coefficient B		
Enth. Coeff. C	Ideal gas enthalpy coefficient C		
Enth. Coeff. D	Ideal gas enthalpy coefficient D		
Enth. Coeff. E	Ideal gas enthalpy coefficient E		
Enth. Coeff. F	Ideal gas enthalpy coefficient F		
Enth. Coeff. G	Ideal gas enthalpy coefficient G		
Heating Value (Btu/gmol)	Heating value		

4.6 Viscosity

The viscosity of the gases is calculated in WinProp and passed to GEM prior to simulation. As this software is primarily designed to handle mixtures of hydrocarbons, some adjustment of the viscosity equations was required when calculating hydrogen viscosities in WinProp. This is discussed below.

Equation (1) shows the Jossi, Stiel and Thodos (JST) correlation (Jossi *et al.* 1962) described in Reid et al. (Reid *et al.* 1977) and was selected in WinProp to calculate the viscosity of different fluid compositions in the fluid model. This correlation was developed using experimental data on 11 pure substances including nitrogen, methane, and ethane, all components of Cousland natural gas making it particularly suitable for purpose and so it was used for the natural gas components in WinProp:

(1) $$[(\mu - \mu^0)\xi + 10^{-4}]^{1/4} = 0.10230 + 0.023364\rho_R + 0.058533{\rho_R}^2 - 0.040758{\rho_R}^3 + 0.0093324{\rho_R}^4$$

where μ is viscosity in centipoise, μ^0 is viscosity at normal pressures (0.1 to 5 atm) in centipoise, ξ is the viscosity parameter, and ρ_R is reduced density (density/density at the critical point). However, as mentioned in the Jossi, Stiel, Thodos paper (Jossi *et al.* 1962), hydrogen deviates from this correlation significantly and therefore another correlation (equation (2)) is given by Jossi, Stiel and Thodos (Jossi *et al.* 1962) to describe its behaviour and was used in WinProp to calculate hydrogen viscosity:

(2) $$[(\mu - \mu^0)\xi + 10^{-4}]^{1/4} = 0.10616 - 0.042426\rho_R + 0.17553{\rho_R}^2 - 0.12295{\rho_R}^3 + 0.028149{\rho_R}^4$$

WinProp allows for the adjustment of the JST correlation to the one suitable for hydrogen, however at low pressures (below 5 atm (Jossi *et al.* 1962)) it reverts to one of two other options. There are two options for calculating the low-pressure mixture viscosity. The first option is to calculate low pressure component viscosities according to a formula by Yoon and Thodos then calculate the mixture viscosity by following the mixing rule of Herning and Zipperer (both described in (Reid *et al.* 1977)). The second option is to calculate the low pressure mixture viscosity directly through a correlation based on the mixture's molecular weight by Lee and Eakin (Lee and Eakin 1964). However, as this correlation only applies at pressures below 5 atm, the correlation is irrelevant for the purposes of the Cousland reservoir itself which is at higher pressures, however it may have a small effect in the wellbore if the pressures drop below the threshold.

4.7 Initialisation

GEM requires the separator and initial conditions to be set prior to simulation runs. The separator is the final stage in the model that brings the produced fluids to standard conditions in order to measure the volumes of each component. The separator is a single stage at STP of the separator are 101.3 kPa (14.7 psi) and 15.6 °C (60 °F), and it has three outputs: oil, gas, or water. The initial conditions are simply the saturations of fluids above and below the gas/water contact in the model.

The water saturation below the gas/water contact (GWC) is 100% and the gas saturation above the GWC is 70%. The gas saturation is based on the relative permeability curves used for the model (see section 4.16)

4.8 Reservoir engineering study of Cousland testing and production data

The reservoir engineering study in this section is performed in order to determine some key parameters and characteristics of the Cousland gas field. These parameters include the inflow performance of the well which determines flow rates at different bottom hole pressures and the theoretical maximum flow rates from the well; a material balance to determine the gas originally in place (GOIP); the damage around the wellbore which can affect the flow rate (also know as skin factor); the permeability; and the initial reservoir pressure. All of these will then be used to match the performance of the model used in the simulation with the original pressure and flow rate data from the Cousland field.

The majority of the methods used in this section are described in great detail in Lee & Wattenbarger (1995) (Lee and Wattenbarger 1995) and the Excel models used are based on those developed by Brandon Tolbert (Tolbert 2021).

4.9 Test and production data quality and reliability

The quality of the data was discussed in the data section of the Geological model of Cousland chapter (see chapter 3.4), however it is worth emphasising that there are two main things to bear in mind about the available data. Firstly there was no downhole pressure measurement, all pressure was measured at wellhead. Secondly, during testing readings were not digitally recorded, they were read by eye from a round pressure gauge with a needle by a worker who then wrote the reading down by hand on paper. This paper was then scanned after being stored in an archive for several decades and added to a pdf file on the UKOGL website (UK Onshore Geophysical Library 2020). These two factors therefore lead to a multitude of ways in which inaccuracies and errors can creep into the data. Namely, as the downhole pressure was not measured, a calculation of bottom hole pressure (BHP) from wellhead pressure (WHP) must be performed which itself relies on the composition analysis of a single sample of Cousland gas and so the accuracy cannot be guaranteed. The other issue is that in some cases the handwriting of the worker who recorded the wellhead pressure was hard to read, there are also cases where they may have written the reading down wrong (some of these tests lasted days and the worker would have been sat in a shed in a field in December throughout the whole night), or missed a reading for some reason (shift changes, falling asleep etc.). Finally there is the accuracy and precision of the pressure

gauges of the 1950s to consider. All of these factors mean that the test data must be treated as less reliable than modern data.

4.10 Bottom hole pressure calculation

In order to analyse pressure test results, bottom hole pressure must be calculated from the well head pressure. This was done using equation (3) (from (Lyons *et al.* 2012)) to determine the bottom hole pressure of a dry gas well:

$$P_{bh} = P_{wh} \times e^{\frac{\left(\frac{S_g}{R}\right)H}{T_{av}}} \quad (3)$$

Where P_{bh} is the bottom hole pressure (psia), P_{wh} is the well head pressure (psia), e is the mathematical constant Euler's number, S_g is the specific gravity of the gas, H is the true vertical depth of the well (in feet), T_{av} is the average temperature in Rankin, and R is the engineering gas constant at API standard conditions (53.36 ft-lb/lb-°R). The correlation can be seen graphically in Figure 46.

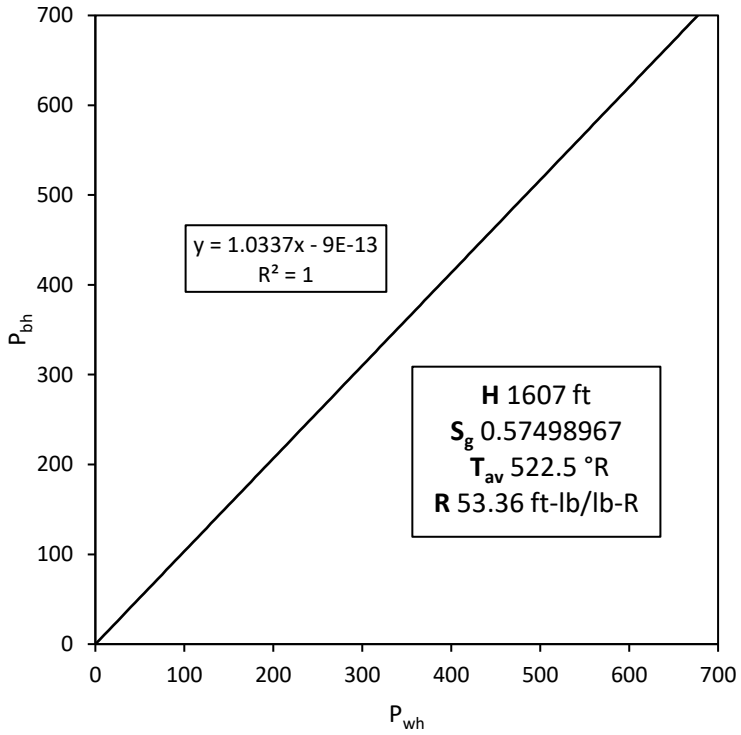

Figure 46: Bottom hole pressure vs well head pressure. This graph shows the correlation between the two using equation (3). The values used are shown in the inset box

4.11 Deliverability testing

During deliverability testing, measures of productivity can be calculated which indicate the potential productivity of a well. In the case of Cousland, a backpressure

test was performed on Cousland 1 on the producing reservoir between the 11th and 12th of November 1956. A backpressure test is conducted by flowing the well at different rates, allowing pressure stabilisation at each rate as the radius of investigation (the area of the reservoir the well is flowing from) reaches the outer edge of the drainage area. These tests are used to calculate a plot of flow rate vs bottom hole pressure, known as the inflow performance relation (IPR) of the well, along with the absolute open flow potential (AOFP) which is a theoretical maximum flow rate for a well when the bottom hole pressure is zero. Both of these measures will be calculated using real data and then used to benchmark the well and reservoir models during history matching in the simulator.

4.11.1 Gas Inflow Performance

The absolute open flow potential (AOFP) is a theoretical maximum flow rate at the sandface against zero backpressure i.e. if the bottom hole pressure is at zero, the AOFP is the maximum theoretical flow rate. The method used to calculate it is described in detail in (Lyons *et al.* 2016). In practice the AOFP is not achievable but is a useful measure for setting maximum allowable flow rates and for regulatory purposes.

Equation (4) (known as the back-pressure equation) was developed by Rawlins and Schellhardt (Rawlins and Schellhardt 1936) is used to relate gas flow rate and flowing bottom hole pressure and can be used to calculate the AOFP and IPR curves:

$$q = C\left(P_r{}^2 - P_{wf}^2\right)^n \tag{4}$$

Where q is the gas flow rate in Mscf/d, C is the stabilised performance coefficient (a dimensionless constant), P_r is the shut-in reservoir pressure in psia, P_{wf} is the flowing bottom hole pressure in psia, n is the numerical exponent (a dimensionless constant).

To calculate n, two arbitrary flow rates (q) are chosen that are separated by one cycle. n is then calculated:

$$n = \frac{1}{slope} = \frac{log\ q_2 - log\ q_1}{\log\left(P_r^2 - P_{wf}^2\right)_2 - \log\left(P_r^2 - P_{wf}^2\right)_1} \tag{5}$$

Next, C is calculated using the backpressure test data:

(6) $$C = \frac{q}{\left(P_r{}^2 - P_{wf}^2\right)^n}$$

And finally the AOFP can be calculated using equation (4) with a value for P_{wf} (bottom hole flowing pressure) of 0. The AOFP for Cousland 1 is 4.6 MMscf/d (million standard cubic feet per day) or 0.13 × 10^6 m^3 per day. Calculated flow rates and AOFP from the Cousland 1 backpressure test is shown in Figure 47.

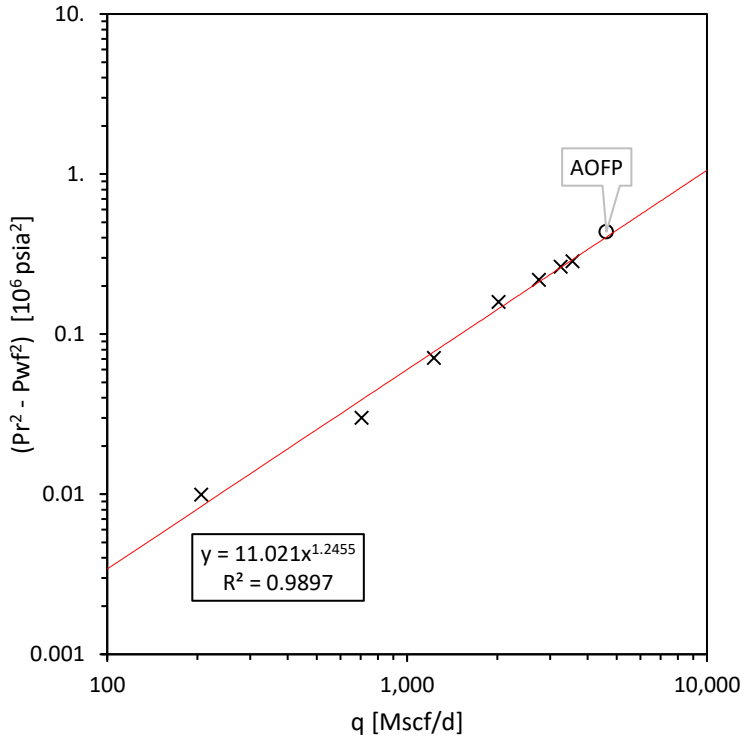

Figure 47: Flow rates from backpressure test data (black crosses), trendline (red line) and AOFP (black circle). AOFP is caluclated from Cousland 1 backpressure test data. The AOFP is 4.6 MMscf/d (Mscf/d = thousand standard cubic feet per day)

Taking arbitrary values of p_{wf} allows the calculation of corresponding flow rates (q) using equation (4) and the construction of an inflow performance relation (IPR) curve. This curve shows the flow rate at a given bottom hole flowing pressure for a given reservoir pressure. As the reservoir is produced, the pressure will decrease and the curve will move down and to the left of the graph. Along with reservoir pressure, the IPR curve is controlled by rock and fluid properties, near-wellbore effects such as skin and heterogeneities in the well's drainage area (Lee and Wattenbarger 1995). Figure 48 shows the calculated IPR curve for Cousland 1 along with the original backpressure test data points.

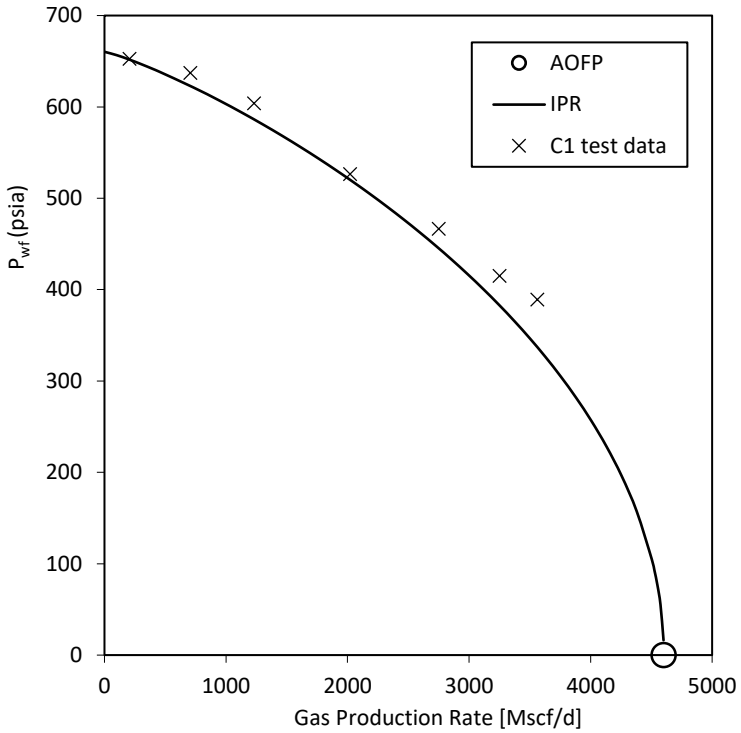

Figure 48: Inflow performace relation curve for Cousland 1 showing the calculated IPR curve (black line) and AOFP (white circle), along with the backpressure test data (black crosses).

This initial IPR curve calculated prior to the production phase of the Cousland gas field will be an essential part of history matching the simulator to real data as near-wellbore damage (skin) and permeability will affect it. Combined with other techniques which will be discussed later, this allows constraining of the model and increases the confidence that the behaviour of the model in the simulator is a close approximation of reality. The IPR curve will also be important in the next chapter on investigating the effects of hydrogen in the wellbore vs natural gas.

4.11.2 Material balance

Determining the GOIP (gas originally in place) is key to history matching the pore volume of the geological model during the simulation study. The pressure testing data (discussed below) suggests that the producing reservoir sand at Cousland is fully enclosed in shales and behaves as a volumetric reservoir (i.e. there is no change in the hydrocarbon pore volume during pressure depletion and therefore the gas/water contact level does not move) which means that a P/Z (pressure over compressibility) plot can be used to determine the GOIP (see chapter 10 of (Lee and Wattenbarger 1995)).

The pressure data between original testing in the 1930s and 1940s and testing and production in the 1950s and 1960s is used to produce the plot of P/Z vs gas produced in Figure 49. The plot is made up of four data points considered to be reliable from between 1939 and 1967, however two of the points (the second and third) overlap and are hard to distinguish as the gas produced during tests in the time between them was small in comparison to the amount produced during commercial production. The first point is the initial reservoir pressure prior to any testing, the second is taken from 1947 after the original series of flow tests in 1939, the third is taken after the flow tests performed in 1956 and the final point is taken over one year after production from the reservoir ceased. Choosing these points spread out in time and allowing enough time (months to years) after flow tests and production should allow the reservoir pressure to reach equilibrium and allow time for any aquifer drive influence to make itself known. The trend does not deviate significantly and so it can be assumed with confidence that the reservoir is volumetric, as any aquifer drive would cause the plot would curve upwards over time. The P/Z plot allows a GOIP (gas originally in place) to be calculated using the intercept with the gas produced axis i.e. where P/Z drops to zero. The plot shows that the GOIP is 0.87 Bcf (billion cubic feet) or 24.7 million m^3.

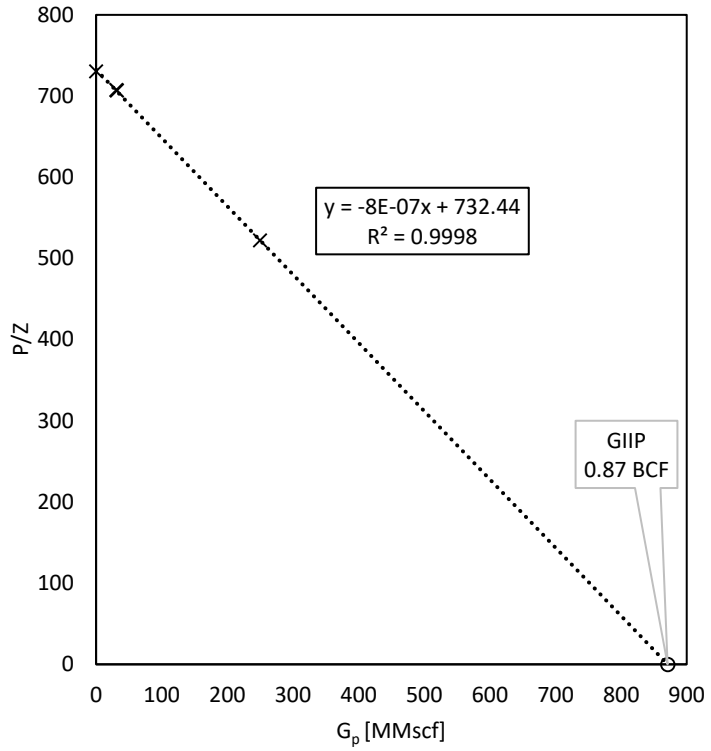

Figure 49: P/Z vs gas produced plot. Crosses show data points, circle with annotation shows GOIP calculation, dashed line is the trend. (MMscf = million standard cubic feet). Two of the four points overlap at the scale of this graph (at P/Z = 707) as the amount of gas produced in the time between them is small compared to the total. The linear nature of the plot indicates that there is no significant aquifer drive and the reservoir is behaving volumetrically.

4.12 1956 buildup test

At the time of the study, only one set of reliable buildup tests data was available for Cousland. That is the buildup after the deliverability testing in 1956 used in the previous section. The analysis used is a semi-log plot of pseudopressure vs Horner time (defined below in section 4.12.2) from which the following can be determined: average reservoir pressure, skin factor, and permeability. All of these variables will be important during history matching of the Cousland gas field model to pressure and production data.

4.12.1 Pseudopressure

Pseudopressure is a mathematical pressure function introduced by Al-Hussainy et al (Al-Hussainy *et al.* 1966b) which accounts for changes in compressibility and viscosity of a gas with pressure and allows for the solving of flow equations without the limiting assumption of gas properties remaining constant with pressure. It is given by equation (7):

(7) $\psi_p = 2\int_{p0}^{p} \frac{p}{\mu Z} \Delta p$

Where ψ_p is pseudopressure (units psia^2/cp), p is the pressure, μ is the viscosity at p, Z is the compressibility at p, and $p0$ is an arbitrary base pressure. A full description of how to calculate pseudopressure using the trapezoidal method is given in the appendix of (Al-Hussainy and Ramey 1967).

4.12.2 Horner Time

Horner time is a time function for analysing buildup test data. When plotted on a semi-log (radial) plot against shut-in pressure, radial flow buildup data becomes a straight line. The slope can then be taken and used to determine permeability and skin. The Horner time function is defined by equation (8):

(8) $\frac{t_p + \Delta t}{\Delta t}$

Where t_p is the time produced (hours between starting the flow test and shutting in the well), and Δt is the time since shut-in (hours).

4.12.3 Semi-log plot

The semi-log plot of pseudopressure vs Horner time is show in Figure 50. This figure has been interpreted to show two key areas which are essential to the analysis. The four points aligned at a shallow angle to the left of the plot show characteristic radial flow and the steeper aligned points to the right are characteristic of wellbore storage effects.

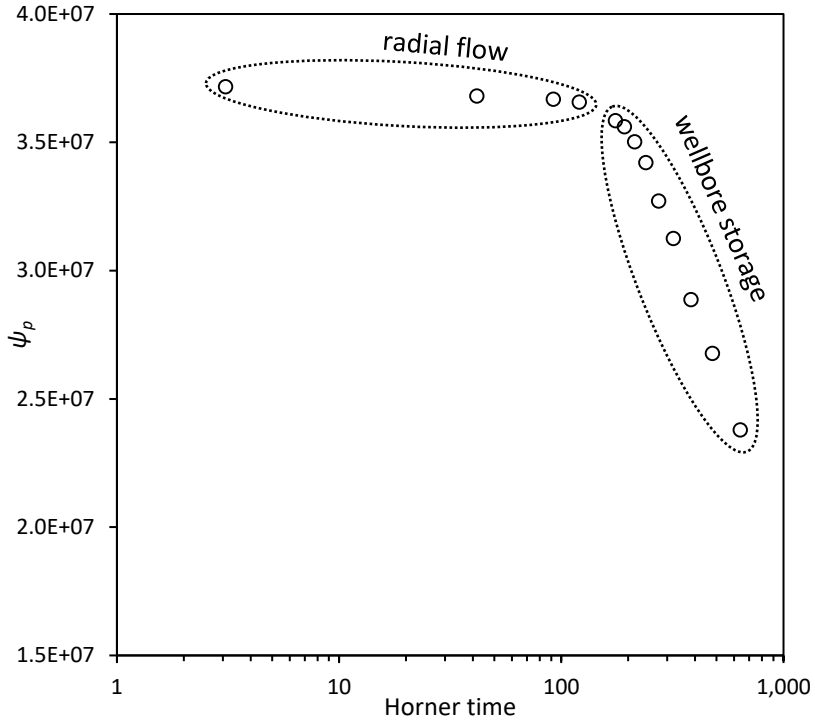

Figure 50: Semi-log plot of pseudopressure vs Horner time for Cousland 1 1956 backpressure test annotated to show radial flow and wellbore storage.

The average reservoir pressure (back calculated from pseudopressure) is given where the slope of the radial flow part of the plot intercepts the y-axis at a Horner time of 1 (which represents infinite shut-in time). The slope can also be used to calculate the permeability using equation (9):

$$k = \frac{1637 q_g T}{m h} \tag{9}$$

Where k is the permeability in millidarcys (mD), q_g is the flow rate prior to shut-in (in Mscfd), T is the reservoir temperature (in Rankine), m is the slope of the radial flow part of the plot (shown by the red line in Figure 51), and h is the pay thickness. Once we have calculated the permeability, the skin factor can be determined using equation (10) (Lee and Wattenbarger 1995):

$$s = 1.151\left[\frac{P_{1hr} - P_{wf}}{m} - log\left(\frac{k}{\phi \mu_g c_t r_w^2}\right) + 3.23\right] \tag{10}$$

Where P_{1hr} is the bottom hole pressure one hour after shut-in, P_{wf} is the bottom hole pressure at shut-in, k is the permeability in millidarcys (mD), ϕ is the porosity (fraction), μ_g is the average gas viscosity (centipoise), c_t total compressibility (sum of water, gas, and formation compressibilities weighted using water and gas

saturations), and r_w is the wellbore radius (feet). Figure 51 shows the semi-log plot with the radial flow slope, P_{1hr}, with average reservoir pressure added.

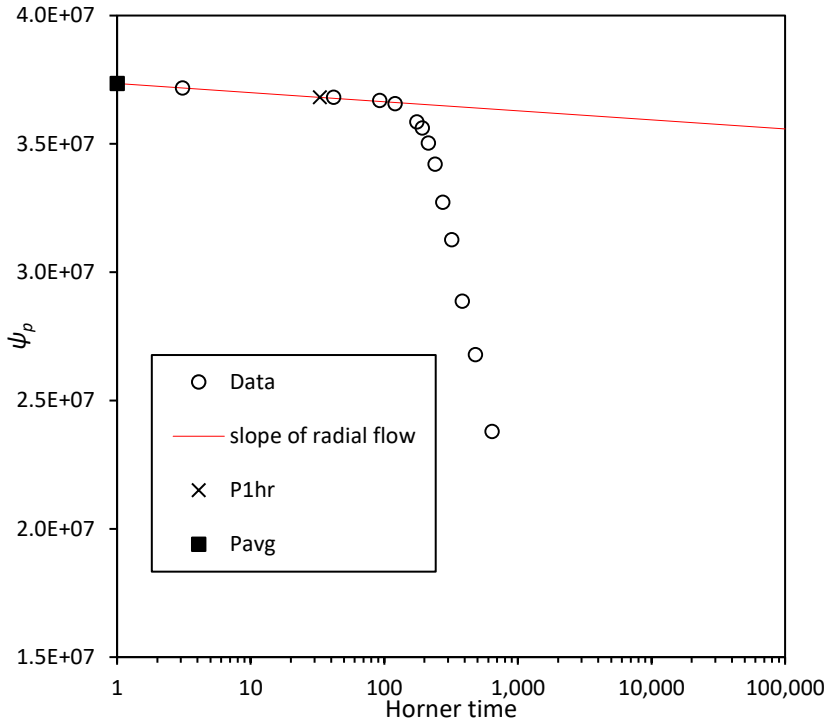

Figure 51: Semi-log plot of pseudopressure vs Horner time for Cousland 1 1956 buildup test. Red line indicates slope of radial flow, cross marks the bottom hole pressure one hour after shut-in (P1hr), and filled square marks the average reservoir pressure at infinite shut-in time (Pavg).

4.12.4 Analysis results

The parameters and fluid properties used in the analysis are given in Table 11 along with the results of the analysis. The permeability of 71.9 mD and skin factor of 49.7 will be used to match the simulator well IPR curve to that of the real Cousland 1 well.

Table 11: Parameters and results of the buildup test analysis.h = net thickness, T = formation temperature, ϕ = porosity, S_g = gas saturation, S_w = water saturation, c_w = water compressibility, c_g = gas compressibility, c_f = formation compressibility, c_t = total compressibility, r_w = wellbore radius, SG = specific gravity (compared to air), μ_g = average gas viscosity, q_g = flow rate prior to shut-in (weighted average), Z = compressibility factor, k = permeability, s = skin factor, P_{avg} = average reservoir pressure.

RESERVOIR PARAMETERS			FLUID PROPERTIES		
variable	**value**	**units**	**variable**	**value**	**units**
h	24	ft	SG	0.5749897	
T	68	F	μ_g	0.0119927	cp
ϕ	0.15		q_g	706.52237	MCFd
S_g	0.5		Z	0.9084699	
S_w	0.5				
c_w	3.60E-06		ANALYSIS RESULTS		
c_g	1.71E-03		**variable**	**value**	**units**
c_f	6.59E-06		k	71.9	mD
c_t	8.66E-04		s	49.7	
r_w	0.365	ft	P_{avg}	639.4	psi

4.13 1939 tests

A backpressure and buildup test was performed on the reservoir interval in 1939 but this test also included another, deeper sand and so the results are not useable for history matching. However, the data illustrates some of the issues noted in the section on data quality and reliability. There are several readings that do not fit with what would be expected (unexpected identical values that form ‘steps’ in the data vs expected smooth curve). These could be the result of human error or the gauge needle sticking. This is highlighted because it makes analysing this data difficult. The semi-log plot below in Figure 52 shows these readings and possible causes.

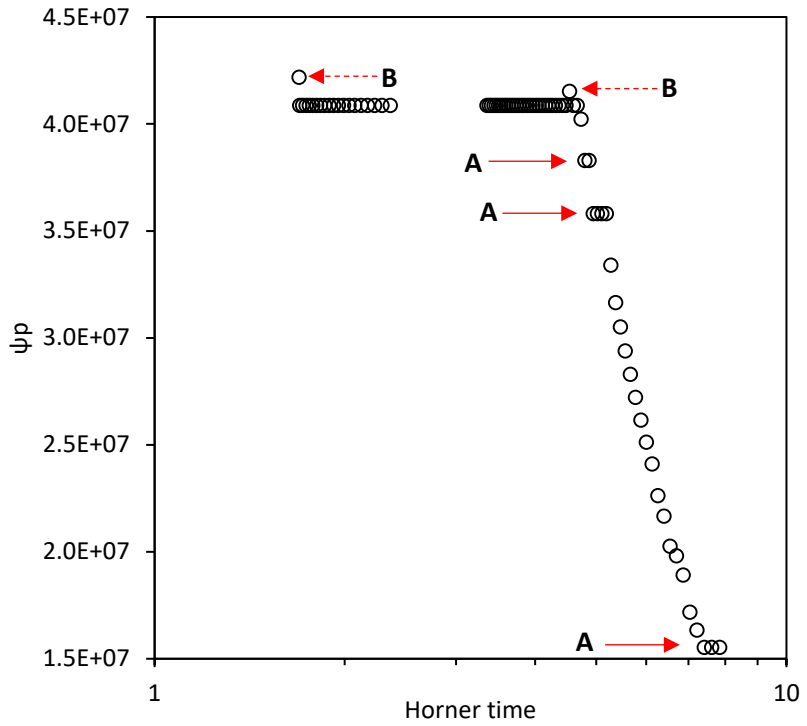

Figure 52: Semi-log plot of pseudopressure (ψp) vs Horner time for Cousland 1 1939 buildup test. This plot highlights potential data issues. Points labelled A (with solid red arrow) show steps in the data possibly caused by a stuck gauge needle. Points labelled B (with broken red arrow) show possible misreading of the gauge.

4.14 History matching

In this section, the history matching process for the Cousland model will be described. The main aims were to match the historical production volumes and pressures of the Cousland field by making adjustments to the reservoir model properties. The key elements for matching were the Cousland 1 IPR curve, the calculated bottom hole pressures for Cousland 1 post-testing in November 1956 , the average permeability of the reservoir calculated from the 1956 pressure testing data, and the production data.

4.15 Well modelling

There are two key areas in which the well is modelled. The first is the flow between the reservoir and the wellbore, known as inflow performance. The second is inside the wellbore to the surface, known as tubing performance.

4.15.1 Tubing performance

In order to history match the well, its tubing performance must be replicated. A key factor in replicating behaviour is an accurate model of the difference between wellhead pressure and bottom hole pressure in the tubing. This is done using the

tubing pressure calculator in CMG Builder (CMG 2019a), a more rigorous process than that used in the reservoir engineering section (equation (3)), which calculates the pressure difference dynamically taking into account the flow regime, changing gas composition, and friction in the tubing.

The calculator was given flow rate and well head pressure data from the 1956 flow test, along with PVT and tubing properties (which are discussed in the tubing model section). It take these and uses different PVT and pressure computation methods to calculate the bottom hole pressure. In this case the Aziz-Govier correlation (Aziz and Govier 1972) was selected in the simulator, a method suitable for vertical producing wells. This gives the tubing performance curves (also known as tubing performance relations or TPR) for Cousland 1 which are shown in Figure 53 with the inflow performance relation (IPR) which was calculated in the reservoir engineering study. The flow rate is given where the TPR and IPR intersect for a given well head pressure.

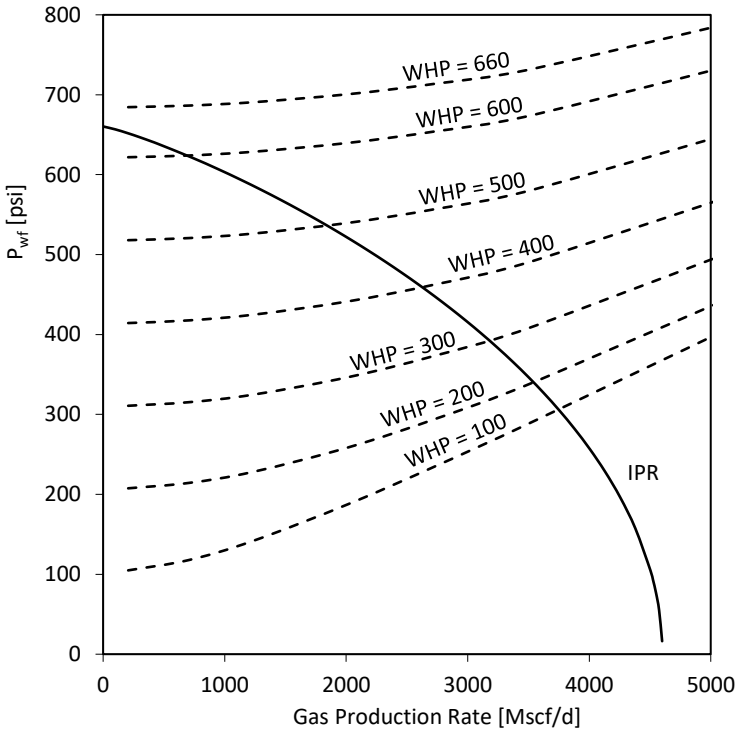

Figure 53: Tubing performance (dashed lines) and IPR (solid line) curves for Cousland 1. WHP = well head pressure; P_{wf} = bottom hole well flowing pressure; Mscf/d = thousand standard cubic feet per day; IPR = inflow performance relation.

4.15.2 Tubing model

The tubing model for the Cousland 1 well consists of a single tube the entire length of the well with an internal diameter of 2 inches (0.0508 metres). The geometric

characteristics of the well are defined in the K (vertical) direction for calculation of the well index internally. The geometric parameter (geofac) depends upon the location of the well within a cell and the location of the cell within the reservoir boundaries, in this case it is 0.37 which means it is in the centre of a cell in the centre of the reservoir. The angular completion fraction (wfrac) describes the fraction of a circle that the well models, and in this case it is 1 as the whole well diameter is within one block. The skin factor (skin) is a measure of the difference in permeability around the wellbore relative to that of the reservoir. A positive number indicates damage to the formation and a reduction in permeability around the well, while a negative number indicates higher permeability around the well relative to the formation. A skin factor of zero implies no alteration to the formation around the well. Prior to history matching, the skin factor was set to zero and would be adjusted based on the IPR output of the simulator. The Cousland 1 well was perforated through the whole reservoir section.

4.15.3 Well constraints

The well was constrained by the gas produced which is known from the production engineering files and relinquishment reports for the Cousland field. This was given at surface volume to the simulator as a field history file. Therefore the reservoir pressure and IPR outputs would need to be matched by adjusting the skin, average reservoir permeability, and total porosity in the model. The gas production data is estimated to have an uncertainty of ±500 SCF (standard cubic feet) as it was measured in MSCF (thousands of standard cubic feet). Figure 54 shows the cumulative gas production over time from the Cousland field.

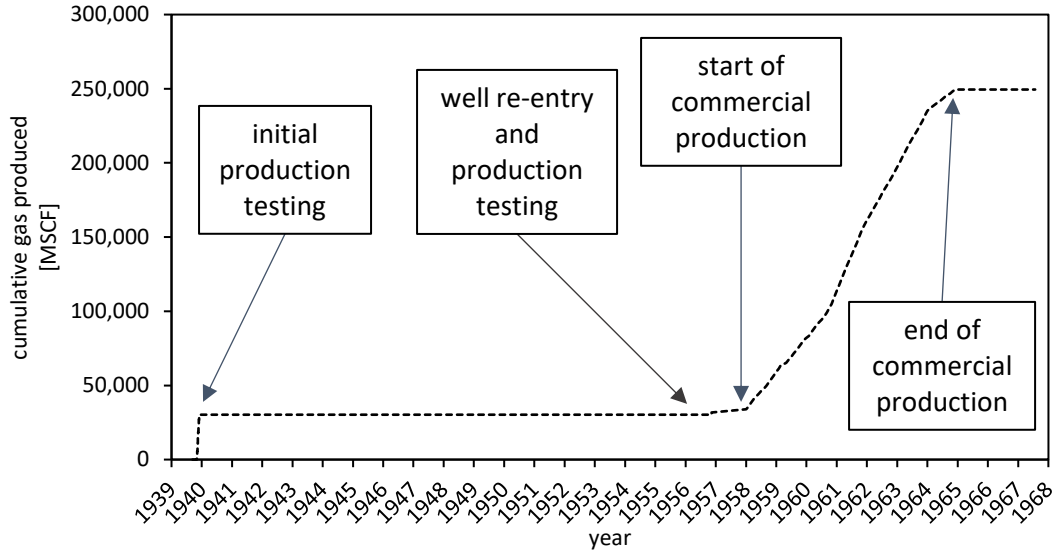

Figure 54: Cousland 1 cumulative gas production from the 1582 sand annotated with key events. MSCF = thousands of standard cubic feet

4.16 Relative permeability curves

Although for the purposes of this simulation only water-gas relative permeability curves are required, GEM requires both a water-oil relative permeability table and a liquid-gas relative permeability table. It then calculates three-phase permeability using Stone's second model as normalized by Aziz and Settari (Aziz and Settari 1979). The relative permeability curves used in the simulation are generic according to L. Schirrer (personal communication, February 20, 2020) and are shown in Figure 55. These were used as no relative permeability measurements were taken for the Cousland field and no relative permeability curves for natural gas/hydrogen mixtures were available at the time this work was done.

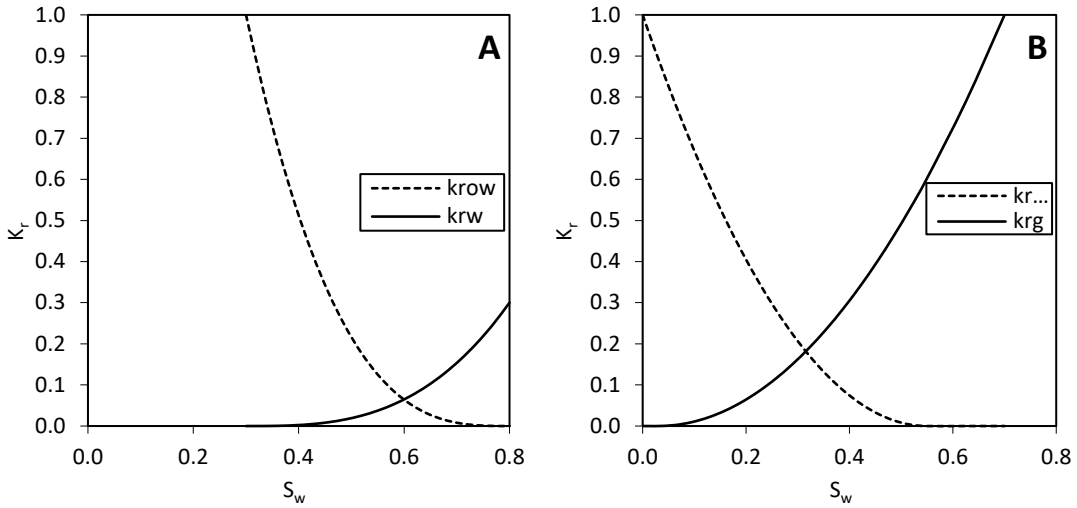

Figure 55: A - relative permeability vs water saturation; B - relative permeability vs gas saturation. Kr = relative permeability, w = water, g = gas, ow = oil/water, og = oil/gas.

.

4.17 Adjustments to the model

Prior to history matching the IPR was much too high, the original reservoir pressure was too low, the amount of gas in the reservoir was too low and the porosity and permeability were both too low. This is reflected in the initial IPR output from the model (Figure 56 A) which shows far higher potential flow rates at lower pressures than the reservoir engineering study concluded from the backpressure test data for Cousland 1. This is to be expected as the geological model was not built based on test data and is a first approximation of the reservoir which was intended for further adjustment based on the results of the reservoir engineering study.

4.17.1 Porosity

The porosity model (see chapter 3.12.1) was adjusted to match the gas originally in place (GOIP) calculated using the P/Z method. The P/Z method (Figure 49) gave a GOIP of 0.87 BCF (billion cubic feet) and the initial model GOIP was 0.66 BCF (see chapter 3.14). A multiplier of 1.32 was applied to the model porosity to bring the GOIP to 0.87 BCF.

4.17.2 Permeability

The average permeability for the blocks in the model which the Cousland 1 well intercepted was 30.9 mD, roughly half of the 71.9 mD determined by the semi-log plot in the reservoir engineering study (see chapter 4.12.3). A multiplier of 2.33 was applied to the permeability to bring the average up to 71.9.

4.17.3 Skin

The skin factor was calculated as 49.7 using the semi-log plot in the reservoir engineering section and this value was used in the simulation.

4.18 Post adjustment reservoir model behaviour

4.18.1 Inflow Performance Relation curves

After the adjustments to the permeability, porosity, and skin in the model were made, the model IPR curve was a good match for the one calculated from the 1956 test data, as shown in Figure 56 B.

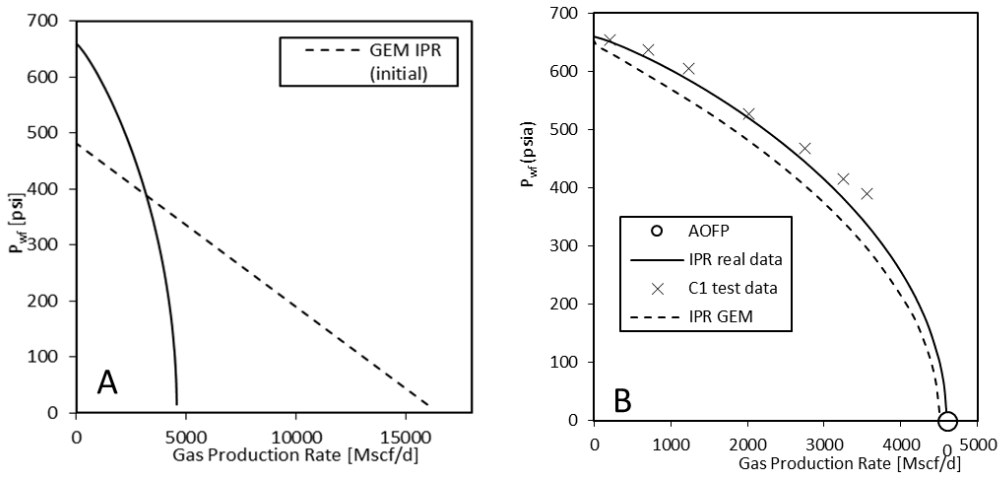

Figure 56: Figure showing the development of GEM IPR curves before and after adjustment. A:Inflow performance relation curves for the Cousland 1 well (1956 test) and the initial GEM simulation well; B: IPR (inflow performance relation) curves for Cousland 1, along with the 1956 flow test data points. This figure shows a close match between the IPR curve calculated from the test data and that outputted by the simulator after history matching the model.

4.18.2 Bottom hole pressures

Bottom hole pressures prior to the 1950s well re-entry and workover are not well matched in the simulator (Figure 57, top). This is because there is test data missing which is mentioned in the production engineering files (Adcock 1939; Martin 1974). Therefore an IPR curve cannot be produced for the well at that time. The bottom hole pressures during production are a much better match due to the available 1956 test data (Figure 57, bottom). The well was reentered in the 1950s and it was found that the original casing perforations were very poor (many of the bullets used were still stuck in the casing itself) (Martin 1974). This would have led to a higher skin factor when compared to the well after it had been reentered. Therefore the IPR curve for the original well would have been shifted to lower flow rates for lower bottom hole pressures with a lower AOFP. Hence the simulator has overestimated

the bottom hole pressure of the well in the 1930s compared with in the 1950s onwards. A comparison of simulator and real bottom hole pressure data can be seen in Figure 57.

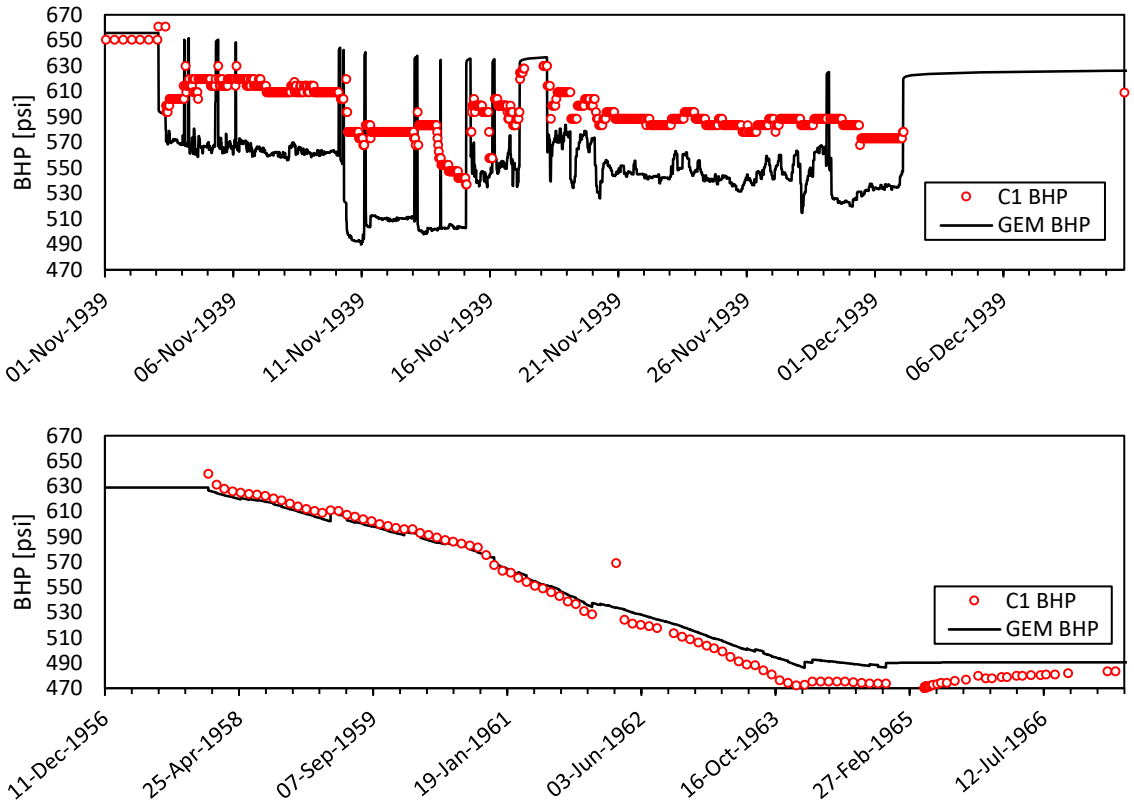

Figure 57: Bottom hole pressures calculated form well head pressure data for Cousland 1 (red circles) and GEM simulator bottom hole pressure output (back lines). The match is not good in the 1939 testing period but much better in the 1950s/60s production period.

4.18.3 Production rate

As the measured production rates were used as a constraint for the model, the simulation output is exactly the same as the Cousland 1 data. Production was severely limited by demand from the local gas works and so does not follow a classic depletion profile as can be seen in Figure 58.

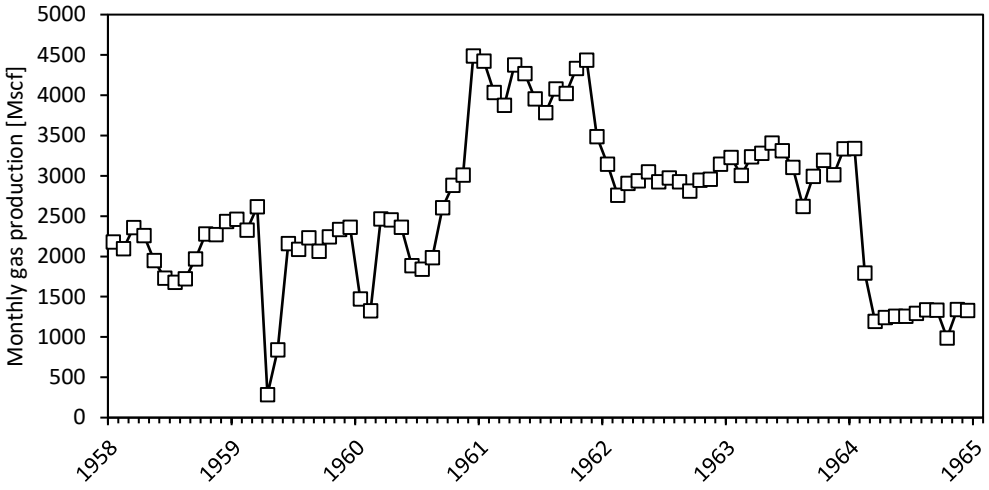

Figure 58: Monthly gas production from the Cousland gas field during commercial production between 1958 and 1965. Production was severely limited by demand.

4.18.4 Next steps

The model has been history matched and the simulator output is reasonably close to the original data. The next step is to design a simulation schedule for hydrogen injection, storage, and production.

4.19 Hatfield Moors Gas storage facility as a basis for the simulated hydrogen storage schedule

This section will provide a brief background on the Hatfield Moors gas storage facility, the similarities with the Cousland gas field, why Hatfield Moors gas storage data was chosen as the basis for the hydrogen storage simulation schedule, and describe the hydrogen storage simulation schedule.

4.19.1 Background

The Hatfield Moors gas storage facility is located around 10 km northeast of the City of Doncaster, Yorkshire, in the UK. It was discovered by accident in 1981 when the Hatfield Moors-1 exploration well blew out from the Late Westphalian B age Oak Rocks sandstone at a depth of 1587 feet. Luckily, there were no casualties but it took 38 days to get the blowout under control and an estimated 1 BCF of gas was lost to the resulting fire (Ward *et al.* 2003). Gas was produced commercially between 1986 to 1998 upon which it was converted to gas storage which has operated since 1999, with the Oaks Rock sandstone used as the storage reservoir (Ward *et al.* 2003).

4.19.2 Comparison to Cousland gas field

This field has some key similarities to the Cousland field, a comparison of basic field data is given in Table 12. The most important from a reservoir engineering perspective are that the original reservoir pressures are similar (650 psig at Hatfield Moors compared to 645 psig at Cousland) and that both reservoirs behave as constant volume reservoirs with pressure depletion as the main drive mechanism (Adcock 1939; Illing 1961; Martin 1974; Exploration Dept. Lasmo 1985; Gralla and Jones 1991). This can be seen in the P/Z plot for Hatfield Moors in Figure 59 from 1998 which, after 11 years of commercial production, has produced a linear response indicating that aquifer activity is absent (Edinburgh Oil & Gas PLC 1999).

Because of the similarity in reservoir pressures and both fields behaving as constant volume reservoirs, the injection and production pressures and rates are likely to be in a similar range. The gas originally in place (GOIP) at Hatfield Moors is also of a similar magnitude to Cousland (6 BCF at Hatfield Moors vs 0.9 BCF at Cousland) which suggests that if Cousland were to be used as a storage site, it would follow a similar storage pattern as Hatfield Moors.

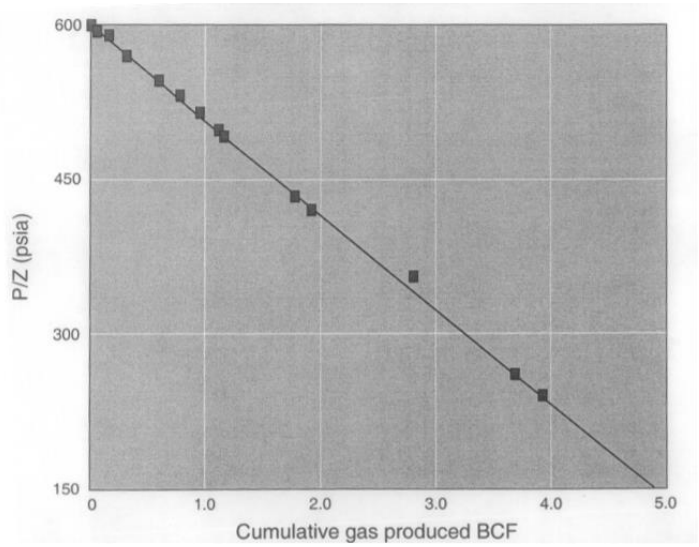

Figure 59: P/Z plot for Hatfield Moors gas field after 11 years of commercial production. The linear response indicates that there is no aquifer activity. Taken from (Edinburgh Oil & Gas PLC 1999)

Table 12: a comparison of key field data for the Hatfield Moors gas storage facility and the Cousland gas field.

	Hatfield Moors Data from (Ward *et al.* 2003)	**Cousland** * = data from this study, otherwise from Exploration Dept. Lasmo (1985)
Trap		
Type	Tilted anticlinal fault block	four way dip closure
Depth to crest	1400 ft TVDss	892 ft TVDss
Gas-water contact	1460 ft TVDss	1110 ft TVDss
Estimated original field pressure	650 psig	660 psia (645 psig)*
Pay zone		
Formation	Oaks Rock Sandstone	1582' sand
Age	Late Westphalian B	Visean
Thickness	25-90 ft	20-50 ft*
Net/gross	0.9	0.7*
Porosity	17.2-25.6%	15%
Average gas saturation	55%	70%*
Permeability	21-1100 mD	71.9 mD (average)*
Hydrocarbons		
Gas gravity (Air = 1)	0.629	0.57*
Gas type	Sweet dry gas	Sweet dry gas
Reserves GOIP	6.1 BCF	0.87 BCF*
Recovery factor	?70%	?70% (assumed)*
Recoverable reserves	4.27 BCF	0.61 BCF*
Drive mechanism	Pressure depletion	Pressure depletion

4.19.3 Natural gas storage schedule

Gas is injected and produced at Hatfield Moors according to market demands and so injection and production take place throughout the year as shown in Figure 60 B and C. However the dominant trend of the storage inventory, the amount of the total working gas volume in the reservoir, is that of a seasonal store with the peak injection through the summer, storage in the autumn/early winter, and production taking place during the colder parts of the winter when gas demand is high, as can be seen in Figure 60 A. As the Cousland gas field volume is of a similar magnitude to Hatfield Moor, it is assumed it would follow a similar schedule.

Storage inventory data (amount of working gas capacity in the reservoir), along with injection and production rates from Hatfield Moors are available from April 2016 onwards (Scottish Power 2020) and displayed graphically in Figure 60. A more detailed look at the data shows the seasonal trend in the storage inventory with distinct peaks between September and January/February and a low in March when the working gas volume is almost entirely depleted. The injection and production rates also show that injection is highest and most sustained between March and August, and production rates are highest and most sustained between January/February and June.

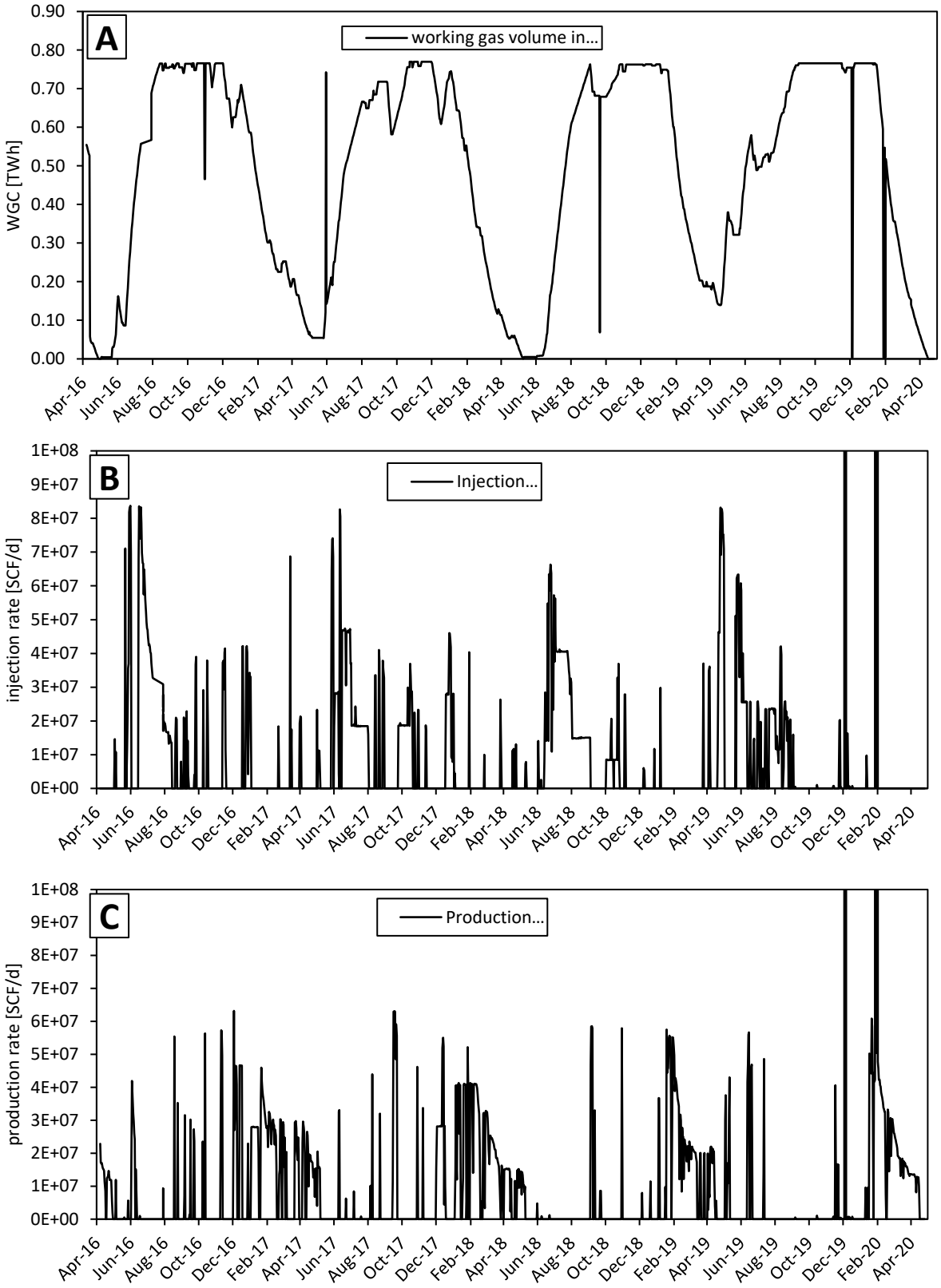

Figure 60: Hatfield Moors storage data (Scottish Power 2020)*; A - working gas storage inventory (TWh = terawatt-hours); B - Injection rates calculated from energy flows using a value of 11.111 kWh per m^3; C - production rates calculated from energy flows using a value of 11.111 kWh per m^3. The two spikes seen in the data in November 2019 and January 2020 are thought to be errors in the data as the flows are higher than any known wells. X-axis format is Month-Year. The seasonal trend mentioned in the text is clearest in A with peak inventory in the summer and lows in the winter. The graphs have all been aligned so that the more subtle seasonal trends in the injection and production rates (also mentioned in the text) in B and C can be matched up to the storage inventory.*

4.19.4 Hydrogen storage schedule

Using the Hatfield Moors data as a basis for the schedule for the simulated hydrogen storage scenarios gives the following schedule which is also summarised in *Table 13*. The injection and production of hydrogen in the model takes place through a single well in the crest of the structure. Initial charging of the reservoir will take two years with a further two years to allow the reservoir to reach equilibrium. Storage cycles are as follows: injection takes place between June and September, the store is full between September and January, production occurs between January and May, and the store is at its lowest working gas volume in May. There will be a total of fourteen storage cycles with the final cycle ending with a one year depletion (well producing at maximum rate) to recover as much hydrogen as possible.

Table 13: hydrogen storage simulation schedule based on data from Hatfield Moor. Simulation dates are arbitrary and run from 2020 to 2040. There is a total of fourteen storage cycles ending in depletion in the final year. There is a single injection/production well in the model.

initial charging of reservoir	**storage cycles (×14)**	**depletion**
Injection: 2 years Settling: 2 years	Extraction phase : Jan – May Empty phase : May Injection phase : Jun – Sep Full phase : Sep – Jan	Depletion of reservoir: 1 year

4.20 Hydrogen storage scenarios

To investigate the pressure response of the reservoir, three different pressure scenarios were simulated: a base case, high pressure case, and a low pressure case. This produced three sets of results and allowed a sensitivity analysis to be conducted. The three scenarios all inject and produce through a single well and are described below.

For the base case, the schedule in *Table 13* is followed with the injection well bottom hole pressure limited to a maximum of 660 psi (the original reservoir pressure) and the production well bottom hole pressure limited to a minimum of 14.7 psi (atmospheric). For the high case, the schedule in *Table 13* is followed with the injection well bottom hole pressure limited to a maximum 744 psi (90% of fracture

pressure - assumed to be enough of a safety margin, calculated using the method of Eaton (1969)) and the production well bottom hole pressure limited to a minimum of 14.7 psi (atmospheric). For the low case, the schedule in *Table 13* is followed with the exception of the initial charging of the reservoir, therefore the first production cycle only produces natural gas. The injection well bottom hole pressure is limited to a maximum of 660 psi (the original reservoir pressure) and the production well bottom hole pressure limited to a minimum of 14.7 psi (atmospheric).

4.21 Results

4.21.1 Compositional changes in the produced gas

Figure 61 shows the mole fraction of hydrogen in the produced gas for the three different scenarios. There is little difference between the scenarios, however the high pressure scenario does show slightly higher mole fractions of hydrogen during the first four production cycles and during depletion in the final year.

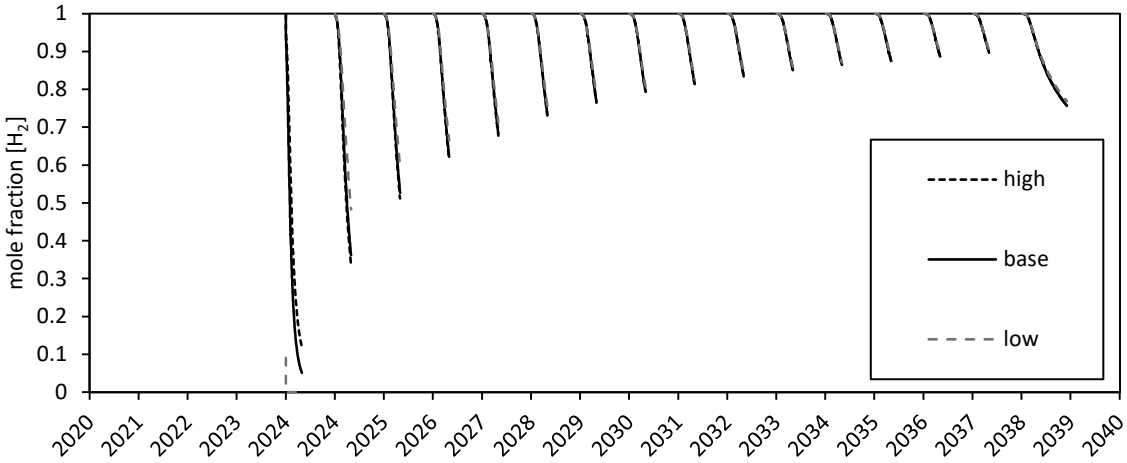

Figure 61: Mole fraction of hydrogen in produced gas for low, base, and high scenarios (black solid and dashed lines) with trendlines (grey solid and dashed lines). Note there is substatial overlap between the three scenarios. The small vertical dashed line at year 2024 between 0 and 0.1 mole fraction H_2 represents natural gas production in the low scenario.

4.21.2 Capacity

Figure 62 shows the average mass of hydrogen injected and recovered per storage cycle. The average mass of hydrogen injected per storage cycle is similar for each scenario between 980,000 and 990,000 kg with the higher figure for the low pressure scenario. The average mass of hydrogen produced per storage cycle differs more, with the high pressure scenario producing 930,000 kg, the base scenario producing 910,000 kg and the low pressure scenario producing 890,000 kg.

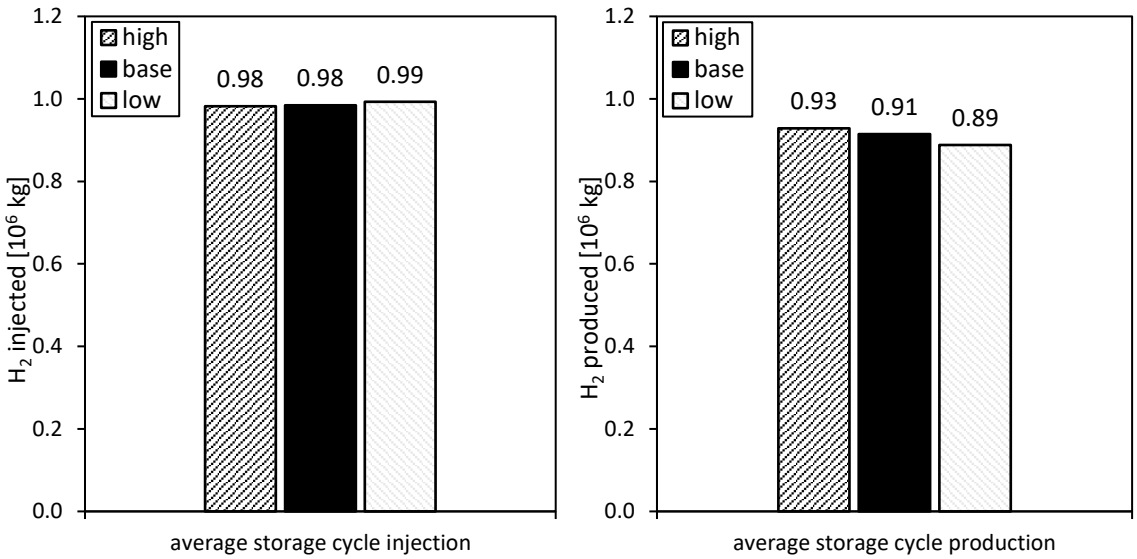

Figure 62: Average mass per storage cycle of injected and produced hydrogen respectively. This figure gives an indication of the hydrogen capacity of the Cousland field.

4.21.3 Recovery factor

Figure 63 shows the hydrogen recovery factor for both the storage cycles average, and the total life of the field which includes both the storage cycles and depletion in the final year. The lifetime recovery factor is similar for each scenario at 98%, however the recovery factor is highest in the high pressure scenario at 95% and lowest in the low pressure scenario at 89% with the base scenario between the two at 93%.

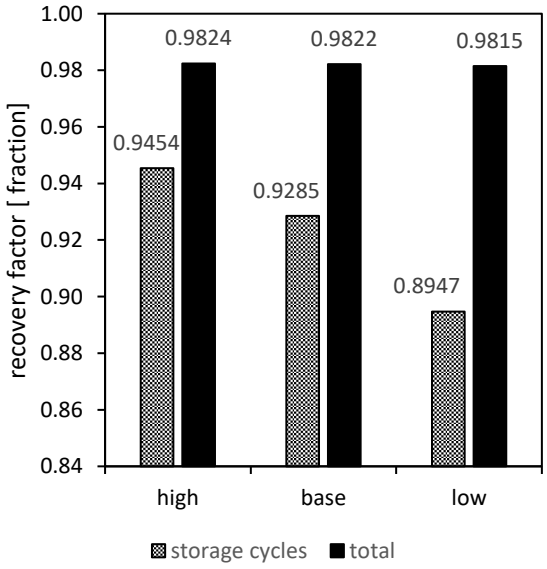

Figure 63: Recovery factor - produced hydrogen as a fraction of injected hydrogen for storage cycle average, and total simulation schedule including depletion in final year.

4.21.4 Pressure response

Figure 64 shows the average pressure in the hydrocarbon/hydrogen containing pore volume in the model over the 20 year storage schedule. For clarification the GEM simulator output calls this the hydrocarbon containing pore volume (HCPV) but here it wil be refered to as the hydrocarbon/hydrogen containing pore volume. The difference between the three scenarios can be seen between 2020 and 2024 during the initial filling and settling phases until the end of the first storage cycle in 2025 at which point the pressures converge and are indistinguishable.

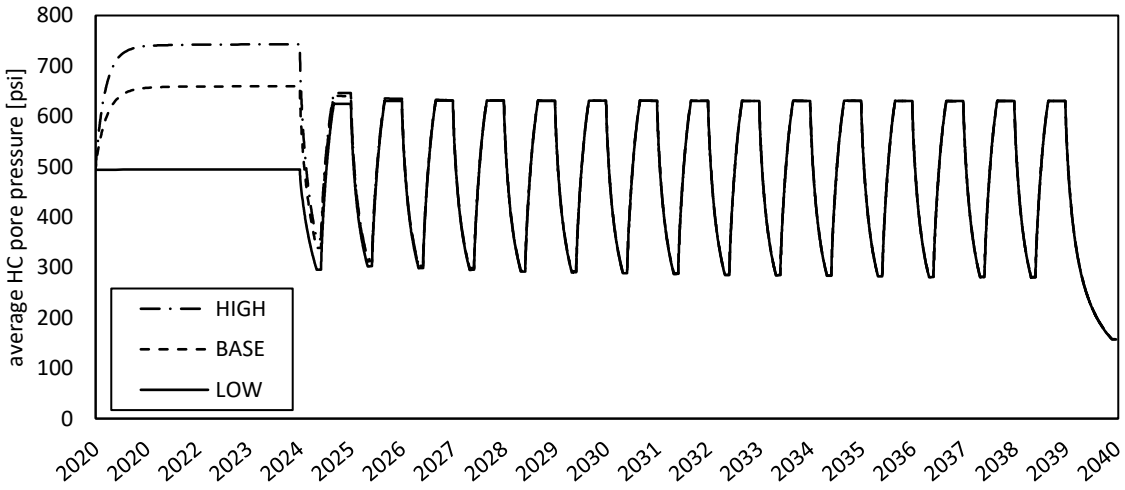

Figure 64: Average hydrocarbon/hydrogen containing pore volume pressure for high, base, and low scenarios. Pressures converge and are indistinguishable after the first storage cycle.

4.21.5 Well flow rates

The hydrogen injection and gas production rates are shown in Figure 65. These rates are in the same order of magnitude as those calculated for Hatfield Moor gas storage in the previous section and show a sharp peak followed by a tailing off. Both the injection and production rates are almost identical for the three scenarios with the high pressure scenario showing slightly higher injection rates during the filling phase in 2020 and higher production rates during the peak of the first production cycle in 2023.

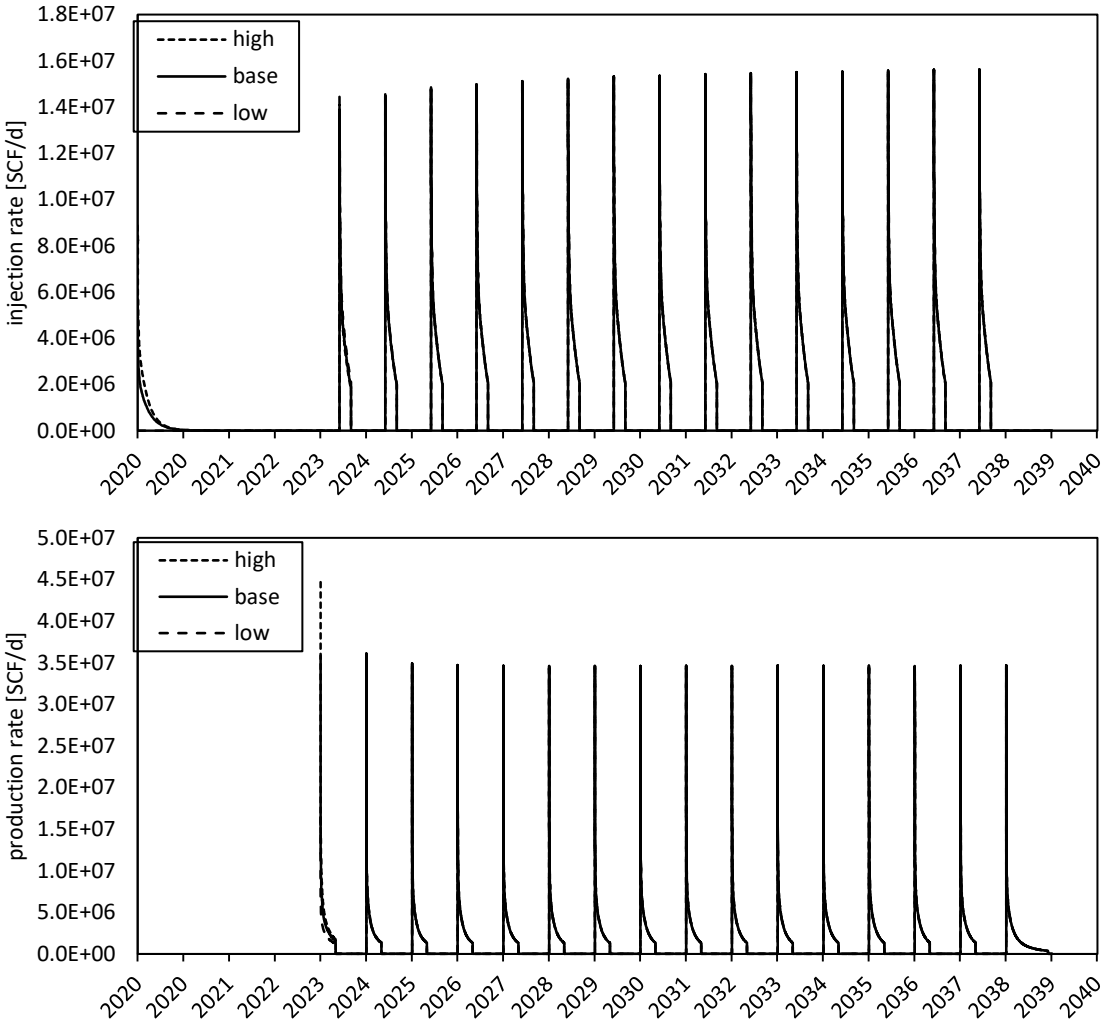

Figure 65: Hydrogen injection and gas production rates during the storage schedule simulation.

4.21.6 Sensitivity analysis

The tornado plot in Figure 66 presents the percentage difference from the base scenario of six key outputs from the hydrogen storage simulation. The greatest variability was in the average recovery factor of the storage cycles, the maximum production flow rate was only affected by the low pressure scenario, and the other variables were affected most by the low pressure scenario as well. The difference is not great with the largest difference being just 3.6%.

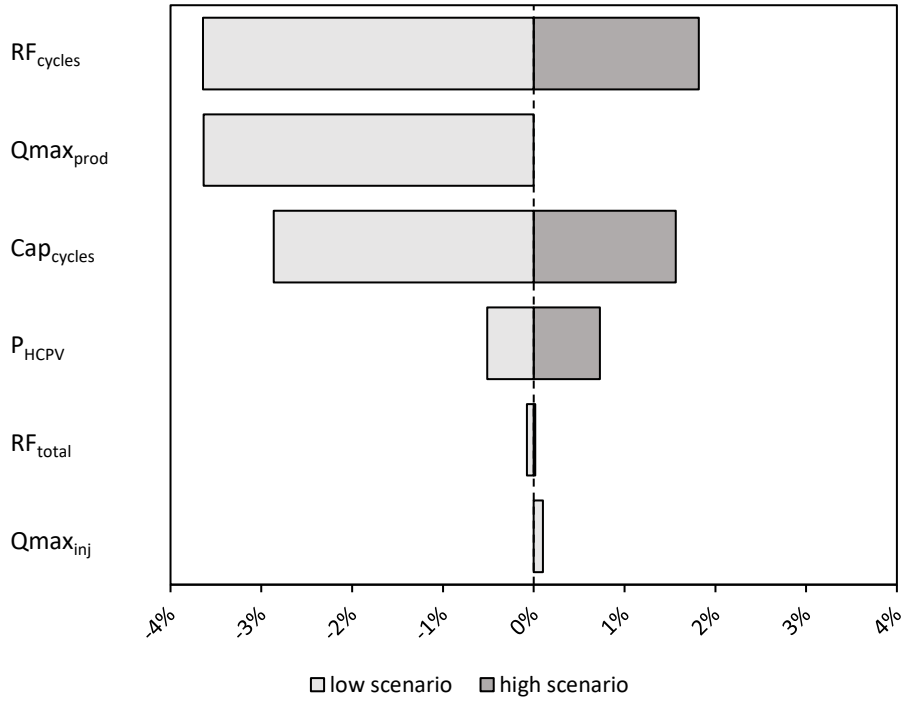

Figure 66: Tornado plot showing difference in % from base scenario of the high and low pressure scenarios. $Qmax_{inj}$ = peak injection rate; RF_{total} = recovery factor total; P_{HCPV} = average hydrocarbon/hydrogen containing pore volume pressure; Cap_{cycles} = capacity (average cycle production); $Qmax_{prod}$ = peak production rate; RF_{cycles} = recovery factor cycles.

4.22 Discussion

This section will discuss the limitations and implications of the simulation results and make some conclusions based upon them. The compositional changes in the gas produced along with that in the reservoir will be discussed in detail with some further analysis to understand those compositional changes over time. Also there will be some discussion of why the three scenarios differ but overall remain extremely similar in their outputs.

4.22.1 Limitations of the simulation study

It is important to remember that this is a simulation based on limited data about which several assumptions have been made as outlined in this chapter and the previous chapter on the geological model. As such, it is only an approximation of reality and is subject to change and refinement in light of new evidence.

Key to the uncertainty is the history matching aspect of the study. History matching is not a well-defined process and does not have a unique solution. The fact that the simulator outputted similar IPR curves and that the model ended up with porosity

and permeabilities that agreed well with the reservoir engineering study does not mean that the model is an accurate representation of reality. The distribution of properties in the reservoir model is the biggest unknown in this study as there is little to no data from the reservoir section itself and the geology is poorly constrained. In most studies the amount of data is exceeded by the number of unknown parameters which makes the problem ill-posed and results in multiple solutions (Tavassoli *et al.* 2004).

Lastly, GEM compositional simulator (CMG 2019b) has been built around PVT equations that were developed empirically for hydrocarbons, and flow equations (such as inflow performance) that have been developed over years of hydrocarbon extraction. Therefore there is inherent uncertainty around how suitable these are for hydrogen.

4.22.2 Compositional changes in produced gas and gas within the reservoir

The proportion of hydrogen in the produced gas increases over time with each cycle, before a slight decrease during depletion in the final year. This trend of increasing proportions of hydrogen in each subsequent cycle is seen in two previous simulation studies which both used nitrogen as a cushion gas in a hydrogen storage (Pfeiffer and Bauer 2015; Feldmann *et al.* 2016). The authors of those studies concluded that this was due to a closed system with minimal losses where impurities are produced and only pure hydrogen is injected leading to an increase in the concentration of hydrogen within the reservoir. However, further investigation of the data reveals that there could be other processes at work. Here I discuss three different processes that could be occurring and how analysis of the gas composition within the model can explain what is going on.

In the first possible process, the natural gas nearest the well is produced and replaced with hydrogen in the next injection cycle and we would expect a small mixed zone with a sudden decrease in the proportion of hydrogen in the produced gas as the mixed zone moves into the well. In the second possible process, the zone of mixing between hydrogen and natural gas moves away from the well, leading to a decrease in the proportion of hydrogen later in each production cycle. And in the third possible process, the mixing zone could be increasing in lateral extent with a longer gradient of mixed gas with a higher proportion of hydrogen closer to the well, which would lead to the rate of the decrease in the proportion of hydrogen to slow with each subsequent cycle.

What we see in the data from Figure 61 is a relatively steady decrease of hydrogen in each cycle, with subsequent cycles showing slower decreases, as indicated by the shallower gradients of the lines in each cycle and the increase in minimum mole fraction in each subsequent storage cycle. There is no sudden decrease in the proportion of hydrogen which leaves the second two situations. The absolute rate change in the proportion of hydrogen can be seen in Figure 67. There is a general slowing of the absolute rate change in each subsequent cycle which suggests that the mixed zone is increasing in lateral extent. Therefore this study suggests that not only is the mixing zone increasing in lateral extent but that the mixing zone is also moving further from the well, i.e. the concentration of hydrogen is increasing closer to the well.

This can be seen in the simulator results by plotting distance from the well against the mole fraction of hydrogen in the gas within the pore space (Figure 68 A) to give an indication of the extent of the mixing zone. The data shows that the concentration close to the well is increasing over time and that the mixing front is being pushed further away. This increase in the lateral extent of the mixing zone is more clearly seen by plotting the lateral extent (from the well out into the reservoir in the I and J directions) of the mixed zone from various mole fractions of hydrogen to a hydrogen mole fraction of 0.1 (Figure 68 B). The mixing zone increases in lateral extent over time which can be seen in Figure 68 B by the increasing distance between a hydrogen mole fraction of 1 (marked by crosses) and a hydrogen mole fraction of 0.5 (marked by triangles). After the final depletion the profile becomes more depressed as natural gas enters the zone previously dominated by hydrogen as the well produces more gas for a longer period than in the storage cycles, bringing the mixed zone fully into the well.

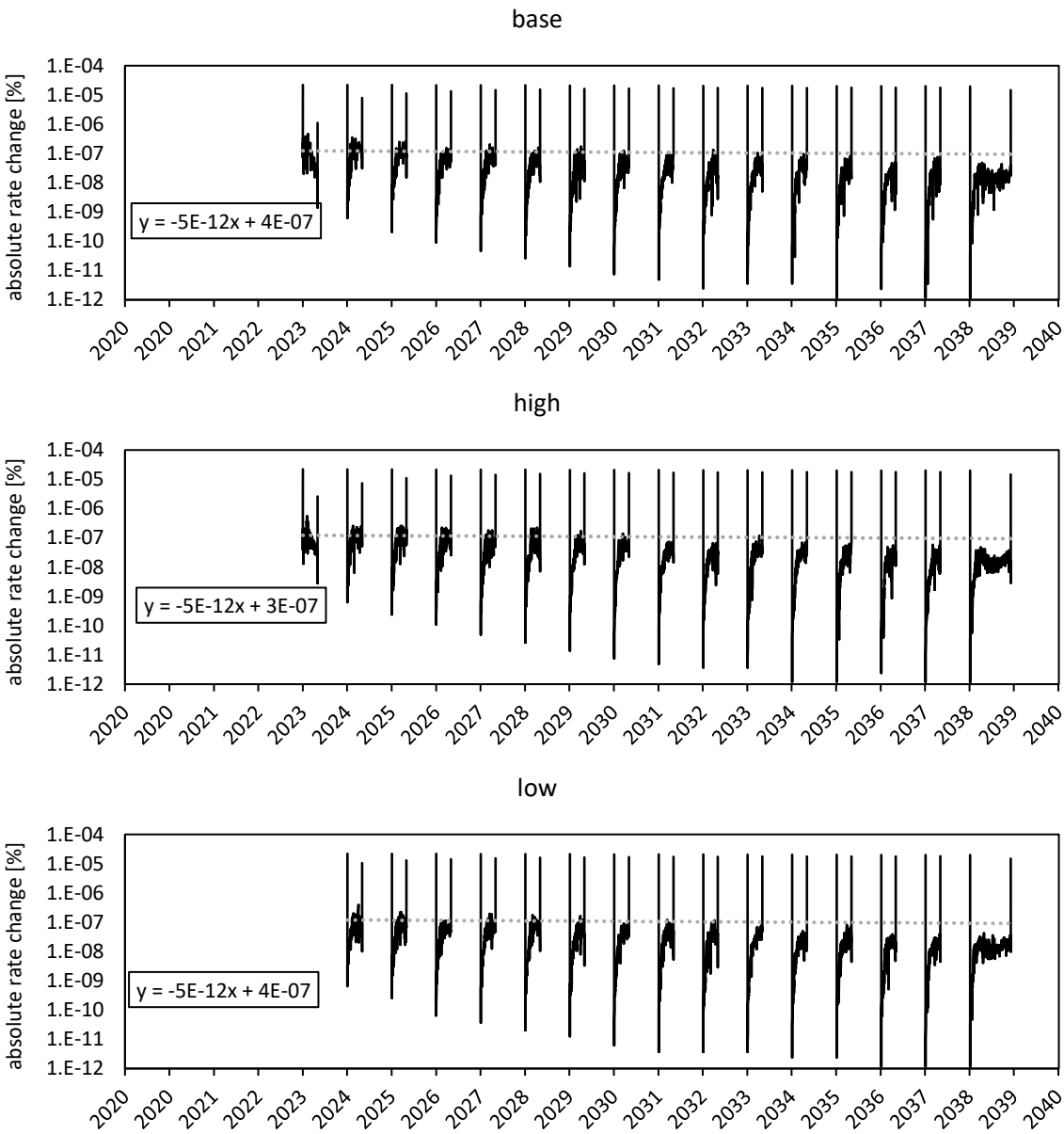

Figure 67: absolute rate of change of hydrogen mole fraction vs year for each of the three scenarios with trendlines and trendline equations. This shows a decrease over time in the absolute rate at which the hydrogen mole fraction is changing in each cycle. This is consistent with the mixed zone of gas in the reservoir increasing in lateral extent with a shallower concentration gradient.

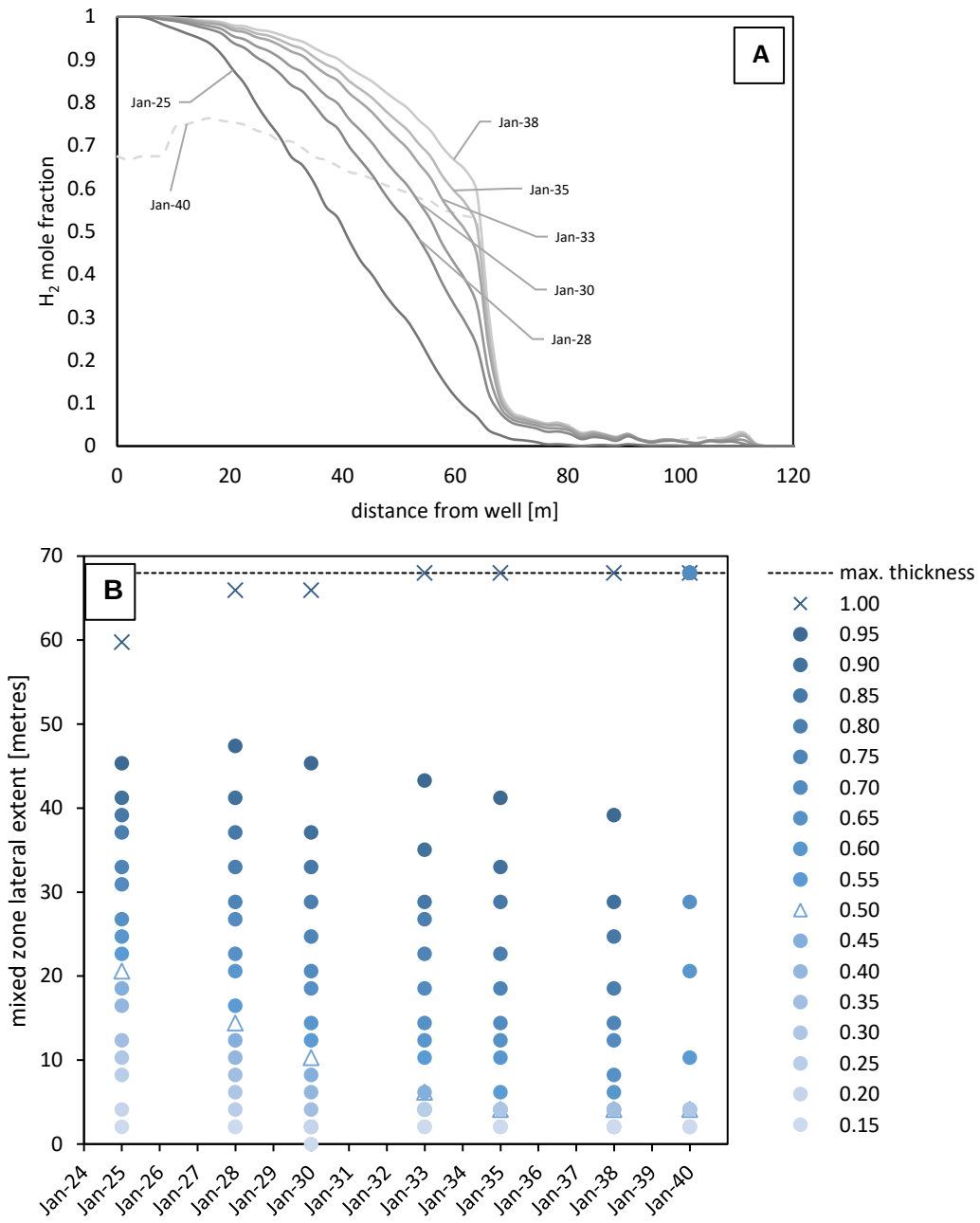

Figure 68: A: Hydrogen mole fraction vs distance from the injection/production well at different times during the simulation. The data is shown for the base case just before production with the exception of the dashed line for January 2040 which is post-depletion. The labels show the month and year. A clear front at around 70 metres from the well can be seen where a sudden increase in the rate at which the hydrogen mole fraction decreases occurs.

B: the lateral extent of the mixed zone where hydrogen and natural gas are mixing from a hydrogen mole fraction of 1 (100% hydrogen: marked with crosses) to a mole fraction of 0.1 (10% hydrogen) which coincides with the front seen in figure A at around 70 metres. The hydrogen mole fraction is an average for that distance from the well in the I and J directions from the well. The hydrogen mole fraction of 0.5 is marked with triangles to highlight the spread over time in the data. The maximum thickness of the mixed zone (68 metres) is marked with a dashed black line.

4.22.3 Capacity

The injected capacity of hydrogen is slightly higher in the low scenario as pure natural gas was produced in the first cycle, which reduced the reservoir pressure compared to the other two scenarios and therefore more hydrogen was injected overall due to higher injection rates. The production capacity is also as expected with the high pressure scenario producing the most gas, and the low pressure scenario producing the least however these are all within a few percent of each other. These results are what is to be expected when looking at the inflow performance relation, as higher production rates would be possible when the average reservoir pressure is higher. As the reservoir pressure lowers, the inflow performance curve moves down and to the left of the inflow performance relation diagram and down the tubing performance curve; this is shown in Figure 69 with IPR curves for the Cousland 1 well and the TPR curve of WHP = 100 psi used as an example only.

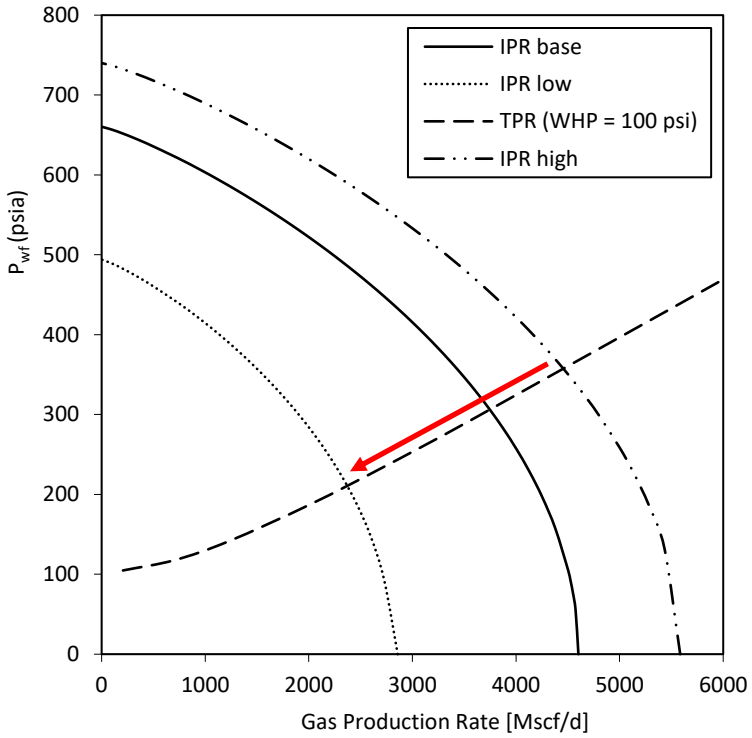

Figure 69: Inflow performance relation curves for the high (dots and dashed line), base (solid line), and low (dotted line) pressure scenarios post inital filling of the reservoir. The reservoir pressures are as follows: high = 740 psia, base = 660 psia, low = 494 psia. The tubing performance curve for a wellhead pressure of 100 psi is also shown (dashed line). Where the tubing performance and inflow performance curves intersect gives the flow rate at that particular reservoir pressure. The red line indicates the effect of declining reservoir pressure on flow rates, moving down the tubing performance curve.

In terms of scale, a comparison with average household domestic demand is useful. The average UK household has an annual gas demand of 12,000 KWh (Ofgem 2020c). Given this, the hydrogen WGC of Cousland could supply approximately 3000 homes, values for each scenario are given in Table 14. As the storage scenarios are seasonal and only producing gas between January and May, the number of homes that could be supplied would be higher however the exact number is highly dependent on a range of factors beyond the scope of this study including weather and gas prices, both of which influence demand.

Table 14: hydrogen working gas capacity, average household domestic demand, and number of houses energy equivalent. HHV of hydrogen = 39.4 kWh/kg

scenario	**high**	**base**	**low**
Cousland H_2 WGC [kg]	9.30E+05	9.10E+05	8.90E+05
home average annual demand [kWh]	12000	12000	12000
no. homes [HHV]	3054	2988	2922

4.22.4 Recovery factor

The hydrogen recovery factor follows the pattern of the production capacity, with the high pressure scenario recovery the highest proportion during the storage cycles. This is likely due to the higher flow rates in the first production cycle as a result of the higher reservoir pressure due to more hydrogen being injected initially. As the reservoir pressure is higher in this first cycle, the inflow performance curve starts further to the right of the diagram and it intersects the tubing performance curve at higher flow rates than the other scenarios. This means that the high pressure scenario will see higher flow rates for longer in the first cycle than the other two scenarios and so more hydrogen can be extracted in that cycle, leading to a higher recovery factor. This could be explained by the higher flow rates allowing the mixed zone of hydrogen and natural gas to be pulled closer to the well.

After final depletion, all scenarios have near identical recovery factors at 98%. However, if a limit on the purity of hydrogen were required by the operator of the storage, this would limit the ability of the well to pull the mixed zone closer to the well as the hydrogen mole fraction of the produced gas fell below some limit. This would then lead to a substantial decrease in the recovery factors, with hydrogen

staying within the mixed zone in the reservoir. However, with efforts such as HyDeploy and HyNet to decarbonise the UK gas grid focussing on blending increasing amounts of hydrogen into the natural gas supply over many years (Isaac 2019), this may not be an issue.

The results suggest that the recovery factor is high over the lifetime of the storage scenarios, however when the inventory (amount of hydrogen in the reservoir at any one time) is taken (shown in Figure 70) a different picture emerges which shows that the proportion of hydrogen in the reservoir is significant. The initial amount in the inventory is relatively small and builds up to around one-third of the working gas mass by the last storage cycle. This means that the natural gas remaining in the reservoir is insufficient to provide the full cushion gas volume required for the flow rates seen at the well and extra hydrogen is playing this role in the reservoir. As the reservoir was more than half full compared to the gas initially in place, this suggests that the cushion gas requirement is higher than the 50% assumed in the first chapter of this thesis. However, the hydrogen that remains in the field as cushion gas as a proportion of the total amount of hydrogen stored and withdrawn decreases significantly over time and so any associated costs could be amortized.

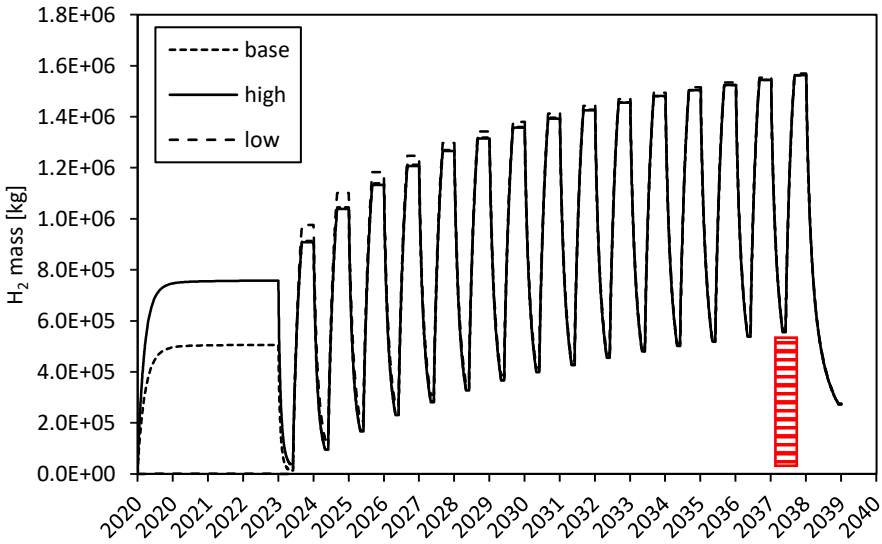

Figure 70: Hydrogen inventory in the reservoir over time (injected hydrogen minus produced hydrogen). The inventory in the reservoir increases over time in all scenarios and reveals an increasing proportion of hydrogen within the field that could be considered cushion gas.The cushion gas mass is the amount under the curve - highlighted for 2037-2038 by the red rectangle with horizontal stripes.

The recovery factors in this simulation study are significantly higher than those in the others considered in the first chapter of this thesis (Sainz-Garcia *et al.* 2017; Luboń

and Tarkowski 2020; Lysyy *et al.* 2021) which ranged from 78% to 89%. This is most likely due to the larger proportion of gas already in the reservoir prior to the injection of hydrogen in this study.

4.22.5 Pressure response and flow rates

Initial differences in the pressure during reservoir charging and the first storage cycle are responsible for all the differences in the other factors such as recovery factor and capacity, as the small differences in flow rates and gas volumes produced in the first cycle are entirely due to the differences in the inflow performance which is affected by the reservoir pressure, as discussed in the Capacity section and demonstrated graphically in Figure 69. After this first cycle the pressure in all the scenarios converges (Figure 64) and this is also seen in well flow rates (Figure 65). Note that no minimum economic flow rate has been accounted for here. This will be investigated in the next chapter and is expected to have a significant effect on the cycle capacity, reservoir pressures, and recovery factors.

4.22.6 Sensitivity analysis

The maximum difference any scenario had was 3.6% on a change from the base case. This effect is insignificant and likely to be much less than the uncertainty of the production data from the 1950s and 1960s. The reason that this difference is so small is that the different constraints used for the three scenarios only really had an effect on the first cycle as the main focus of them was the initial charging of the reservoir. After that, the well behaved in a very similar manner in all three scenarios allowing the pressures, well flow rates, and volumes injected/produced to converge.

4.23 Conclusions

A reservoir engineering study was performed on well testing and production data from the Cousland gas field and the results used to tune a model of the field. The model was then history matched using the aforementioned data before a hydrogen storage simulation investigation was performed. The initial volume of hydrogen injected into the reservoir had little effect on the recovery factor, capacity, well flow rates, produced gas composition, and pressure response during the subsequent storage cycles and final depletion. It is also clear from the pressure and hydrogen inventory results that the well constraints are not leading to an equilibrium situation in the reservoir: the mixing front is being pushed out and spread into the reservoir over time. The purity of recovered hydrogen appears to be controlled by the distance of the mixing front from the well which means that injecting more hydrogen

to push it further away should result in purer hydrogen being produced. This has implications for cushion gas requirements even where existing natural gas in the reservoir is intended to be used for this purpose. The Cousland gas field could potentially store and recover close to 1000 tonnes of hydrogen without significant losses over 20 years, however the purity may cause some issues if a pure stream of hydrogen is required, as purification would affect the pressure limits, well flow rates, and storage capacity which in turn would have an effect on the economics of the storage site.

Chapter 5 An open-source tool for the calculation of field deliverability and cushion gas requirements in volumetric gas reservoir storage sites

The full code is available in Appendix 5.

5.1 Introduction

Recent studies have investigated the regional potential of porous rocks for hydrogen storage (Heinemann *et al.* 2018a; Gasanzade *et al.* 2021; Mouli-Castillo *et al.* 2021; Scafidi *et al.* 2021). However the cushion gas proportion (the volume of gas that must remain in the reservoir to maintain the pressure and allow a certain minimum deliverability) has to be assumed in most cases based on figures given in the literature. These range from 22% for one reservoir simulation study (Sainz-Garcia *et al.* 2017) to two thirds or more in a general study (Foh *et al.* 1979). As these estimates either tend to be for specific reservoirs under specific conditions in the case of reservoir simulations or very vague and generalised in the case of general studies they are unsuitable for use in regional capacity estimates. There exists therefore a gap between regional capacity estimates, estimates based on reservoir engineering (Amid *et al.* 2016) and reservoir simulation studies of individual fields (Pfeiffer and Bauer 2015; Feldmann *et al.* 2016; Pfeiffer *et al.* 2016, 2017; Sainz-Garcia *et al.* 2017; Luboń and Tarkowski 2020; Lysyy *et al.* 2021) into which a method for more reliable cushion gas volume estimates fits.

This gap between static capacity estimates using basic reservoir data and dynamic capacity estimates using reservoir simulation can be filled by estimating well performance through the use of the laminar-inertial-turbulent (or LIT) equations (Houpeurt 1959) (sometimes known as the Forchheimer equation) along with outflow or tubing performance equations. Using the LIT and outflow equations, the plateau rate (well flow rate which can be held constant for a given amount of time) can be calculated and from this the cushion gas requirement determined. The model has been validated using data from real gas storage facilities and can therefore be applied to potential sites with a reasonably high level of confidence. The only data required for the calculations is the original reservoir pressure, average permeability, average porosity, formation thickness, depth, gas initially in place, and reservoir temperature: the same data that is generally used to make regional estimates and exists in databases such as CO_2Stored (Bentham *et al.* 2014).

The following chapter will describe the equations used to build a program which calculates the inflow/outflow performance of gas storage sites and determines the cushion gas requirements. The equations are given in field units for two reasons: firstly to avoid the need for conversion factors in the equations which make checking them against the original references difficult for those who wish to scrutinise the method further or replicate it, and secondly because these units are in common use in the oil and gas industry to whom this tool will be of most value. The program is validated using data from four different gas reservoirs of varying size, depth, and pressure: Cousland (UK), Hatfield Moors (UK), Rough (UK), and Grijpskerk (Netherlands). Of these, Hatfield Moors, Rough, and Grijpskerk have all been used for seasonal gas storage, and Cousland has been investigated for hydrogen storage in chapter 4 of this thesis. Table 15 shows the input variables for these fields.

Table 15: input variables for the four differnt fields used to test the inflow/outflow performance program

field	**reservoir pressure**	**permeability**	**porosity**	**thickness**	**depth**	**GIIP**	**temperature**	**ref.**
	[psia]	[mD]	[frac]	[ft]	[ft]	[MMSCF]	[Rankine]	
Grijpskerk	5700	25	0.15	590	11220.5	381000	702.27	(Juez-Larré *et al.* 2016)
Cousland	660	70	0.15	48	1582	870	527.67	This thesis
Rough	4533	75	0.125	95	9000	366000	656.67	(Stuart 1991)
Hatfield Moors	650	143.2	19.1	57.5	1400	6100	527.67	(Ward *et al.* 2003)

This program can be used to estimate the working and cushion gas volumes, expected flow rates, and well performance of closed gas reservoirs. This study modelled methane and hydrogen storage but the program can be adjusted for other gases and gas mixes.

The inflow/outflow model was created in Python (Van Rossum and Drake 2009) utitlising the open-source thermophysical property library CoolProp (Bell *et al.* 2014) which implements the full capabilities of NIST REFPROP (National Institute of Standards and Tehcnology Standard Reference Fluid Thermodynamic And

Transport Properties Database) from the U.S. Department of Commerce (Lemmon *et al.* 2013). The full python code is included in Appendix 5.

5.2 Methods

5.2.1 Fluid property modelling

CoolProp (Bell *et al.* 2014) is used to calculate the compressibility factors and viscosities of both hydrogen and methane in this study. The viscosity correlation used for hydrogen is that of Muzny et al. (Muzny *et al.* 2013), and the density and compressibility is calculated using the equation of state of Leachman et al. (Leachman *et al.* 2009). For methane, the viscosity correlation used is that of Quiñones-Cisneros and Deiters (Quiñones-Cisneros and Deiters 2006), and the density and compressibility is calculated using the equation of state of Setzmann and Wagner (Setzmann and Wagner 1991).

5.2.2 Well inflow performance model

The following methods for calculating the theoretical deliverability of a gas well are based on the methods outlined in chapter 4 Lee and Wattenbarger (1995). We use the theoretical LIT (laminar-inertial-turbulent) equations developed by Houpert (1959) which are exact solutions to the generalized radial-flow diffusivity equation. These equations account for variation of fluid properties and non-Darcy flow and so are suitable for gas inflow performance at all reservoir pressures. The pseudosteady-state inflow equation is:

$$p_p(\bar{p}) - p_p(p_{wf}) = aq_g + bq_g^2$$

Where $p_p(\bar{p})$ is the real-gas pseudopressure at the average reservoir pressure, $p_p(p_{wf})$ is the real-gas pseudopressure at bottom hole flowing, a is a coefficient that includes the Darcy flow and skin effects with the units [(psia^{2}cP)/(MMSCF/d)], b is the non-Darcy flow coefficient with the units [(psia^{2}cP)/(MMSCF/d)^2], and q_g is the gas flow rate at surface conditions with the units MMSCF/D.

Pseudopressure is an integral function introduced by Al-Hussainy et al. (Al-Hussainy *et al.* 1966a) which accounts for changes in compressibility and viscosity of a gas with pressure and allows for the solving of flow equations without the limiting assumption of gas properties remaining constant with pressure. It is defined as:

$$p_p(p) = 2\int_{p0}^{p} \frac{p}{\mu Z} \Delta p$$

Where $p_p(p)$ is pseudopressure (units psia^2/cp), p is the pressure, μ is the viscosity at pressure p, Z is the compressibility at p, and $p0$ is an arbitrary base pressure (1 psi in this model). A full description with example data of how to calculate pseudopressure using the trapezoidal method is given in the appendix of Al-Hussainy and Ramey (1967).

Parameter a, related to the drainage area, reservoir thickness and permeability, and skin factor is pressure independent. This equation form is for a circular drainage area with a well in the middle (Houpeurt 1959):

$$a = \frac{1.422 \times 10^6 T}{k_g h}\left[1.151\log\left(\frac{10.06A}{C_A r_w^2}\right) - \frac{3}{4} + s\right]$$

Where T is the reservoir temperature in degrees Rankine (°R), k_g is the formation's permeability to gas in millidarcies (mD), h is the formation thickness in feet (ft), A is the drainage area in feet^2 (ft^2), C_A is the Dietz shape factor with a value of 31.62 for a circular drianage area with a well in the middle, r_w is the wellbore radius in feet (ft), and s is the skin factor.

Parameter b reflects the non-Darcy flow effect and is dependent on pressure though the gas viscosity (Houpeurt 1959):

$$b = \frac{1.422 \times 10^6 TD}{k_g h}$$

Where T is the reservoir temperature in degrees Rankine (°R), k_g is the formation's permeability to gas in millidarcies (mD), h is the formation thickness in feet (ft), and D is the non-Darcy coefficient which accounts for the inertial and turbulent flow effects which results from the high gas velocities near the wellbore.

Parameter D is the non-Darcy flow factor which is inversely proportional to the viscosity at the bottom hole pressure (Houpeurt 1959):

$$D = \frac{2.715 \times 10^{-12} \beta k_g M p_{sc}}{h \mu_g (p_{wf}) r_w T_{sc}}$$

where k_g is the formation's permeability to gas in millidarcies (mD), h is the formation thickness in feet (ft), μ_g is the gas viscosity in centipoise (cP) evaluated at p_{wf}, M is the molecular weight of the gas or gas mixture, p_{sc} is the pressure at standard conditions (14.5038 psi), p_{wf} is the bottom hole flowing pressure in psi, r_w

is the wellbore radius in feet (ft), T_{sc} is the temperature at standard conditions in degrees Rankine (491.67 °R), β is the inertial coefficient (Jones 1987) given by

$$\beta = 1.88 \times 10^{10} k^{-1.47} \phi^{-0.53}$$

Where k is the permeability in millidarcies (mD), and ϕ is the porosity (fraction).

To find the gas flow rate we rearrange the pseudosteady-state inflow equation to give:

$$\mathrm{q_{sc}} = \frac{-a + \sqrt{a^2 + 4b\left[p_p(\bar{p}) - p_p(p_{wf})\right]}}{2b}$$

5.2.3 Well outflow performance model

The outflow performance was calculated by computing the bottom hole flowing pressure (BHFP) using the average temperature and compressibility method outlined in chapter 4 of Lee and Wattenbarger (1995). This method considers the wellhead pressure, energy losses from friction between the gas and the tubing, and the weight of the gas column. The average temperature and compressibility method assumes that the temperature and compressibility can be represented by the average values of surface and bottom hole temperatures and pressures. The average temeprature and viscosity are required to determine the compressibility and are obtained by an initial estimate followed by iteration until convergence. This process can require more than one iteration and is outlined below:

1. An approximation of the BHFP is required to start:

$$p_{wf} \approx p_{tf} + 0.25\left(\frac{p_{tf}}{100}\right)\left(\frac{L\cos\,\theta}{100}\right)$$

Where p_{wf} is the bottom hole flowing pressure (BHFP) in psi, p_{tf} is the wellhead flowing pressure in psi (in this model it is set to 50% of the reservoir pressure but is adjustable), L is the length of the tubing in feet (ft), and θ is the angle of the well (in this study the well is assumed to be veritcal; θ = 0°).

2. The arithmetic average of the wellbore pressure and temperature are calculated using the temperature and pressure at bottom hole and wellhead.
3. The average compressibility and viscosity are calculated using the average pressure and temperature of the wellbore calculated in step 2.

4. Calculate the Reynold's number which is the dimensionless ratio of fluid inertial forces to the viscous forces and is used to determine the nature of the flow regime

$$N_{\mathrm{Re}} = \frac{20\gamma_g q_g}{\mu_g \mathrm{d}}$$

Where N_{Re} is the Reynold's number (dimensionless), γ_g is the specific gravity of the gas (air = 1), q_g is the gas flow rate in thousands of cubic feet per day (MSCF/d), μ_g is the viscosity in centipoise (cP), and d is the pipe diameter in inches (in).

5. Depending on the value of the Reynold's number, the Moody friction factor is calculated in one of two ways:

Where the Reynold's number is less than or equal to 2000 the flow is characterised as laminar and the Moody friction factor is inversely proportional to it:

$$f = 64/N_{\mathrm{Re}}$$

Where f is the Moody friction factor, and N_{Re} is the Reynold's number (dimensionless).

Unstable flow occurs where the Reynold's number is between 2000 and 4000, and above 4000 the flow is determined to be fully turbulent. In this study we use the correlation by Swamee and Jain (1976) for unstable and turbulent conditions where the Reynold's number is higher than 2000:

$$f = 4\left[2.28 - 4\log\left(\frac{\varepsilon}{d} + \frac{21.25}{N_{\mathrm{Re}}^{0.9}}\right)\right]^{-2}$$

Where f is the Moody friction factor, ε is the pipe roughness in inches (assumed to be 0.0006 inches in this study), d is the pipe diameter in inches (in), and N_{Re} is the Reynold's number (dimensionless). The model will print the flow regime as it iterates.

6. The BHFP is calculated using the following equation as per Lee and Wattenbarger (1995)

$$p_{wf}^2 = p_{tf}^2 e^s + \frac{6.67 \times 10^{-4} q_g^2 f \bar{T}^2 \bar{z}^2}{d^5 \cos\,\theta}(e^s - 1)$$

Where p_{wf} is the bottom hole flowing pressure (BHFP) in psi, p_{tf} is the wellhead flowing pressure in psi (in this model it is set to 50% of the reservoir pressure but is

adjustable), q_g is the gas flow rate at surface conditions with the units MMSCF/D, f is the Moody friction factor, $\bar{T}$ is the average temperature in degrees Rankine (°R) calculated in step 2, $\bar{z}$ is the average compressibility factor calculated in step 2, d is the pipe diameter in inches (in), e is the natural logarithmic base, θ is the angle of the well (in this study the well is assumed to be veritcal; θ = 0°), and s is the average temperature and compressibility factor method parameter defined as follows after Lee and Wattenbarger (1995):

$$s = \frac{0.0375\gamma_g L\cos\,\theta}{\bar{z}\bar{T}}$$

Where γ_g is the specific gravity of the gas (air = 1), L is the length of the tubing in feet (ft), θ is the angle of the well (in this study the well is assumed to be veritcal; θ = 0°), $\bar{z}$ is the average compressibility factor calculated in step 2, and $\bar{T}$ is the average temperature in degrees Rankine (°R) calculated in step 2.

7. The model then iterates on steps 2 to 6 until p_{wf} converges with a tolerance of 0.5%.

5.2.4 Erosional velocity

In order to prevent a loss of thickness in the wall of the wellbore through corrosion and erosion associated with high fluid velocities, sand production, and the presence of corrosive contaminants such as CO_2, the erosional velocity should be considered. The erosional velocity limit is normally determined through in field testing, however the American Petroleum Institute (American Petroleum Institute 1991) published a simple equation to determine an approximate value:

$$V_e = \frac{c}{\sqrt{\rho_m}}$$

Where V_e is the erosional velocity in feet per second (ft s^{-1}), c is an empricial constant that has values of 100 for continous service and 150 for intermittent service (this model assumes the well is used intermittently for seasonal storage), ρ_m is the fluid density at flowing pressure and temperature in pounds per cubic foot (lbs ft^{-3}). This equation has limits to its accuracy and conditions where it can be used (Madani Sani *et al.* 2019) however, it is used in this study as an indication of whether theoretical well flow rates are unreasonably high.

5.2.5 Gas initially in place (GIIP) adjustments

GIIP is given in the input data from the literature. It is assumed to be 100% methane. For hydrogen, the expansion factors are calculated for both methane and hydrogen and the expansion factor ratio is used to adjust the GIIP, which assumes it is 100% hydrogen (Guo 2019)

$$e = 35.3 \times \frac{P}{Z \times T}$$

Where e is the expansion factor, P is the reservoir pressure in psia, Z is the gas compressibility factor at reservoir conditions, and T is the reservoir temperature in Rankine (°R).

5.2.6 Plateau rate calculation

The plateau rate is the constant flow rate that can be maintained for a given length of time and is calculated using the following equation from Juez-Larré *et al.* (2016):

$$Q_p = \frac{1}{\left(\frac{1}{Q_{ini}}\right) + \left(\frac{T_p}{GIIP}\right)}$$

Where Q_p is the plateau rate in MMSCF/D is, T_p is the number of days of constant production, Q_{ini} is the initial gas low rate in MMSCF/D (assumed to be the operating rate where the inflow and tubing performance curves intersect), and $GIIP$ is the gas initially in place in MMSCF. In this study it is assumed that a seasonal gas storage will need to deliver at a constant flow rate for 90 days, however this can be changed in the input file. Therefore this equation will give the maximum flow rate acheivable for this time for the reservoir.

5.2.7 Working and cushion gas volume calculations

It is assumed that 10% of the GIIP is unrecoverable and it is therefore excluded from working and cushion gas volume calculations, as recovery factors of 90% are achievable from volumetric gas reservoirs (Lee and Wattenbarger 1995). The working gas capacity is given by:

$$V_{gw} = Q_p \times T_p$$

Where V_{gw} is the working gas volume in MMSCF, Q_p is the plateau rate in MMSCF/D, and T_p is the number of days of constant production. The cushion gas volume is given by:

$$V_{gc} = (GIIP \times 0.9) - V_{gw}$$

Where V_{gc} is the cushion gas volume in MMSCF, V_{gw} is the working gas volume in MMSCF, $GIIP$ is the gas initially in place in MMSCF, and 0.9 is the recoverable gas in the reservoir.

5.2.8 Well power capacity calculation

It is useful when comparing hydrogen and methane wells to not only consider the flow rates but the flow of energy. The model computes the power capacity of each well from its 90 day plateau rate using the higher heating value (HHV, for values used see Table 16) of each gas.

$$W_P = (\frac{q_g * 10^6}{35.315}) * \rho * (HHV * 0.001)/24$$

Where W_P is the well power capacity in megawatts (MW), q_g is the flow rate in MMSCF/D (10^6 converts from million cubic feet to cubic feet and 35.315 converts to m^3), ρ is the density of the gas in kg/m^3 at surface conditions (as calculated in CoolProp), HHV is the higher heating value of the gas in kWh (0.001 converts to MWh), and 24 converts from MWh per day to MW.

5.2.9 Well performance forecasting

All the above calculations are performed at decreasing reservoir pressures in order to forecast well performance. It is then possible to do step-wise calculations of gas produced in order to determine the natural flow rate over time of the reservoir as per the methods in chapter 4 of Lee and Wattenbarger (1995).

5.2.10 Model assumptions

The model assumptions are described in Table 16 below which shows the assumption, the value where applicable, and whether or not it can be adjusted in the model. Where the adjustable column simply says no, code would need to be added in order to change it.

Table 16: assumptions used in the inflow/outflow performance program

assumption variable	assumed value	adjustable in model?
skin	1	yes
P_{wh} (wellhead pressure)	P_r (reservoir pressure) * 0.3	yes
r_e (effective radius)	1500m (4920ft)	yes
pipe roughness	1.524e-5 metres (0.0006 inches)	yes
gas recovery factor	0.9	yes
Dietz shape factor	31.62	yes
H_2 HHV (higher heating value)	39.4 kWh/kg	yes
CH_4 HHV (higher heating value)	15.4 kWh/kg	yes
c factor (erosional velocity eq.)	150 for intermittent service	yes
gas injection	not considered - assumed reservoir can be fully refilled in the other 275 days of the year	no
plateau rate time	90 days	yes adjustable in input files
pure gases	n/a	no
no temperature changes during production	n/a	no
net:gross	1	no - adjust reservoir thickness in input file to account for changes

5.2.11 Summary of model calculations

The model generates a range of pressures from 1 psi up to the inputted reservoir pressure in 1 psi increments. It then uses the inputted temperature and each pressure increment to calculate the viscosity, density, and compressibility using the CoolProp python package (Bell *et al.* 2014) as detailed in the fluid properties section above. From this, the pseudopressure is calculated using the trapezoidal method (Al-Hussainy and Ramey 1967). Then, the inflow performance is calculated using the pseudosteady state equation method of Houpeurt (Houpeurt 1959). For the

tubing performance, the average temperature and compressibility factor method is implemented and iterated over until it converges. The erosional velocity, plateau rate, working and cushion gas volumes are then calculated. The whole process is repeated for several different initial reservoir pressures and the timestep calculations are performed.

All the data is then saved as csv (comma separated value) files. The inflow performance, tubing performance, and erosional velocity are all plotted in graphs and the operating point where the inflow and tubing performance curves intersect is calculated and labelled. The well performance forecast is also plotted from the timestep calculations. The model then automatically names and saves these plots as png files.

5.3 Model validation

The model was validated against natural gas storage data from three real gas storage sites: Hatfield Moors (UK), Rough (UK), and Grijpskerk (Netherlands), and the Cousland (UK) gas field which was investigated in detail through reservoir simulation and a reservoir engineering study in chapter 4 of this thesis. These sites differ in size and pressure by orders of magnitude (see Table 15) with Cousland being by far the smallest and Grijpskerk the largest.

For natural gas, the Grijpskerk gas storage in the Netherlands has a reported cushion gas requirement of 88.5% (Juez-Larré *et al.* 2016): the model outputs a CH_4 cushion gas requirement of 88.6% for a single well scenario with 8 inch tubing. Modelling work on the gas storage potential of Griijpskerk by Juez-Larré *et al.* (2016) found a single well withdrawal rate of 7.6 million Sm^3/day (268.4 MMSCF/d) for 7 inch tubing for natural gas: the model also outputs a single well withdrawal rate for Grijpskerk of 7.6 million Sm^3/day (269.4 MMSCF/d) which is within the rounding error of conversion between cubic metres and cubic feet. Hatfield Moors has 7 inch tubing and two horizontal wells (Ward *et al.* 2003) with a natural gas cushion gas requirement of 66.7% (Chaudry *et al.* 2008): the model outputs a cushion gas requirement of 67.6% for a two well scenario with 8 inch tubing for CH_4. The Rough gas storage facility used up to 30 wells (Stuart 1991; Competition & Markets Authority 2017) and an unknown tubing size with a natural gas cushion gas requirement of 64.2% (Chaudry *et al.* 2008): the model outputs a cushion gas requirement of 35.0% for a 30 well scenario with 8 inch tubing and a cushion gas requirement of 69.6% for a 30 well scenario with 2 inch tubing. A 2016 reservoir

engineering study on hydrogen storage at the Rough gas field (Amid *et al.* 2016) found a cushion gas requirement for natural gas of around 70%. The discrepancies between the real reported cushion gas requirement and this study are likely due to uncertainties around the number of wells in use on average at the Rough gas storage facility as well as the well diameter. The Cousland gas field was never used for gas storage however it was estimated in the chapter 4 of this thesis that the cushion gas requirement would be greater than 50% when hydrogen is injected above the existing natural gas in the field using 2 inch tubing. The model outputs a cushion gas requirement of 63.2% with a single well using 2 inch tubing for CH_4 and a cushion gas requirement of 53.2% with a single well using 2 inch tubing for H_2.

5.4 Results and discussion

The full output of the model run is available in the data package with a summary available in Appendix 5 and consists of a table of the results for each field by gas, number of wells, and well diameter. The results discussed here will focus on the cushion gas requirements for the different scenarios and the energy flows from the wells. The low, medium, and high scenarios referred to are the number of wells in each run which are given in Table 17:

Table 17: Number of wells in each scenario

	scenario			
Field	low	medium	high	source
Grijpskerk	5	11	20	https://www.nlog.nl/datacenter/field-overview
Rough	15	30	45	https://assets.publishing.service.gov.uk/media/5a30ff94ed915d2cf25281 final-decision.pdf
Cousland	1	2	3	thesis
Hatfield Moors	1	2	4	https://doi.org/10.1144/GSL.MEM.2003.020.01.76

5.4.1 Plateau rates and cushion gas requirement

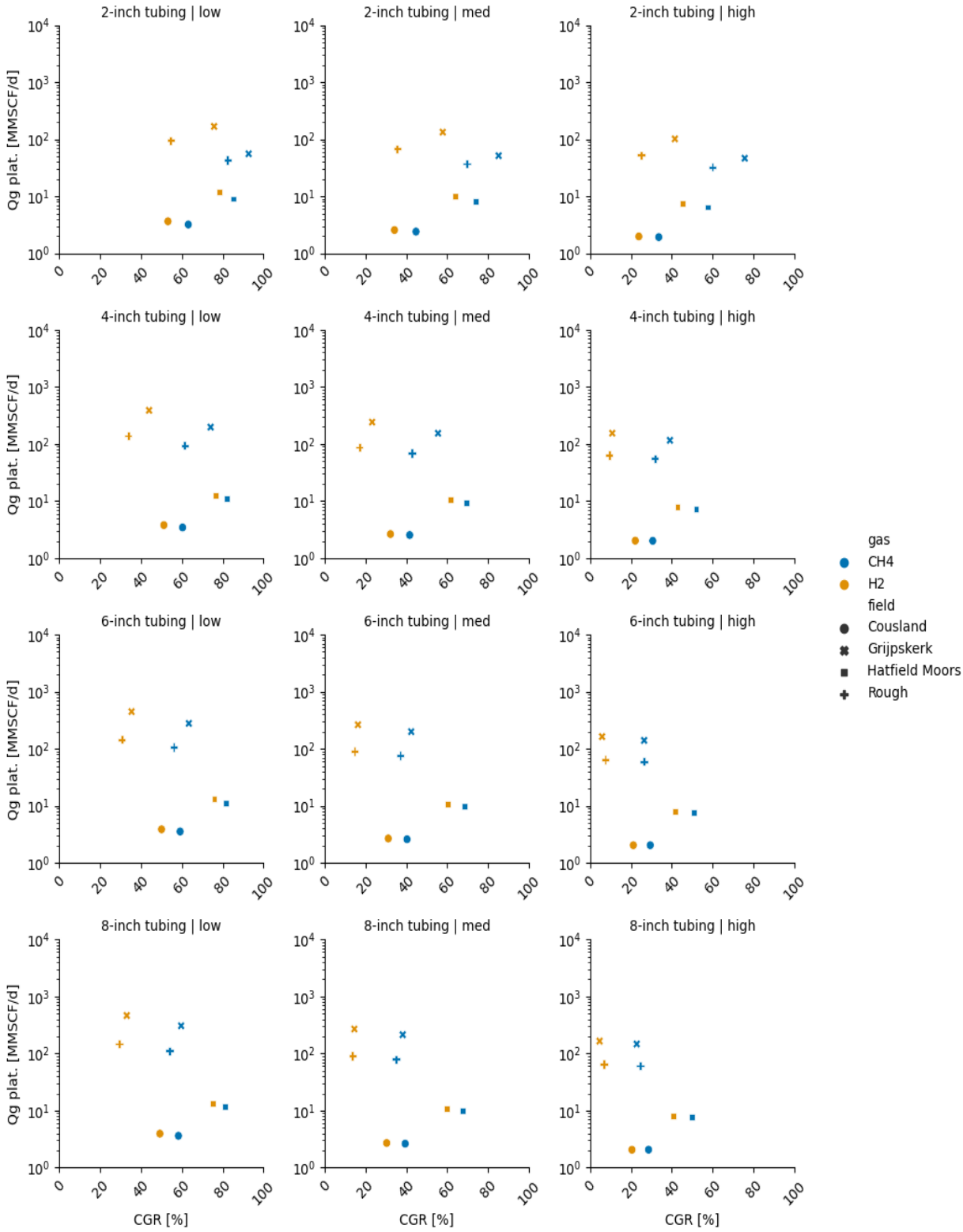

Figure 71: Plateau flow rate of individual wells [MMSCF/d] vs. the cushion gas requirement [%] for each of the three well scenarios (low, med, high) and the four different tubing sizes (2, 4, 6, 8 inches). The y-axis is the flow rate on a log scale and the x-axis is the cushion gas requirment on a linear scale. Blue indicates the datapoint is for CH_4 and gold/yellow indicates H_2. Gas fields are differentiated by shape as per the legend: Cousland is a filled circle, Grijpskerk is a diagonal cross, Hatfield Moors is a square, and Rough is a vertical/horizontal cross. The key trends are that cushion gas requirements decrease with increasing numbers of wells and increasing sizes of tubing.

Figure 71 shows the individual well flow rate vs the cushion gas requirement for each of the three well scenarios low, med, and high, with the four different tubing sizes 2, 4, 6, and 8 inches. The two different colours represent the values for hydrogen and methane, and the different symbols are for the four different gas fields: Cousland, Grijpskerk, Hatfield Moors, and Rough. The results are displayed in this manner in order to highlight the effects of changing the variables, in this case the number of wells (Table 17), diameter of the tubing, and type of gas. From left to right shows the effect of increasing the number of wells, and top to bottom shows the effect of increasing the diameter of the tubing. The y-axis scale for flow rates is logarithmic in order to display the results from all the gas fields simultaneously on each graph.

There are several trends to be observed which will be discussed below. Firstly, hydrogen flow rates are higher than those for methane in each scenario for each field and so appear higher on the y-axis. Hydrogen cushion gas requirements are also lower than those for methane in all scenarios for all fields. Increasing the number of wells (going from left to right across the three columns in Figure 71) does two things: firstly, it decreases the cushion gas requirement for both methane and hydrogen scenarios, with a larger decrease for hydrogen scenarios . Secondly it reduces the flow rate of the wells slightly with the hydrogen flow rates showing a larger decrease than methane flow rates. Increasing the diameter of the tubing (going from top to bottom in Figure 71) also has two effects: the first is to increase the well flow rates and the second is the reduce the cushion gas requirement. If we compare the two end members in this series of scenarios (2-inch tubing low and 8-inch tubing high) we can see that the cushion gas requirement is reduced significantly for all fields with the hydrogen scenario for Grijpskerk showing the biggest decrease from 75.8% for the 2-inch tubing low scenario to 4.6% for the 8-inch tubing high scenario.

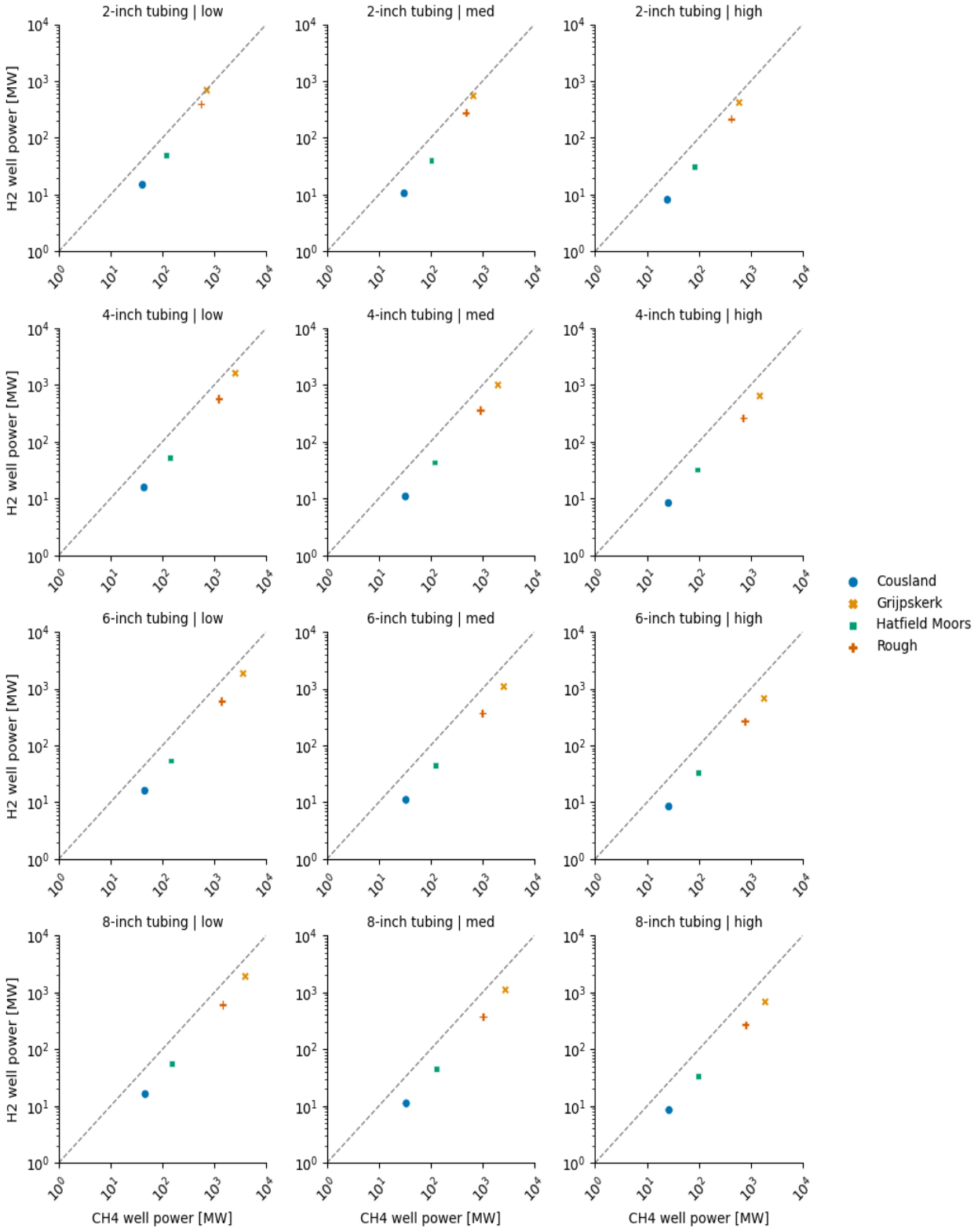

Figure 72: A log-log plot of power delivered by a single H_2 well [MW] vs power delivered by a single CH_4 well [MW] for each of the three well scenarios (low, med, high) and the four different tubing sizes (2, 4, 6, 8 inches). Fields are differentiated by coloured symbols: Cousland is a blue filled circle, Grijpskerk is a gold/yellow diagonal cross, Hatfield Moors is a green square, and Rough is a red vertical/horizontal cross. The dashed grey lines show where the well power for each gas would be equal. Key trends are that increasing the number of wells decreases the power delivered by a single well, whereas increasing the tubing size increases the power delivered by a single well.

Figure 72 shows the power delivered by a single well during the 90-day plateau rate for hydrogen (y-axis) vs methane (x-axis) scenarios for each of the three well scenarios low, med, and high, with the four different tubing sizes 2, 4, 6, and 8 inches. The four different fields (Cousland, Grijpskerk, Hatfield Moors, and Rough) are shown by different coloured symbols.

The results are displayed in this manner in order to highlight the effects of changing the variables, in this case the number of wells and the diameter of the tubing. From left to right shows the effect of increasing the number of wells, and top to bottom shows the effect of increasing the diameter of the tubing. The x and y axes scales are logarithmic in order to display the results from all the gas fields simultaneously on each graph. The dashed grey line on each graph represents the values at which the hydrogen and methane well powers are equal and shall be referred to as the line of equality from hereon in.

The trends in this figure are subtle but can be described as follows. Increasing the number of wells (going from left to right across the three columns Figure 72) has the effect of reducing the power delivered by a single well for both hydrogen and methane wells but there is a larger decrease for hydrogen wells which pushes the values further below the line of equality. Increasing the size of the tubing (going from top to bottom in Figure 72) has the effect of increasing the individual well power for both hydrogen and methane but at a slightly higher rate for methane. The lowest ratio of H_2 well power to CH_4 well power is for the high wells scenario with an 8-inch tubing in the Cousland field where the H_2 well power is only 31.9% of the CH_4 well power. The highest ratio belongs to the Grijpskerk field in the low wells scenario with 2 inch tubing where H_2 well power is 96.8% of the CH_4 well power.

5.4.2 *Field power – total flow rates of all wells in terms of energy delivered*

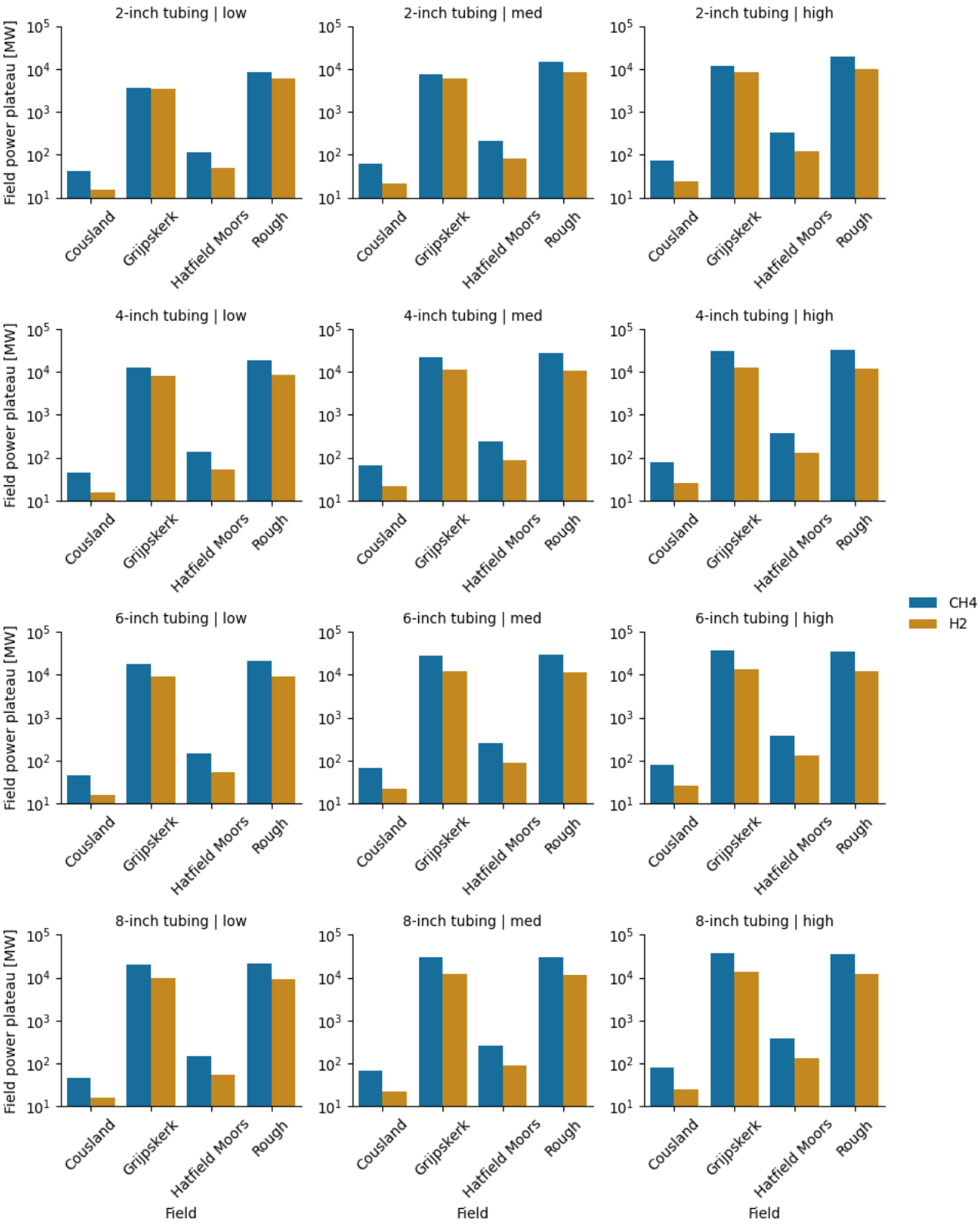

Figure 73: Total field power at plateau rate [MW]. Blue shows results for CH_4 and gold/yellow shows results for H_2. Key trends are that increasing the number of wells increases the total field power, as does increasing the tubing size.

The total field deliverability in terms of well power for each of the scenarios is shown in Figure 73. Increasing the number of wells (going from left to right across the three columns in Figure 73) increases the total field deliverability, as does increasing the size of the tubing. The differences between hydrogen and methane in the rates at which the deliverability increases is more apparent in Figure 73 than in Figure 72 with the most apparent example that of Grijpskerk which in the 2-inch tubing low scenario shows that hydrogen and methane are capable of delivering almost the same power at 3572 MW for CH_4 and 3459 MW for H_2 , whereas in the 8-inch high scenario the same field shows 37850 MW for methane which is 2.8 times as high as the 13635 MW for hydrogen.

5.4.3 Sensitivity analysis

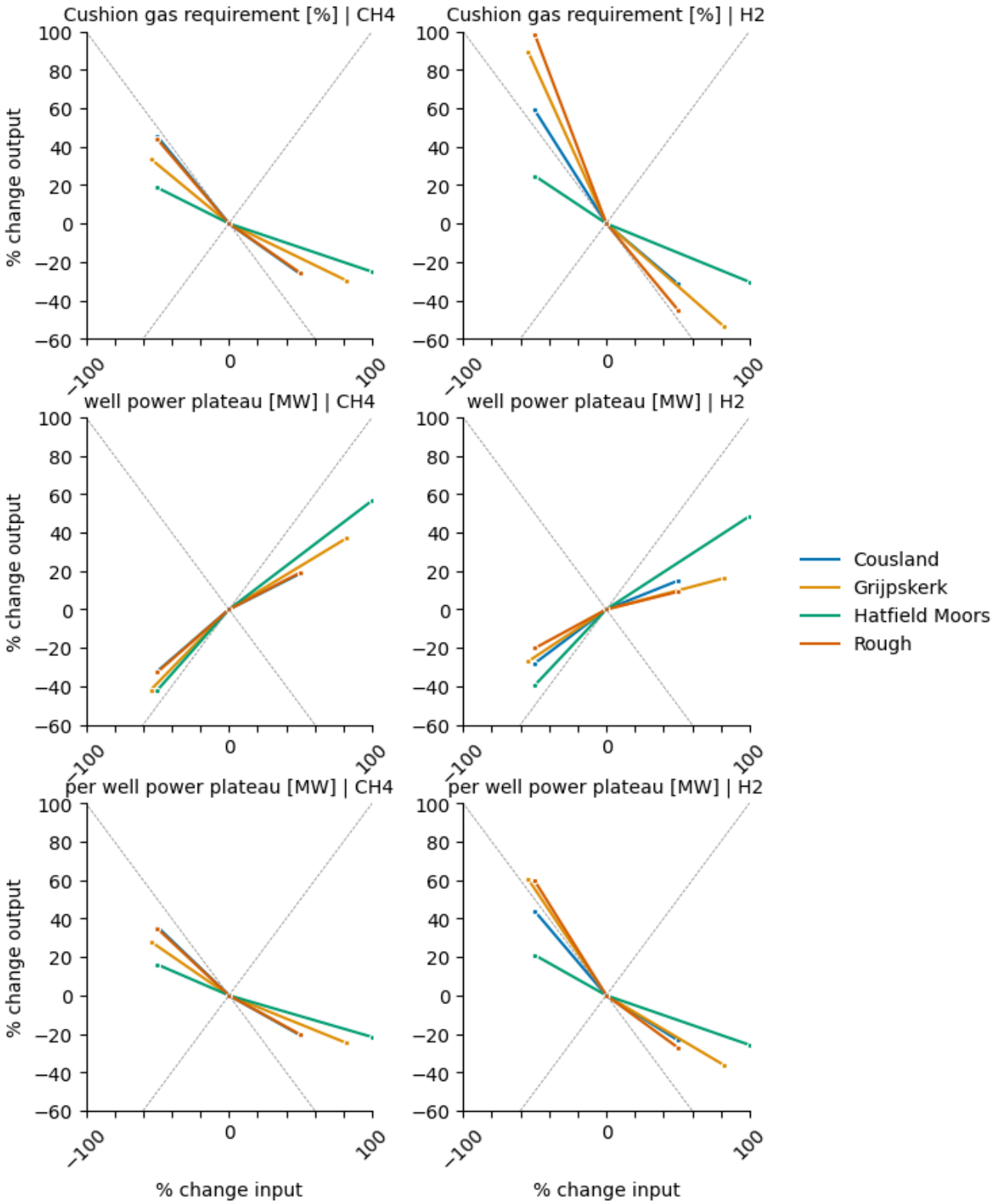

Figure 74: Sensitivity plots for the three different number of well scenarios (low, med, high). Left and right columns are CH_4 and H_2 respectively. Top row shows the effect on cushion gas requirement [%], middle row shows the effect on total well power/total field power at plateau rate [MW], and the bottom row shows the effect on individual well power at plateau rate [MW]. Fields are differentiated by colour: Cousland is blue, Grijpskerk is gold/yellow, Hatfield Moors is green, and Rough is red/orange. Grey dashed lines indicate an equal relationship between change in input and change in output. Key trends are described in the text.

Figure 74 shows the sensitivity analysis for the different numbers of wells in each scenario with the x-axis showing the percentage change of wells from the base case and the y-axis showing the percentage change of the three different outputs from the base case. The graphs are split as follows: the top row shows the effect of changing the number of wells on the cushion gas requirement, the middle row shows the effect of changing the number of wells on the field plateau rate in energy terms (labelled as well power plateau [MW] i.e. the total power of all wells combined), and the bottom row shows effect of changing the number of wells on the individual well plateau rate in energy terms. The left hand column of the figure shows the results for CH_4 and the right hand column of the figure shows the results for H_2. The fields are differentiated by colour and the results shown as points connected by lines. The light grey dashed lines show where there would be a 1:1 effect e.g. a 10% change in the input results in a 10% change of the output.

The relationship between the number of wells and the change in cushion gas requirement is not linear according to Figure 74. Decreasing the number of wells has a bigger impact on the cushion gas requirement than increasing the number of wells which can be seen from the steeper lines to the left of zero on the x-axis. The general trend is that less wells means a larger cushion gas requirement. The opposite goes for the field plateau rate in energy terms, with less wells reducing the rate from the base case at a greater rate than increasing the number of wells increases it. Finally, the individual well plateau rate in energy terms increases with less wells and decreases at a slower rate with more wells. The individual fields show a considerable range of differences in (10s of%) for each of the different outputs with hydrogen showing a much greater spread between fields, but all follow the aforementioned trends.

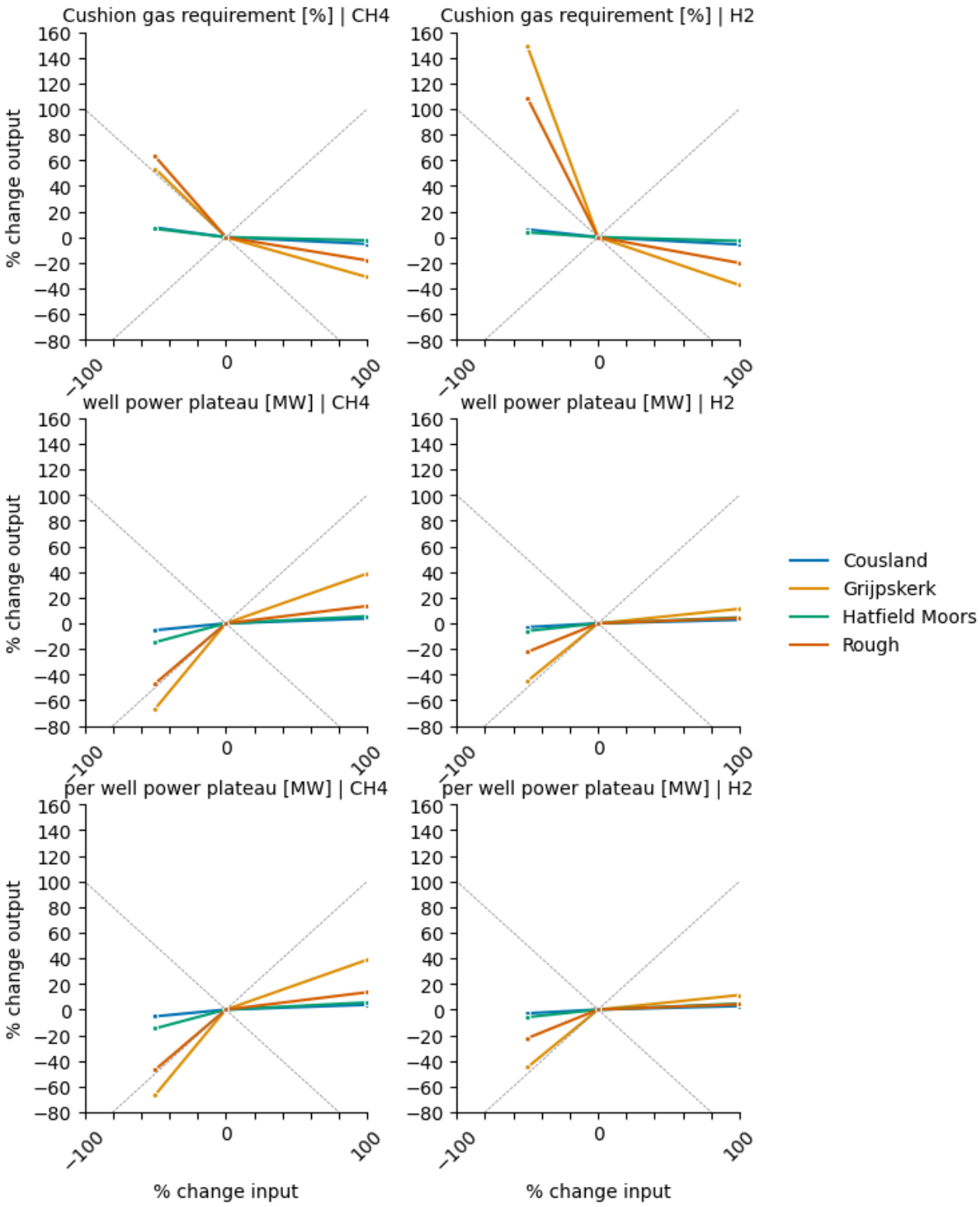

Figure 75: Sensitivity plots for three different tubing sizes (2, 4,and 8 inches).Left and right columns are CH_4 and H_2 respectively. Top row shows tthe effect on cushion gas requirement [%], middle row shows the effect on total well power/total field power at plateau rate [MW], and the bottom row shows the effect on individual well power at plateau rate [MW]. Fields are differentiated by colour: Cousland is blue, Grijpskerk is gold/yellow, Hatfield Moors is green, and Rough is red/orange. Grey dashed lines indicate an equal relationship between change in input and change in output. Key trends are described in the text.

Figure 75 shows the sensitivity analysis for the different sizes of tubing in each scenario with the x-axis showing the percentage change of wells from the base case and the y-axis showing the percentage change of the three different outputs from the base case. The graphs are split as follows: the top row shows the effect of changing the tubing size on the cushion gas requirement, the middle row shows the effect of changing the tubing size on the field plateau rate in energy terms (labelled as well power plateau [MW] i.e. the total power of all wells combined), and the bottom row shows effect of changing the tubing size on the individual well plateau rate in energy terms. The left hand column of the figure shows the results for CH_4 and the right hand column of the figure shows the results for H_2. The fields are differentiated by colour and the results shown as points connected by lines. The light grey dashed lines show where there would be a 1:1 effect e.g. a 10% change in the input results in a 10% change of the output.

Decreasing the tubing size in the wells reduces both the individual and field scale plateau rates in energy terms, and increases the cushion gas requirements. This is true for all fields and both CH_4 and H_2. However there is a significant difference between the two pairs of fields Cousland and Hatfield Moors, and Grijpskerk and Rough. The former show an almost linear relationship across the different outputs whereas the latter fo not with great increases seen with a reduction in tubing size than with an increase in tubing size. The tubing size also seems to have a much greater effect on the cushion gas requirement than the number of wells did, with a reduction from 4 to 2 inches resulting in a 150% increase in the Grijpskerk H_2 scenario and a 110% increase shown for the Rough H_2 scenario.

5.4.4 Cushion gas requirement – H_2 vs CH_4

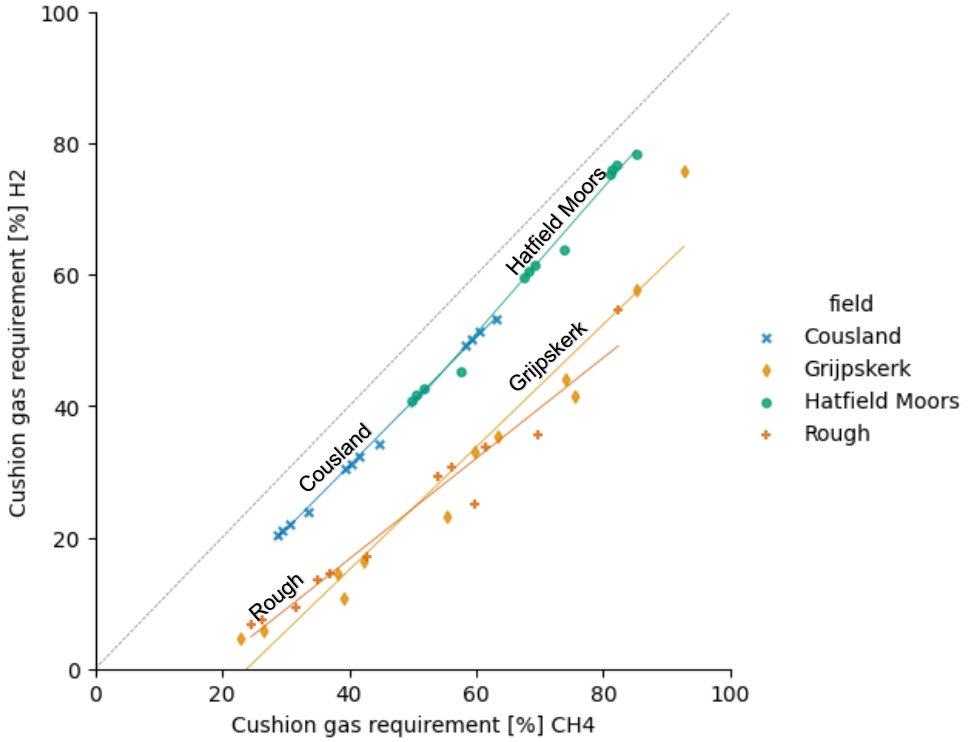

Figure 76: Cushion gas requirement for H_2 [%] vs cushion gas requirement for CH_4 [%]. Data is represented by markers with trendlines added. Fields are differentiated by colour: Cousland is blue diagonal crosses, Grijpskerk is gold/yellow elongted diamonds, Hatfield Moors is green filled circles, and Rough is red/orange vertical crosses. Grey dashed line indicates a 1:1 ratio bewtween H_2 cushion gas requirment and that of CH_4. Key trends are that H_2 requires a lower proportion of cushion gas than CH_4 with the larger fields (Grijpskerk and Rough) showing this trend more storngly than the smaller fields (Cousland and Hatfield Moors).

Figure 76 shows the cushion gas requirement percentage for both hydrogen and methane plotted against each other for all the different scenarios, categorised by field in the same colours as used for the previous plots. The crosses indicate the data points and the lines show the trends, with the grey dashed line showing where the cushion gas requirement for H_2 is equal to that for CH_4. The Cousland and Hatfield Moors fields are closer to this line of equality than the Grijpskerk and Rough fields and show almost identical trends with a ratio of around 1.5:1 between CH_4 and H_2. The Grijpskerk and Rough fields also occupy a similar part of the graph with a ratio of around 2:1 between CH_4 and H_2, however the Grijpskerk trend is similar to those of Cousland and Hatfield Moors, whereas the trend for Rough is slightly shallower.

5.4.5 Insights from the test data

The model output and sensitivity analysis shows that the cushion gas requirement for a particular field can be adjusted considerably through the drilling of more wells or the use of larger diameter tubing. This is true for both CH_4 and H_2. Therefore the question of the capacity of a field in terms of working and cushion gas volumes is more a question of the number of wells that can be drilled than inherent reservoir characteristics. The same goes for deliverability: more wells with a bigger diameter mean that more gas can be extracted from the field in the production window, which in this study was 90 days. The well power difference between CH_4 and H_2 could be an issue in smaller fields like Cousland where the difference is great, however with larger fields like Grijpskerk the difference is only a few percent. If a certain level of deliverability in energy terms is required then tubing size or number of wells could be adjusted, and since H_2 has a smaller cushion gas requirement than CH_4 , it could still be competitive given the smaller initial investment in cushion gas required. This study focussed solely on closed reservoirs without significant aquifer drive, in reservoirs with aquifer drive other factors are likely to be more significant, such as steepness of structure and permeability (Heinemann *et al.* 2021b).

5.4.6 Utility of the model

The sensitivity analysis suggests a non-linear relationship between the inputs (number of wells, size of tubing) and the cushion gas requirement and flow rates of the wells. Therefore, given well and gas cost data, a levelized cost of storage could be determined for different numbers of wells and tubing diameters. Coupled with constraints on minimum energy flow rate requirements and plateau durations fields, an optimal scenario could be determined with the lowest levelized cost.

This will lead more accurate and realistic regional capacity estimates, and allow a ranking of sites based on their costs which is something of great interest to industry when selecting potential storage locations and comparing them with other storage options. Given the need for storage below a certain cost, this ranking could also be developed into an extremely valuable screening tool in itself.

5.4.7 Limitations of the model

However the model does have some limitations. The equations developed by Houpert (1959) and used in the model do not take into account changes in temperature in the reservoir during production. It is also assumed that the reservoir is volumetric (i.e. it behaves as a closed system without any aquifer drive) and no

well interference is modelled. But, due to the open-source nature of the model (it is available in Appendix 5) these features could easily be added to it if needed. This means that anyone can run the model to gain insights into gas storage sites without the need for a software licence, and hopefully over time it can continue to develop.

5.4.8 A brief note on economics

A very simple use case of the model is to compare the cost of the wells with the cost of the cushion gas. In this way, the benefit of adding more wells can be measured. Assuming a hydrogen cost of 2 US$/kg, an injection cost of 0.015 US$/m^3 (Almeida *et al.* 2018), and a well cost calculated using the following basic well drilling cost estimation equation developed for onshore US wells (Ogden and Johnson 2010)

$$C_{\text{drill}} = ((-3.9 \times 10^{-8} d^3 + 4.00 \times 10^{-4} d^2 - 0.84d + 903)d) \times 1.42$$

where d is well depth (m) and C_{drill} is the drilling cost (2021 US$/well), and 1.42 is the conversion factor to 2021 US$.

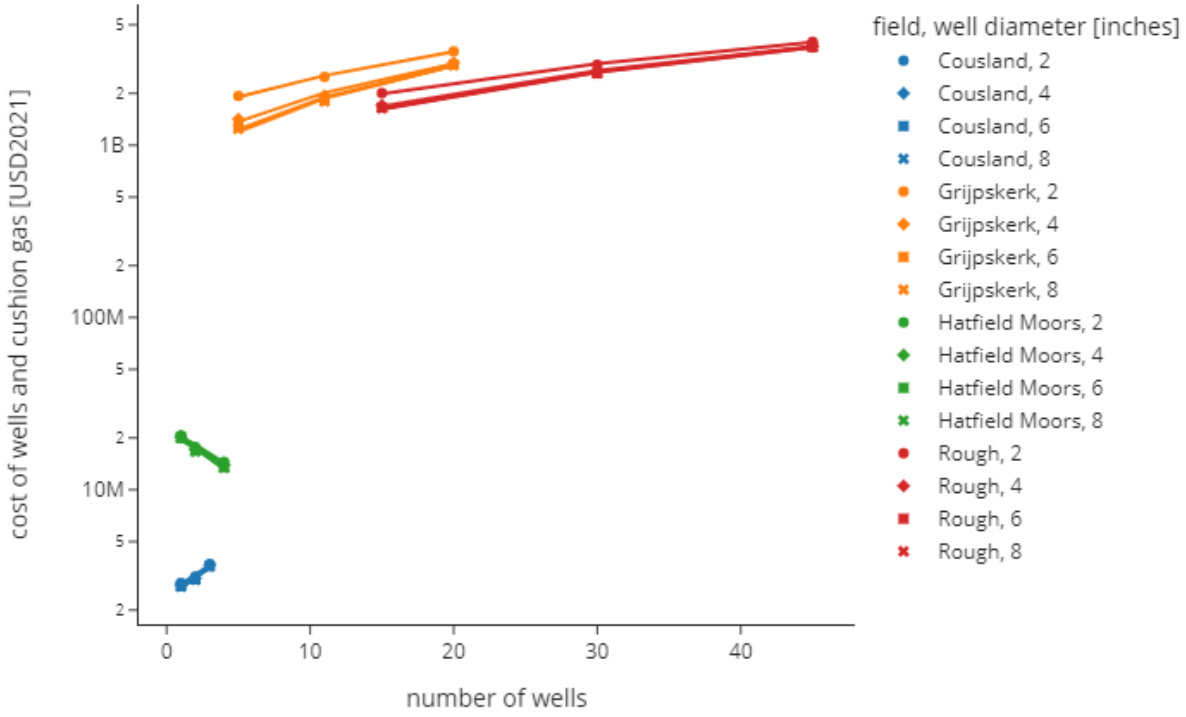

Figure 77: The total cost (in USD2021) of well drilling, cushion gas, and cushion gas injection vs the number of wells for the Cousland (blue), Grijpskerk (orange), Hatfield Moors (green), and Rough (red) fields. All fields show that increasing the number of wells increases the total costs expect for Hatfield Moors where drilling more wells reduces the total cost as the cost of the proportion of cushion gas required decreases faster than the drilling of new wells increases the total cost. Note the y-axis is in a log scale; M stands for million and B stands for billion.

The decrease in the proportion of cushion gas required that follows the drilling of more wells does not decrease the total costs for three of the fields studied: Cousland, Grijpskerk, and Rough (Figure 77). However Hatfield Moors shows the opposite trend with increasing wells correlating with decreasing total costs (Figure 77). This does not take into account the extra working gas that can be utilised over the lifetime of the storage site with lower cushion gas requirements, but shows an interesting trend which may also be the case for other fields. This demonstrates that the model can be useful in gaining insights about the costs associated with potential hydrogen storage sites.

5.5 Conclusions

This study has found that cushion gas requirements and deliverability are not entirely dependent on reservoir properties but can be changed significantly by adjusting the number of wells and well diameter. H_2 and CH_4 storage sites can be engineered to deliver comparable amounts of gas in energy terms, however H_2 will generally deliver less for a given scenario. The program created in this study will be useful for future researchers engaged in regional gas storage estimation projects, particularly as hydrogen storage capacity estimates are of key interest at the current time. A simple demonstration of adding economics to the model shows that for some fields, drilling more wells could reduce combined well drilling and cushion gas costs.

Chapter 6 Conclusions

The aim of this thesis was to investigate the capacity and behaviour of porous rock hydrogen storage sites with a focus on the UK. This was achieved by analysing gas demand data to determine the seasonal hydrogen storage requirement for the total UK gas demand. Screening criteria was developed and implemented in R to provide a robust figure for the amount of hydrogen that could reasonably be stored in porous rock formations on the UK continental shelf (UKCS). The Cousland gas field was selected and modelled using original exploration and production data to determine the static volume available for hydrogen storage, and simulation of hydrogen injection and recovery in the modelled reservoir was performed to determine the dynamic hydrogen storage capacity and investigate the use of natural gas as cushion gas. Finally, an open-source program was developed in Python to investigate the well performance of hydrogen storage sites with the intention of improving cushion gas requirement estimates using basic reservoir data.

6.1 Model development

The seasonal storage requirement for the UK was calculated using monthly gas demand data with the sources from which that demand was satisfied. A simple model was developed in Excel in order to determine the difference between summer lows in demand and winters peaks. The mid-point between these was used as the benchmark from which the requirement was measured, in essence saying that hydrogen production, most likely by steam methane reformation, would occur at one rate throughout the year with storage used as a buffer. The capacity of the UKCS entailed the selection of screening criteria which was implemented in R to find the static capacity of gas fields and saline aquifers. It was determined that the lack of accurate data around saline aquifers prevented any meaningful storage capacity from being calculated. Gas field storage capacity estimates were found to be much more reliable, with the Rough gas field being benchmarked against an existing study. Modelling of the Cousland gas field was achieved through the digitization of a substantial quantity of poor quality, unsearchable hand and typewritten publicly available data from the 1930s to 1960s. Data included well logs, pressure tests, geological reports, petroleum and reservoir engineering reports, and chemical analyses. From these a geological model of the Cousland gas field was developed in Petrel. Sensitivity analyses was performed on the model before it was loaded into CMG builder and hydrogen storage simulation runs performed in CMG GEM. Fluid models were developed in CMG WinProp and the model was history matched

against original production and testing data before 20 year hydrogen storage runs were performed at various pressures to understand the physical behaviour of hydrogen in the semi-depleted gas field. Finally, an open-source program was developed which takes simple reservoir data such as pressure, temperature, and gas-initially-in-place (GIIP) and calculates the cushion gas requirements and deliverability of wells. The tool was benchmarked against real gas storage site data and gave very good matches. The aim of this tool is to improve estimates of cushion gas requirements for hydrogen storage sites which are currently assumed based on various estimates and studies.

6.2 Findings

Using the gas demand data, an inter-seasonal storage requirement of ~150 TWh was calculated for the UK. This was in line with other estimates found in the literature using different methods. 95 depleted gas fields and 82 saline aquifers on the UKCS were identified as suitable for hydrogen storage with an available pore space of 62.9 billion cubic metres. A total working gas capacity of 9100 TWh energy equivalent of hydrogen was calculated. Gas fields account for 6,900 TWh of working gas capacity, saline aquifers with identified structures account for 2,100 TWh of working gas capacity, and saline aquifers with no identified structures account for 70 TWh of working gas capacity, however the estimates for saline aquifers come with a low degree of certainty.

The geological model of Cousland contains 716,380 cells. With 119 × 86 × 70 cells in the I,J, and K directions respectively. The resolution is 25 metres in both the I and J directions and averages 0.23 metres in the K direction. Key features of the model are that the reservoir is volumetric (i.e. and enclosed sand with no-flow boundaries), highly heterogeneous in terms of both porosity and permeability, with shales within the reservoir section also treated as no-flow boundaries. The volumetric sensitivity analysis found that porosity had the biggest impact on the gas volume followed by the irreducible water saturation. Initially, the model had a pore volume of 10.2 million m^3 (360 million ft^3) which was then adjusted during history matching of the model in CMG GEM.

The history matching and hydrogen storage simulation of the Cousland model found that both porosity and permeability in the model needed to be increased to match the inflow/outflow performance calculated from testing and production data. Once a good match was found the hydrogen storage schedule was simulated over a 20 year

period. The initial volume of hydrogen injected into the reservoir had little effect on the recovery factor, capacity, well flow rates, produced gas composition, and pressure response during subsequent storage cycles and final depletion of the reservoir. It was observed that the purity of the recovered hydrogen increased over time as the mixing front between the injected hydrogen and natural gas was pushed further into the reservoir with each injection cycle. The simulation showed that the Cousland gas field could potentially store and recover close to 1000 tonnes of hydrogen without significant losses over 20 years, and that the existing natural gas in the field acted as an effective cushion gas.

The open-source Python program developed to investigate the well performance of hydrogen storage found that cushion gas requirements and deliverability are not entirely dependent on reservoir properties but can be changed significantly by adjusting the number of wells and well diameter. H_2 and CH_4 storage sites can be engineered to deliver comparable amounts of gas in energy terms, however H_2 will generally deliver less for a given scenario. The program created in this study will be useful for future researchers engaged in regional gas storage estimation projects, particularly as hydrogen storage capacity estimates are of key interest at the current time. A simple demonstration of adding economics to the model shows that for some fields, drilling more wells could reduce combined well drilling and cushion gas costs.

6.3 Recommendations for further work

Application of the methods outlined in chapter one on UKCS storage capacities to other regional CO_2 Atlases and to the UK onshore. This would provide a valuable resource for both public and private players in the hydrogen field, allowing a high level screening for the best potential storage sites/regions and allowing a narrower focus for further studies. For example: onshore gas fields and structures were under investigation by the gas council for storage of town gas during the 1960s before North Sea gas was discovered (Adcock 1969). As hydrogen production will follow a similar model to town gas production it follows that smaller, distributed storage sites in different parts of the UK gas network would provide robust and flexible storage options. The addition of economics to the Cousland model and simulation would make a useful case study and could determine whether the site has any value as a real project at full or pilot scale, with any lessons learned applied to other sites identified across the UK.

Applying the open-source Python program described in chapter five to the CO_2Stored database would require a licence and special permission to acquire detailed data for all the fields in the database. However, using the screening process from chapter one combined with the Python program in chapter five would give much more accurate estimates for the working gas capacity of UK offshore gas fields. Further to this, applying some simple economics and a sensitivity analysis of well numbers would determine the best case storage sites that warrant further investigation including reservoir engineering and simulation studies as described in chapters three and four. Further development of the open-source python program in chapter five to include injection would then allow very basic black-box simulation of storage sites at a very low computational cost. This would be of value to all researchers but particularly to those without access to funding and expensive software licences.

Chapter 7 References

Adcock, C.M. 1939. *COUSLAND 1 Production Engineering File 1*.

Adcock, C.M. 1969. *Oil and Gas Fields of Britain*.

Al-Hussainy, R. and Ramey, H.J. 1967. Application of Real Gas Flow Theory to Well Testing and Deliverability Forecasting. *SPE 1234B*.

Al-Hussainy, R., Ramey, H.J. and Crawford, P.B. 1966a. The Flow of Real Gases Through Porous Media. *Journal of Petroleum Technology*, **18**, 624–636, https://doi.org/10.2118/1243-A-PA.

Al-Hussainy, R., Ramey, H.J. and Crawford, P.B. 1966b. The Flow of Real Gases Through Porous Media. *Journal of Petroleum Technology*, **18**, 624–636, https://doi.org/10.2118/1243-A-PA.

Albadi, M.H. and El-Saadany, E.F. 2010. Overview of wind power intermittency impacts on power systems. *Electric Power Systems Research*, **80**, 627–632, https://doi.org/10.1016/j.epsr.2009.10.035.

Alcalde, J., Heinemann, N., et al. 2019. Acorn: Developing full-chain industrial carbon capture and storage in a resource- and infrastructure-rich hydrocarbon province. *Journal of Cleaner Production*, **233**, 963–971, https://doi.org/10.1016/J.JCLEPRO.2019.06.087.

Allen, K. 1985. CAES: The Underground Portion. *IEEE Power Engineering Review*, **PER**-**5**, 35, https://doi.org/10.1109/MPER.1985.5528813.

Allen, R.D., Doherty, T.J., Erikson, R.L. and Wiles, L.E. 1983. Factors affecting storage of compressed air in porous-rock reservoirs.

Almeida, J.R.U.C., Fagundes De Almeida, E.L., Torres, E.A. and Freires, F.G.M. 2018. Economic value of underground natural gas storage for the Brazilian power sector. *Energy Policy*, **121**, 488–497, https://doi.org/10.1016/j.enpol.2018.07.005.

American Petroleum Institute. 1991. *API RP 14E: Recommended Practice for Design and Installation of Offshore Production Platform Piping Systems*.

Amid, A., Mignard, D. and Wilkinson, M. 2016. Seasonal storage of hydrogen in a

depleted natural gas reservoir. *International Journal of Hydrogen Energy*, **41**, 5549–5558, https://doi.org/10.1016/j.ijhydene.2016.02.036.

Anglo-American Oil Company. 1939. Midlothian 1 Petroleum Engineering File.

Aprea, J.L. and Bolcich, J.C. 2020. The energy transition towards hydrogen utilization for green life and sustainable human development in Patagonia. *International Journal of Hydrogen Energy*, **45**, 25627–25645, https://doi.org/10.1016/J.IJHYDENE.2020.01.246.

Asquith, G. and Krygowski, D. 2004. *Basic Well Log Analysis, 2nd Edition*, 2nd ed.

Aziz, K. and Govier, G.W. 1972. Pressure Drop In Wells Producing Oil And Gas. *Journal of Canadian Petroleum Technology*, **11**, 38–48, https://doi.org/10.2118/72-03-04.

Aziz, K. and Settari, A. 1979. *Petroleum Reservoir Simulation*.

Babarit, A., Gilloteaux, J.-C., Clodic, G., Duchet, M., Simoneau, A. and Platzer, M.F. 2018. Techno-economic feasibility of fleets of far offshore hydrogen-producing wind energy converters. *International Journal of Hydrogen Energy*, **43**, 7266–7289, https://doi.org/10.1016/J.IJHYDENE.2018.02.144.

Bagnall, A.C. 1979. The Search for Natural Petroleum in the Lothians. *Edinburgh Geologist - issue 5*, 12–14.

Basniev, K.S., Omelchenko, R.J.. . J., et al. 2010. Underground Hydrogen Storage Problems in Russia. *In*: Stolten, D. and Grube, T. (eds) *18th World Hydrogen Energy Conference 2010*. 1–7.

BEIS. 2018. DUKES chapter 4: statistics on supply and demand for natural gas. *In*: *Digest of UK Energy Statistics (DUKES): Natural Gas*. 15.

BEIS. 2020a. *DUKES_4.3 UK Continental Shelf and Onshore Natural Gas Production and Supply*.

BEIS. 2020b. *Supply and Consumption of Natural Gas and Colliery Methane (DUKES 4.2)*.

Bell, I.H., Wronski, J., Quoilin, S. and Lemort, V. 2014. Pure and Pseudo-pure Fluid Thermophysical Property Evaluation and the Open-Source Thermophysical Property Library CoolProp. *Industrial and Engineering Chemistry Research*, **53**,

2498–2508, https://doi.org/10.1021/IE4033999.

Bentham, M., Mallows, T., Lowndes, J. and Green, A. 2014. CO2STORage evaluation database (CO2Stored). The UK's online storage atlas. *Energy Procedia*, **63**, 5103–5113, https://doi.org/10.1016/j.egypro.2014.11.540.

Beutel, T. and Black, S. 2004. Salt deposits and gas cavern storage in the UK with a case study of salt exploration from Cheshire. *In*: *Fall 2004 Conference*.

Biegger, P., Kittinger, F. and Lehner, M. 2018. Underground Sun Conversion. *In*: *14th Minisymposium Chemical & Process Engineering - Johannes Kepler Universität, Linz, Austria*.

Bolton, W. 2006. *Engineering Science*, 5th ed.

BP. 1960a. Cousland 6 Geological Completion Report.

BP. 1960b. Cousland 6 Geological Completion Report - Enclosure.

British Geological Survey. 2008. An appraisal of underground gas storage technologies and incidents, for the development of risk assessment methodology, Volume Two - Figures and Tables. *British: Health and Safety Executive*.

British Geological Survey. 2020a. Borehole materials databasehttps://www.bgs.ac.uk/technologies/databases/borehole-materials-database/.

British Geological Survey. 2020b. National Geoscience Data Centre (NGDC)https://www.bgs.ac.uk/geological-data/national-geoscience-data-centre/.

Buzek, F., Onderka, V., Vancura, P. and Wolf, I. 1994. Carbon isotope study of methane production in a town gas storage reservoir. *Fuel*, **73**, 747–752, https://doi.org/10.1016/0016-2361(94)90019-1.

Caglayan, D.G., Weber, N., Heinrichs, H.U., Linßen, J., Robinius, M., Kukla, P.A. and Stolten, D. 2020. Technical potential of salt caverns for hydrogen storage in Europe. *International Journal of Hydrogen Energy*, **45**, 6793–6805, https://doi.org/10.1016/j.ijhydene.2019.12.161.

Caine, D., Iliffe, M., Kinsella, K., Wahyuni, W. and Bond, L. 2019. *Dolphyn Hydrogen*

Phase 1 - Final Report.

Cant, D.J. 1992. Subsurface Facies Analysis. *In*: *Facies Models: Response to Sea Level Change*.

Carbon Storage Taskforce. 2010. *National Carbon Mapping and Infrastructure Plan – Australia*.

Carden, P. and Paterson, L. 1979. Physical, chemical and energy aspects of underground hydrogen storage. *International Journal of Hydrogen Energy*, **4**, 559–569, https://doi.org/10.1016/0360-3199(79)90083-1.

Carmichael, R.S. 1982. *Handbook of Physical Properties of Rocks*, https://doi.org/10.1201/9780203712115.

Cartwright, J., Stewart, S. and Clark, J. 2001. Salt dissolution and salt-related deformation of the Forth Approaches Basin, UK North Sea. *Marine and Petroleum Geology*, **18**, 757–778, https://doi.org/10.1016/S0264-8172(01)00019-8.

Chadwick, A., Arts, R., Bernstone, C., May, F., Thibeau, S. and Zweigel, P. 2008. *Best Practice for the Storage of CO2 in Saline Aquifers - Observations and Guidelines from the SACS and CO2STORE Projects*, https://doi.org/ISBN: 978-0-85272-610-5.

Chaudry, M., Jenkins, N. and Strbac, G. 2008. Multi-time period combined gas and electricity network optimisation. *Electric Power Systems Research*, **78**, 1265–1279, https://doi.org/10.1016/j.epsr.2007.11.002.

Chen, J., Ren, S., Yang, C., Jiang, D. and Li, L. 2013. Self-healing characteristics of damaged rock salt under different healing conditions. *Materials*, **6**, 3438–3450, https://doi.org/10.3390/ma6083438.

Clavier, C., Hoyle, W. and Meunier, D. 1971. Quantitative Interpretation of Thermal Neutron Decay Time Logs: Part I. Fundamentals and Techniques. *Journal of Petroleum Technology*, **23**, 743–755, https://doi.org/10.2118/2658-A-PA.

Climate Change Committee. 2015. *The Fifth Carbon Budget*.

Climate Change Committee. 2016. *Next Steps for UK Heat Policy - Annex 2. Heat in UK Buildings Today*.

Climate Change Committee. 2020. *The Sixth Carbon Budget*.

CMG. 2019a. Builder.

CMG. 2019b. GEM.

CMG. 2019c. WinProp.

Collins, D.A., Nghlem, L.X., Li, V. ·k and Grabenstetter, J.E. 1992. *An Efficient Approach to Adaptive-Implicit Compositional Simulation With an Equation of State*.

Competition & Markets Authority. 2017. *Rough Gas Storage Undertakings Review Final Decision*.

COMSOL Inc. 2016. COMSOL Reference Manual (version 5.2a). 1–1378.

CONOCO (U.K.) Limited and ENTERPRISE OIL p.l.c. 1991. *EXL 026 (FIRTH OF FORTH) RELINQUISHMENT REPORT*.

Cornot-Gandolphe, S. 2017. *Underground Gas Storage in the World - 2017 Status*.

Cornot-Gandolphe, S. 2018. *Underground Gas Storage in the World - 2018 Status*.

Cranfield University, The Gas Technology Institute and Doosan Babcock. 2019. *Bulk Hydrogen Production by Sorbent Enhanced Steam Reforming (HyPER)*.

Crotogino, F., Schneider, G.S. and Evans, D.J. 2018. Renewable energy storage in geological formations. *Proceedings of the Institution of Mechanical Engineers, Part A: Journal of Power and Energy*, **232**, 100–114, https://doi.org/10.1177/0957650917731181.

Crown Estate Scotland. 2018. Maps & Publications. *Crown Estate Scotland website*.

Dahowski, R.T., Li, X., Davidson, C.L., Wei, N. and Dooley, J.J. 2009. Regional Opportunities for Carbon Dioxide Capture and Storage in China. 85.

Dawood, F., Anda, M. and Shafiullah, G.M. 2020. Hydrogen production for energy: An overview. *International Journal of Hydrogen Energy*, **45**, 3847–3869, https://doi.org/10.1016/j.ijhydene.2019.12.059.

Dean, G. 2018. The Scottish oil-shale industry from the viewpoint of the modern-day shale-gas industry. *Geological Society, London, Special Publications*, **465**, 53–69, https://doi.org/10.1144/sp465.13.

Department for Business Energy & Industrial Strategy. 2018a. *2016 UK GREENHOUSE GAS EMISSIONS, FINAL FIGURES Statistical Release: National Statistics*.

Department for Business Energy & Industrial Strategy. 2018b. *SUB-NATIONAL ELECTRICITY AND GAS CONSUMPTION STATISTICS*.

East Lothian Antiquarians and Field Naturalists Society. 2018a. Inveresk Musselburgh | Homes. *The Fourth Statistical Account of East Lothian*https://el4.org.uk/parish/inveresk-musselburgh/homes/.

East Lothian Antiquarians and Field Naturalists Society. 2018b. Prestonpans | Homes. *The Fourth Statistical Account of East Lothian*https://el4.org.uk/parish/prestonpans/homes/.

Eaton, B.A. 1969. Fracture Gradient Prediction and Its Application in Oilfield Operations. *Journal of Petroleum Technology*, **21**, 1353–1360, https://doi.org/10.2118/2163-PA.

Edinburgh Oil & Gas PLC. 1999. *Hatfield Moors - Addendum to Annex B*.

Ehrenberg, S.N. and Nadeau, P.H. 2005. Sandstone vs. carbonate petroleum reservoirs: A global perspective on porosity-depth and porosity-permeability relationships. *AAPG Bulletin*, **89**, 435–445, https://doi.org/10.1306/11230404071.

Element Energy. 2020. *Gigastack: Bulk Supply of Renewable Hydrogen - Public Report*.

Energy Research Partnership. 2016. *Potential Role of Hydrogen in the UK Energy System*.

Energy Technology Training Center. 2001. Module 1 : Hydrogen Properties. *In*: *Hydrogen Fuel Cell Engines and Related Technologies - Technical Report, PB2003-100184*.

Equinor. 2013. Open datasets | OPM. *The Open Porous Media Initiative*https://opm-project.org/?page_id=559.

Evans, D., Graham, C., Armour, A. and Bathurst, P. 2003. *The Millennium Atlas: Petroleum Geology of the Central and Northern North Sea*, 2003/08/05. Evans, D., Graham, C., Armour, A. and Bathurst, P. (eds), https://doi.org/DOI:

10.1017/S0016756803218124.

Evans, D., Highley, D., Gale, I., Cowley, J., Rayner, D. and Hill, A. 2008. *Mineral Planning Factsheet - Underground Storage*.

Evans, D.J. and Holloway, S. 2009. A review of onshore UK salt deposits and their potential for underground gas storage. *In*: Evans, D. J. and Chadwick, R. A. (eds) *Underground Gas Storage: Worldwide Experiences and Future Development in the UK and Europe*, https://doi.org/10.1144/SP313.5.

Evans, D.J. and West, J.M. 2008. *An Appraisal of Underground Gas Storage Technologies and Incidents, for the Development of Risk Assessment Methodology*.

Exploration Dept. Lasmo. 1985. U.K. Onshore Licence PL177 - Evaluation of the remaining hydrocarbon prospects. 113.

Falcon, N.L. 1938. *COUSLAND 1 TO 3 GEOLOGICAL COMPLETION REPORT*.

Falcon, N.L. and Kent, P.E. 1960. Geological Results of Petroleum Exploration in Britain 1945-1957. *Geological Society Memoir*, **2**, 5–56, https://doi.org/10.1144/GSL.MEM.1960.002.01.01.

Feldmann, F., Hagemann, B., Ganzer, L. and Panfilov, M. 2016. Numerical simulation of hydrodynamic and gas mixing processes in underground hydrogen storages. *Environmental Earth Sciences*, **75**, 1–15, https://doi.org/10.1007/s12665-016-5948-z.

Fisher, W.D. 1945. P001637.

Flemisch, B., Darcis, M., et al. 2011. DuMux: DUNE for multi-{phase,component,scale,physics,…} flow and transport in porous media. *Advances in Water Resources*, **34**, 1102–1112, https://doi.org/10.1016/j.advwatres.2011.03.007.

Foh, S., Novil, M., Rockar, E. and Randolph, P. 1979. *Underground Hydrogen Storage Final Report*.

Friend, D.G., Ely, J.F. and Ingham, H. 1989. Thermophysical Properties of Methane. *Journal of Physical and Chemical Reference Data*, **18**, 583–638, https://doi.org/10.1063/1.555828.

Gasanzade, F., Pfeiffer, W.T., Witte, F., Tuschy, I. and Bauer, S. 2021. Subsurface renewable energy storage capacity for hydrogen, methane and compressed air – A performance assessment study from the North German Basin. *Renewable and Sustainable Energy Reviews*, **149**, 111422, https://doi.org/10.1016/J.RSER.2021.111422.

Gazprom. 2018. *A Leader of Gas Science: 70th Anniversary of VNIIGAZ*. Gritsenko, A. I., Grigoryev, B. A. and Dzhafarov, K. I. (eds).

Gluyas, J.G. and Hichens, H.M. 2003. United Kingdom oil and gas fields. Commemorative millennium volume. *Geological Society Memoir*, **20**, 1006, https://doi.org/10.1144/GSL.MEM.2003.020.

Gluyas, J.G., De-Paola, N., et al. 2020. The Humbly Grove, Herriard and Hester's Copse fields, UK Onshore. *Geological Society, London, Memoirs*, **52**, 74 LP – 81, https://doi.org/10.1144/M52-2018-78.

Gralla, D.S. and Jones, R.E. 1991. *Hatfield Moors Gas Field - Annual Reservoir Performance Report 1990*.

Graupner, B.J., Li, D. and Bauer, S. 2011. The coupled simulator ECLIPSE–OpenGeoSys for the simulation of CO2 storage in saline formations. *Energy Procedia*, **4**, 3794–3800, https://doi.org/10.1016/J.EGYPRO.2011.02.314.

Greensmith, J.T. 1961. The petrology of the Oil-Shale Group sandstones of west Lothian and southern Fifeshire. *Proceedings of the Geologists' Association*, **72**, 49–71, https://doi.org/10.1016/S0016-7878(61)80026-6.

Greensmith, J.T. 1962. Rhythmic Deposition in the Carboniferous Oil-Shale Group of Scotland. *The Journal of Geology*, **70**, 355–364, https://doi.org/10.1086/626825.

Greensmith, J.T. 1965. Calciferous Sandstone Series Sedimentation at the Eastern End of the Midland Valley of Scotland. *SEPM Journal of Sedimentary Research*, **Vol. 35**, 223–242, https://doi.org/10.1306/74d71226-2b21-11d7-8648000102c1865d.

Groenenberg, R.M., Juez-Larre, J., et al. 2020. *Techno-Economic Modelling of Large-Scale Energy Storage Systems*.

Guo, B. 2019. Petroleum reservoir properties. *In*: *Well Productivity Handbook*. 17–

51., https://doi.org/10.1016/B978-0-12-818264-2.00002-6.

HAESELDONCKX, D. and DHAESELEER, W. 2007. The use of the natural-gas pipeline infrastructure for hydrogen transport in a changing market structure. *International Journal of Hydrogen Energy*, **32**, 1381–1386, https://doi.org/10.1016/j.ijhydene.2006.10.018.

Hagemann, B., Rasoulzadeh, M., Panfilov, M., Ganzer, L. and Reitenbach, V. 2016. Hydrogenization of underground storage of natural gas: Impact of hydrogen on the hydrodynamic and bio-chemical behavior. *Computational Geosciences*, **20**, 595–606, https://doi.org/10.1007/s10596-015-9515-6.

Haldane, J.B.S. 1924. Daedalus, or science and the future. *The Eugenics review*, **16**, 143–145, https://doi.org/10.2307/2014395.

Hallett, D., Durant, G.P. and Farrow, G.E. 1985. Oil exploration and production in Scotland. *Scottish Journal of Geology*, **21**, 547–570, https://doi.org/10.1144/sjg21040547.

Hart, D., Howes, J., et al. 2015. *Scenarios for Deployment of Hydrogen in Contributing to Meeting Carbon Budgets and the 2050 Target*.

Harvie, B.A. and Hobbs, R.J. 2013. Case Study: Shale Bings in Central Scotland: From Ugly Blots on the Landscape to Cultural and Biological Heritage. *In*: *Novel Ecosystems: Intervening in the New Ecological World Order*, https://doi.org/10.1002/9781118354186.ch35.

Hassanpouryouzband, A., Joonaki, E., Edlmann, K., Heinemann, N. and Yang, J. 2020. Thermodynamic and transport properties of hydrogen containing streams. *Scientific Data*, **7**, 222, https://doi.org/10.1038/s41597-020-0568-6.

Heinemann, N., Booth, M.G., Haszeldine, R.S., Wilkinson, M., Scafidi, J. and Edlmann, K. 2018a. Hydrogen storage in porous geological formations – onshore play opportunities in the midland valley (Scotland, UK). *International Journal of Hydrogen Energy*, **43**, 20861–20874, https://doi.org/10.1016/j.ijhydene.2018.09.149.

Heinemann, N., Booth, M.G., Haszeldine, R.S., Wilkinson, M., Scafidi, J. and Edlmann, K. 2018b. Hydrogen storage in porous geological formations – onshore play opportunities in the midland valley (Scotland, UK). *International*

Journal of Hydrogen Energy, **43**, 20861–20874, https://doi.org/10.1016/J.IJHYDENE.2018.09.149.

Heinemann, N., Alcalde, J., et al. 2021a. Enabling large-scale hydrogen storage in porous media-the scientific challenges, https://doi.org/10.1039/d0ee03536j.

Heinemann, N., Scafidi, J., et al. 2021b. Hydrogen storage in saline aquifers: The role of cushion gas for injection and production. *International Journal of Hydrogen Energy*, **46**, 39284–39296, https://doi.org/10.1016/j.ijhydene.2021.09.174.

Helmholtz Centre Potsdam. 2015. H2STORE. *GFZ German Research Centre for Geosciences*https://www.gfz-potsdam.de/en/section/geoenergy/projects/completed-projects/h2store/.

Hévin, G. 2019. Underground storage of Hydrogen in salt caverns. *In*: *European Workshop on Underground Energy Storage November 7th-8th 2019, Paris*.

Horseman, S., Evans, D., Rowley, J. and Chadwick, A. 2008. Underground gas storage: Geology, technology, planning and regulation. *Earthwise*, 12–13.

Houpeurt, A. 1959. On the Flow of Gases in Porous Media. *Revue de L'Institut Francais du Petrole*, **XIV**, 1468–1684.

HyWeb. 2007. Hydrogen Data. *The Hydrogen and Fuel Cell Information System*.

IEA. 2019. GECO 2019. *International Energy Agency Website*https://www.iea.org/geco/.

Illing, V.C. 1961. *Further Drilling at Cousland*.

Isaac, T. 2019. HyDeploy: The UK's First Hydrogen Blending Deployment Project. *Clean Energy*, **3**, 114–125, https://doi.org/10.1093/ce/zkz006.

ITN. 1957. ENERGY: Natural gas switched on in Scotlandhttps://www.gettyimages.co.uk/detail/video/natural-gas-switched-on-in-scotland-scotland-lothian-news-footage/813093966?adppopup=true&uiloc=thumbnail_more_search_results_adp&uiloc=thumbnail_more_search_results_adp.

Johnston, I.A. 2005. The Noble-Abel Equation of State: Thermodynamic Derivations for Ballistics Modelling. *DSTO-TN-0670*.

Jones, S.C. 1987. Using the Inertial Coefficient, β, To Characterize Heterogeneity in Reservoir Rock. *Society of Petroleum Engineers of AIME, (Paper) SPE*, **Pi**, 165–174, https://doi.org/10.2118/16949-MS.

Jossi, J.A., Stiel, L.I. and Thodos, G. 1962. The viscosity of pure substances in the dense gaseous and liquid phases. *AIChE Journal*, **8**, 59–63, https://doi.org/10.1002/aic.690080116.

Juez-Larré, J., Remmelts, G., Breunese, J.N., van Gessel, S.F. and Leeuwenburgh, O. 2016. Using underground gas storage to replace the swing capacity of the giant natural gas field of Groningen in the Netherlands. A reservoir performance feasibility study. *Journal of Petroleum Science and Engineering*, **145**, 34–53, https://doi.org/10.1016/j.petrol.2016.03.010.

Katzenstein, W. and Apt, J. 2012. The cost of wind power variability. *Energy Policy*, **51**, 233–243, https://doi.org/10.1016/j.enpol.2012.07.032.

Ketzer, J.M., Machado, C.X., Rockett, G.C. and Iglesias, R.S. 2015. *Brazilian Atlas of CO2 Capture and Geological Storage*.

Khaledi, K., Mahmoudi, E., Datcheva, M. and Schanz, T. 2016. Stability and serviceability of underground energy storage caverns in rock salt subjected to mechanical cyclic loading. *International Journal of Rock Mechanics and Mining Sciences*, **86**, 115–131, https://doi.org/10.1016/j.ijrmms.2016.04.010.

Kilgallon, R., Gilfillan, S.M. V, Edlmann, K., McDermott, C.I., Naylor, M. and Haszeldine, R.S. 2018. Experimental determination of noble gases and SF6, as tracers of CO2flow through porous sandstone. *Chemical Geology*, **480**, 93–104, https://doi.org/10.1016/j.chemgeo.2017.09.022.

Kopal, L., Cizek, P. and Milička, J. 2016. Geological model of Lobodice underground gas storage facility based on 3D seismic interpretation. *Contributions to Geophysics and Geodesy*, **46**, 125–135, https://doi.org/10.1515/CONGEO-2016-0009.

Korte, C., Mandt, T. and Bergholz, T. 2016. Physics of Hydrogen. *In*: *Hydrogen Science and Engineering: Materials, Processes, Systems and Technology*. 563–600.

Kruck, O., Crotogino, F., Prelicz, R. and Rudolph, T. 2013. *'Assessment of the*

Potential, the Actors and Relevant Business Cases for Large Scale and Seasonal Storage of Renewable Electricity by Hydrogen Underground Storage in Europe' Overview on All Known Underground Storage Technologies for Hydrogen Status: D(4).

Landinger, H., Bünger, U., Raksha, T., Weindorf, W., Simón, J., Correas, L. and Crotogino, F. 2014. Assessment of the Potential, the Actors and Relevant Business Cases for Large Scale and Long Term Storage of Renewable Electricity by Hydrogen Underground Storage in Europe.

Lanz, A. 2001. Module 1: Hydrogen Properties. *In*: *Hydrogen Fuel Cell Engines and Related Technologies*. 41.

Larionov, V. V. 1969. *Borehole Radiomentry*.

Le Fevre, C. 2013. *Gas Storage in Great Britain*.

Leachman, J.W., Jacobsen, R.T., Penoncello, S.G. and Lemmon, E.W. 2009. Fundamental Equations of State for Parahydrogen, Normal Hydrogen, and Orthohydrogen. *Journal of Physical and Chemical Reference Data*, **38**, 721, https://doi.org/10.1063/1.3160306.

Lee, A.L. and Eakin, B.E. 1964. Gas-Phase Viscosity of Hydrocarbon Mixtures. *Society of Petroleum Engineers Journal*, **4**, 247–249, https://doi.org/10.2118/872-pa.

Lee, W.J. and Wattenbarger, R.A. 1995. *Gas Reservoir Engineering*.

Lees, G.M., Cox, P.T. and Weald, S. 1937. The Geological Basis of the Present Search for Oil in Great Britain by the D'Arcy Exploration Company, Ltd. *Quarterly Journal of the Geological Society*, **93**, 156–194, https://doi.org/10.1144/gsl.jgs.1937.093.01-04.09.

Lemmon, E.W., Huber, M.L. and Leachman, J.W. 2008. Revised Standardized Equation for Hydrogen Gas Densities for Fuel Consumption Applications. *Journal of Research of the National Institute of Standards and Technology*, https://doi.org/10.6028/jres.113.028.

Lemmon, E.W., Huber, M.L. and McLinden, M.O. 2013. NIST Standard Reference Database 23: Reference Fluid Thermodynamic and Transport Properties-REFPROP, Version 9.1.

Lemmon, E.W., McLinden, M.O. and Friend, D.G. 2021. ‘Thermophysical Properties of Fluid Systems’. *In*: Linstrom, P. J. and Mallard, W. G. (eds) *NIST Chemistry WebBook, NIST Standard Reference Database Number 69*, https://doi.org/https://doi.org/10.18434/T4D303.

Liebensteiner, M. and Wrienz, M. 2019. Do Intermittent Renewables Threaten the Electricity Supply Security? *Energy Economics*, 104499, https://doi.org/10.1016/j.eneco.2019.104499.

Liebscher, A., Wackerl, J. and Streibel, M. 2016. Geologic Storage of Hydrogen - Fundamentals, Processing, and Projects. *In*: *Hydrogen Science and Engineering : Materials, Processes, Systems and Technology*. 629–658., https://doi.org/10.1002/9783527674268.ch26.

Loftus, G.W.F. and Greensmith, J.T. 1988. The lacustrine Burdiehouse Limestone Formation-a key to the deposition of the Dinantian Oil Shales of Scotland. *Geological Society Special Publication*, **40**, 219–234, https://doi.org/10.1144/GSL.SP.1988.040.01.19.

Luboń, K. and Tarkowski, R. 2020. Numerical simulation of hydrogen injection and withdrawal to and from a deep aquifer in NW Poland. *International Journal of Hydrogen Energy*, **45**, 2068–2083, https://doi.org/10.1016/j.ijhydene.2019.11.055.

Lyons, W., Carter, T. and Lapeyrousse, N.J. 2012. Air and Gas Calculations. *In*: Lyons, W., Carter, T. and Lapeyrousse Production, and Workover (Third Edition), N. J. B. T.-F. and C. for D. (eds) *Formulas and Calculations for Drilling, Production, and Workover*. 253–266., https://doi.org/10.1016/B978-1-85617-929-4.00006-3.

Lyons, W.C., Plisga, G.J. and Lorenz, M.D. 2016. Chapter 6 - Production Engineering. *In*: Lyons, W. C., Plisga, G. J. and Lorenz, M. D. (eds) *Standard Handbook of Petroleum and Natural Gas Engineering (Third Edition)*. 6–529., https://doi.org/https://doi.org/10.1016/B978-0-12-383846-9.00006-0.

Lysyy, M., Fernø, M. and Ersland, G. 2021. Seasonal hydrogen storage in a depleted oil and gas field. *International Journal of Hydrogen Energy*, **46**, 25160–25174, https://doi.org/10.1016/j.ijhydene.2021.05.030.

Madani Sani, F., Huizinga, S., Esaklul, K.A. and Nesic, S. 2019. Review of the API

RP 14E erosional velocity equation: Origin, applications, misuses, limitations and alternatives. *Wear*, **426**–**427**, 620–636, https://doi.org/10.1016/J.WEAR.2019.01.119.

Martens, S., Liebscher, A., et al. 2013. CO2 storage at the Ketzin pilot site, Germany: Fourth year of injection, monitoring, modelling and verification. *Energy Procedia*, **37**, 6434–6443, https://doi.org/10.1016/j.egypro.2013.06.573.

Martin, D.L. 1974. *COUSLAND 1 Production Engineering File 2*.

McCarty, R.D., Hord, J. and Roder, H.M. 1981. *Selected Properties of Hydrogen (Engineering Design Data)*, National B.

Michalski, J., Bünger, U., et al. 2017. Hydrogen generation by electrolysis and storage in salt caverns: Potentials, economics and systems aspects with regard to the German energy transition. *International Journal of Hydrogen Energy*, **42**, 13427–13443, https://doi.org/10.1016/j.ijhydene.2017.02.102.

Microsoft Corporation. 2016. Microsoft Excel 2016.

Monaghan, A.A. 2014. The Carboniferous shales of the Midland Valley of Scotland : geology and resource estimation. *British Geological Survey for Department of Energy and Climate Change*.

Mostaghimi, P., Kamali, F., Jackson, M.D., Muggeridge, A.H. and Pain, C.C. 2016. Adaptive Mesh Optimization for Simulation of Immiscible Viscous Fingering. *SPE Journal*, **21**, 2250–2259, https://doi.org/10.2118/173281-PA.

Mouli-Castillo, J. 2018. *Assessing the Potential for Compressed Air Energy Storage Using the Offshore UK Saline Aquifer Resource*. The University of Edinburgh.

Mouli-Castillo, J., Wilkinson, M., Mignard, D., McDermott, C., Haszeldine, R.S. and Shipton, Z.K. 2018. Inter-seasonal compressed air energy storage using saline aquifers (Manuscript submitted for publication).

Mouli-Castillo, J., Heinemann, N. and Edlmann, K. 2021. Mapping geological hydrogen storage capacity and regional heating demands: An applied UK case study. *Applied Energy*, **283**, 116348, https://doi.org/10.1016/j.apenergy.2020.116348.

Muzny, C.D., Huber, M.L. and Kazakov, A.F. 2013. Correlation for the viscosity of normal hydrogen obtained from symbolic regression. *Journal of Chemical and*

Engineering Data, **58**, 969–979, https://doi.org/10.1021/je301273j.

National Grid. 2018. *Gas Ten Year Statement 2018*.

NETL and US DOE. 2015. Carbon Storage Atlas - Fifth Edition (Atlas V). **5**, 114.

Nghiem, L.X. and Heidemann, R.A. 1982. General Acceleration Procedure for Multiphase Flash Calculation With Application to Oil-Gas-Water Systems. *In*: *2nd European Symposium on Enhanced Oil Recovery,*. 8–10.

Nghiem, L.X., Aziz, K. and Li, Y.K. 1983. ROBUST ITERATIVE METHOD FOR FLASH CALCULATIONS USING THE SOAVE-REDLICH-KWONG OR THE PENG-ROBINSON EQUATION OF STATE. *Society of Petroleum Engineers journal*, **23**, 521–530, https://doi.org/10.2118/8285-pa.

Northern Gas Networks. 2016. *H21 Leeds City Gate*.

Northern Gas Networks. 2018. *H21 North of England*.

Norwegian Petroleum Directorate. 2011. CO2 Storage Atlas Norwegian North Sea. 2011. *Norwegian Petroleum Directorate: Stavanger, Norway*, **1**, 72.

Ofgem. 2020a. Gas demand and supply source by month (GB). *Ofgem data portal*https://www.ofgem.gov.uk/data-portal/gas-demand-and-supply-source-month-gb.

Ofgem. 2020b. *GB Gas Storage Facilities*.

Ofgem. 2020c. Typical Domestic Consumption Valueshttps://www.ofgem.gov.uk/gas/retail-market/monitoring-data-and-statistics/typical-domestic-consumption-values.

Ogden, J. and Johnson, N. 2010. Techno-economic analysis and modeling of carbon dioxide (CO2) capture and storage (CCS) technologies. *In*: *Developments and Innovation in Carbon Dioxide (CO2) Capture and Storage Technology*. 27–63., https://doi.org/10.1533/9781845699574.1.27.

Oil & Gas Authority. 2020. OGA Field Production, PPRS (WGS84) | Oil and Gas Authorityhttps://data-ogauthority.opendata.arcgis.com/datasets/oga-field-production-pprs-wgs84/data.

Panfilov, M. 2010. Underground Storage of Hydrogen: In Situ Self-Organisation and Methane Generation. *Transport in Porous Media*, **85**, 841–865,

https://doi.org/10.1007/s11242-010-9595-7.

Panfilov, M. 2016. *4 – Underground and Pipeline Hydrogen Storage*, https://doi.org/10.1016/B978-1-78242-362-1.00004-3.

Panfilov, M., Reitenbach, V. and Ganzer, L. 2016. Self-organization and shock waves in underground methanation reactors and hydrogen storages. *Environmental Earth Sciences*, **75**, 313, https://doi.org/10.1007/s12665-015-5048-5.

Paterson, L. 1983. *THE IMPLICATIONS OF FINGERING IN UNDERGROUND HYDROGEN STORAGE*.

Peng, D.Y. and Robinson, D.B. 1976. A New Two-Constant Equation of State. *Industrial and Engineering Chemistry Fundamentals*, **15**, 59–64, https://doi.org/10.1021/i160057a011.

Pérez, A., Pérez, E., Dupraz, S. and Bolcich, J. 2016. Patagonia Wind-Hydrogen Project: Underground Storage and Methanation. *In*: *21st World Hydrogen Energy Conference 2016. Zaragoza, Spain. 13-16 Th June, 2016*.

Pfeiffer, W.T. and Bauer, S. 2015. Subsurface Porous Media Hydrogen Storage – Scenario Development and Simulation. *Energy Procedia*, **76**, 565–572, https://doi.org/10.1016/j.egypro.2015.07.872.

Pfeiffer, W.T., Graupner, B. and Bauer, S. 2016. The coupled non-isothermal, multiphase-multicomponent flow and reactive transport simulator OpenGeoSys–ECLIPSE for porous media gas storage. *Environmental Earth Sciences*, **75**, 1347, https://doi.org/10.1007/s12665-016-6168-2.

Pfeiffer, W.T., Beyer, C. and Bauer, S. 2017. Hydrogen storage in a heterogeneous sandstone formation: dimensioning and induced hydraulic effects. *Petroleum geoscience*, **23**, 315–326, https://doi.org/10.1144/petgeo2016-050.

Plaat, H. 2009. Underground gas storage: Why and how. *Geological Society, London, Special Publications*, **313**, 25 LP-- 37, https://doi.org/10.1144/SP313.4.

Poling, B.E. 2001. *The Properties of Gases and Liquids*, 5th edition / Bru... Prausnitz, J. M. (John M., O'Connell, J. P. (John P. and Reid, R. C. (Robert C. (eds). book.

Primary Energy - BP Statistical Review of World Energy 2019 | *68th Edition*. 2019.

Prime Minister's Office. 2019. *The Queen's Speech 2019*.

Progressive Energy. 2019. HyNet Low Carbon Hydrogen Plant - Phase 1 Report for BEIS.

Pruess, K., Oldenburg, C. and Moridis, G. 1999. TOUGH2 User's Guide. 1–197.

QGIS Development Team. 2020. QGIS Geographic Information System.

Qian, J.W., Jaubert, J.N. and Privat, R. 2013. Phase equilibria in hydrogen-containing binary systems modeled with the Peng-Robinson equation of state and temperature-dependent binary interaction parameters calculated through a group-contribution method. *Journal of Supercritical Fluids*, **75**, 58–71, https://doi.org/10.1016/j.supflu.2012.12.014.

Quiñones-Cisneros, S.E. and Deiters, U.K. 2006. Generalization of the Friction Theory for Viscosity Modeling. *The Journal of Physical Chemistry B*, **110**, 12820–12834, https://doi.org/10.1021/jp0618577.

R Core Team. 2019. R: A Language and Environment for Statistical Computing.

RAG Austria AG, AXIOM angewandte Prozesstechnik GesmbH, VERBUND AG, MONTANUNIVERSITÄT LEOBEN, UNIVERSITÄT für Bodenkultur Wien and ENERGIEINSTITUT an der Johannes Kepler Universität Linz. 2017. *Underground Sun Storage - Final Report*.

Rawlins, E.L. and Schellhardt, M.A. 1936. *Back-Pressure Data on Natural Gas Wells and Their Application to Production Practices*.

Raza, A., Rezaee, R., Gholami, R., Bing, C.H., Nagarajan, R. and Hamid, M.A. 2016. A screening criterion for selection of suitable CO2 storage sites. *Journal of Natural Gas Science and Engineering*, **28**, 317–327, https://doi.org/10.1016/j.jngse.2015.11.053.

Reid, R.C., Prausnitz, J.M. and Sherwood, T.K. 1977. *The Properties of Gases and Liquids*, 3rd Editio.

Ren, G., Wan, J., Liu, J., Yu, D. and Söder, L. 2018. Analysis of wind power intermittency based on historical wind power data. *Energy*, **150**, 482–492, https://doi.org/10.1016/j.energy.2018.02.142.

Rohatgi, A. 2020. WebPlotDigitizer.

Sadler, D., Cargill, A., et al. 2016. *Leeds City Gate*.

Sainz-Garcia, A., Abarca, E., Rubi, V. and Grandia, F. 2017. Assessment of feasible strategies for seasonal underground hydrogen storage in a saline aquifer. *International Journal of Hydrogen Energy*, **42**, 16657–16666, https://doi.org/10.1016/j.ijhydene.2017.05.076.

San Marchi, C. and Somerday, B.P.P. 2008. Thermodynamics of Gaseous Hydrogen and Hydrogen Transport in Metals. *In*: *MRS Spring 2008 Meeting, Session HH: "The Hydrogen Economy"*.

Scafidi, J., Wilkinson, M., Gilfillan, S.M.V., Heinemann, N. and Haszeldine, R.S. 2021. A quantitative assessment of the hydrogen storage capacity of the UK continental shelf. *International Journal of Hydrogen Energy*, **46**, 8629–8639, https://doi.org/10.1016/j.ijhydene.2020.12.106.

Schlumberger. 2014. ECLIPSE.

Schlumberger. 2019. Petrel 2019.

Scottish Power. 2020. Hatfield Moor - Gas Flows - ScottishPower. *Segmental Generation & Supply Statements*https://www.scottishpower.com/pages/hatfieldmoor_gas_flows.aspx .

Senseny, P.E., Hansen, F.D., Russell, J.E., Carter, N.L. and Handin, J.W. 1992. Mechanical behaviour of rock salt: Phenomenology and micromechanisms. *International Journal of Rock Mechanics and Mining Sciences and*, **29**, 363–378, https://doi.org/10.1016/0148-9062(92)90513-Y.

Setzmann, U. and Wagner, W. 1991. A New Equation of State and Tables of Thermodynamic Properties for Methane Covering the Range from the Melting Line to 625 K at Pressures up to 100 MPa. *Journal of Physical and Chemical Reference Data*, **20**, 1061–1155, https://doi.org/10.1063/1.555898.

Simbeck, D.R. 2004. CO2capture and storage-the essential bridge to the hydrogen economy. *Energy*, **29**, 1633–1641, https://doi.org/10.1016/j.energy.2004.03.065.

Šmigáň, P., Greksák, M., Kozánková, J., Buzek, F., Onderka, V. and Wolf, I. 1990.

Methanogenic bacteria as a key factor involved in changes of town gas stored in an underground reservoir. *FEMS Microbiology Letters*, **73**, 221–224, https://doi.org/10.1016/0378-1097(90)90733-7.

Stieber, S.J. 1970. Pulsed Neutron Capture Log Evaluation - Louisiana Gulf Coast. *Fall Meeting of the Society of Petroleum Engineers of AIME*, 7, https://doi.org/10.2118/2961-MS.

Stone, H.B.J., Veldhuis, I. and Richardson, R.N. 2009. Underground hydrogen storage in the UK. *Geological Society, London, Special Publications*, **313**, 217–226, https://doi.org/10.1144/SP313.13.

Storengy France. 2018. Beynes - Storengy. *Storengy France Website*.

Strobel, G., Hagemann, B., Huppertz, T.M. and Ganzer, L. 2020. Underground bio-methanation: Concept and potential. *Renewable and Sustainable Energy Reviews*, **123**, 109747, https://doi.org/10.1016/J.RSER.2020.109747.

Stuart, I.A. 1991. The Rough Gas Storage Field, Blocks 47/3d, 47/8b, UK North Sea. *Geological Society, London, Memoirs*, **14**, 477–484, https://doi.org/10.1144/gsl.mem.1991.014.01.59.

Swamee, P.K. and Jain, A.K. 1976. Explicit Equations for Pipe-Flow Problems. *Journal of the Hydraulics Division*, **102**, 657–664, https://doi.org/10.1061/JYCEAJ.0004542.

Tavassoli, Z., Carter, J.N. and King, P.R. 2004. Errors in History Matching - SPE-86883-PA. *SPE Journal*, **9**, 352–361.

Thaysen, E.M., McMahon, S., et al. 2021. Estimating microbial growth and hydrogen consumption in hydrogen storage in porous media. *Renewable and Sustainable Energy Reviews*, **151**, 111481, https://doi.org/10.1016/J.RSER.2021.111481.

The Crown Estate. 2018. Maps and GIS Data. *The Crown Estate website*.

The UK government. 2008. *Climate Change Act 2008*.

Tolbert, B. 2021. Top Dog Engineer https://topdogengineer.com/.

UK Onshore Geophysical Library. 2020. UK Onshore Geophysical Libraryhttps://ukogl.org.uk/.

Underhill, J.R., Monaghan, A.A. and Browne, M.A.E. 2008. Controls on structural styles, basin development and petroleum prospectivity in the Midland Valley of Scotland. *Marine and Petroleum Geology*, **25**, 1000–1022, https://doi.org/10.1016/j.marpetgeo.2007.12.002.

UNFCCC. 2015. Paris Agreement. *Conference of the Parties on its twenty-first session*, **21932**, 32, https://doi.org/FCCC/CP/2015/L.9/Rev.1.

Van Rossum, G. and Drake, F.L. 2009. Python 3 Reference Manual.

Vangkilde-Pedersen, T., Anthonsen, K.L., et al. 2009. Assessing European capacity for geological storage of carbon dioxide–the EU GeoCapacity project. *Energy Procedia*, **1**, 2663–2670, https://doi.org/10.1016/J.EGYPRO.2009.02.034.

VNIPITRANSGAZ. 2013. Подземные хранилища газа (underground gas storage)http://www.vtg.com.ua/experience/main/ugs.html?lang=en.

Vogel, J.V. 1968. Inflow Performance Relationships for Solution-Gas Drive Wells. *Journal of Petroleum Technology*, **20**, 83–92, https://doi.org/10.2118/1476-PA.

Ward, J., Chan, A. and Ramsay, B. 2003. The Hatfield Moors and Hatfield West Gas (Storage) Fields, South Yorkshire. *Geological Society, London, Memoirs*, **20**, 903–910, https://doi.org/10.1144/GSL.MEM.2003.020.01.76.

Watson, S.D., Lomas, K.J. and Buswell, R.A. 2019. Decarbonising domestic heating: What is the peak GB demand? *Energy Policy*, **126**, 533–544, https://doi.org/10.1016/J.ENPOL.2018.11.001.

Watts, J.W. 1997. Reservoir Simulation: Past, Present, and Future. *SPE Computer Applications*, **9**, 171–176, https://doi.org/10.2118/38441-PA.

Wickham, H. 2016. *Ggplot2: Elegant Graphics for Data Analysis*.

Williams, A. 2003. *Free Energy Relationships in Organic and Bio-Organic Chemistry*, https://doi.org/10.1039/9781847550927.

Williams, D.M. and Harper, A.T. 1988. *A Basin Model for the Silurian of the Midland Valley of Scotland and Ireland*.

Wilson, G. and Rowley, P. 2019. *Flexibility in Great Britain's Gas Networks : Analysis of Linepack and Linepack Flexibility Using Hourly Data*.

Wyllie, M.R.J., Gregory, A.R. and Gardner, L.W. 1956. ELASTIC WAVE

VELOCITIES IN HETEROGENEOUS AND POROUS MEDIA. *GEOPHYSICS*, **21**, 41–70, https://doi.org/10.1190/1.1438217.

Xia, C. and Wilkinson, M. 2017. The geological risks of exploring for a CO2 storage reservoir. *International Journal of Greenhouse Gas Control*, **63**, 272–280, https://doi.org/10.1016/j.ijggc.2017.05.016.

Yekta, A.E., Manceau, J.-C., Gaboreau, S., Pichavant, M. and Audigane, P. 2018. Determination of Hydrogen–Water Relative Permeability and Capillary Pressure in Sandstone: Application to Underground Hydrogen Injection in Sedimentary Formations. *Transport in Porous Media*, **122**, 333–356, https://doi.org/10.1007/s11242-018-1004-7.

Yu, L. and Liu, J. 2015. Stability of interbed for salt cavern gas storage in solution mining considering cusp displacement catastrophe theory. *Petroleum*, **1**, 82–90, https://doi.org/10.1016/j.petlm.2015.03.006.

Zivar, D., Kumar, S. and Foroozesh, J. 2020. Underground hydrogen storage: A comprehensive review. *International Journal of Hydrogen Energy*, https://doi.org/https://doi.org/10.1016/j.ijhydene.2020.08.138.

Chapter 8 Appendices

8.1 Appendix 1 – Publication: A quantitative assessment of the hydrogen storage capacity of the UK continental shelf

8.1.1 Journal publication

Published as: Scafidi, J. *et al.* (2021) ‘A quantitative assessment of the hydrogen storage capacity of the UK continental shelf’, *International Journal of Hydrogen Energy*. Elsevier Ltd, 46(12), pp. 8629–8639. doi: 10.1016/j.ijhydene.2020.12.106.

INTERNATIONAL JOURNAL OF HYDROGEN ENERGY 46 (2021) 8629–8639

Available online at www.sciencedirect.com

ScienceDirect

journal homepage: www.elsevier.com/locate/he

A quantitative assessment of the hydrogen storage capacity of the UK continental shelf

Jonathan Scafidi[*], *Mark Wilkinson*, *Stuart M.V. Gilfillan*, *Niklas Heinemann*, *R. Stuart Haszeldine*

School of GeoSciences, University of Edinburgh, James Hutton Road, Edinburgh, EH9 3FE, UK

HIGHLIGHTS

- UK requires 150 TWh of seasonal hydrogen storage capacity to decarbonise gas.
- First quantification of hydrogen storage capacity in gas fields.
- 6900 TWh hydrogen working gas capacity in UK offshore gas fields.
- Low temperature/high pressure capacity storage sites are best.
- Offshore gas fields and wind could develop offshore hydrogen production.

GRAPHICAL ABSTRACT

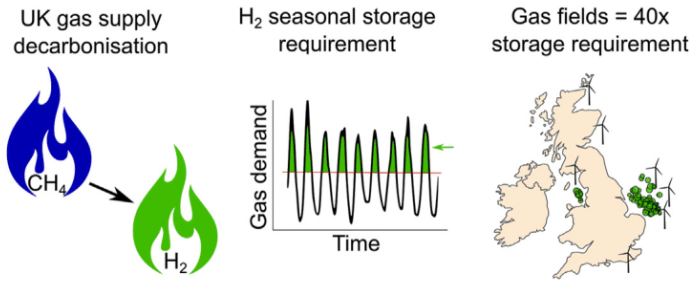

ARTICLE INFO

Article history:
Received 17 August 2020
Received in revised form
16 November 2020
Accepted 13 December 2020
Available online 4 January 2021

Keywords:
Seasonal hydrogen storage
Depleted gas fields
Offshore hydrogen production
Seasonal storage capacity quantification
Decarbonisation

ABSTRACT

Increased penetration of renewable energy sources and decarbonisation of the UK's gas supply will require large-scale energy storage. Using hydrogen as an energy storage vector, we estimate that 150 TWh of seasonal storage is required to replace seasonal variations in natural gas production. Large-scale storage is best suited to porous rock reservoirs. We present a method to quantify the hydrogen storage capacity of gas fields and saline aquifers using data previously used to assess CO_2 storage potential. We calculate a P50 value of 6900 TWh of working gas capacity in gas fields and 2200 TWh in saline aquifers on the UK continental shelf, assuming a cushion gas requirement of 50%. Sensitivity analysis reveals low temperature storage sites with sealing rocks that can withstand high pressures are ideal sites. Gas fields in the Southern North Sea could utilise existing infrastructure and large offshore wind developments to develop large-scale offshore hydrogen production.

* *Corresponding author.*
E-mail address: jonathan.scafidi@ed.ac.uk (J. Scafidi).
https://doi.org/10.1016/j.ijhydene.2020.12.106

Introduction

In 2018, fossil fuels accounted for 85% of global primary energy demand [1], resulting in the release of 33.1 billion tons of carbon dioxide into the atmosphere [2]. The Paris agreement, reached in December 2015 by 196 members of the United Nations Framework Convention on Climate Change (UNFCCC), aims to keep the increase in global average temperature to well below 2 °C above pre-industrial levels (preferably less than 1.5 °C) in order to substantially reduce the risks and effects of climate change [3]. Meeting these targets requires rapid decarbonisation of power generation, heating, industry, and transport.

Success in decarbonising the UK electricity sector has led to increased deployment of renewable energy sources such as wind and solar. Whilst this increase in renewable energy sources will reduce CO_2 emissions intensity, economic security of supply and grid balancing issues associated with variations in wind, solar and water energy production are likely to increase [4–7].

Decarbonising heating has proven to be more challenging. The UK relies heavily on natural gas for heating with 23 million homes connected to the existing gas grid [8]. Heating and hot water in buildings alone accounts for 20% of the UK's total greenhouse gas emissions [8]. The CCC (Committee on Climate Change) recommended a reduction in these specific emissions of 20% below 1990 levels by 2030 [8] and a target of 57% reduction for all emissions from 1990 levels by 2030 [9].

A major challenge is replacing the seasonal flexibility of the natural gas supply with a low carbon alternative that can match the peak winter demand. Currently production rates from UK gas fields, along with imports from Norway, are increased in the winter to match peak demand and satisfy 70% of UK gas demand [10]. The seasonal difference in gas demand between summer and winter is between 45 and 75 TWh (calculated from Ofgem data [10], 2009–2018).

The key to solving issues of intermittency is the coupling of low carbon energy sources with large-scale energy storage systems capable of storing several TWh across seasonal timescales [11]. Large-scale natural gas (CH_4) storage is a proven technology where subsurface stores are filled during periods of low demand (i.e. summer) and emptied during high demand periods in winter.

Large-scale hydrogen production coupled with storage in geological structures is a technically feasible method for seasonal energy balancing [11–13] and could play an important role in enabling a low carbon energy system. However, this requires a decarbonised source of hydrogen either through steam methane reforming of natural gas combined with carbon capture and storage, or electrolysis using low carbon energy sources, with both sources being the subject of investigation on the UK continental shelf [14–20].

With 8.4 GW of existing offshore wind capacity in the UK and a government commitment of increasing that figure to 40 GW by 2030 [21], large-scale production and storage of hydrogen on the UK continental shelf could provide inter-seasonal balancing of renewable energy production while making use of existing oil and gas infrastructure. 40 GW of offshore wind with a load factor of 60% and an electrolyser efficiency of 70% could produce 147.17 TWh of hydrogen per year. Supplying the whole UK gas demand of 877.51 TWh [22] would require around six times this amount of offshore wind. Steam methane reformation of natural gas is therefore the more likely source for hydrogen to replace natural gas, but hydrogen production via electrolysis could still play an important role in balancing renewable electricity generation.

Underground hydrogen storage

Similar to natural gas, hydrogen can be stored in subsurface salt caverns, providing energy densities around 100 times greater than compressed air energy storage [23]. Hydrogen storage in salt caverns has been implemented commercially for industrial feedstock in three caverns at Teeside (UK) since the 1970s [24] and in two at the US Gulf Coast since the 1980s [25]. Salt cavern natural gas storage is important for short term energy demand fluctuations as they allow multiple injection and withdrawal cycles per year. However, salt caverns currently contribute only 20% of the total worldwide gas storage capacity [26] and their availability is limited to areas with thick subsurface salt deposits.

Hydrogen can also be stored in the pore space within a geological structure, displacing formation waters or, in the case of depleted gas fields, residual gases, which offers a geographically more independent and flexible solution for large-scale hydrogen storage [27]. Leakage is prevented by the presence of a caprock with a high capillary entry pressure above the reservoir and a trap structure will prevent the hydrogen from migrating laterally to guarantee its reproduction [28]. To date, pure hydrogen has not been stored in porous rocks, however, hydrogen-rich town gas (typically ~50% by volume) has been stored in porous rocks in Germany, France, and the Czech Republic [29].

As of 2018 there are 46 billion cubic metres (bcm) of natural gas storage in 75 saline aquifer storage sites and 334 bcm in 492 depleted hydrocarbon fields worldwide [26]. Whilst no commercial projects currently store hydrogen in porous rocks, no physical or chemical barriers have been identified that could not be addressed using the knowledge gained from decades of experience in underground natural gas storage, and it was concluded early on that the physical and chemical challenges associated with hydrogen storage were manageable [12,13,30]. Several modelling studies investigate the cyclic injection and storage of hydrogen in geological formations using standard industry software and no major technical obstacles have been reported [31–33].

Recent work compared the possibility of hydrogen storage with natural gas storage at the Rough Gas Storage Facility [34], which at 3.3 bcm was the UK's largest porous rock gas store until it ceased to operate as a storage site in 2017. The hydrogen storage capacity (in terms of energy) was found to be approximately one third that of natural gas, due to its lower energy density [35]. The same study found that losses through dissolution and bacterial action would be negligible [34].

Replacement of natural gas in the UK gas grid will require large-scale storage and, to date, no large-scale quantitative assessment of the potential hydrogen storage capacity available in subsurface porous rock has been undertaken. Here, we estimate the hydrogen storage capacity of the porous rocks on

the UK continental shelf using a database originally compiled for geological CO_2 storage. The methodology outlined here is directly applicable to other national databases for carbon storage where they exist, paving the way for the compilation of robust hydrogen storage capacities for other large sedimentary basins. Furthermore we also calculate the proximity to storage sites to existing and planned offshore wind developments on the UK continental shelf which could provide a source of low carbon hydrogen in the future and may require large-scale energy storage.

Hydrogen storage capacity requirements for the UK

Replacement of existing storage

The current total natural gas storage capacity for the UK is 16.56 TWh [36], which is equivalent to 6.89 days' average supply based on 2019 UK gas demand of 877.51 TWh [22]. This is spread across 1.50 billion cubic metres (bcm) of underground gas storage [37], 0.37 bcm of which is in porous rocks at Humbly Grove and Hatfield Moor [38]. This equates to a porous rock working gas capacity of 2.34 TWh for natural gas [39]. If the UK moves to a 100% hydrogen gas network, only one third of the energy can be stored in these porous rock sites, equivalent to 0.78 TWh (assuming a similar cushion gas requirement as per a study on the Rough Gas Storage Facility study [34]) due to the lower energy density of hydrogen [34]. This would require an extra 1.56 TWh of working gas capacity to be found.

Further to additional porous rock storage capacity, the natural gas that is stored within the gas network itself, known as linepack, also needs to be considered. The energy density of hydrogen at linepack pressures can be four times lower than that of natural gas [40], so replacement of natural gas with hydrogen would, in the worst case, result in four times less energy stored in the linepack. Currently the UK national transmissions system and local gas grids contain 4.88 TWh at their maximum and 3.84 TWh at their minimum, with an average of 4.41 TWh [41]. Assuming that energy needs to be accessible for grid functionality then a further 2.88 to 3.66 TWh of working gas capacity will be required.

This means that replacing natural gas with hydrogen in the UK grid will require 4.44 to 5.22 TWh of additional working gas capacity to compensate for hydrogen's lower energy density.

Estimates of inter-seasonal storage requirements

Estimates from demand

The H21 Leeds City Gate project produced by utility network provider Northern Gas Networks, focused on the provision of heat through a 100% hydrogen gas network for the Yorkshire city of Leeds in northern England, UK [42]. This was based on converting the existing natural gas network of the city entirely to hydrogen. The study calculated that the conversion of the city's natural gas network to hydrogen would require 40 days of maximum average daily demand for inter-seasonal storage [42]. Extrapolating this 40 day storage requirement to a national level using the maximum 3 hourly change in the gas network as peak demand of 251 GWh [41] (from data between January 2013 and March 2018) results in a maximum daily demand of 2.0 TWh which translates to a storage requirement of 80.3 TWh.

Using the same assumption of a 40 day requirement but using a peak demand figure of 170 GW calculated from household user data [43] (collected between May 2009 and July 2010) gives a maximum daily demand of 4.1 TWh. Multiplying this maximum daily demand by the 40 day requirement equates to a storage requirement of 163.2 TWh. Finally, using the 2018 UK gas demand of 881 TWh [44], 40 days of seasonal storage would equal 96.5 TWh.

Estimates from supply

Over 70% of UK gas demand is supplied by gas fields located within the UK continental shelf (UKCS) and Norway, with storage, LNG (liquefied natural gas) and pipeline imports making up the balance [10]. Fig. 1 shows the UK gas demand and supply source between October 2009 and October 2018 (data from Ofgem [10]). Negative values indicate exports and injection into storage. Over the past decade, seasonal variations in demand are increasingly accommodated by imports

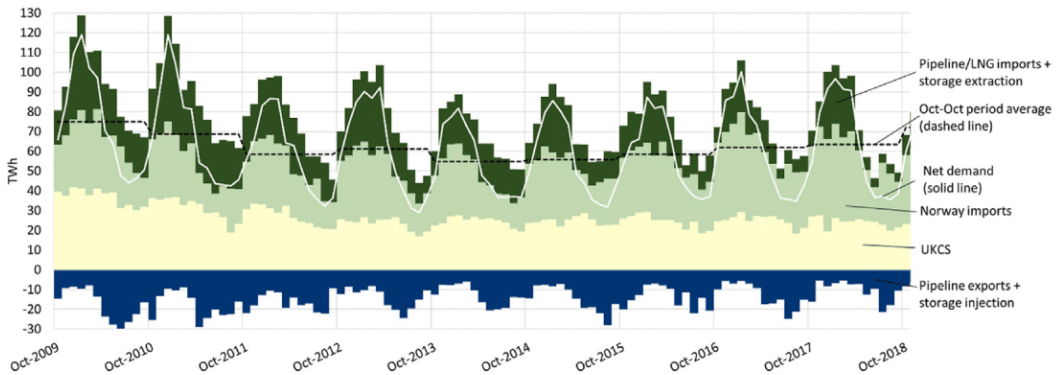

Fig. 1 – UK gas demand and supply source from October 2009 to October 2018 made using data from Ofgem [10]. Gas supplied from the UK continental shelf (UKCS) and Norway respectively makes up over 70% of demand. Negative values indicate injection into storage and pipeline exports. The dashed line is the yearly average from October to October, and the white line is the net demand.

from Norway and other pipelines from Europe due to a reduction in supplies from the UK continental shelf and LNG imports.

We have calculated the average monthly demand for each 12 month period from October to September in order to capture the full range of seasonal change in gas demand. The difference from this average for each month is shown in Fig. 2. In the winter period of 2017/18 total demand above the period average was 133.49 TWh. Assuming a constant hydrogen production rate of 63.35 TWh per month (the October 2017 to October 2018 average monthly demand) and no imports then the 133.49 TWh figure would be indicative of the level of working gas capacity required for seasonal storage of hydrogen. However, it is worth noting that this figure represents a maximum required working gas capacity as hydrogen production via steam methane reformation (SMR) could still utilise the seasonal variations in production rates of natural gas fields by building more capacity [45].

The Energy Research Partnership (ERP), a UK public-private partnership seeking to guide and accelerate innovation in the energy sector through enhancing dialogue and collaboration, investigated the potential role of hydrogen in the UK energy system [45]. This work found that if the full UK domestic heat and industrial demand of 424 TWh for the year 2013 was switched to hydrogen produced by SMR, as little as 54 GW of installed SMR capacity could be used (run continuously at a >90% load factor with 1 month downtime per year) if combined with 75 TWh of storage capacity (it is assumed that this figure is working gas capacity) [45]. Assuming the relationship between storage capacity and gas demand is linear, then the 2018 UK gas demand of 881 Twh [44] would require around double this amount of working gas capacity, ~150 TWh. This is consistent with the 133.5 TWh figure calculated previously from the 2008 to 2018 Ofgem data [10].

Methods and data

The CO_2 stored database

The CO_2 Stored database was developed by the UK Storage Appraisal Project, a consortium of Universities and the British Geological Survey (BGS), funded by the Energy Technologies Institute and published in 2012. It was developed to ascertain the geological storage capacity of the UK continental shelf for CO_2, and was maintained by the Crown Estate and BGS between 2013 and 2018 [46]. It is now maintained and developed solely by the BGS.

The database includes saline aquifers (porous rock formations saturated with saline, non-potable water), depleted and active hydrocarbon fields, and consists of some 574 entries. Information contained in the database includes porosity and permeability, areal extent, thickness, pore volume, pressure regime, location, and type of storage site. Entries are classified as either having identified structures/traps or not, and being open or closed pressure systems. Storage volumes in the database were calculated using Monte Carlo analysis and are provided in tonnes. However, calculations in this study are given in TWh to allow comparison between hydrogen and natural gas. P50 values (meaning that 50% of volumes exceed the P50 estimate and hence 50% of volumes are less than the P50 vol) for formation pore volumes in the CO_2 Stored database were used in this study and therefore all hydrogen storage capacities are also P50 values.

Methodology

The method used to calculate the hydrogen storage capacity of the UK continental shelf from the database comprised of three stages:

1) Filtering: The database was filtered for depth, reservoir quality, type (oil fields, gas fields, aquifers), along with removal of inappropriate entries.
2) Aquifer efficiency calculations: The calculation of storage efficiency to estimate useable pore volumes within saline aquifers with and without identified structures.
3) Hydrogen capacity calculation: Conversion of the available pore volume for hydrogen storage into hydrogen energy equivalent.

The stages were coded in "R" programming language [47] and run using the CO_2 Stored database as input. The code used is available in the supplementary information Appendix 2.

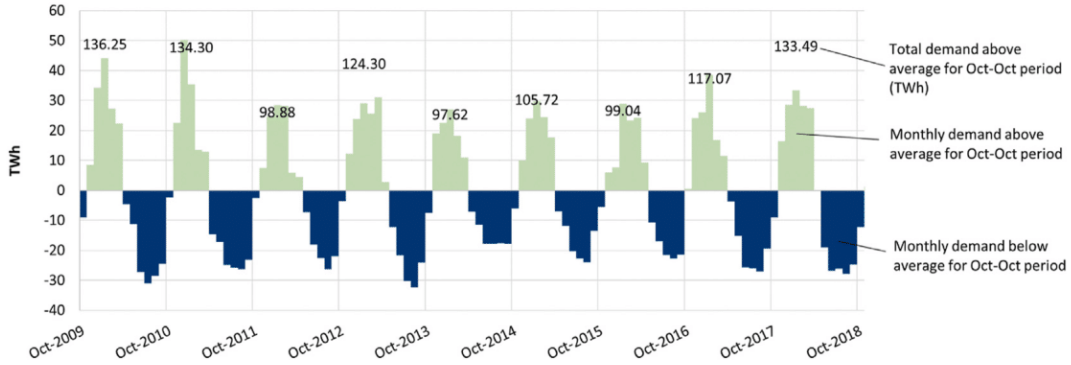

Fig. 2 – UK gas demand difference from yearly October to October average (see dashed line on Fig. 1). Positive values are supply above average and negative values are supply below average. This graph quantifies the seasonal changes in gas demand over each October–October period. The difference between winter peaks and summer lows are 45–75 TWh depending on the year.

Stage one: filtering

Site selection. Sites containing oil or gas condensates were considered unsuitable due to the potential for contamination of stored hydrogen. These were removed and only gas fields and saline aquifers were considered, bringing the total number of entries in the database down to 470.

Saline aquifers are far less well understood than hydrocarbon fields due their size and lack of discovered commercially exploitable hydrocarbon fields. However, they can contain traps that may be suitable for hydrogen storage. Whilst some of these traps have been studied during oil and gas exploration, there are likely to be many undiscovered or undocumented traps not present in the CO_2 Stored database, which relies heavily on hydrocarbon industry data. Hence, we deem saline aquifers to be suitable for hydrogen storage and include them in the hydrogen storage capacity estimate.

Reservoir quality filtering of saline aquifers. Gas fields are deemed to be highly suitable for hydrogen storage as they have trapped and stored buoyant natural gas for geological periods of time. Therefore, gas fields were not filtered for depth and other reservoir properties due to their proven ability to store gas over long time scales.

Saline aquifers were filtered for a minimum permeability of 100 mD and porosity of 10% based on CO_2 storage parameters [48]. However, hydrogen is a much smaller molecule and based on recent work on helium [49], it may be diverted into disconnected and dead-end pores not accessed by larger molecules. This means that lower porosities and permeabilities than those required for CO_2 storage may be acceptable, but further investigation is needed to verify this. Porous rock natural gas storage sites in the UK show average permeabilities of less than 100 mD. The Rough gas storage facility in the UKCS has well average permeabilities ranging between 2 mD – 184 mD [50], the average core permeabilities for the two wells at the UK Hatfield Moors gas storage facility are 38.4 and 248 mD [51], and the average permeability for the UK Humbly Grove gas storage facility is only 20 mD in the storage formation (Great Oolite Group) [52]. However, we apply the precautionary principle and filtering for reservoir quality reduced the number of entries to 325.

Depth filtering of saline aquifers. The saline aquifers were then filtered for depth, using a minimum value of 200 m TVDSS based on accepted compressed air storage guidance [53]. As hydrogen requires more work to compress than CO_2 or natural gas, having a shallow minimum depth would save on compression costs. This reduced the number of entries in the database considered in this study to 317.

A maximum depth filter of 2500 m TVDSS was applied to the mean depth of saline aquifers. This depth was chosen as porosity in sandstone reservoirs typically declines to less than 10% below these depths [54], meaning a lack of available effective pore space for storage. 2500 m is also the maximum depth cited for best practice in CO_2 storage [55]. This brought the number of entries considered down to 202.

Duplicate entries and missing data. Some sites were duplicated as result of subdivision of larger units. For example, the Bunter sandstone which has entries for the full extent, zones, and closures. The full extent and zones were filtered out as the closures had been identified as separate entries in the database. This brought the number of entries considered down to 191.

Not all entries in the CO_2 Stored database were complete, with some missing key data required for the hydrogen capacity calculation. These were filtered out bringing the number of entries in the database considered down to 177.

Stage two: efficiency calculations for saline aquifers

After the filtering stage, 82 saline aquifers remained. Of these 12 have no identified structures or traps. In order to store hydrogen in a porous rock formation we assume that, as with natural gas storage, a trap (a physical shape to the rock layers) is required to contain injected hydrogen within the areal extent that allows production wells to recover it. As there are no identified traps in these 12 saline aquifers we must estimate the likely pore volume of unidentified traps within them. Based on a method recently developed for compressed air energy storage [56] we determined that there were very low storage capacities in these saline aquifers. Combining this with the low confidence of location, and lack of data we do not consider these saline aquifers further. More details on these calculations and their results are provided for interest in appendices 1 and 3 in the supplementary information.

Estimating useable pore volumes in saline aquifers with identified structures and/or traps. A storage efficiency of 1% was applied to the 70 saline aquifers with identified structures and traps based on the conservative estimate of the proportion of pore volume available for CO_2 storage in the CO_2 Stored database [46]. This assumption was required as no information on trap geometries and their suitability for seasonal gas storage exists in the CO_2 Stored database.

Stage three: hydrogen capacity estimation

For depleted gas fields and saline aquifers, the estimated reservoir pore volumes were converted into hydrogen energy equivalent in TWh, allowing direct comparison to estimated energy storage requirements.

Pore volumes were converted to equivalent hydrogen volumes at STP using equation (1) adapted from the Rough Gas Storage Facility study [34].

$$V_{H(STP)} = \frac{V_{H2}(1 - S_{wi})P}{ZP_0}\frac{T_0}{T} \quad (1)$$

where $V_{H(STP)}$ is the volume of hydrogen at STP, V_{H2} is the volume of pore space suitable for hydrogen storage, S_{wi} is the irreducible water saturation (defined as the lowest water saturation that can be achieved by displacing the water with oil or gas and given in the CO_2 Stored database as 0.423), P_0 is pressure at STP, P is reservoir pressure (hydrostatic, calculated from depth), T_0 is temperature at STP, T is reservoir temperature, and Z is the compressibility factor of hydrogen which was linked to the temperature and pressure of the reservoir using an equation of state [57]. The irreducible water saturation in the CO_2 Stored database was used as a conservative estimate. We are currently aware of only one laboratory measurement of hydrogen-water relative permeability in

sandstone from Yekta et al. [58] which gives a value of ~0.13. The calculation was also run using this value to see what effect it had on the hydrogen storage capacity. Eq. (1) was also subject to a sensitivity analysis to determine the influence of each variable.

Only a proportion of the total volume calculated using Eq. (1) comprises the working gas capacity (WGC) i.e. the gas that could be economically stored and removed each cycle. The gas required to keep reservoir pressure at a suitable level to allow efficient production of stored gas is called the cushion gas requirement (CGR). We assumed a cushion gas requirement of 50% based on the Rough Gas Storage Facility study [34]. Hydrogen volume was converted using density at STP to calculate mass using the Nobel-Abel equation of state [59] (Eq. (2)).

$$\rho = P/(RT + bP) \quad (2)$$

where ρ is density, P is pressure, R is the gas constant (4160 J/kg K for hydrogen [60]), T is temperature, and b is the co-volume (15.84 cm^3/mol for hydrogen [61]). Mass was converted to energy using the higher heating value (HHV) for hydrogen (39.41 kWh/kg [62]) to allow a comparison to energy demand in the UK.

Offshore wind development proximity calculation

After filtering and volumetric calculations were completed, the remaining gas field and saline aquifer data were tabulated and loaded into QGIS geographical information software [63]. Crown estate offshore wind installation data [64,65] was also loaded into the GIS software and a nearest neighbour analysis was performed to calculate how close each of the remaining gas fields and saline aquifers were to existing or planned offshore wind installations. For the locations of saline aquifers without identified structures the geographic centres given in the CO_2 Stored database were used.

Results

Using the methods outlined and the irreducible water saturation of 0.423 given in the CO_2 Stored database, 95 depleted gas fields and 82 saline aquifers were identified as suitable for hydrogen storage. Using an available pore space of 62.9 billion cubic metres, a total working gas capacity of 9100 TWh energy equivalent of hydrogen was calculated. A full list of sites and calculated capacities is available in the supplementary information, appendix 4.

Gas fields account for 6900 TWh of working gas capacity, saline aquifers with identified structures account for 2100 TWh of working gas capacity, and saline aquifers with no identified structures account for 70 TWh of working gas capacity (see Table 1). Calculated figures are given to 2 significant figures for gas fields and saline aquifers with identified structures, and 1 significant figure for saline aquifers with no identified structures based on the differing uncertainties associated with them. Table 1 also shows the capacity estimates where $S_{wi} = 0.13$ (from Yekta et al. [58]), an increase of 51% (see section on sensitivity analysis below).

Fig. 3 shows the location of all identified hydrogen storage sites and the location of active, under construction, and planned offshore wind developments.

Twenty-nine of the gas fields are 10 km or less from wind developments with the maximum distance being 46 km. Twenty-one of the saline aquifer storage sites with identified structures are 10 km or less from wind developments, with twenty-two sites at a distance of 100 km or greater, with the maximum distance being 186 km. Four of the saline aquifer storage sites with no identified structures are 10 km or less from wind developments with seven sites at a distance of 100 km or greater with the maximum distance being 189 km. As the distances for saline aquifers with no identified structures are measured from centroids rather than identified sites these hold little meaning.

85% of identified gas field storage capacity is located in the Southern North Sea (SNS) and the remaining 15% is located in the East Irish Sea (EIS). Fig. 4 shows the Southern North Sea gas fields and offshore wind developments. The Rough gas field (previously Rough gas storage facility) mentioned earlier is highlighted along with the largest gas field, Leman.

The majority of storage sites have a capacity between 1 and 100 TWh. Size distribution of storage sites by type and geographic area is given in Fig. 5.

Sensitivity analysis and factors affecting hydrogen storage capacity estimates

A base case scenario was created from average values in the CO_2 Stored database (with an arbitrary 1 bcm pore volume), along with high and low values for each variable based on extremes. This data is shown in Fig. 6 as a tornado plot, with the base case values shown in the middle of each bar and the extreme values on the ends (labelled high and low).

The variables that are least well known are the storage pressure (P), working gas capacity fraction (WGC), and

Table 1 – Filtering parameters, final number of entries from the CO_2 Stored database post-filtering, and storage capacities by site type and S_{wi} value used. Storage capacities given to 2 significant figures.

	Depth	Porosity & Permeability	No. of entries	Working gas capacity (TWh) $S_{wi} = 0.423$	Working gas capacity (TWh) $S_{wi} = 0.13$
Gas fields	n/a	n/a	95	6900	10,000
Saline aquifer with identified structure	>200 m <2500 m	≥10% ≥100mD	70	2100	3200
Saline aquifer with no identified structure	>200 m <2500 m	≥10% ≥100mD	12	70	100
Total			177	9100	14,000

irreducible water saturation (S_{wi}). All three will be site specific to some degree, affected by the geology of the storage site and in the case of WGC and pressure, economics of compression and storage. Irreducible water saturation is likely to be lower than the base case as evidenced by the work of Yekta et al. [58]. Z (compressibility factor) has relatively little effect as hydrogen compressibility does not change significantly across the temperature/pressure range encountered in the CO_2 Stored database.

A sensitivity analysis was performed to determine which of the variables in equation (1) had the biggest influence on working gas capacity estimates for hydrogen. Fig. 7 shows the influence of each variable in equation (1) on the output (working gas capacity) as they are varied by ±10%. Compressibility (Z) has the biggest influence with a change of −1.006% in output with every increase of 1%, however as this is directly linked to temperature and pressure, it is ultimately these variables that result in changes in compressibility. Irreducible water saturation (S_{wi}) has the smallest effect of −0.733% with every increase of 1%.

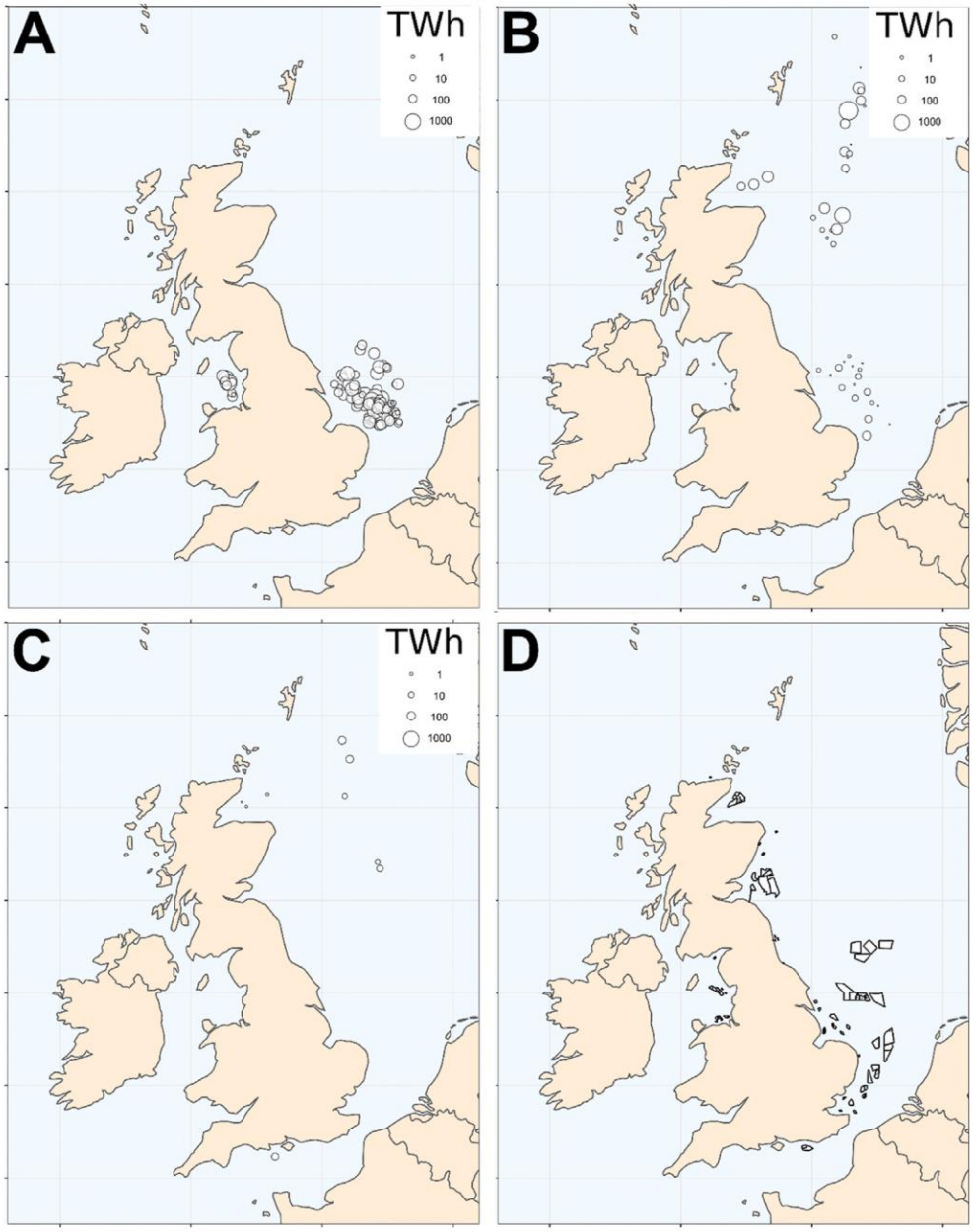

Fig. 3 – Location and relative sizes of different storage types and offshore wind on the UK continental shelf. A = Gas fields; B = Saline Aquifers with Identified Structures; C = Aquifers with no identified structures; D = location of existing and planned offshore wind developments. The majority of storage exists in the gas fields of the Southern North Sea, in close proximity to the majority of offshore wind developments. Figure generated in R using gplot2 [72].

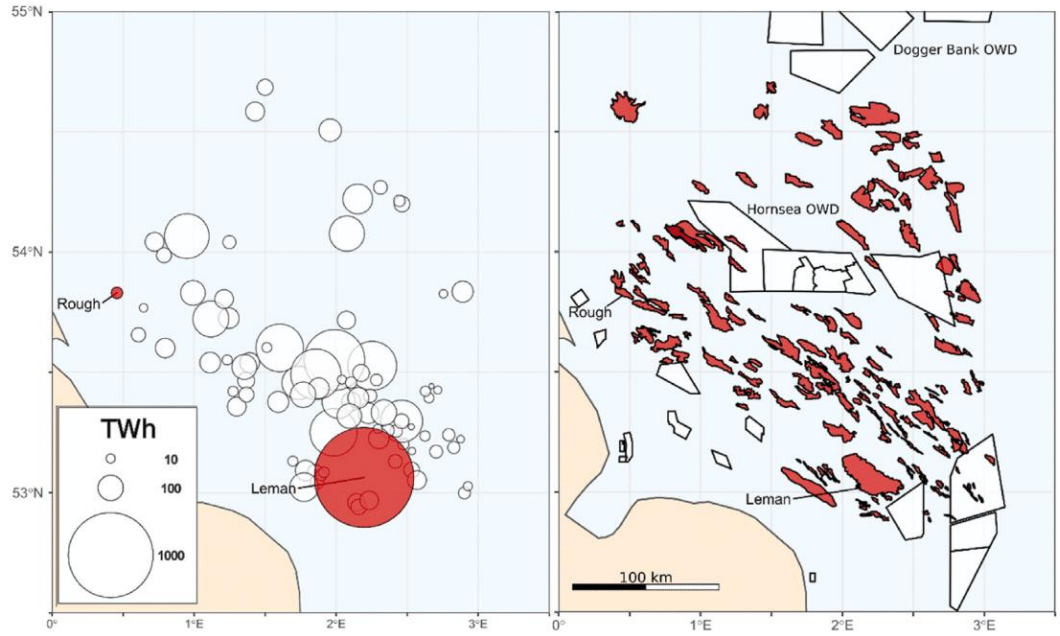

Fig. 4 – Detailed view of the Southern North Sea gas fields. Left panel shows gas fields and their relative storage capacities in TWh. Right panel shows the locations of the gas fields relative to planned and visiting offshore wind developments (OWD). The Rough (12 TWh) and Leman (1200 TWh) gas fields are highlighted in both panels.

Discussion

Our results show that there is a potential 6900 TWh of high confidence (P50) working gas capacity for hydrogen in gas fields in the Southern North Sea and East Irish Sea.

This is greater than any estimates of seasonal storage capacity requirements given earlier, the highest of which was ~150 TWh. The majority of this storage capacity is located in the Southern North Sea close to existing and planned large offshore wind developments which could be used to produce hydrogen that could be injected into seasonal energy stores in

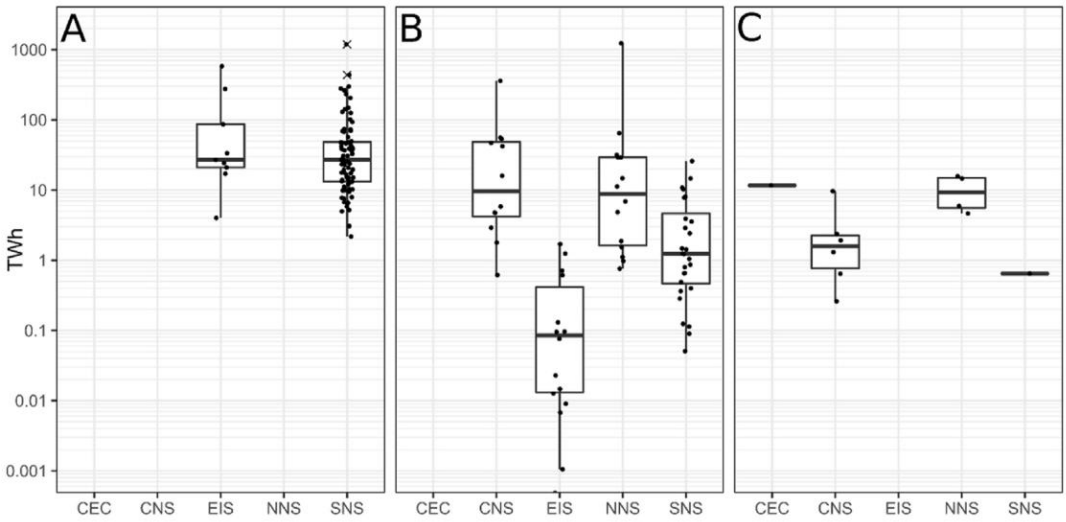

Fig. 5 – Boxplot diagram showing storage site size distribution by geographic region. A = Gas fields; B = Saline aquifers with identified structures; C = Saline aquifers with no identified structures. White boxes extend to the 25th and 75th percentiles, bold horizontal lines within boxes represent the median value, whiskers extend 1.5 times the distance between the first and third quartiles, crosses represent outliers and black points represent data points. CEC = Central English Channel; CNS = Central North Sea; EIS = East Irish Sea Basin; NNS = Northern North Sea; SNS = Southern North Sea. The SNS gas fields provide the largest number and diversity of site sizes.

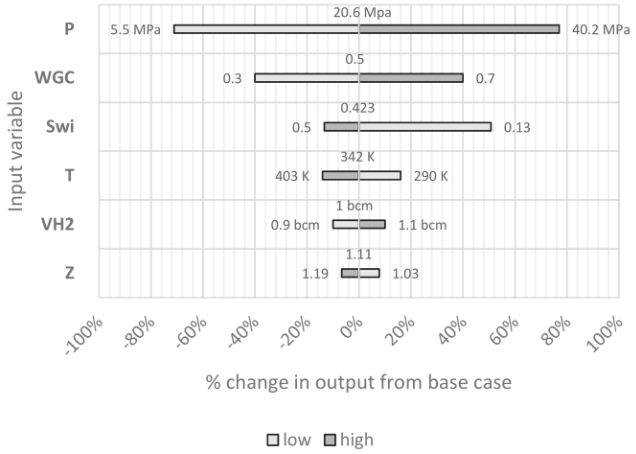

Fig. 6 – Tornado plot showing the base, high and low for variables in equation (1) and their effect on the output (hydrogen storage capacity). Uncertainty in P, WGC, and Swi have the biggest potential to change the storage capacity estimate P = reservoir pressure; WGC = the working gas capacity fraction; Swi = the irreducible water saturation; T = reservoir temperature; VH2 = the volume of pore space suitable for hydrogen storage; and Z = the compressibility factor of hydrogen.

hydrogen stored would be low temperature reservoirs capable of containing high pressure while allowing for a relatively high working gas capacity fraction i.e. a higher working gas capacity would make a storage site more economically viable. Further refinement of ideal storage site parameters for site selection would need to take this into account.

As the relative permeability of hydrogen in water is not well defined it is unclear as to whether viscous fingering would dominate over capillary limited flow. As viscous fingering can be controlled to some degree by injection rate it is not unlikely that the low irreducible water saturations demonstrated by Yekta et al. [58] could be achieved in real storage sites.

This high-level study sought to estimate total hydrogen storage capacity in the UK continental shelf. Further refinement would need to take into consideration the potential conflict with CO_2 storage sites, potential reactions between hydrogen and existing fluids in the gas fields such as natural gas, carbon dioxide, and hydrogen sulphide, and well integrity.

This methodology can also be applied to other carbon storage databases where they exist to provide an estimate of hydrogen storage capacity at a national level. Such databases currently exist in Australia [66], Brazil [67], China [68], Europe

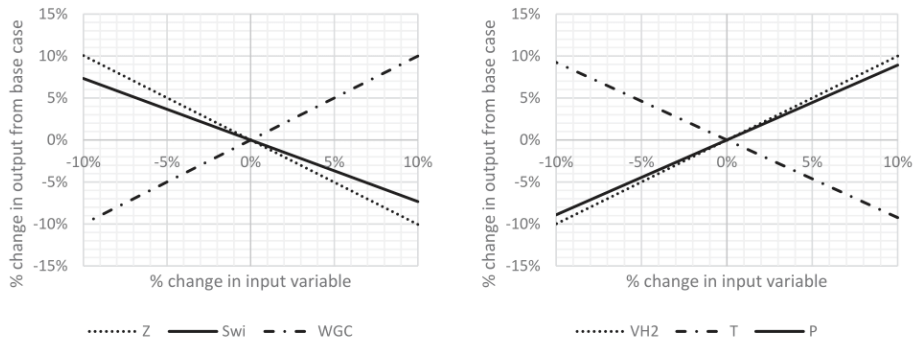

Fig. 7 – Sensitivity of variables in Eq. (1). All variables are positively correlated with changes in output except temperature, irreducible water saturation, and compressibility factor. P = reservoir pressure; WGC = the working gas capacity fraction; Swi = the irreducible water saturation; T = reservoir temperature; VH2 = the volume of pore space suitable for hydrogen storage; and Z = the compressibility factor of hydrogen.

the future. Individual gas fields offer a range of storage capacities between <10 TWh to >1000 TWh. Offshore hydrogen production is currently being investigated along with energy hubs which combine hydrogen and electricity production from offshore wind with existing oil and gas infrastructure [14–19].

We also show that there is a potential 2200 TWh of working gas capacity for hydrogen in saline aquifers, however there are considerable hurdles to providing accurate estimations of hydrogen storage capacity in saline aquifers in the CO_2 Stored database. This is due to the amount of uncertainty in the size and location of useable pore space within suitable structures, especially in aquifers with no identified structures, making this a low confidence estimate.

Sensitivity analysis of Eq. (1) and the tornado plot in Fig. 6 shows that the ideal storage sites in terms of capacity of [69], Norway [70], and North America [71].

Conclusions

We present a methodology to estimate hydrogen storage capacity in porous rocks at a national level using a carbon dioxide storage database for the UK. We find a P50 estimate of 6900 TWh of hydrogen storage capacity in the gas fields of the UK continental shelf and a lower confidence estimate of 2200 TWh in saline aquifers. These figures are an order of magnitude greater than all known estimates for the seasonal storage requirement for the UK. This methodology can be applied to other national carbon dioxide storage databases where they exist to provide a high-level quantified estimate of hydrogen storage potential.

Declaration of competing interest

The authors declare that they have no known competing financial interests or personal relationships that could have appeared to influence the work reported in this paper.

Acknowledgements

JS is supported by a Natural Environment Research Council (NERC) National Productivity Investment Fund PhD 460 studentship NE/R009228/1. MW, NH and RSH are supported by funding from the Engineering and Physical Sciences Research Council (EPSRC) grant number EP/S027815/1. SMVG is supported by funding from the UKCCS Research centre, Total, and NERC grant number NE/R018049/1. The authors would also like to thank the British Geological Survey for providing access to the CO_2 Stored database. Finally, the authors would like to thank the reviewers for their comments and feedback on the manuscript which have significantly improved the final version.

Appendix A. Supplementary data

Supplementary data to this article can be found online at https://doi.org/10.1016/j.ijhydene.2020.12.106.

REFERENCES

[1] Primary energy - BP statistical review of world energy 2019 | 68th ed.. 2019.
[2] IEA., GECO. Int energy agency website 2019. https://www.iea.org/geco/. [Accessed 6 August 2019].
[3] UNFCCC. Paris agreement. In: Conf parties its twenty-first sess, vol. 21932; 2015. p. 32. https://doi.org/FCCC/CP/2015/L.9/Rev.1.
[4] Liebensteiner M, Wrienz M. Do intermittent renewables threaten the electricity supply security? Energy Econ 2019:104499. https://doi.org/10.1016/j.eneco.2019.104499.
[5] Ren G, Wan J, Liu J, Yu D, Söder L. Analysis of wind power intermittency based on historical wind power data. Energy 2018;150:482–92. https://doi.org/10.1016/j.energy.2018.02.142.
[6] Katzenstein W, Apt J. The cost of wind power variability. Energy Pol 2012;51:233–43. https://doi.org/10.1016/j.enpol.2012.07.032.
[7] Albadi MH, El-Saadany EF. Overview of wind power intermittency impacts on power systems. Elec Power Syst Res 2010;80:627–32. https://doi.org/10.1016/j.epsr.2009.10.035.
[8] CCC. Next steps for UK heat policy - annex 2. Heat in UK buildings today. 2016.
[9] CCC. Committe on climate change - The fifth carbon budget - the next step towards a low-carbon economy - November 2015. 2015.
[10] Ofgem. Gas demand and supply source by month (GB). Ofgem Data Portal; 2020. https://www.ofgem.gov.uk/data-portal/gas-demand-and-supply-source-month-gb. [Accessed 27 October 2020].
[11] Crotogino F, Schneider GS, Evans DJ. Renewable energy storage in geological formations. Proc Inst Mech Eng Part A J Power Energy 2018;232:100–14. https://doi.org/10.1177/0957650917731181.
[12] Stone HBJ, Veldhuis I, Richardson RN. Underground hydrogen storage in the UK. Geol Soc London, Spec Publ 2009;313:217–26. https://doi.org/10.1144/SP313.13.
[13] Foh S, Novil M, Rockar E, Randolph P. Underground hydrogen storage final report. 1979. Chicago.
[14] Caine D, Iliffe M, Kinsella K, Wahyuni W, Bond L. Dolphyn hydrogen phase 1 - final report. 2019.
[15] Cranfield University. The gas technology Institute, doosan babcock. Bulk hydrogen production by sorbent enhanced steam reforming. HyPER; 2019.
[16] Element Energy. Gigastack: bulk supply of renewable hydrogen - public report. 2020.
[17] Alcalde J, Heinemann N, Mabon L, Worden RH, de Coninck H, Robertson H, et al. Acorn: developing full-chain industrial carbon capture and storage in a resource- and infrastructure-rich hydrocarbon province. J Clean Prod 2019;233:963–71. https://doi.org/10.1016/J.JCLEPRO.2019.06.087.
[18] Progressive Energy. Phase 1 Report - Progressive Energy: HyNet low carbon hydrogen plant [n.d].
[19] Babarit A, Gilloteaux J-C, Clodic G, Duchet M, Simoneau A, Platzer MF. Techno-economic feasibility of fleets of far offshore hydrogen-producing wind energy converters. Int J Hydrogen Energy 2018;43:7266–89. https://doi.org/10.1016/J.IJHYDENE.2018.02.144.
[20] Dawood F, Anda M, Shafiullah GM. Hydrogen production for energy: an overview. Int J Hydrogen Energy 2020;45:3847–69. https://doi.org/10.1016/j.ijhydene.2019.12.059.
[21] Prime Minister's Office. The queen's speech 2019. 2019.
[22] BEIS. Supply and consumption of natural gas and colliery methane (DUKES 4.2). 2020.
[23] Hart D, Howes J, Lehner F, Dodds PE, Hughes N, Fais B, et al. Scenarios for deployment of hydrogen in contributing to meeting carbon budgets and the 2050 target. 2015.
[24] Evans DJ, Holloway S. A review of onshore UK salt deposits and their potential for underground gas storage. In: Evans DJ, Chadwick RA, editors. Undergr. Gas storage worldw. Exp. Futur. Dev. UK Eur. The Geological Society, London, Special Publications; 2009. https://doi.org/10.1144/SP313.5.
[25] Panfilov M. 4 – underground and pipeline hydrogen storage. Elsevier Ltd.; 2016. https://doi.org/10.1016/B978-1-78242-362-1.00004-3.
[26] Cornot-Gandolphe S. Underground gas storage in the world - 2018 status. 2018.
[27] Zivar D, Kumar S, Foroozesh J. Underground hydrogen storage: a comprehensive review. Int J Hydrogen Energy 2020. https://doi.org/10.1016/j.ijhydene.2020.08.138. In press.
[28] Heinemann N, Booth MG, Haszeldine RS, Wilkinson M, Scafidi J, Edlmann K. Hydrogen storage in porous geological formations – onshore play opportunities in the midland valley (Scotland, UK). Int J Hydrogen Energy 2018;43:20861–74. https://doi.org/10.1016/j.ijhydene.2018.09.149.
[29] Kruck O, Crotogino F, Prelicz R, Rudolph T. "Assessment of the potential, the actors and relevant business cases for large scale and seasonal storage of renewable electricity by hydrogen underground storage in Europe" overview on all known underground storage technologies for hydrogen status: D(4). 2013.
[30] Carden PO, Paterson L. Physical, chemical and energy aspects of underground hydrogen storage. Int J Hydrogen Energy 1979;4:559–69. https://doi.org/10.1016/0360-3199(79)90083-1.
[31] Sainz-Garcia A, Abarca E, Rubi V, Grandia F. Assessment of feasible strategies for seasonal underground hydrogen storage in a saline aquifer. Int J Hydrogen Energy

2017;42:16657–66. https://doi.org/10.1016/j.ijhydene.2017.05.076.
[32] Luboń K, Tarkowski R. Numerical simulation of hydrogen injection and withdrawal to and from a deep aquifer in NW Poland. Int J Hydrogen Energy 2020;45:2068–83. https://doi.org/10.1016/j.ijhydene.2019.11.055.
[33] Pfeiffer WT, Bauer S. Subsurface porous media hydrogen storage – scenario development and simulation. Energy Procedia 2015;76:565–72. https://doi.org/10.1016/J.EGYPRO.2015.07.872.
[34] Amid A, Mignard D, Wilkinson M. Seasonal storage of hydrogen in a depleted natural gas reservoir. Int J Hydrogen Energy 2016;41:5549–58. https://doi.org/10.1016/j.ijhydene.2016.02.036.
[35] Hassanpouryouzband A, Joonaki E, Edlmann K, Heinemann N, Yang J. Thermodynamic and transport properties of hydrogen containing streams. Sci Data 2020;7:222. https://doi.org/10.1038/s41597-020-0568-6.
[36] BEIS. DUKES_4.3 UK continental shelf and onshore natural gas production and supply. 2020.
[37] Ofgem. GB Gas storage facilities. 2020.
[38] National Grid. Gas ten year statement 2018. 2018.
[39] Horseman S, Evans D, Rowley J, Chadwick A. Underground gas storage: geology, technology, planning and regulation. Earthwise 2008;12–3.
[40] Haeseldonckx D, D'haeseleer W. The use of the natural-gas pipeline infrastructure for hydrogen transport in a changing market structure. Int J Hydrogen Energy 2007;32:1381–6. https://doi.org/10.1016/J.IJHYDENE.2006.10.018.
[41] Wilson G, Rowley P. Flexibility in Great Britain's gas networks : analysis of linepack and linepack flexibility using hourly data. 2019.
[42] Northern Gas Networks. H21 Leeds city gate. 2016. https://doi.org/10.1155/2008/830474.
[43] Watson SD, Lomas KJ, Buswell RA. Decarbonising domestic heating: what is the peak GB demand? Energy Pol 2019;126:533–44. https://doi.org/10.1016/J.ENPOL.2018.11.001.
[44] BEIS. DUKES chapter 4: statistics on supply and demand for natural gas. Dig. UK Energy Stat. Nat. gas 2018:15.
[45] Energy Research Partnership. Potential role of hydrogen in the UK energy system. 2016.
[46] Bentham M, Mallows T, Lowndes J, Green A. CO2STORage evaluation database (CO2Stored). The UK's online storage atlas. Energy Procedia 2014;63:5103–13. https://doi.org/10.1016/j.egypro.2014.11.540.
[47] R Core Team. R. A language and environment for statistical computing. 2019.
[48] Raza A, Rezaee R, Gholami R, Bing CH, Nagarajan R, Hamid MA. A screening criterion for selection of suitable CO2 storage sites. J Nat Gas Sci Eng 2016;28:317–27. https://doi.org/10.1016/j.jngse.2015.11.053.
[49] Kilgallon R, Gilfillan SMV, Edlmann K, McDermott CI, Naylor M, Haszeldine RS. Experimental determination of noble gases and SF6, as tracers of CO2flow through porous sandstone. Chem Geol 2018;480:93–104. https://doi.org/10.1016/j.chemgeo.2017.09.022.
[50] Stuart IA. The Rough gas storage field, blocks 47/3d, 47/8b, UK North Sea. Geol Soc London, Mem 1991;14:477–84. https://doi.org/10.1144/gsl.mem.1991.014.01.59.
[51] Ward J, Chan a, Ramsay B. The Hatfield Moors and Hatfield west gas (storage) fields , south Yorkshire. United Kingdom oil gas fields. Commem Millenium 2003;20:905–10. https://doi.org/10.1144/GSL.MEM.2003.020.01.76.
[52] Gluyas JG, De-Paola N, Imber J, Jezierski TM, Jones RR, Jordan P, et al. The humbly Grove, herriard and hester's copse fields, UK onshore. Geol Soc London, Mem 2020;52:74 LP–81. https://doi.org/10.1144/M52-2018-78.
[53] Allen RD, Doherty TJ, Erikson RL, Wiles LE. Factors affecting storage of compressed air in porous-rock reservoirs. 1983.
[54] Ehrenberg SN, Nadeau PH. Sandstone vs. carbonate petroleum reservoirs: a global perspective on porosity-depth and porosity-permeability relationships. Am Assoc Petrol Geol Bull 2005;89:435–45. https://doi.org/10.1306/11230404071.
[55] Chadwick A, Arts R, Bernstone C, May F, Thibeau S, Zweigel P. Best practice for the storage of CO2 in saline aquifers - observations and guidelines from the SACS and CO2STORE projects, vol. 14; 2008, ISBN 978-0-85272-610-5.
[56] Mouli-Castillo J. Assessing the potential for compressed air energy storage using the offshore UK saline aquifer resource. The University of Edinburgh; 2018.
[57] Lemmon EW, Huber ML, Leachman JW. Revised standardized equation for hydrogen gas densities for fuel consumption applications. J Res Natl Inst Stand Technol 2008;113(6):341–50. https://doi.org/10.6028/jres.113.028.
[58] Yekta AE, Manceau JC, Gaboreau S, Pichavant M, Audigane P. Determination of hydrogen–water relative permeability and capillary pressure in sandstone: application to underground hydrogen injection in sedimentary formations. Transp Porous Media 2018;122:1–24. https://doi.org/10.1007/s11242-018-1004-7.
[59] Johnston IA. The noble-abel equation of state: thermodynamic derivations for ballistics modelling. 2005. DSTO-TN-0670.
[60] Bolton W. Engineering science. 5th ed. Oxford: Newnes; 2006.
[61] San Marchi C, Somerday B. Thermodynamics of gaseous hydrogen and hydrogen transport in metals. In: MRS Proceedings; 2008. p. 1098.
[62] HyWeb. Hydrogen data. Hydrog Fuel Cell Inf Syst 2007. http://www.h2data.de/. [Accessed 31 December 2020].
[63] QGIS Development Team. QGIS geographic information system. 2020.
[64] Crown Estate Scotland. Maps & publications. Crown Estate Scotl Website; 2018.
[65] The Crown Estate. Maps and GIS data. The Crown Estate Website; 2018.
[66] Carbon Storage Taskforce. National carbon mapping and infrastructure plan – Australia. 2010.
[67] Ketzer JM, Machado CX, Rockett GC, Iglesias RS. Brazilian atlas of CO2 capture and geological storage. 2015.
[68] Dahowski RT, Li X, Davidson CL, Wei N, Dooley JJ. Regional opportunities for carbon dioxide capture and storage in China. 2009. p. 85.
[69] Vangkilde-Pedersen T, Anthonsen KL, Smith N, Kirk K, Neele F, van der Meer B, et al. Assessing European capacity for geological storage of carbon dioxide–the EU GeoCapacity project. Energy Procedia 2009;1:2663–70. https://doi.org/10.1016/J.EGYPRO.2009.02.034.
[70] Norwegian Petroleum Directorate. CO2 storage atlas Norwegian North Sea. Nor Pet Dir Stavanger, Norw 2011 2011;1:72.
[71] NETL, US DOE. Carbon storage atlas - 5th ed. (Atlas V), vol. 5; 2015. p. 114.
[72] Wickham H. ggplot2: elegant graphics for data analysis. New York: Springer-Verlag; 2016.

8.1.2 Estimating useable pore volumes in saline aquifers without identified structures or traps

The methodology used to estimate pore volume in saline aquifers without identified structures or traps was adapted from a compressed air energy storage capacity study(Mouli-Castillo 2018). This combined hydrocarbon exploration well success rates and oil field production data in order to estimate the likely volumes of pore space within traps that are suitable for fluid storage.

It was assumed that all hydrocarbon exploration wells are drilled into some form of trap within an aquifer, identified by exploration techniques such as seismic interpretation. Since the success rate of hydrocarbon exploration wells from 1963 to 2002 is 30%(Xia and Wilkinson 2017), the relationship between the volume of hydrocarbons produced from these structures and the average success rate of hydrocarbon exploration wells provides an estimate of the total volume of effective fluid traps(Mouli-Castillo *et al.* 2018).

Using this total volume, an estimate of the proportion suitable for hydrogen storage can be made, using the difference between the proportion of traps suitable for fluid storage and the proportion of traps that contain hydrocarbons. This provides the volume of traps that do not contain hydrocarbons and are therefore suitable for hydrogen storage. This process is visualised in Figure 78.

It is unknown if the successful exploration wells found gas or oil or both so the entire 30% of the total volume was assumed to contain oil and therefore considered unsuitable for hydrogen storage. However, traps with wells which found gas are accounted for separately in the calculation for depleted gas fields based on data from the CO_2 database. Where available, oil production figures were taken from Oil & Gas Authority data(Oil & Gas Authority 2020) for each oilfield in the list. Formation volume factors (FVF, the volume change upon bringing fluids from a reservoir to the surface) are from Gluyas and Hichens (2003)(Gluyas and Hichens 2003) and from Evans et al. (eds) (2003)(Evans *et al.* 2003). As there was little to no available data on FVF for most North Sea fields, an average was used, calculated from the available data. This data and calculation is given in spreadsheet form in appendix 3.

The volume of the traps was calculated from the oil production and FVF data and compared with that given in the database for a given saline aquifer to provide an estimate of the proportion of pore volume suitable for hydrogen storage. This proportion is known as the storage efficiency and was averaged using the available

data and applied to all saline aquifers with no identified structures/traps, resulting in a storage efficiency of 0.1% ± 0.04% $\sigma_{\bar{x}}$.

Equation (1)(Mouli-Castillo *et al.* 2018) was used to estimate the pore volume of useable structures within a single aquifer.

$$(3)\ V_{H2} = (V_{oil(STP)} * FVF/R_{ow}) * S_{H2}$$

Where V_{H2} is the volume of pore space suitable for hydrogen storage, $V_{oil(STP)}$ is the total volume of produced oil at STP (standard temperature and pressure), *FVF* is the average formation volume factor (1.28 ± 0.04 $\sigma_{\bar{x}}$), R_{ow} is the success rate of oil wells, and S_{H2} is the proportion of structures suitable for hydrogen storage. The latter is estimated from the proportion of total traps in an aquifer that are suitable for fluid storage where drilling has penetrated sealing/reservoir formation pairs(Xia and Wilkinson 2017) (49 ± 8%; this includes structures containing oil). The success rate of exploration wells is 30%(Xia and Wilkinson 2017) and as structures that contain oil are deemed unsuitable for hydrogen storage these are subtracted. This leaves a figure of 19 ± 8% of structures suitable for hydrogen storage. A visual representation of this method is shown in Figure 78.

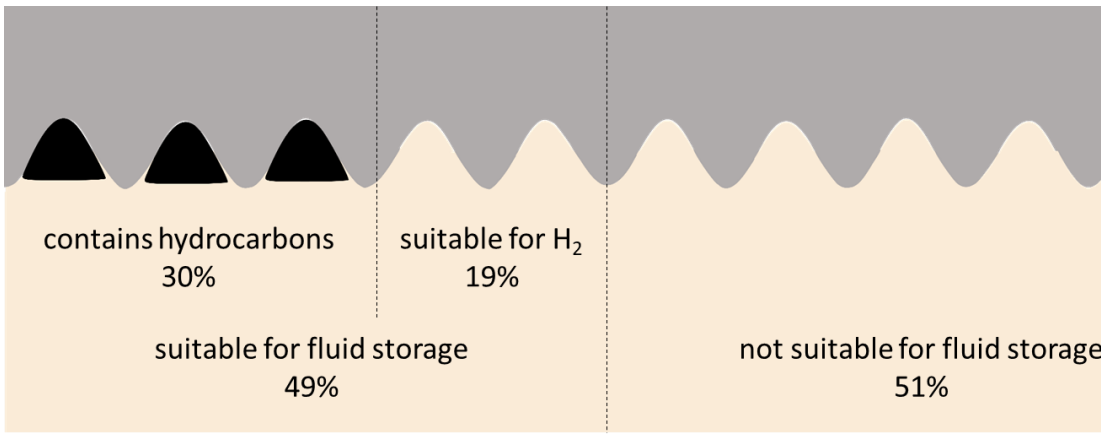

Figure 78: Schematic saline aquifer and seal to visualise the variables in the efficiency calculation. The grey area represents the sealing formation above the saline aquifer (pale yellow area). Small structures exist at the top of the saline aquifer, 30% of which contain hydrocarbons represented by black fill. The 51% of structures on the right are not suitable for fluid storage (e.g. due to poor reservoir quality or compartmentalisation) which leaves the 19% structures in the middle which are suitable for fluid storage but do not contain hydrocarbons available for hydrogen storage. Dashed lines represent the boundaries between the various portions of the saline aquifer. NB this schematic is not to scale nor is it intended to be a realistic representation of an actual saline aquifer. It merely visualises the logic of the calculation.

8.1.3 References

Adcock, C.M. 1939. *COUSLAND 1 Production Engineering File 1*.

Adcock, C.M. 1969. *Oil and Gas Fields of Britain*.

Al-Hussainy, R. and Ramey, H.J. 1967. Application of Real Gas Flow Theory to Well Testing and Deliverability Forecasting. *SPE 1234B*.

Al-Hussainy, R., Ramey, H.J. and Crawford, P.B. 1966a. The Flow of Real Gases Through Porous Media. *Journal of Petroleum Technology*, **18**, 624–636, https://doi.org/10.2118/1243-A-PA.

Al-Hussainy, R., Ramey, H.J. and Crawford, P.B. 1966b. The Flow of Real Gases Through Porous Media. *Journal of Petroleum Technology*, **18**, 624–636, https://doi.org/10.2118/1243-A-PA.

Albadi, M.H. and El-Saadany, E.F. 2010. Overview of wind power intermittency impacts on power systems. *Electric Power Systems Research*, **80**, 627–632, https://doi.org/10.1016/j.epsr.2009.10.035.

Alcalde, J., Heinemann, N., et al. 2019. Acorn: Developing full-chain industrial carbon capture and storage in a resource- and infrastructure-rich hydrocarbon province. *Journal of Cleaner Production*, **233**, 963–971, https://doi.org/10.1016/J.JCLEPRO.2019.06.087.

Allen, K. 1985. CAES: The Underground Portion. *IEEE Power Engineering Review*, **PER**-**5**, 35, https://doi.org/10.1109/MPER.1985.5528813.

Allen, R.D., Doherty, T.J., Erikson, R.L. and Wiles, L.E. 1983. Factors affecting storage of compressed air in porous-rock reservoirs.

Almeida, J.R.U.C., Fagundes De Almeida, E.L., Torres, E.A. and Freires, F.G.M. 2018. Economic value of underground natural gas storage for the Brazilian power sector. *Energy Policy*, **121**, 488–497, https://doi.org/10.1016/j.enpol.2018.07.005.

American Petroleum Institute. 1991. *API RP 14E: Recommended Practice for Design and Installation of Offshore Production Platform Piping Systems*.

Amid, A., Mignard, D. and Wilkinson, M. 2016. Seasonal storage of hydrogen in a depleted natural gas reservoir. *International Journal of Hydrogen Energy*, **41**, 5549–5558, https://doi.org/10.1016/j.ijhydene.2016.02.036.

Anglo-American Oil Company. 1939. Midlothian 1 Petroleum Engineering File.

Aprea, J.L. and Bolcich, J.C. 2020. The energy transition towards hydrogen utilization for green life and sustainable human development in Patagonia. *International Journal of Hydrogen Energy*, **45**, 25627–25645, https://doi.org/10.1016/J.IJHYDENE.2020.01.246.

Asquith, G. and Krygowski, D. 2004. *Basic Well Log Analysis, 2nd Edition*, 2nd ed.

Aziz, K. and Govier, G.W. 1972. Pressure Drop In Wells Producing Oil And Gas. *Journal of Canadian Petroleum Technology*, **11**, 38–48, https://doi.org/10.2118/72-03-04.

Aziz, K. and Settari, A. 1979. *Petroleum Reservoir Simulation*.

Babarit, A., Gilloteaux, J.-C., Clodic, G., Duchet, M., Simoneau, A. and Platzer, M.F. 2018. Techno-economic feasibility of fleets of far offshore hydrogen-producing wind energy converters. *International Journal of Hydrogen Energy*, **43**, 7266–7289, https://doi.org/10.1016/J.IJHYDENE.2018.02.144.

Bagnall, A.C. 1979. The Search for Natural Petroleum in the Lothians. *Edinburgh Geologist - issue 5*, 12–14.

Basniev, K.S., Omelchenko, R.J.. . J., et al. 2010. Underground Hydrogen Storage Problems in Russia. *In*: Stolten, D. and Grube, T. (eds) *18th World Hydrogen Energy Conference 2010*. 1–7.

BEIS. 2018. DUKES chapter 4: statistics on supply and demand for natural gas. *In*: *Digest of UK Energy Statistics (DUKES): Natural Gas*. 15.

BEIS. 2020a. *DUKES_4.3 UK Continental Shelf and Onshore Natural Gas Production and Supply*.

BEIS. 2020b. *Supply and Consumption of Natural Gas and Colliery Methane (DUKES 4.2)*.

Bell, I.H., Wronski, J., Quoilin, S. and Lemort, V. 2014. Pure and Pseudo-pure Fluid Thermophysical Property Evaluation and the Open-Source Thermophysical Property Library CoolProp. *Industrial and Engineering Chemistry Research*, **53**, 2498–2508, https://doi.org/10.1021/IE4033999.

Bentham, M., Mallows, T., Lowndes, J. and Green, A. 2014. CO2STORage

evaluation database (CO2Stored). The UK's online storage atlas. *Energy Procedia*, **63**, 5103–5113, https://doi.org/10.1016/j.egypro.2014.11.540.

Beutel, T. and Black, S. 2004. Salt deposits and gas cavern storage in the UK with a case study of salt exploration from Cheshire. *In*: *Fall 2004 Conference*.

Biegger, P., Kittinger, F. and Lehner, M. 2018. Underground Sun Conversion. *In*: *14th Minisymposium Chemical & Process Engineering - Johannes Kepler Universität, Linz, Austria*.

Bolton, W. 2006. *Engineering Science*, 5th ed.

BP. 1960a. Cousland 6 Geological Completion Report.

BP. 1960b. Cousland 6 Geological Completion Report - Enclosure.

British Geological Survey. 2008. An appraisal of underground gas storage technologies and incidents, for the development of risk assessment methodology, Volume Two - Figures and Tables. *British: Health and Safety Executive*.

British Geological Survey. 2020a. Borehole materials databasehttps://www.bgs.ac.uk/technologies/databases/borehole-materials-database/.

British Geological Survey. 2020b. National Geoscience Data Centre (NGDC)https://www.bgs.ac.uk/geological-data/national-geoscience-data-centre/.

Buzek, F., Onderka, V., Vancura, P. and Wolf, I. 1994. Carbon isotope study of methane production in a town gas storage reservoir. *Fuel*, **73**, 747–752, https://doi.org/10.1016/0016-2361(94)90019-1.

Caglayan, D.G., Weber, N., Heinrichs, H.U., Linßen, J., Robinius, M., Kukla, P.A. and Stolten, D. 2020. Technical potential of salt caverns for hydrogen storage in Europe. *International Journal of Hydrogen Energy*, **45**, 6793–6805, https://doi.org/10.1016/j.ijhydene.2019.12.161.

Caine, D., Iliffe, M., Kinsella, K., Wahyuni, W. and Bond, L. 2019. *Dolphyn Hydrogen Phase 1 - Final Report*.

Cant, D.J. 1992. Subsurface Facies Analysis. *In*: *Facies Models: Response to Sea*

Level Change.

Carbon Storage Taskforce. 2010. *National Carbon Mapping and Infrastructure Plan – Australia*.

Carden, P. and Paterson, L. 1979. Physical, chemical and energy aspects of underground hydrogen storage. *International Journal of Hydrogen Energy*, **4**, 559–569, https://doi.org/10.1016/0360-3199(79)90083-1.

Carmichael, R.S. 1982. *Handbook of Physical Properties of Rocks*, https://doi.org/10.1201/9780203712115.

Cartwright, J., Stewart, S. and Clark, J. 2001. Salt dissolution and salt-related deformation of the Forth Approaches Basin, UK North Sea. *Marine and Petroleum Geology*, **18**, 757–778, https://doi.org/10.1016/S0264-8172(01)00019-8.

Chadwick, A., Arts, R., Bernstone, C., May, F., Thibeau, S. and Zweigel, P. 2008. *Best Practice for the Storage of CO2 in Saline Aquifers - Observations and Guidelines from the SACS and CO2STORE Projects*, https://doi.org/ISBN: 978-0-85272-610-5.

Chaudry, M., Jenkins, N. and Strbac, G. 2008. Multi-time period combined gas and electricity network optimisation. *Electric Power Systems Research*, **78**, 1265–1279, https://doi.org/10.1016/j.epsr.2007.11.002.

Chen, J., Ren, S., Yang, C., Jiang, D. and Li, L. 2013. Self-healing characteristics of damaged rock salt under different healing conditions. *Materials*, **6**, 3438–3450, https://doi.org/10.3390/ma6083438.

Clavier, C., Hoyle, W. and Meunier, D. 1971. Quantitative Interpretation of Thermal Neutron Decay Time Logs: Part I. Fundamentals and Techniques. *Journal of Petroleum Technology*, **23**, 743–755, https://doi.org/10.2118/2658-A-PA.

Climate Change Committee. 2015. *The Fifth Carbon Budget*.

Climate Change Committee. 2016. *Next Steps for UK Heat Policy - Annex 2. Heat in UK Buildings Today*.

Climate Change Committee. 2020. *The Sixth Carbon Budget*.

CMG. 2019a. Builder.

CMG. 2019b. GEM.

CMG. 2019c. WinProp.

Collins, D.A., Nghlem, L.X., Li, V. ·k and Grabenstetter, J.E. 1992. *An Efficient Approach to Adaptive-Implicit Compositional Simulation With an Equation of State*.

Competition & Markets Authority. 2017. *Rough Gas Storage Undertakings Review Final Decision*.

COMSOL Inc. 2016. COMSOL Reference Manual (version 5.2a). 1–1378.

CONOCO (U.K.) Limited and ENTERPRISE OIL p.l.c. 1991. *EXL 026 (FIRTH OF FORTH) RELINQUISHMENT REPORT*.

Cornot-Gandolphe, S. 2017. *Underground Gas Storage in the World - 2017 Status*.

Cornot-Gandolphe, S. 2018. *Underground Gas Storage in the World - 2018 Status*.

Cranfield University, The Gas Technology Institute and Doosan Babcock. 2019. *Bulk Hydrogen Production by Sorbent Enhanced Steam Reforming (HyPER)*.

Crotogino, F., Schneider, G.S. and Evans, D.J. 2018. Renewable energy storage in geological formations. *Proceedings of the Institution of Mechanical Engineers, Part A: Journal of Power and Energy*, **232**, 100–114, https://doi.org/10.1177/0957650917731181.

Crown Estate Scotland. 2018. Maps & Publications. *Crown Estate Scotland website*.

Dahowski, R.T., Li, X., Davidson, C.L., Wei, N. and Dooley, J.J. 2009. Regional Opportunities for Carbon Dioxide Capture and Storage in China. 85.

Dawood, F., Anda, M. and Shafiullah, G.M. 2020. Hydrogen production for energy: An overview. *International Journal of Hydrogen Energy*, **45**, 3847–3869, https://doi.org/10.1016/j.ijhydene.2019.12.059.

Dean, G. 2018. The Scottish oil-shale industry from the viewpoint of the modern-day shale-gas industry. *Geological Society, London, Special Publications*, **465**, 53–69, https://doi.org/10.1144/sp465.13.

Department for Business Energy & Industrial Strategy. 2018a. *2016 UK GREENHOUSE GAS EMISSIONS, FINAL FIGURES Statistical Release:*

National Statistics.

Department for Business Energy & Industrial Strategy. 2018b. *SUB-NATIONAL ELECTRICITY AND GAS CONSUMPTION STATISTICS*.

East Lothian Antiquarians and Field Naturalists Society. 2018a. Inveresk Musselburgh | Homes. *The Fourth Statistical Account of East Lothian*https://el4.org.uk/parish/inveresk-musselburgh/homes/.

East Lothian Antiquarians and Field Naturalists Society. 2018b. Prestonpans | Homes. *The Fourth Statistical Account of East Lothian*https://el4.org.uk/parish/prestonpans/homes/.

Eaton, B.A. 1969. Fracture Gradient Prediction and Its Application in Oilfield Operations. *Journal of Petroleum Technology*, **21**, 1353–1360, https://doi.org/10.2118/2163-PA.

Edinburgh Oil & Gas PLC. 1999. *Hatfield Moors - Addendum to Annex B*.

Ehrenberg, S.N. and Nadeau, P.H. 2005. Sandstone vs. carbonate petroleum reservoirs: A global perspective on porosity-depth and porosity-permeability relationships. *AAPG Bulletin*, **89**, 435–445, https://doi.org/10.1306/11230404071.

Element Energy. 2020. *Gigastack: Bulk Supply of Renewable Hydrogen - Public Report*.

Energy Research Partnership. 2016. *Potential Role of Hydrogen in the UK Energy System*.

Energy Technology Training Center. 2001. Module 1 : Hydrogen Properties. *In*: *Hydrogen Fuel Cell Engines and Related Technologies - Technical Report, PB2003-100184*.

Equinor. 2013. Open datasets | OPM. *The Open Porous Media Initiative*https://opm-project.org/?page_id=559.

Evans, D., Graham, C., Armour, A. and Bathurst, P. 2003. *The Millennium Atlas: Petroleum Geology of the Central and Northern North Sea*, 2003/08/05. Evans, D., Graham, C., Armour, A. and Bathurst, P. (eds), https://doi.org/DOI: 10.1017/S0016756803218124.

Evans, D., Highley, D., Gale, I., Cowley, J., Rayner, D. and Hill, A. 2008. *Mineral Planning Factsheet - Underground Storage*.

Evans, D.J. and Holloway, S. 2009. A review of onshore UK salt deposits and their potential for underground gas storage. *In*: Evans, D. J. and Chadwick, R. A. (eds) *Underground Gas Storage: Worldwide Experiences and Future Development in the UK and Europe*, https://doi.org/10.1144/SP313.5.

Evans, D.J. and West, J.M. 2008. *An Appraisal of Underground Gas Storage Technologies and Incidents, for the Development of Risk Assessment Methodology*.

Exploration Dept. Lasmo. 1985. U.K. Onshore Licence PL177 - Evaluation of the remaining hydrocarbon prospects. 113.

Falcon, N.L. 1938. *COUSLAND 1 TO 3 GEOLOGICAL COMPLETION REPORT*.

Falcon, N.L. and Kent, P.E. 1960. Geological Results of Petroleum Exploration in Britain 1945-1957. *Geological Society Memoir*, **2**, 5–56, https://doi.org/10.1144/GSL.MEM.1960.002.01.01.

Feldmann, F., Hagemann, B., Ganzer, L. and Panfilov, M. 2016. Numerical simulation of hydrodynamic and gas mixing processes in underground hydrogen storages. *Environmental Earth Sciences*, **75**, 1–15, https://doi.org/10.1007/s12665-016-5948-z.

Fisher, W.D. 1945. P001637.

Flemisch, B., Darcis, M., et al. 2011. DuMux: DUNE for multi-{phase,component,scale,physics,…} flow and transport in porous media. *Advances in Water Resources*, **34**, 1102–1112, https://doi.org/10.1016/j.advwatres.2011.03.007.

Foh, S., Novil, M., Rockar, E. and Randolph, P. 1979. *Underground Hydrogen Storage Final Report*.

Friend, D.G., Ely, J.F. and Ingham, H. 1989. Thermophysical Properties of Methane. *Journal of Physical and Chemical Reference Data*, **18**, 583–638, https://doi.org/10.1063/1.555828.

Gasanzade, F., Pfeiffer, W.T., Witte, F., Tuschy, I. and Bauer, S. 2021. Subsurface renewable energy storage capacity for hydrogen, methane and compressed air

– A performance assessment study from the North German Basin. *Renewable and Sustainable Energy Reviews*, **149**, 111422, https://doi.org/10.1016/J.RSER.2021.111422.

Gazprom. 2018. *A Leader of Gas Science: 70th Anniversary of VNIIGAZ*. Gritsenko, A. I., Grigoryev, B. A. and Dzhafarov, K. I. (eds).

Gluyas, J.G. and Hichens, H.M. 2003. United Kingdom oil and gas fields. Commemorative millennium volume. *Geological Society Memoir*, **20**, 1006, https://doi.org/10.1144/GSL.MEM.2003.020.

Gluyas, J.G., De-Paola, N., et al. 2020. The Humbly Grove, Herriard and Hester's Copse fields, UK Onshore. *Geological Society, London, Memoirs*, **52**, 74 LP – 81, https://doi.org/10.1144/M52-2018-78.

Gralla, D.S. and Jones, R.E. 1991. *Hatfield Moors Gas Field - Annual Reservoir Performance Report 1990*.

Graupner, B.J., Li, D. and Bauer, S. 2011. The coupled simulator ECLIPSE–OpenGeoSys for the simulation of CO2 storage in saline formations. *Energy Procedia*, **4**, 3794–3800, https://doi.org/10.1016/J.EGYPRO.2011.02.314.

Greensmith, J.T. 1961. The petrology of the Oil-Shale Group sandstones of west Lothian and southern Fifeshire. *Proceedings of the Geologists' Association*, **72**, 49–71, https://doi.org/10.1016/S0016-7878(61)80026-6.

Greensmith, J.T. 1962. Rhythmic Deposition in the Carboniferous Oil-Shale Group of Scotland. *The Journal of Geology*, **70**, 355–364, https://doi.org/10.1086/626825.

Greensmith, J.T. 1965. Calciferous Sandstone Series Sedimentation at the Eastern End of the Midland Valley of Scotland. *SEPM Journal of Sedimentary Research*, **Vol. 35**, 223–242, https://doi.org/10.1306/74d71226-2b21-11d7-8648000102c1865d.

Groenenberg, R.M., Juez-Larre, J., et al. 2020. *Techno-Economic Modelling of Large-Scale Energy Storage Systems*.

Guo, B. 2019. Petroleum reservoir properties. *In*: *Well Productivity Handbook*. 17–51., https://doi.org/10.1016/B978-0-12-818264-2.00002-6.

HAESELDONCKX, D. and DHAESELEER, W. 2007. The use of the natural-gas

pipeline infrastructure for hydrogen transport in a changing market structure. *International Journal of Hydrogen Energy*, **32**, 1381–1386, https://doi.org/10.1016/j.ijhydene.2006.10.018.

Hagemann, B., Rasoulzadeh, M., Panfilov, M., Ganzer, L. and Reitenbach, V. 2016. Hydrogenization of underground storage of natural gas: Impact of hydrogen on the hydrodynamic and bio-chemical behavior. *Computational Geosciences*, **20**, 595–606, https://doi.org/10.1007/s10596-015-9515-6.

Haldane, J.B.S. 1924. Daedalus, or science and the future. *The Eugenics review*, **16**, 143–145, https://doi.org/10.2307/2014395.

Hallett, D., Durant, G.P. and Farrow, G.E. 1985. Oil exploration and production in Scotland. *Scottish Journal of Geology*, **21**, 547–570, https://doi.org/10.1144/sjg21040547.

Hart, D., Howes, J., et al. 2015. *Scenarios for Deployment of Hydrogen in Contributing to Meeting Carbon Budgets and the 2050 Target*.

Harvie, B.A. and Hobbs, R.J. 2013. Case Study: Shale Bings in Central Scotland: From Ugly Blots on the Landscape to Cultural and Biological Heritage. *In*: *Novel Ecosystems: Intervening in the New Ecological World Order*, https://doi.org/10.1002/9781118354186.ch35.

Hassanpouryouzband, A., Joonaki, E., Edlmann, K., Heinemann, N. and Yang, J. 2020. Thermodynamic and transport properties of hydrogen containing streams. *Scientific Data*, **7**, 222, https://doi.org/10.1038/s41597-020-0568-6.

Heinemann, N., Booth, M.G., Haszeldine, R.S., Wilkinson, M., Scafidi, J. and Edlmann, K. 2018a. Hydrogen storage in porous geological formations – onshore play opportunities in the midland valley (Scotland, UK). *International Journal of Hydrogen Energy*, **43**, 20861–20874, https://doi.org/10.1016/j.ijhydene.2018.09.149.

Heinemann, N., Booth, M.G., Haszeldine, R.S., Wilkinson, M., Scafidi, J. and Edlmann, K. 2018b. Hydrogen storage in porous geological formations – onshore play opportunities in the midland valley (Scotland, UK). *International Journal of Hydrogen Energy*, **43**, 20861–20874, https://doi.org/10.1016/J.IJHYDENE.2018.09.149.

Heinemann, N., Alcalde, J., et al. 2021a. Enabling large-scale hydrogen storage in porous media-the scientific challenges, https://doi.org/10.1039/d0ee03536j.

Heinemann, N., Scafidi, J., et al. 2021b. Hydrogen storage in saline aquifers: The role of cushion gas for injection and production. *International Journal of Hydrogen Energy*, **46**, 39284–39296, https://doi.org/10.1016/j.ijhydene.2021.09.174.

Helmholtz Centre Potsdam. 2015. H2STORE. *GFZ German Research Centre for Geosciences*https://www.gfz-potsdam.de/en/section/geoenergy/projects/completed-projects/h2store/.

Hévin, G. 2019. Underground storage of Hydrogen in salt caverns. *In*: *European Workshop on Underground Energy Storage November 7th-8th 2019, Paris*.

Horseman, S., Evans, D., Rowley, J. and Chadwick, A. 2008. Underground gas storage: Geology, technology, planning and regulation. *Earthwise*, 12–13.

Houpeurt, A. 1959. On the Flow of Gases in Porous Media. *Revue de L'Institut Francais du Petrole*, **XIV**, 1468–1684.

HyWeb. 2007. Hydrogen Data. *The Hydrogen and Fuel Cell Information System*.

IEA. 2019. GECO 2019. *International Energy Agency Website*https://www.iea.org/geco/.

Illing, V.C. 1961. *Further Drilling at Cousland*.

Isaac, T. 2019. HyDeploy: The UK's First Hydrogen Blending Deployment Project. *Clean Energy*, **3**, 114–125, https://doi.org/10.1093/ce/zkz006.

ITN. 1957. ENERGY: Natural gas switched on in Scotlandhttps://www.gettyimages.co.uk/detail/video/natural-gas-switched-on-in-scotland-scotland-lothian-news-footage/813093966?adppopup=true&uiloc=thumbnail_more_search_results_adp&uiloc=thumbnail_more_search_results_adp.

Johnston, I.A. 2005. The Noble-Abel Equation of State: Thermodynamic Derivations for Ballistics Modelling. *DSTO-TN-0670*.

Jones, S.C. 1987. Using the Inertial Coefficient, β, To Characterize Heterogeneity in Reservoir Rock. *Society of Petroleum Engineers of AIME, (Paper) SPE*, **Pi**,

165–174, https://doi.org/10.2118/16949-MS.

Jossi, J.A., Stiel, L.I. and Thodos, G. 1962. The viscosity of pure substances in the dense gaseous and liquid phases. *AIChE Journal*, **8**, 59–63, https://doi.org/10.1002/aic.690080116.

Juez-Larré, J., Remmelts, G., Breunese, J.N., van Gessel, S.F. and Leeuwenburgh, O. 2016. Using underground gas storage to replace the swing capacity of the giant natural gas field of Groningen in the Netherlands. A reservoir performance feasibility study. *Journal of Petroleum Science and Engineering*, **145**, 34–53, https://doi.org/10.1016/j.petrol.2016.03.010.

Katzenstein, W. and Apt, J. 2012. The cost of wind power variability. *Energy Policy*, **51**, 233–243, https://doi.org/10.1016/j.enpol.2012.07.032.

Ketzer, J.M., Machado, C.X., Rockett, G.C. and Iglesias, R.S. 2015. *Brazilian Atlas of CO2 Capture and Geological Storage*.

Khaledi, K., Mahmoudi, E., Datcheva, M. and Schanz, T. 2016. Stability and serviceability of underground energy storage caverns in rock salt subjected to mechanical cyclic loading. *International Journal of Rock Mechanics and Mining Sciences*, **86**, 115–131, https://doi.org/10.1016/j.ijrmms.2016.04.010.

Kilgallon, R., Gilfillan, S.M. V, Edlmann, K., McDermott, C.I., Naylor, M. and Haszeldine, R.S. 2018. Experimental determination of noble gases and SF6, as tracers of CO2flow through porous sandstone. *Chemical Geology*, **480**, 93–104, https://doi.org/10.1016/j.chemgeo.2017.09.022.

Kopal, L., Cizek, P. and Milička, J. 2016. Geological model of Lobodice underground gas storage facility based on 3D seismic interpretation. *Contributions to Geophysics and Geodesy*, **46**, 125–135, https://doi.org/10.1515/CONGEO-2016-0009.

Korte, C., Mandt, T. and Bergholz, T. 2016. Physics of Hydrogen. *In*: *Hydrogen Science and Engineering: Materials, Processes, Systems and Technology*. 563–600.

Kruck, O., Crotogino, F., Prelicz, R. and Rudolph, T. 2013. *'Assessment of the Potential, the Actors and Relevant Business Cases for Large Scale and Seasonal Storage of Renewable Electricity by Hydrogen Underground Storage*

in Europe' Overview on All Known Underground Storage Technologies for Hydrogen Status: D(4).

Landinger, H., Bünger, U., Raksha, T., Weindorf, W., Simón, J., Correas, L. and Crotogino, F. 2014. Assessment of the Potential, the Actors and Relevant Business Cases for Large Scale and Long Term Storage of Renewable Electricity by Hydrogen Underground Storage in Europe.

Lanz, A. 2001. Module 1: Hydrogen Properties. *In*: *Hydrogen Fuel Cell Engines and Related Technologies*. 41.

Larionov, V. V. 1969. *Borehole Radiomentry*.

Le Fevre, C. 2013. *Gas Storage in Great Britain*.

Leachman, J.W., Jacobsen, R.T., Penoncello, S.G. and Lemmon, E.W. 2009. Fundamental Equations of State for Parahydrogen, Normal Hydrogen, and Orthohydrogen. *Journal of Physical and Chemical Reference Data*, **38**, 721, https://doi.org/10.1063/1.3160306.

Lee, A.L. and Eakin, B.E. 1964. Gas-Phase Viscosity of Hydrocarbon Mixtures. *Society of Petroleum Engineers Journal*, **4**, 247–249, https://doi.org/10.2118/872-pa.

Lee, W.J. and Wattenbarger, R.A. 1995. *Gas Reservoir Engineering*.

Lees, G.M., Cox, P.T. and Weald, S. 1937. The Geological Basis of the Present Search for Oil in Great Britain by the D'Arcy Exploration Company, Ltd. *Quarterly Journal of the Geological Society*, **93**, 156–194, https://doi.org/10.1144/gsl.jgs.1937.093.01-04.09.

Lemmon, E.W., Huber, M.L. and Leachman, J.W. 2008. Revised Standardized Equation for Hydrogen Gas Densities for Fuel Consumption Applications. *Journal of Research of the National Institute of Standards and Technology*, https://doi.org/10.6028/jres.113.028.

Lemmon, E.W., Huber, M.L. and McLinden, M.O. 2013. NIST Standard Reference Database 23: Reference Fluid Thermodynamic and Transport Properties-REFPROP, Version 9.1.

Lemmon, E.W., McLinden, M.O. and Friend, D.G. 2021. 'Thermophysical Properties of Fluid Systems'. *In*: Linstrom, P. J. and Mallard, W. G. (eds) *NIST Chemistry*

WebBook, NIST Standard Reference Database Number 69, https://doi.org/https://doi.org/10.18434/T4D303.

Liebensteiner, M. and Wrienz, M. 2019. Do Intermittent Renewables Threaten the Electricity Supply Security? *Energy Economics*, 104499, https://doi.org/10.1016/j.eneco.2019.104499.

Liebscher, A., Wackerl, J. and Streibel, M. 2016. Geologic Storage of Hydrogen - Fundamentals, Processing, and Projects. *In*: *Hydrogen Science and Engineering : Materials, Processes, Systems and Technology*. 629–658., https://doi.org/10.1002/9783527674268.ch26.

Loftus, G.W.F. and Greensmith, J.T. 1988. The lacustrine Burdiehouse Limestone Formation-a key to the deposition of the Dinantian Oil Shales of Scotland. *Geological Society Special Publication*, **40**, 219–234, https://doi.org/10.1144/GSL.SP.1988.040.01.19.

Luboń, K. and Tarkowski, R. 2020. Numerical simulation of hydrogen injection and withdrawal to and from a deep aquifer in NW Poland. *International Journal of Hydrogen Energy*, **45**, 2068–2083, https://doi.org/10.1016/j.ijhydene.2019.11.055.

Lyons, W., Carter, T. and Lapeyrousse, N.J. 2012. Air and Gas Calculations. *In*: Lyons, W., Carter, T. and Lapeyrousse Production, and Workover (Third Edition), N. J. B. T.-F. and C. for D. (eds) *Formulas and Calculations for Drilling, Production, and Workover*. 253–266., https://doi.org/10.1016/B978-1-85617-929-4.00006-3.

Lyons, W.C., Plisga, G.J. and Lorenz, M.D. 2016. Chapter 6 - Production Engineering. *In*: Lyons, W. C., Plisga, G. J. and Lorenz, M. D. (eds) *Standard Handbook of Petroleum and Natural Gas Engineering (Third Edition)*. 6–529., https://doi.org/https://doi.org/10.1016/B978-0-12-383846-9.00006-0.

Lysyy, M., Fernø, M. and Ersland, G. 2021. Seasonal hydrogen storage in a depleted oil and gas field. *International Journal of Hydrogen Energy*, **46**, 25160–25174, https://doi.org/10.1016/j.ijhydene.2021.05.030.

Madani Sani, F., Huizinga, S., Esaklul, K.A. and Nesic, S. 2019. Review of the API RP 14E erosional velocity equation: Origin, applications, misuses, limitations and alternatives. *Wear*, **426**–**427**, 620–636,

https://doi.org/10.1016/J.WEAR.2019.01.119.

Martens, S., Liebscher, A., et al. 2013. CO2 storage at the Ketzin pilot site, Germany: Fourth year of injection, monitoring, modelling and verification. *Energy Procedia*, **37**, 6434–6443, https://doi.org/10.1016/j.egypro.2013.06.573.

Martin, D.L. 1974. *COUSLAND 1 Production Engineering File 2*.

McCarty, R.D., Hord, J. and Roder, H.M. 1981. *Selected Properties of Hydrogen (Engineering Design Data)*, National B.

Michalski, J., Bünger, U., et al. 2017. Hydrogen generation by electrolysis and storage in salt caverns: Potentials, economics and systems aspects with regard to the German energy transition. *International Journal of Hydrogen Energy*, **42**, 13427–13443, https://doi.org/10.1016/j.ijhydene.2017.02.102.

Microsoft Corporation. 2016. Microsoft Excel 2016.

Monaghan, A.A. 2014. The Carboniferous shales of the Midland Valley of Scotland : geology and resource estimation. *British Geological Survey for Department of Energy and Climate Change*.

Mostaghimi, P., Kamali, F., Jackson, M.D., Muggeridge, A.H. and Pain, C.C. 2016. Adaptive Mesh Optimization for Simulation of Immiscible Viscous Fingering. *SPE Journal*, **21**, 2250–2259, https://doi.org/10.2118/173281-PA.

Mouli-Castillo, J. 2018. *Assessing the Potential for Compressed Air Energy Storage Using the Offshore UK Saline Aquifer Resource*. The University of Edinburgh.

Mouli-Castillo, J., Wilkinson, M., Mignard, D., McDermott, C., Haszeldine, R.S. and Shipton, Z.K. 2018. Inter-seasonal compressed air energy storage using saline aquifers (Manuscript submitted for publication).

Mouli-Castillo, J., Heinemann, N. and Edlmann, K. 2021. Mapping geological hydrogen storage capacity and regional heating demands: An applied UK case study. *Applied Energy*, **283**, 116348, https://doi.org/10.1016/j.apenergy.2020.116348.

Muzny, C.D., Huber, M.L. and Kazakov, A.F. 2013. Correlation for the viscosity of normal hydrogen obtained from symbolic regression. *Journal of Chemical and Engineering Data*, **58**, 969–979, https://doi.org/10.1021/je301273j.

National Grid. 2018. *Gas Ten Year Statement 2018*.

NETL and US DOE. 2015. Carbon Storage Atlas - Fifth Edition (Atlas V). **5**, 114.

Nghiem, L.X. and Heidemann, R.A. 1982. General Acceleration Procedure for Multiphase Flash Calculation With Application to Oil-Gas-Water Systems. *In*: *2nd European Symposium on Enhanced Oil Recovery,*. 8–10.

Nghiem, L.X., Aziz, K. and Li, Y.K. 1983. ROBUST ITERATIVE METHOD FOR FLASH CALCULATIONS USING THE SOAVE-REDLICH-KWONG OR THE PENG-ROBINSON EQUATION OF STATE. *Society of Petroleum Engineers journal*, **23**, 521–530, https://doi.org/10.2118/8285-pa.

Northern Gas Networks. 2016. *H21 Leeds City Gate*.

Northern Gas Networks. 2018. *H21 North of England*.

Norwegian Petroleum Directorate. 2011. CO2 Storage Atlas Norwegian North Sea. 2011. *Norwegian Petroleum Directorate: Stavanger, Norway*, **1**, 72.

Ofgem. 2020a. Gas demand and supply source by month (GB). *Ofgem data portal*https://www.ofgem.gov.uk/data-portal/gas-demand-and-supply-source-month-gb.

Ofgem. 2020b. *GB Gas Storage Facilities*.

Ofgem. 2020c. Typical Domestic Consumption Valueshttps://www.ofgem.gov.uk/gas/retail-market/monitoring-data-and-statistics/typical-domestic-consumption-values.

Ogden, J. and Johnson, N. 2010. Techno-economic analysis and modeling of carbon dioxide (CO2) capture and storage (CCS) technologies. *In*: *Developments and Innovation in Carbon Dioxide (CO2) Capture and Storage Technology*. 27–63., https://doi.org/10.1533/9781845699574.1.27.

Oil & Gas Authority. 2020. OGA Field Production, PPRS (WGS84) | Oil and Gas Authorityhttps://data-ogauthority.opendata.arcgis.com/datasets/oga-field-production-pprs-wgs84/data.

Panfilov, M. 2010. Underground Storage of Hydrogen: In Situ Self-Organisation and Methane Generation. *Transport in Porous Media*, **85**, 841–865, https://doi.org/10.1007/s11242-010-9595-7.

Panfilov, M. 2016. *4 – Underground and Pipeline Hydrogen Storage*, https://doi.org/10.1016/B978-1-78242-362-1.00004-3.

Panfilov, M., Reitenbach, V. and Ganzer, L. 2016. Self-organization and shock waves in underground methanation reactors and hydrogen storages. *Environmental Earth Sciences*, **75**, 313, https://doi.org/10.1007/s12665-015-5048-5.

Paterson, L. 1983. *THE IMPLICATIONS OF FINGERING IN UNDERGROUND HYDROGEN STORAGE*.

Peng, D.Y. and Robinson, D.B. 1976. A New Two-Constant Equation of State. *Industrial and Engineering Chemistry Fundamentals*, **15**, 59–64, https://doi.org/10.1021/i160057a011.

Pérez, A., Pérez, E., Dupraz, S. and Bolcich, J. 2016. Patagonia Wind-Hydrogen Project: Underground Storage and Methanation. *In*: *21st World Hydrogen Energy Conference 2016. Zaragoza, Spain. 13-16 Th June, 2016*.

Pfeiffer, W.T. and Bauer, S. 2015. Subsurface Porous Media Hydrogen Storage – Scenario Development and Simulation. *Energy Procedia*, **76**, 565–572, https://doi.org/10.1016/j.egypro.2015.07.872.

Pfeiffer, W.T., Graupner, B. and Bauer, S. 2016. The coupled non-isothermal, multiphase-multicomponent flow and reactive transport simulator OpenGeoSys–ECLIPSE for porous media gas storage. *Environmental Earth Sciences*, **75**, 1347, https://doi.org/10.1007/s12665-016-6168-2.

Pfeiffer, W.T., Beyer, C. and Bauer, S. 2017. Hydrogen storage in a heterogeneous sandstone formation: dimensioning and induced hydraulic effects. *Petroleum geoscience*, **23**, 315–326, https://doi.org/10.1144/petgeo2016-050.

Plaat, H. 2009. Underground gas storage: Why and how. *Geological Society, London, Special Publications*, **313**, 25 LP-- 37, https://doi.org/10.1144/SP313.4.

Poling, B.E. 2001. *The Properties of Gases and Liquids*, 5th edition / Bru... Prausnitz, J. M. (John M., O'Connell, J. P. (John P. and Reid, R. C. (Robert C. (eds). book.

Primary Energy - BP Statistical Review of World Energy 2019 | *68th Edition*. 2019.

Prime Minister's Office. 2019. *The Queen's Speech 2019*.

Progressive Energy. 2019. HyNet Low Carbon Hydrogen Plant - Phase 1 Report for BEIS.

Pruess, K., Oldenburg, C. and Moridis, G. 1999. TOUGH2 User's Guide. 1–197.

QGIS Development Team. 2020. QGIS Geographic Information System.

Qian, J.W., Jaubert, J.N. and Privat, R. 2013. Phase equilibria in hydrogen-containing binary systems modeled with the Peng-Robinson equation of state and temperature-dependent binary interaction parameters calculated through a group-contribution method. *Journal of Supercritical Fluids*, **75**, 58–71, https://doi.org/10.1016/j.supflu.2012.12.014.

Quiñones-Cisneros, S.E. and Deiters, U.K. 2006. Generalization of the Friction Theory for Viscosity Modeling. *The Journal of Physical Chemistry B*, **110**, 12820–12834, https://doi.org/10.1021/jp0618577.

R Core Team. 2019. R: A Language and Environment for Statistical Computing.

RAG Austria AG, AXIOM angewandte Prozesstechnik GesmbH, VERBUND AG, MONTANUNIVERSITÄT LEOBEN, UNIVERSITÄT für Bodenkultur Wien and ENERGIEINSTITUT an der Johannes Kepler Universität Linz. 2017. *Underground Sun Storage - Final Report*.

Rawlins, E.L. and Schellhardt, M.A. 1936. *Back-Pressure Data on Natural Gas Wells and Their Application to Production Practices*.

Raza, A., Rezaee, R., Gholami, R., Bing, C.H., Nagarajan, R. and Hamid, M.A. 2016. A screening criterion for selection of suitable CO2 storage sites. *Journal of Natural Gas Science and Engineering*, **28**, 317–327, https://doi.org/10.1016/j.jngse.2015.11.053.

Reid, R.C., Prausnitz, J.M. and Sherwood, T.K. 1977. *The Properties of Gases and Liquids*, 3rd Editio.

Ren, G., Wan, J., Liu, J., Yu, D. and Söder, L. 2018. Analysis of wind power intermittency based on historical wind power data. *Energy*, **150**, 482–492, https://doi.org/10.1016/j.energy.2018.02.142.

Rohatgi, A. 2020. WebPlotDigitizer.

Sadler, D., Cargill, A., et al. 2016. *Leeds City Gate*.

Sainz-Garcia, A., Abarca, E., Rubi, V. and Grandia, F. 2017. Assessment of feasible strategies for seasonal underground hydrogen storage in a saline aquifer. *International Journal of Hydrogen Energy*, **42**, 16657–16666, https://doi.org/10.1016/j.ijhydene.2017.05.076.

San Marchi, C. and Somerday, B.P.P. 2008. Thermodynamics of Gaseous Hydrogen and Hydrogen Transport in Metals. *In*: *MRS Spring 2008 Meeting, Session HH: "The Hydrogen Economy"*.

Scafidi, J., Wilkinson, M., Gilfillan, S.M.V., Heinemann, N. and Haszeldine, R.S. 2021. A quantitative assessment of the hydrogen storage capacity of the UK continental shelf. *International Journal of Hydrogen Energy*, **46**, 8629–8639, https://doi.org/10.1016/j.ijhydene.2020.12.106.

Schlumberger. 2014. ECLIPSE.

Schlumberger. 2019. Petrel 2019.

Scottish Power. 2020. Hatfield Moor - Gas Flows - ScottishPower. *Segmental Generation & Supply Statements*https://www.scottishpower.com/pages/hatfieldmoor_gas_flows.aspx .

Senseny, P.E., Hansen, F.D., Russell, J.E., Carter, N.L. and Handin, J.W. 1992. Mechanical behaviour of rock salt: Phenomenology and micromechanisms. *International Journal of Rock Mechanics and Mining Sciences and*, **29**, 363–378, https://doi.org/10.1016/0148-9062(92)90513-Y.

Setzmann, U. and Wagner, W. 1991. A New Equation of State and Tables of Thermodynamic Properties for Methane Covering the Range from the Melting Line to 625 K at Pressures up to 100 MPa. *Journal of Physical and Chemical Reference Data*, **20**, 1061–1155, https://doi.org/10.1063/1.555898.

Simbeck, D.R. 2004. CO2capture and storage-the essential bridge to the hydrogen economy. *Energy*, **29**, 1633–1641, https://doi.org/10.1016/j.energy.2004.03.065.

Šmigáň, P., Greksák, M., Kozánková, J., Buzek, F., Onderka, V. and Wolf, I. 1990. Methanogenic bacteria as a key factor involved in changes of town gas stored

in an underground reservoir. *FEMS Microbiology Letters*, **73**, 221–224, https://doi.org/10.1016/0378-1097(90)90733-7.

Stieber, S.J. 1970. Pulsed Neutron Capture Log Evaluation - Louisiana Gulf Coast. *Fall Meeting of the Society of Petroleum Engineers of AIME*, 7, https://doi.org/10.2118/2961-MS.

Stone, H.B.J., Veldhuis, I. and Richardson, R.N. 2009. Underground hydrogen storage in the UK. *Geological Society, London, Special Publications*, **313**, 217–226, https://doi.org/10.1144/SP313.13.

Storengy France. 2018. Beynes - Storengy. *Storengy France Website*.

Strobel, G., Hagemann, B., Huppertz, T.M. and Ganzer, L. 2020. Underground bio-methanation: Concept and potential. *Renewable and Sustainable Energy Reviews*, **123**, 109747, https://doi.org/10.1016/J.RSER.2020.109747.

Stuart, I.A. 1991. The Rough Gas Storage Field, Blocks 47/3d, 47/8b, UK North Sea. *Geological Society, London, Memoirs*, **14**, 477–484, https://doi.org/10.1144/gsl.mem.1991.014.01.59.

Swamee, P.K. and Jain, A.K. 1976. Explicit Equations for Pipe-Flow Problems. *Journal of the Hydraulics Division*, **102**, 657–664, https://doi.org/10.1061/JYCEAJ.0004542.

Tavassoli, Z., Carter, J.N. and King, P.R. 2004. Errors in History Matching - SPE-86883-PA. *SPE Journal*, **9**, 352–361.

Thaysen, E.M., McMahon, S., et al. 2021. Estimating microbial growth and hydrogen consumption in hydrogen storage in porous media. *Renewable and Sustainable Energy Reviews*, **151**, 111481, https://doi.org/10.1016/J.RSER.2021.111481.

The Crown Estate. 2018. Maps and GIS Data. *The Crown Estate website*.

The UK government. 2008. *Climate Change Act 2008*.

Tolbert, B. 2021. Top Dog Engineer https://topdogengineer.com/.

UK Onshore Geophysical Library. 2020. UK Onshore Geophysical Libraryhttps://ukogl.org.uk/.

Underhill, J.R., Monaghan, A.A. and Browne, M.A.E. 2008. Controls on structural

styles, basin development and petroleum prospectivity in the Midland Valley of Scotland. *Marine and Petroleum Geology*, **25**, 1000–1022, https://doi.org/10.1016/j.marpetgeo.2007.12.002.

UNFCCC. 2015. Paris Agreement. *Conference of the Parties on its twenty-first session*, **21932**, 32, https://doi.org/FCCC/CP/2015/L.9/Rev.1.

Van Rossum, G. and Drake, F.L. 2009. Python 3 Reference Manual.

Vangkilde-Pedersen, T., Anthonsen, K.L., et al. 2009. Assessing European capacity for geological storage of carbon dioxide–the EU GeoCapacity project. *Energy Procedia*, **1**, 2663–2670, https://doi.org/10.1016/J.EGYPRO.2009.02.034.

VNIPITRANSGAZ. 2013. Подземные хранилища газа (underground gas storage)http://www.vtg.com.ua/experience/main/ugs.html?lang=en.

Vogel, J.V. 1968. Inflow Performance Relationships for Solution-Gas Drive Wells. *Journal of Petroleum Technology*, **20**, 83–92, https://doi.org/10.2118/1476-PA.

Ward, J., Chan, A. and Ramsay, B. 2003. The Hatfield Moors and Hatfield West Gas (Storage) Fields, South Yorkshire. *Geological Society, London, Memoirs*, **20**, 903–910, https://doi.org/10.1144/GSL.MEM.2003.020.01.76.

Watson, S.D., Lomas, K.J. and Buswell, R.A. 2019. Decarbonising domestic heating: What is the peak GB demand? *Energy Policy*, **126**, 533–544, https://doi.org/10.1016/J.ENPOL.2018.11.001.

Watts, J.W. 1997. Reservoir Simulation: Past, Present, and Future. *SPE Computer Applications*, **9**, 171–176, https://doi.org/10.2118/38441-PA.

Wickham, H. 2016. *Ggplot2: Elegant Graphics for Data Analysis*.

Williams, A. 2003. *Free Energy Relationships in Organic and Bio-Organic Chemistry*, https://doi.org/10.1039/9781847550927.

Williams, D.M. and Harper, A.T. 1988. *A Basin Model for the Silurian of the Midland Valley of Scotland and Ireland*.

Wilson, G. and Rowley, P. 2019. *Flexibility in Great Britain's Gas Networks : Analysis of Linepack and Linepack Flexibility Using Hourly Data*.

Wyllie, M.R.J., Gregory, A.R. and Gardner, L.W. 1956. ELASTIC WAVE VELOCITIES IN HETEROGENEOUS AND POROUS MEDIA. *GEOPHYSICS*,

21, 41–70, https://doi.org/10.1190/1.1438217.

Xia, C. and Wilkinson, M. 2017. The geological risks of exploring for a CO2 storage reservoir. *International Journal of Greenhouse Gas Control*, **63**, 272–280, https://doi.org/10.1016/j.ijggc.2017.05.016.

Yekta, A.E., Manceau, J.-C., Gaboreau, S., Pichavant, M. and Audigane, P. 2018. Determination of Hydrogen–Water Relative Permeability and Capillary Pressure in Sandstone: Application to Underground Hydrogen Injection in Sedimentary Formations. *Transport in Porous Media*, **122**, 333–356, https://doi.org/10.1007/s11242-018-1004-7.

Yu, L. and Liu, J. 2015. Stability of interbed for salt cavern gas storage in solution mining considering cusp displacement catastrophe theory. *Petroleum*, **1**, 82–90, https://doi.org/10.1016/j.petlm.2015.03.006.

Zivar, D., Kumar, S. and Foroozesh, J. 2020. Underground hydrogen storage: A comprehensive review. *International Journal of Hydrogen Energy*, https://doi.org/https://doi.org/10.1016/j.ijhydene.2020.08.138.

8.1.4 Results

Table 18: Results from the investication of hydrogen storage capacity of the UKCS. capacity is working gas capacity

name	**lat**	**lon**	**unit type**	**capacity (twh)**	**closest wind development**	**distance (km)**
Esmond	54.583221	1.428973	gas field	39.9	Z3 Creyke Beck A OFTO	20
Forbes	54.683773	1.499463	gas field	27.5	Z3 Creyke Beck A OFTO	9
Gordon	54.505503	1.957469	gas field	56.7	Z3 Creyke Beck A	17
Caister_B	54.19862	2.463122	gas field	26.6	Hornsea Project Three (HOW03)	24
Leman	53.062638	2.196042	gas field	1188.7	East Anglia North Tranche One West (Norfolk Vanguard West)	16
Barque	53.601201	1.601773	gas field	265.6	Hornsea Project 1 Transmission Asset (OFTO)	18
Amethyst_East	53.600446	0.795735	gas field	42.1	Hornsea Project 1 Transmission Asset (OFTO)	0
Camelot_North	52.959285	2.142056	gas field	32.8	East Anglia North Tranche One West (Norfolk Vanguard West)	12
Camelot_Central_South	52.940538	2.157195	gas field	25.6	East Anglia North Tranche One West (Norfolk Vanguard West)	10
Camelot__Northeast	52.967641	2.232372	gas field	36.8	East Anglia North Tranche One West (Norfolk Vanguard West)	6

Cleeton	54.041875	0.721038	gas field	38.9	Hornsea Project Four (HOW04)	20
Clipper_North	53.455531	1.736011	gas field	129.8	Dudgeon	28
Corvette	53.235392	2.625324	gas field	10.2	East Anglia North Tranche 2 (Norfolk Boreas)	16
Davy	52.998409	2.902582	gas field	14.3	East Anglia North Tranche 2 (Norfolk Boreas)	0
Bessemer	53.20185	2.472358	gas field	13.0	East Anglia North Tranche One West (Norfolk Vanguard West)	19
Beaufort	53.172681	2.532864	gas field	5.0	East Anglia North Tranche One West (Norfolk Vanguard West)	15
Brown	53.026738	2.92691	gas field	7.9	East Anglia North Tranche 2 (Norfolk Boreas)	0
Gawain	53.17035	2.703799	gas field	16.8	East Anglia North Tranche 2 (Norfolk Boreas)	8
Guinevere	53.42024	1.273852	gas field	10.3	Dudgeon	13
Deborah	53.086962	1.851217	gas field	22.8	Dudgeon	31
Big_Dotty	53.091643	1.784571	gas field	46.4	Dudgeon	27
Little_Dotty_(Leman_Sdst)	53.04442	1.865417	gas field	19.6	East Anglia North Tranche 2 (Norfolk Boreas)	27
Della	53.07218	1.895105	gas field	12.1	East Anglia North Tranche 2 (Norfolk Boreas)	30
Dawn	53.130539	1.694635	gas field	9.9	Dudgeon	20
Delilah	53.084599	1.913129	gas field	11.1	East Anglia North Tranche One West (Norfolk Vanguard West)	31

Indefatigable	53.296441	2.460179	gas field	205.3	East Anglia North Tranche One West (Norfolk Vanguard West)	29
Johnston	54.040604	1.247792	gas field	17.4	Hornsea Project Four (HOW04)	0
Malory	53.550605	1.232497	gas field	9.9	Hornsea Project 1 Transmission Asset (OFTO)	15
Mercury	53.767896	0.643787	gas field	6.6	Hornsea Project 2 OFTO	19
Neptune	53.986194	0.787381	gas field	23.8	Hornsea Project Four (HOW04)	21
Pickerill	53.539872	1.11212	gas field	47.0	Hornsea Project 1 Transmission Asset (OFTO)	12
North_Sean	53.239903	2.79265	gas field	15.0	East Anglia North Tranche 2 (Norfolk Boreas)	10
South_Sean	53.187541	2.827992	gas field	14.9	East Anglia North Tranche 2 (Norfolk Boreas)	4
East_Sean	53.221801	2.875965	gas field	5.2	East Anglia North Tranche 2 (Norfolk Boreas)	5
Vanguard	53.378	2.105641	gas field	38.6	Dudgeon	46
Vulcan	53.250026	1.981406	gas field	261.1	Dudgeon	36
North_Valiants	53.377162	2.016299	gas field	125.6	Dudgeon	40
Vikings	53.526552	2.253237	gas field	280.5	Hornsea Project 1 Transmission Asset (OFTO)	32
Anglia	53.376415	1.591555	gas field	48.1	Dudgeon	15
Ann	53.716145	2.072232	gas field	35.5	Hornsea Project 1 Transmission Asset (OFTO)	10
Audrey	53.550552	1.987359	gas field	435.5	Hornsea Project 1 Transmission Asset (OFTO)	29
Baird	53.272899	2.528135	gas field	3.1	East Anglia North Tranche 2 (Norfolk Boreas)	24

Waveney	53.356853	1.299396	gas field	38.9	Dudgeon	5
Bell	53.255268	2.422808	gas field	15.5	East Anglia North Tranche One West (Norfolk Vanguard West)	26
Callisto	53.257401	2.361244	gas field	17.7	East Anglia North Tranche One West (Norfolk Vanguard West)	28
Europa	53.224839	2.300154	gas field	45.8	East Anglia North Tranche One West (Norfolk Vanguard West)	27
Excalibur	53.464615	1.365214	gas field	30.6	Dudgeon	17
Galahad	53.539587	1.389982	gas field	43.3	Hornsea Project 1 Transmission Asset (OFTO)	20
Galleon	53.491337	1.856954	gas field	299.1	Hornsea Project 1 Transmission Asset (OFTO)	34
Ganymede	53.32906	2.226863	gas field	47.0	East Anglia North Tranche One West (Norfolk Vanguard West)	39
Hyde	53.829514	0.991344	gas field	69.0	Hornsea Project Four (HOW04)	14
Lancelot	53.406662	1.367423	gas field	23.7	Dudgeon	10
Mordred	53.521873	1.353082	gas field	69.9	Hornsea Project 1 Transmission Asset (OFTO)	21
Newsham	53.724659	1.243678	gas field	47.8	Hornsea Project 2 OFTO	1
Ravenspurn	54.065469	0.948175	gas field	232.6	Hornsea Project Four (HOW04)	7
Sinope	53.264778	2.29308	gas field	7.7	East Anglia North Tranche One West (Norfolk Vanguard West)	31
Skiff	53.433243	1.877184	gas field	47.5	Dudgeon	34

Thames	53.093842	2.530741	gas field	26.0	East Anglia North Tranche One West (Norfolk Vanguard West)	6
Victor	53.332015	2.335615	gas field	74.0	East Anglia North Tranche One West (Norfolk Vanguard West)	36
Vixen	53.401741	2.239164	gas field	18.0	Hornsea Project 1 Transmission Asset (OFTO)	45
West_Sole	53.721458	1.117158	gas field	148.9	Hornsea Project 2 OFTO	3
Windermere	53.825977	2.754488	gas field	6.7	Hornsea Project Three (HOW03)	1
Alison	53.49683	2.175066	gas field	30.6	Hornsea Project 1 Transmission Asset (OFTO)	34
Amethyst_West	53.655426	0.60749	gas field	20.8	Hornsea Project 2 OFTO	10
Barque_South	53.602825	1.511394	gas field	9.5	Hornsea Project 1 Transmission Asset (OFTO)	16
Bure	53.129283	2.416744	gas field	19.4	East Anglia North Tranche One West (Norfolk Vanguard West)	14
Clipper_South	53.406266	1.767085	gas field	73.0	Dudgeon	26
Indefatigiable_South_West	53.29644	2.46018	gas field	23.3	East Anglia North Tranche One West (Norfolk Vanguard West)	29
Rough	53.829899	0.456151	gas field	13.0	Westermost Rough	16
Yare	53.051765	2.568526	gas field	38.8	East Anglia North Tranche One West (Norfolk Vanguard West)	1
Markham	53.834911	2.890449	gas field	49.6	Hornsea Project Three (HOW03)	10
Vampire	53.469246	2.040144	gas field	7.5	Hornsea Project 1 Transmission Asset (OFTO)	38

Valkyrie	53.456959	2.105176	gas field	13.2	Hornsea Project 1 Transmission Asset (OFTO)	39
Victoria	53.467546	2.283344	gas field	14.0	Hornsea Project Three (HOW03)	37
Viscount	53.393005	2.155652	gas field	48.4	Hornsea Project 1 Transmission Asset (OFTO)	46
Valiant_South	53.317707	2.0926	gas field	67.5	East Anglia North Tranche One West (Norfolk Vanguard West)	43
Hoton	53.804363	1.209999	gas field	38.1	Hornsea Project Four (HOW04)	3
Brigantine_A	53.393234	2.653017	gas field	9.5	East Anglia North Tranche 2 (Norfolk Boreas)	29
Brigantine_B	53.420746	2.628058	gas field	10.2	Hornsea Project Three (HOW03)	32
Brigantine_C	53.425451	2.715192	gas field	5.8	East Anglia North Tranche 2 (Norfolk Boreas)	30
Brigantine_D	53.441868	2.671291	gas field	2.2	Hornsea Project Three (HOW03)	29
Hamilton	53.568347	-3.450813	gas field	33.5	Burbo Bank Extension	9
Hamilton_North	53.645936	-3.47204	gas field	17.1	Burbo Bank Extension	17
North_Morecambe	53.964246	-3.673617	gas field	275.7	Walney Extension Transmission Asset	4
South_Morecambe	53.872332	-3.598405	gas field	580.2	Walney Extension Transmission Asset	9
Hamilton_East	53.603283	-3.407324	gas field	4.0	Burbo Bank Extension	11

Millom	54.017144	-3.808132	gas field	86.7	Walney Extension Transmission Asset	5
Bains	53.875693	-3.463778	gas field	21.0	Walney Extension Transmission Asset	6
Dalton	53.897447	-3.728957	gas field	24.3	Walney Extension Transmission Asset	12
Calder	53.806281	-3.665614	gas field	26.9	Walney Extension Transmission Asset	18
Hewett	53.022614	1.773482	gas field	93.1	East Anglia North Tranche 2 (Norfolk Boreas)	24
Murdoch	54.267967	2.311171	gas field	19.4	Hornsea Project Three (HOW03)	31
Schooner	54.075801	2.075275	gas field	142.0	Hornsea Project Two (HOW02)	9
Boulton	54.219636	2.151279	gas field	101.4	Hornsea Project Three (HOW03)	26
Caister_C	54.211971	2.445023	gas field	13.3	Hornsea Project Three (HOW03)	26
Fulmar_028_05	56.877812	0.821726	Saline aquifer with identified structure	5.8	Hywind (Scotland) Ltd	146
Fulmar_021_28	57.023636	0.586666	Saline aquifer with identified structure	1.8	Hywind (Scotland) Ltd	125
Fulmar_021_29	57.182104	0.753223	Saline aquifer with identified structure	2.9	Hywind (Scotland) Ltd	129

Fulmar_021_23	57.193361	0.39953	Saline aquifer with identified structure	4.8	Hywind (Scotland) Ltd	108
Fulmar_021_18	57.358078	0.449926	Saline aquifer with identified structure	0.6	Hywind (Scotland) Ltd	107
Fulmar_021_16	57.457633	0.052782	Saline aquifer with identified structure	4.7	Hywind (Scotland) Ltd	82
Bunter_Closure_1	54.0251	1.76661	Saline aquifer with identified structure	8.0	Hornsea Project 2 OFTO	3
Bunter_Closure_4	54.384764	1.623913	Saline aquifer with identified structure	0.1	Hornsea Project Four (HOW04)	33
Bunter_Closure_5	54.466272	1.421954	Saline aquifer with identified structure	2.4	Hornsea Project Four (HOW04)	32
Bunter_Closure_7	54.101063	0.98824	Saline aquifer with identified structure	0.1	Hornsea Project Four (HOW04)	2
Bunter_Closure_35	54.215727	1.027245	Saline aquifer with identified structure	10.3	Hornsea Project Four (HOW04)	1

Bunter_Closure_38	54.311859	1.920562	Saline aquifer with identified structure	0.8	Hornsea Project 2 OFTO	35
Bunter_Closure_39	54.173271	1.821028	Saline aquifer with identified structure	2.9	Hornsea Project 2 OFTO	19
Bunter_Closure_40	54.248415	1.551506	Saline aquifer with identified structure	1.2	Hornsea Project Four (HOW04)	18
Bunter_Closure_41	54.341867	1.235258	Saline aquifer with identified structure	1.2	Hornsea Project Four (HOW04)	15
Bunter_Closure_42	54.408695	1.084344	Saline aquifer with identified structure	0.7	Hornsea Project Four (HOW04)	22
Bunter_Closure_46	54.049356	0.712246	Saline aquifer with identified structure	1.4	Hornsea Project Four (HOW04)	20
Bunter_Closure_32	53.978083	0.417206	Saline aquifer with identified structure	0.4	Z3 Creyke Beck A OFTO	22
Rannoch_210_25	61.363752	0.866452	Saline aquifer with identified structure	4.8	Nova Innovation Ltd	124

Carr_012_22	58.127854	-2.691303	Saline aquifer with identified structure	16.0	MacColl Offshore Windfarm Ltd	0
Punt_012_24	58.172	-2.213	Saline aquifer with identified structure	42.1	Moray Offshore Wind Farm (East	21
Captain_013_17	58.337	-1.677	Saline aquifer with identified structure	53.4	MacColl Offshore Windfarm Ltd	54
Bunter_Closure_29	54.164407	0.259956	Saline aquifer with identified structure	3.9	Z3 Creyke Beck A OFTO	0
Bunter_Closure_18	52.955722	2.143609	Saline aquifer with identified structure	0.5	East Anglia North Tranche One West (Norfolk Vanguard West)	11
Bunter_Closure_2	53.778113	1.145496	Saline aquifer with identified structure	8.1	Hornsea Project Four (HOW04)	7
Bunter_Closure_21	53.551834	1.642516	Saline aquifer with identified structure	7.8	Hornsea Project 1 Transmission Asset (OFTO)	24
Bunter_Closure_22	53.595038	1.356559	Saline aquifer with identified structure	0.4	Hornsea Project 1 Transmission Asset (OFTO)	14

Bunter_Closure_23	53.476887	1.563445	Saline aquifer with identified structure	0.1	Dudgeon	23
Bunter_Closure_24	53.464106	1.355361	Saline aquifer with identified structure	0.7	Dudgeon	17
Bunter_Closure_25	53.538117	1.208355	Saline aquifer with identified structure	0.3	Hornsea Project 1 Transmission Asset (OFTO)	15
Bunter_Closure_26	53.846642	1.620278	Saline aquifer with identified structure	1.5	Hornsea Project 2 OFTO	0
Bunter_Closure_9	53.103944	2.162435	Saline aquifer with identified structure	14.7	East Anglia North Tranche One West (Norfolk Vanguard West)	21
Bunter_Closure_17	53.387944	2.530687	Saline aquifer with identified structure	1.0	East Anglia North Tranche 2 (Norfolk Boreas)	33
Bunter_Closure_20	53.178646	2.698508	Saline aquifer with identified structure	0.1	East Anglia North Tranche 2 (Norfolk Boreas)	9
Bunter_Closure_28	53.68426	2.121505	Saline aquifer with identified structure	10.8	Hornsea Project 1 Transmission Asset (OFTO)	13

Bunter_Closure_3	53.451501	2.301575	Saline aquifer with identified structure	3.6	Hornsea Project Three (HOW03)	39
Frigg_Sandstone_Member	60.262987	1.788166	Saline aquifer with identified structure	64.7	Nova Innovation Ltd	160
Heimdal_Sandstone_Member	59.764412	1.391094	Saline aquifer with identified structure	1234.4	P/f SHEFA	144
Tay_Sandstone_Member	57.214001	0.95326	Saline aquifer with identified structure	55.7	Hywind (Scotland) Ltd	140
Cromarty_Sandstone_Member	57.66	0.484214	Saline aquifer with identified structure	46.9	Hywind (Scotland) Ltd	109
Flugga_Sandstone_Member	58.884766	1.244936	Saline aquifer with identified structure	29.3	P/f SHEFA	156
Hermod_Sandstone_Member	59.863137	2.005782	Saline aquifer with identified structure	1.9	P/f SHEFA	178
Skadan_Sandstone_Member	58.842275	1.431641	Saline aquifer with identified structure	6.9	P/f SHEFA	167

Teal_Sandstone_Member	59.987419	1.863455	Saline aquifer with identified structure	29.2	P/f SHEFA	170
Skroo_Sandstone_Member_1	59.036395	1.491254	Saline aquifer with identified structure	0.8	P/f SHEFA	162
Skroo_Sandstone_Member_2	58.75416	1.365673	Saline aquifer with identified structure	1.0	P/f SHEFA	169
Skroo_Sandstone_Member_3	58.446585	1.328304	Saline aquifer with identified structure	1.5	P/f SHEFA	186
Ormskirk_closure_1	53.527505	-3.757251	Saline aquifer with identified structure	0.0	Gwynt y Mor	9
Ormskirk_Closure_2	53.492623	-3.758859	Saline aquifer with identified structure	0.0	Gwynt y Mor	6
Ormskirk_closure_3	53.474974	-3.674108	Saline aquifer with identified structure	0.0	Gwynt y Mor	1
Ormskirk_closure_4	53.45949	-3.651525	Saline aquifer with identified structure	0.1	Gwynt y Mor	0

Ormskirk_closure_5	53.662459	-3.750253	Saline aquifer with identified structure	0.1	Gwynt y Mor	21
Ormskirk_closure_6	53.444253	-3.587288	Saline aquifer with identified structure	0.7	Gwynt y Mor	0
Ormskirk_closure_7	53.747504	-3.198678	Saline aquifer with identified structure	0.6	Walney 2 OFTO	17
Ormskirk_closure_8	53.7799	-3.181389	Saline aquifer with identified structure	0.0	Walney 2 OFTO	13
Ormskirk_closure_9	53.860054	-3.313529	Saline aquifer with identified structure	1.2	Walney Extension Transmission Asset	6
Ormskirk_closure_10	54.022795	-3.335328	Saline aquifer with identified structure	0.0	Walney 1 OFTO	0
Ormskirk_closure_11	54.104443	-3.366852	Saline aquifer with identified structure	0.0	Ormonde	3
Ormskirk_closure_12	54.104782	-3.416483	Saline aquifer with identified structure	0.1	Ormonde	1

Ormskirk_closure_13	54.142195	-3.380432	Saline aquifer with identified structure	0.0	Ormonde	6
Ormskirk_closure_14	54.212677	-3.468196	Saline aquifer with identified structure	0.0	Ormonde	12
Ormskirk_closure_15	54.146463	-3.541296	Saline aquifer with identified structure	0.1	Walney 2	6
Ormskirk_closure_16	54.291616	-3.756797	Saline aquifer with identified structure	1.7	Walney Extension 3	15
Balder_Sandstone_Member_1	59.482459	1.265716	Saline aquifer with identified structure	31.6	BT Openreach	141
Balder_Sandstone_Member_2	58.526197	1.275758	Saline aquifer with identified structure	14.7	P/f SHEFA	178
Balder_Formation_Sandstone_Member_3	60.207579	1.867762	Saline aquifer with identified structure	11.2	Nova Innovation Ltd	166
Balder_Formation_Sandstone_Member_4	60.70069	1.851479	Saline aquifer with identified structure	1.1	Nova Innovation Ltd	155

Hewett_Sandstone_Bed	52.750845	2.097506	Saline aquifer with identified structure	25.9	East Anglia North Tranche 2 (Norfolk Boreas)	0
Spilsby_Sandstone_Formation_2	52.990776	2.973943	Saline aquifer with identified structure	0.9	East Anglia North Tranche 2 (Norfolk Boreas)	0
Forties_5	57.506401	1.16623	Saline aquifer with identified structure	359.3	Hywind (Scotland) Ltd	149
Mains_012_26	58.020657	-2.882098	Saline aquifer with no identified structure	1.9	Moray Offshore Windfarm (West)	5
Orrin_012_26	58.117854	-3.067867	Saline aquifer with no identified structure	1.3	Moray Offshore Windfarm (West)	0
Louise_012_22	58.141262	-2.836619	Saline aquifer with no identified structure	0.6	Moray Offshore Windfarm (West)	0
Coracle_012_20	58.279	-2.093	Saline aquifer with no identified structure	2.4	MacColl Offshore Windfarm Ltd	29

Mousa_Formation_1	59.052561	1.055292	Saline aquifer with no identified structure	14.6	P/f SHEFA	138
Otter_Sandstone_Formation	50.457417	-1.795488	Saline aquifer with no identified structure	11.7	Rampion (Southern Array)	104
Spilsby_Sandstone_Formation_3	52.506911	2.842884	Saline aquifer with no identified structure	0.6	Z5 East Anglia Three OFTO	2
Mousa_Formation_2	58.270479	0.170599	Saline aquifer with no identified structure	0.3	Hywind (Scotland) Ltd	124
Dornoch_Formation	59.455341	0.762061	Saline aquifer with no identified structure	15.7	P/f SHEFA	113
Grid_Sandstone_Member	58.244087	0.863274	Saline aquifer with no identified structure	5.9	Hywind (Scotland) Ltd	154

Mey_1	56.68334	2.20503	Saline aquifer with no identified structure	9.7	Z3 Teesside (Lackenby) B	173
Maureen_1	56.821499	2.11464	Saline aquifer with no identified structure	4.6	Z3 Teesside (Lackenby) B	189

8.2 Appendix 2 – Hydrogen storage capacity calculator code for R

This code will replicate the results of Scafidi *et al.* (2021). You will need two input files: the reservoir database in csv format in the structure given in Table 19 and the constants from Table 20 saved in a csv file named cons.csv.

Table 19: structure of the input table with column names, variable, units, example data, and data type

column	**variable**	**units**	**example data**	**type**
code	index		1	int
unitdesignate_trans	saline aquifer = 1, gas = 2, gas condensate = 3, oil & gas = 4		2	int
stratigraphy_age_trans	age		Whyassic	str
stratigraphy_group_trans	group		Dinosaur_Group	str
stratigraphy_form_trans	formation		Seagull_Formation	str
stratigraphy_member_trans	member		NA	str
stratigraphy_bed	bed		NA	str
geographic_area_trans	geographic area		Northern_North_Sea	str
description	name		Banana_gas_field_	str
lat	latitude		55.55	float
lon	longitude		1.55	float

storage_unit_type_trans	1 = no identified structure, 2 = identified structure		2	int
grossthicknessml_metres	thickness	metres	600.7	float
areaml_km_2	area	km2	250.5	float
porosityml_frac	porosity	fraction	0.15	float
porevolume_10E6m_3	pore volume	m3	17000.5	float
formationtempml_deg_C	formation temperature	degrees celcius	150.5	float
fracturepressureml_Mpa	fracture pressure	Megapascals (Mpa)	100.5	float
0.75_of_fracture_pressure_Mpa	75% of fracture pressure (not used in final version)	Megapascals (Mpa)	75.5	float
Hydrostatic_pressure_Mpa	hydrostatic pressure	Megapascals (Mpa)	60.5	float
Pressure_diff_hydrostatic_and_0.75_fracture	difference between hydrostatic and 75% of fracture pressures (not used in final version)	Megapascals (Mpa)	30.5	float
pressure_gradient_of_0.0102_Mpa_per_metre_(from_https://bugs.freedesktop.org/attachment.cgi?id=44605)	pressure if gradient of 0.0102 MPa per metres		50.5	float

shallowestdepthml_mTVDSS	shallowest depth	metres TVDSS	5000.5	float
meandepthml_mTVDSS	mean depth	metres TVDSS	5100.5	float
salinity_ppm	salinty	parts per million ppm	55000.3	float
formationtempml_Kelvin	formation temperature	degrees Kelvin	400.5	float
storagepermeabilityml_md	permeability	millidarcies (mD)	40.8	float
irreducible_water_saturationml_frac	irreducible water saturation	fraction	0.423	float
fluidviscocity_cp	fluid viscosity	centipose (cP)	0.2	float

Table 20: constants for cons.csv from table 1 in Lemmon, Huber and Leachman (2008)

ai	bi	ci
5.89E-02	1.325	1
-6.14E-02	1.87	1
-2.65E-03	2.5	2
2.73E-03	2.8	2
1.80E-03	2.938	2.42
-1.15E-03	3.14	2.63
9.59E-05	3.37	3
-1.11E-07	3.75	4
1.26E-10	4	5

```
##########################################################################
###################
#
# hydrogen storage capacity estimate for UK offshore code using CO2Stored
database
#
##########################################################################
###################

# preamble
install.packages("knitr")
install.packages("asserthat")
install.packages("assertthat")
library("asserthat")
library(dplyr)
library(knitr)
```

```
# load CO2stored database
CO2STORED_for_use_in_R <- read.csv("R:/CO2STORED_for_use_in_R.csv")

# set hydrogen values
gasdensitystp <- 0.0899 #kg/m3
h2energydensity <- 120 #Mj/m3
MJ2kWh <- 0.277778 #kwh/Mj
twhperkg <- 3.941e-08 #twh/kg HHV
h2gasconstant <- 4160 #R: j/kg K from engineering science page 88
h2covol <- 1.58e-05 #b: m3/mol

# constants
stpp <- 0.101325 #MPa@stp
stpt <- 273.15 #kelvin@stp
iws <- 0.423 #irreducible water sat from database
wgc <- 0.5 #working gas capacity

#conversions
MMtom <- 1e+06 #millions cubic metres to cubic metres
MPatopa <- 1e+06 #megapascals to pascals

#########################################################################
###################
#
# STAGE 1 : FILTERING
#
#########################################################################
###################
# filter so only saline aquifers and gas sites (s.a. = 1, gas = 2, gas condensate = 3,
oil & gas = 4)

h2store <- subset(CO2STORED_for_use_in_R,
CO2STORED_for_use_in_R$unitdesignate_trans < 3)
```

```
# H2 compressibility factor for each reservoir (constants & formula from lemmon et
al 2008)
# cons.csv is the constants from table 1 in Lemmon et al 2008 (Revised
Standardized #Equation for Hydrogen #Gas Densities for Fuel Consumption
Applications)
cons <- read.csv("R:/cons.csv", T)

for (i in 1:nrow(h2store)) {
  h2store$Z[i] <- 1 + sum(cons$ai *
(100/h2store$formationtempml_Kelvin[i])^cons$bi *
(h2store$Hydrostatic_pressure_Mpa[i]/1)^cons$ci)
}

filter1 <- nrow(h2store)

# POROPERM

# storage parameter filter for permeability
h2store <- subset(h2store, !(h2store$unitdesignate_trans == 1 &
h2store$storagepermeabilityml_md < 100))

filter2 <- nrow(h2store)

# storage paramter filter for porosity
h2store <- subset(h2store, !(h2store$unitdesignate_trans == 1 &
h2store$porosityml_frac < 0.1))

filter3 <- nrow(h2store)

# all code above working fine

# filter for min depth based on min CAES
h2store <- subset(h2store, !(h2store$unitdesignate_trans == 1 &
h2store$shallowestdepthml_mTVDSS < 200))
```

```
filter4 <- nrow(h2store)

# max depth from chadwick 2008
h2store <- subset(h2store, !(h2store$unitdesignate_trans == 1 &
h2store$meandepthml_mTVDSS > 2500))

filter5 <- nrow(h2store)



# number of sites left
n_saline <- sum(with(h2store, unitdesignate_trans == 1))
n_gas <- sum(with(h2store, unitdesignate_trans == 2))

# remove all identified unsuitable saline aquifers: Bunter zones and extent as
closures identified, Ormskirk Zones
# as closures identified, Leman extent as fields identified.

tomatch <- list(128, 138, 139, 141, 153, 154, 225, 226, 227, 228, 229, 230, 231,
248, 256, 257, 258, 259, 260, 303,
  304, 306, 307)
h2store <- h2store[!h2store$code%in% tomatch, ]

filter6 <- nrow(h2store)

# remove na values

cols <- c(17, 21, 28)
h2store <- h2store[complete.cases(h2store[, cols]), ]

filter7 <- nrow(h2store)

#########################################################################
###################
#
# STAGE 2 : EFFICIENCY CALCULATION FOR SALINE AQUIFERS
```

```
#
#########################################################################
##################

# no identified structure as per paper section
for (i in 1:length(h2store$unitdesignate_trans)) {
  if (h2store$storage_unit_type_trans[i] == 1 && h2store$unitdesignate_trans[i] == 1)
{
    h2store$porevolume_10E6m_3[i] <- h2store$porevolume_10E6m_3[i] * 0.001
  }
}

# identified structure 1% as per CO2Stored database minimum efficiency
# conservative estimate based on lack of data

for (i in 1:length(h2store$unitdesignate_trans)) {
  if (h2store$storage_unit_type_trans[i] != 1 && h2store$unitdesignate_trans[i] == 1)
{
    h2store$porevolume_10E6m_3[i] <- h2store$porevolume_10E6m_3[i] * 0.01
  }
}

#########################################################################
##################
#
# STAGE 3 : HYDROGEN CAPACITY CALCULATION
#
#########################################################################
##################

# equation 2 from paper
h2store$capacity_m3 <- ((h2store$porevolume_10E6m_3 * MMtom) * (1 - iws) *
h2store$Hydrostatic_pressure_Mpa * stpt)/(h2store$Z *
  stpp * h2store$formationtempml_Kelvin)
```

```
# working gas capacity

h2store$capacity_m3 <- h2store$capacity_m3 * wgc

# density at reservoir conditions

h2store$density <- (h2store$Hydrostatic_pressure_Mpa * MPatopa)/(h2gasconstant
* h2store$formationtempml_Kelvin + h2covol *
  (h2store$Hydrostatic_pressure_Mpa * MPatopa))

# density at stp

h2densstp <- (stpp * MPatopa)/(h2gasconstant * stpt + h2covol * (stpp * MPatopa))

h2store$h2mass_kg <- h2store$capacity_m3 * h2densstp

# conversion to TWh

h2store$twh <- h2store$h2mass_kg * twhperkg

# tabulate results

# GRAND TOTAL
grandtotaltwh <- colSums(h2store["twh"], na.rm = TRUE, dims = 1)

# saline aquifer TOTAL
aquifers <- subset(h2store, h2store$unitdesignate_trans == 1)

nostructure_aquiferstoretwh <- subset(aquifers, aquifers$storage_unit_type_trans
== 1)
withstructure_aquiferstoretwh <- subset(aquifers,
!(aquifers$storage_unit_type_trans == 1))

withstructure_aquifertotaltwh <- colSums(withstructure_aquiferstoretwh["twh"],
na.rm = TRUE, dims = 1)
```

```
nostructure_aquifertotaltwh <- colSums(nostructure_aquiferstoretwh["twh"], na.rm =
TRUE, dims = 1)

# gas field TOTAL

gasfieldstoretwh <- subset(h2store, h2store$unitdesignate_trans == 2)
gasfieldtotaltwh <- colSums(gasfieldstoretwh["twh"], na.rm = TRUE, dims = 1)

# numbersleft after everything
ngas <- nrow(gasfieldstoretwh)
nsa_ns <- nrow(nostructure_aquiferstoretwh)
nsa_ws <- nrow(withstructure_aquiferstoretwh)

post_n_saline <- sum(with(h2store, unitdesignate_trans == 1))
post_n_gas <- sum(with(h2store, unitdesignate_trans == 2))

# make table of results
Results_twh_h2 <- c(gasfieldtotaltwh, withstructure_aquifertotaltwh,
nostructure_aquifertotaltwh, grandtotaltwh)

# label results
names(Results_twh_h2) <- c("Gas field capacity/twh", "Saline aquifer with id
structure capacity/twh", "Saline aquifer no id structure capacity/twh",
  "Total capacity/twh")

# export data to GIS for visualisation

write.csv(h2store,
"R:/PhD/h2store_offshore_resources/h2store_r_processed_update", row.names =
TRUE) #open excel, open file, save as .csv



filters <- c(filter1, filter2, filter3, filter4, filter5, filter6, filter7)

filters
```

```
Results_twh_h2

final_numbers <- c(ngas, nsa_ns, nsa_ws)

final_numbers

#########################################################################
###################
#
# END OF CODE
#########################################################################
###################
```

8.3 Appendix 3 – Digitized data from the Cousland gas field

8.3.1 Core data

Table 21: Cousland core porosity and permeability data. Reports can be found at the UK onshore geophysical library interactive map, just search for Cousland

blank = no data							
well	reports (OKUGL.org.uk)	page number	depth [ft]	depth [m]	perm [mD]	por [%]	por [frac]
C1	petroleum engineering file 1	85	1724.5	525.6	2.15		
C1	petroleum engineering file 1	85	928	282.9	8.02		
C1	petroleum engineering file 1	85	928	282.9	37.2		
C1	petroleum engineering file 1	85	950	289.6	1.31		
C1	petroleum engineering file 1	85	950	289.6	10		
C1	petroleum engineering file 1	85	971	296.0	1.02		
C1	petroleum engineering file 1	85	1200	365.8	0.74		
C1	petroleum engineering file 1	85	1248	380.4	4.24		
C1	petroleum engineering file 1	85	1265	385.6	12.91		
C1	petroleum engineering file 1	85	1791.5	546.0	172.1		
C1	petroleum engineering file 1	85	1804.5	550.0	154.9		
C1	petroleum engineering file 1	85	1724.5	525.6	3		
C1	petroleum engineering file 1	85	928	282.9	11.08		
C1	petroleum engineering file 1	85	928	282.9	33.51		
C1	petroleum engineering file 1	85	950	289.6	1.26		
C1	petroleum engineering file 1	85	950	289.6			
C1	petroleum engineering file 1	85	971	296.0	0.76		
C1	petroleum engineering file 1	85	1200	365.8	1.5		
C1	petroleum engineering file 1	85	1248	380.4			
C1	petroleum engineering file 1	85	1265	385.6			
C1	petroleum engineering file 1	85	1791.5	546.0	172.1		
C1	petroleum engineering file 1	85	1804.5	550.0	154.9		
C1	petroleum engineering file 1	76	2187	666.6	24.23		
C1	petroleum engineering file 1	76	2188	666.9	9.24		
C1	petroleum engineering file 1	76	2189	667.2	2.4		
C1	petroleum engineering file 1	76	2187	666.6	36.57		
C1	petroleum engineering file 1	76	2188	666.9	8.52		
C1	petroleum engineering file 1	76	2189	667.2	2.33		
C1	petroleum engineering file 1	78	2015	614.2	9.45	1.9	0.019
C1	petroleum engineering file 1	78	2026.5	617.7	6.42	2.5	0.025
C1	petroleum engineering file 1	78	2105.5	641.8	166.8	1.5	0.015
C1	petroleum engineering file 1	78	2015	614.2	9.42	2	0.02

C1	petroleum engineering file 1	78	2026.5	617.7	4.84	1.8	0.018
C1	petroleum engineering file 1	78	2105.5	641.8	190.6	1.6	0.016
C1	petroleum engineering file 1	83	1791.5	546.0	172.1		
C1	petroleum engineering file 1	83	1791.5	546.0	172.1		
C1	petroleum engineering file 1	83	1804.5	550.0	154.9		
C1	petroleum engineering file 1	83	1804.5	550.0	154.9		
C1	petroleum engineering file 1	90	1590	484.6	269.8		
C1	petroleum engineering file 1	90	1590	484.6	303.2		
C1	petroleum engineering file 1	90	1613	491.6	41.36		
C1	petroleum engineering file 1	90	1613	491.6	25.78		
C1	petroleum engineering file 1	90	1631	497.1	1.94		
C1	petroleum engineering file 1	90	1631	497.1	2.73		
C1	petroleum engineering file 1	90	1631	497.1	2.75		
C1	petroleum engineering file 1	90	1631	497.1	2.55		
C1	petroleum engineering file 1	93	1587	483.7		17	0.17
C1	petroleum engineering file 1	93	1625.5	495.5		15.4	0.154
C1	petroleum engineering file 1	95	1590	484.6	256		
C1	petroleum engineering file 1	95	1590	484.6	280		
C1	petroleum engineering file 1	95	1613	491.6	72.8		
C1	petroleum engineering file 1	95	1613	491.6	26.55		
C1	petroleum engineering file 1	95	1631	497.1	1.94		
C1	petroleum engineering file 1	95	1631	497.1	2.73		
C1	petroleum engineering file 1	100	1262	384.7		18.1	0.181
C1	petroleum engineering file 1	100	1253	381.9		23	0.23
C2	petroleum engineering file	20-21	2057	627.0		6.6	0.066
C2	petroleum engineering file	20-21	2072.5	631.7		3.6	0.036
C2	petroleum engineering file	20-21	2056	626.7	16.28		
C2	petroleum engineering file	20-21	2071.5	631.4	19		
C2	petroleum engineering file	20-21	2286	696.8	2.16	5.6	0.056
C2	petroleum engineering file	20-21	2295	699.5	10.46	11.7	0.117
C2	petroleum engineering file	20-21	2310	704.1	19.39	9.4	0.094
C2	petroleum engineering file	20-21	2330	710.2	451	5.2	0.052
C2	petroleum engineering file	20-21	2340	713.2	3.08	7.2	0.072
C2	petroleum engineering file	20-21	2360	719.3	3.73	3.1	0.031
C2	petroleum engineering file	20-21	2365	720.9	7.08	4.1	0.041
C2	petroleum engineering file	20-21	2375	723.9	37.36	11.1	0.111
C2	petroleum engineering file	20-21	2385	726.9	45.76	10.7	0.107
C2	petroleum engineering file	20-21	2392	729.1	6.02	4.6	0.046
C2	petroleum engineering file	20-21	2404	732.7	2.16	7.5	0.075
C2	petroleum engineering file	20-21	2056	626.7	6.94		
C2	petroleum engineering file	20-21	2071.5	631.4	19.9		

C2	petroleum engineering file	20-21	2286	696.8	2.26		
C2	petroleum engineering file	20-21	2295	699.5	11.98		
C2	petroleum engineering file	20-21	2310	704.1	24.07		
C2	petroleum engineering file	20-21	2330	710.2	451		
C2	petroleum engineering file	20-21	2340	713.2	4.15		
C2	petroleum engineering file	20-21	2360	719.3	3.39		
C2	petroleum engineering file	20-21	2365	720.9	4.2		
C2	petroleum engineering file	20-21	2375	723.9	38.44		
C2	petroleum engineering file	20-21	2385	726.9	42.5		
C2	petroleum engineering file	20-21	2392	729.1	5.92		
C2	petroleum engineering file	20-21	2404	732.7	2.26		
C2	petroleum engineering file	22	1496	456.0	197	8.6	0.086
C2	petroleum engineering file	22	1512	460.9	1.88	1.2	0.012
C2	petroleum engineering file	22	1515	461.8	2.96	10.4	0.104
C2	petroleum engineering file	22	2028	618.1	53.72	10.2	0.102
C2	petroleum engineering file	22	2095	638.6	186.3	6.7	0.067
C2	petroleum engineering file	24	1496	456.0	198.3		
C2	petroleum engineering file	24	1512	460.9	3.32		
C2	petroleum engineering file	24	1515	461.8	2.73		
C2	petroleum engineering file	24	2028	618.1	55.2		
C2	petroleum engineering file	24	2095	638.6	186.3		
C4	petroleum engineering file	38	299	91.1	0	6.9	0.069
C4	petroleum engineering file	38	301	91.7	1.8	14.2	0.142
C4	petroleum engineering file	38	307	93.6	3.4	17.8	0.178
C4	petroleum engineering file	38	310	94.5			
C4	petroleum engineering file	38	318	96.9	0.2	13.2	0.132
C4	petroleum engineering file	38	496	151.2		29.5	0.295
C4	petroleum engineering file	38	498	151.8	1.9	13.8	0.138
C4	petroleum engineering file	38	500	152.4	0	14.2	0.142
C4	petroleum engineering file	38	507	154.5	12.3	16.2	0.162
C4	petroleum engineering file	38	750	228.6	0.2	9.3	0.093
C4	petroleum engineering file	38	750.5	228.8	10.8	17.6	0.176
C4	petroleum engineering file	38	880	268.2	1.1	17.8	0.178
C4	petroleum engineering file	38	931	283.8	0.3	10	0.1
C4	petroleum engineering file	38	934	284.7	0.4	7	0.07
C4	petroleum engineering file	38	936	285.3	0.3	9.8	0.098
C4	petroleum engineering file	38	942	287.1	0.6	12	0.12
C4	petroleum engineering file	38	943.5	287.6	0.2	6.4	0.064
C4	petroleum engineering file	38	1160	353.6	0.4	3.4	0.034
C4	petroleum engineering file	38	1243	378.9	170	16.4	0.164
C4	petroleum engineering file	38	1247.5	380.2			

C4	petroleum engineering file	38	1486	452.9	43	16.1	0.161
C4	petroleum engineering file	38	1487.5	453.4	1.2	14.2	0.142
C4	petroleum engineering file	38	1489	453.8		8.8	0.088
C4	petroleum engineering file	38	1524	464.5			
C4	petroleum engineering file	38	1540	469.4	0.1	5.6	0.056
C4	petroleum engineering file	38	1594	485.9	0.8	7.7	0.077
C4	petroleum engineering file	38	1595	486.2	6	11.8	0.118
C4	petroleum engineering file	38	1597	486.8			
C4	petroleum engineering file	38	1598.5	487.2	9.8	12.2	0.122
C4	petroleum engineering file	38	1600	487.7	33	13.1	0.131
C5	petroleum engineering file	28	892.5	272.0		10.2	0.102
C5	petroleum engineering file	28	897	273.4	8.6	14.6	0.146
C5	petroleum engineering file	28	901.5	274.8	439.8	15.5	0.155
C5	petroleum engineering file	28	928	282.9		0.7	0.007
C5	petroleum engineering file	28	1065	324.6	7.8	13	0.13
C5	petroleum engineering file	28	1074	327.4	0.77	10.7	0.107
C5	petroleum engineering file	28	1083	330.1	7.88	14.1	0.141
C5	petroleum engineering file	28	1352	412.1	265.1	16.4	0.164
C5	petroleum engineering file	28	1356	413.3	213.9	15.3	0.153
C5	petroleum engineering file	28	1359	414.2	10.03	12	0.12
C5	petroleum engineering file	28	1365	416.1	0.39	7.9	0.079
C5	petroleum engineering file	28	1519	463.0	67.9	14.2	0.142
C5	petroleum engineering file	28	1523	464.2	57.28	14.3	0.143
C5	petroleum engineering file	28	1661	506.3	161.1	15.5	0.155
C5	petroleum engineering file	28	1663	506.9	40.8	13.8	0.138
C5	petroleum engineering file	28	1694.5	516.5	1.93	10.8	0.108
C5	petroleum engineering file	28	1695.5	516.8	3.66	9.1	0.091
C5	petroleum engineering file	28	1715	522.7	123.9	13.3	0.133
C5	petroleum engineering file	28	1718.5	523.8	96.3	12.3	0.123
C5	petroleum engineering file	28	1735	528.8	1	7.7	0.077
C5	petroleum engineering file	28	1739	530.0	0.59	9.5	0.095
C5	petroleum engineering file	28	1858	566.3	1.4	7.8	0.078
C5	petroleum engineering file	28	1887	575.2	0.08	5	0.05
C5	petroleum engineering file	28	1890	576.1	0.24	6.2	0.062
C6	geological report on cores	8	1366	416.4		14.4	0.144
C6	geological report on cores	8	1366	416.4		13.7	0.137
C6	geological report on cores	8	1389	423.4		10.1	0.101
C6	geological report on cores	8	1390	423.7		7.4	0.074
C6	geological report on cores	8	1402	427.3		9.3	0.093
C6	geological report on cores	8	1409	429.5		12.1	0.121
C6	geological report on cores	8	1494	455.4		2.1	0.021

C6	geological report on cores	8	1500	457.2		12.1	0.121
C6	geological report on cores	8	1500	457.2		10.8	0.108
C6	geological report on cores	8	1514	461.5		10.7	0.107
C6	geological report on cores	8	1526	465.1		13.8	0.138
C6	geological report on cores	8	1526	465.1		12.5	0.125
C6	geological report on cores	8	1532	467.0		14.2	0.142
C6	geological report on cores	8	1532	467.0		13	0.13
C6	geological report on cores	8	1537	468.5		7.1	0.071

8.3.2 Gas analysis

Table 22: gas analysis from Cousland 1. C1,C2,C3,and C4 refer to hydrocarbons with the corresponding number of carbon atoms (a standard format in the hydrocarbon industry) and N2 is nitrogen

Interval (MD) [feet]	**C1**	**C2**	**C3**	**C4**	**N_2**
1188-1279	95.85	2.3	1.24	0.6	-
1248-1279	90.75	3.1	3.5	2.65	-
1582-1632	95.85	2.6	-	-	1.55
1720-1800	94	2.9	0.6	-	2.59
2094-2122	87.9	3.85	1.05	0.65	6.53
from p85	LASMO relinquishment report (UKOGL.org.uk)				

8.3.3 Pressure and production data

Table 23: field history file formatted for CMG software. 'Well Head Pressure', 'Gas Rate SC', and 'Cumulative Gas SC' are WHP [psi], gas rate [ft3/day], and cumulative gas produced [ft3] respectively, in columns 2, 3, and 4. Column 1 is time in ISO format

2020-06-10T15:40:00			
'C1 full production history - psia'			
1939-09-11T07:00:03			
'ISO_DATE_FORMAT'			
3			
'Well Head Pressure' 'Gas Rate SC' 'Cumulative Gas SC'			
'psi' 'ft3/day' 'ft3'			
1			
'C1'			
1939-09-11T07:00:03	583.7	0	0
1939-09-11T09:00:03	585.7	0	0
1939-09-11T11:00:03	587.7	0	0
1939-09-11T13:00:03	589.7	0	0
1939-09-11T14:00:03	590.7	0	0
1939-09-11T16:00:03	590.7	0	0
1939-09-11T18:00:03	590.9	0	0
1939-09-11T20:00:03	591.1	0	0
1939-09-11T22:00:03	591.7	0	0
1939-09-12T10:00:03	592.2	0	0
1939-09-12T20:00:03	593	0	0
1939-09-13T12:00:03	594.9	0	0
1939-09-14T12:00:03	596.6	0	0
1939-09-15T12:00:03	597.4	0	0
1939-09-16T12:00:03	598.1	0	0

1939-09-17T12:00:03	-99999	0	0
1939-09-18T12:00:03	-99999	0	0
1939-09-19T12:00:03	599.2	0	0
1939-09-20T12:00:03	599.7	0	0
1939-09-21T12:00:03	600.3	0	0
1939-09-22T12:00:03	600.3	0	0
1939-09-23T12:00:03	600.4	0	0
1939-09-24T12:00:03	-99999	0	0
1939-09-25T12:00:03	600.7	0	0
1939-09-26T12:00:03	600.9	0	0
1939-09-27T12:00:03	601	0	0
1939-09-28T12:00:03	601.1	0	0
1939-09-29T12:00:03	601.2	0	0
1939-09-30T12:00:03	601.5	0	0
1939-10-07T12:00:03	601.3	0	0
1939-10-08T12:00:03	-99999	0	0
1939-10-09T12:00:03	601.6	0	0
1939-10-10T12:00:03	601.3	0	0
1939-10-11T12:00:03	601.4	0	0
1939-10-12T12:00:03	601.1	0	0
1939-10-13T12:00:03	600.9	0	0
1939-10-21T14:00:03	-99999	0	0
1939-10-21T15:00:03	-99999	0	0
1939-10-21T16:00:03	-99999	0	0
1939-10-21T17:00:03	-99999	0	0
1939-10-21T18:00:03	-99999	0	0
1939-10-21T19:00:03	-99999	0	0

1939-10-21T20:00:03	-99999	0	0
1939-10-21T21:00:03	-99999	0	0
1939-10-21T22:00:03	-99999	0	0
1939-10-21T23:00:03	-99999	0	0
1939-10-22T00:00:03	-99999	0	0
1939-10-22T01:00:03	24.7	0	0
1939-10-22T02:00:03	24.7	0	0
1939-10-22T03:00:03	24.7	0	0
1939-10-22T04:00:03	24.7	0	0
1939-10-22T05:00:03	24.7	0	0
1939-10-22T06:00:03	44.7	0	0
1939-10-22T07:00:03	44.7	0	0
1939-10-22T08:00:03	174.7	0	0
1939-10-22T09:00:03	179.7	0	0
1939-10-22T10:00:03	189.7	0	0
1939-10-22T11:00:03	199.7	0	0
1939-10-22T12:00:03	209.7	0	0
1939-10-22T13:00:03	219.7	0	0
1939-10-22T14:00:03	229.7	0	0
1939-10-22T15:00:03	239.7	0	0
1939-10-22T16:00:03	249.7	0	0
1939-10-22T17:00:03	259.7	0	0
1939-10-22T18:00:03	269.7	0	0
1939-10-22T19:00:03	279.7	0	0
1939-10-22T20:00:03	289.7	0	0
1939-10-22T21:00:03	299.7	0	0
1939-10-22T22:00:03	309.7	0	0

1939-10-22T23:00:03	319.7	0	0
1939-10-23T00:00:03	329.7	0	0
1939-10-23T01:00:03	339.7	0	0
1939-10-23T02:00:03	344.7	0	0
1939-10-23T03:00:03	359.7	0	0
1939-10-23T04:00:03	369.7	0	0
1939-10-23T05:00:03	374.7	0	0
1939-10-23T06:00:03	384.7	0	0
1939-10-23T07:00:03	404.7	0	0
1939-10-23T08:00:03	404.7	0	0
1939-10-23T09:00:03	404.7	0	0
1939-10-23T10:00:03	414.7	0	0
1939-10-23T11:00:03	424.7	0	0
1939-10-23T12:00:03	444.7	0	0
1939-10-23T13:00:03	454.7	0	0
1939-10-23T14:00:03	459.7	0	0
1939-10-23T15:00:03	474.7	0	0
1939-10-23T16:00:03	484.7	0	0
1939-10-23T17:00:03	499.7	0	0
1939-10-23T18:00:03	509.7	0	0
1939-10-23T19:00:03	519.7	0	0
1939-10-23T20:00:03	529.7	0	0
1939-10-23T21:00:03	539.7	0	0
1939-10-23T22:00:03	549.7	0	0
1939-10-23T23:00:03	559.7	0	0
1939-10-24T00:00:03	569.7	0	0
1939-10-24T01:00:03	584.7	0	0

1939-10-24T02:00:03	604.7	0	0
1939-10-24T03:00:03	604.7	0	0
1939-10-24T04:00:03	604.7	0	0
1939-10-24T05:00:03	604.7	0	0
1939-10-24T06:00:03	624.7	0	0
1939-10-24T07:00:03	624.7	0	0
1939-10-24T08:00:03	639.7	0	0
1939-10-24T09:00:03	644.7	0	0
1939-10-24T10:00:03	644.7	0	0
1939-10-24T11:00:03	649.7	0	0
1939-10-24T12:00:03	644.7	0	0
1939-10-24T13:00:03	644.7	0	0
1939-10-24T14:00:03	644.7	0	0
1939-10-24T15:00:03	644.7	0	0
1939-10-24T16:00:03	644.7	0	0
1939-10-24T17:00:03	644.7	0	0
1939-10-24T18:00:03	644.7	0	0
1939-10-24T19:00:03	644.7	0	0
1939-10-24T20:00:03	644.7	0	0
1939-10-24T21:00:03	644.7	0	0
1939-10-24T22:00:03	644.7	0	0
1939-10-24T23:00:03	644.7	0	0
1939-10-25T00:00:03	644.7	0	0
1939-10-25T01:00:03	644.7	0	0
1939-10-25T02:00:03	644.7	0	0
1939-10-25T03:00:03	644.7	0	0
1939-10-25T04:00:03	644.7	0	0

1939-10-25T05:00:03	644.7	0	0
1939-10-25T06:00:03	644.7	0	0
1939-10-25T07:00:03	644.7	0	0
1939-10-25T08:00:03	644.7	0	0
1939-10-25T09:00:03	644.7	0	0
1939-10-25T10:00:03	644.7	0	0
1939-10-25T11:00:03	644.7	0	0
1939-10-25T12:00:03	644.7	0	0
1939-10-25T13:00:03	644.7	0	0
1939-10-25T14:00:03	644.7	0	0
1939-10-25T15:00:03	644.7	0	0
1939-10-25T16:00:03	644.7	0	0
1939-10-28T08:00:03	644.7	0	0
1939-10-28T16:00:03	644.7	0	0
1939-10-29T00:00:03	644.7	0	0
1939-10-29T08:00:03	644.7	0	0
1939-10-29T16:00:03	644.7	0	0
1939-10-30T00:00:03	644.7	0	0
1939-10-30T08:00:03	644.7	0	0
1939-10-30T16:00:03	644.7	0	0
1939-10-31T00:00:03	644.7	0	0
1939-10-31T08:00:03	644.7	0	0
1939-10-31T16:00:03	644.7	0	0
1939-11-01T00:00:03	644.7	0	0
1939-11-01T08:00:03	644.7	0	0
1939-11-01T16:00:03	644.7	0	0
1939-11-02T00:00:03	644.7	0	0

1939-11-02T08:00:03	644.7	0	0
1939-11-02T16:00:03	644.7	0	0
1939-11-03T00:00:03	644.7	0	0
1939-11-03T08:00:03	644.7	0	0
1939-11-03T09:00:03	654.7	0	0
1939-11-03T15:30:03	654.7	800000	216667
1939-11-03T16:00:03	594.7	950000	236458
1939-11-03T16:30:03	589.7	1060000	258542
1939-11-03T17:00:03	589.7	1030000	280000
1939-11-03T17:30:03	589.7	1000000	300834
1939-11-03T18:00:03	594.7	1080000	323334
1939-11-03T18:30:03	594.7	1040000	345000
1939-11-03T19:00:03	594.7	950000	364792
1939-11-03T19:30:03	599.7	980000	385209
1939-11-03T20:00:03	599.7	1050000	407084
1939-11-03T20:30:03	599.7	1060000	429167
1939-11-03T21:00:03	599.7	1050000	451042
1939-11-03T21:30:03	599.7	1050000	472917
1939-11-03T22:00:03	599.7	1050000	494792
1939-11-03T22:30:03	599.7	1040000	516459
1939-11-03T23:00:03	599.7	1020000	537709
1939-11-03T23:30:03	599.7	1030000	559168
1939-11-04T00:00:03	599.7	1020000	580418
1939-11-04T00:30:03	599.7	1030000	601876
1939-11-04T01:00:03	599.7	1020000	623126
1939-11-04T01:30:03	599.7	1020000	644376
1939-11-04T02:00:03	599.7	1020000	665626

1939-11-04T02:30:03	599.7	1020000	686876
1939-11-04T03:00:03	599.7	1040000	708543
1939-11-04T03:30:03	599.7	1050000	730418
1939-11-04T04:00:03	599.7	1050000	752293
1939-11-04T04:30:03	599.7	1050000	774168
1939-11-04T05:00:03	599.7	1050000	796043
1939-11-04T05:30:03	599.7	1060000	818127
1939-11-04T06:00:03	599.7	1050000	840002
1939-11-04T06:30:03	599.7	1050000	861877
1939-11-04T07:00:03	599.7	1050000	883752
1939-11-04T07:30:03	599.7	1060000	905835
1939-11-04T08:00:03	599.7	970000	926044
1939-11-04T08:30:03	609.7	1000000	946877
1939-11-04T09:00:03	599.7	1040000	968544
1939-11-04T09:15:03	-99999	0	968544
1939-11-04T10:15:03	624.7	1070000	1013127
1939-11-04T10:30:03	609.7	1050000	1024067
1939-11-04T11:00:03	604.7	1050000	1045942
1939-11-04T11:30:03	609.7	1040000	1067609
1939-11-04T12:00:03	609.7	1060000	1089692
1939-11-04T12:30:03	609.7	1070000	1111984
1939-11-04T13:30:03	-99999	0	1111984
1939-11-04T13:45:03	614.7	1045000	1122867
1939-11-04T14:00:03	609.7	1090000	1134223
1939-11-04T14:30:03	609.7	1140000	1157974
1939-11-04T15:00:03	609.7	1095000	1180786
1939-11-04T15:30:03	609.7	1100000	1203703

1939-11-04T16:00:03	609.7	1095000	1226515
1939-11-04T16:30:03	609.7	984000	1247015
1939-11-04T17:00:03	614.7	996000	1267765
1939-11-04T17:30:03	604.7	1135000	1291411
1939-11-04T18:00:03	614.7	1024000	1312745
1939-11-04T18:30:03	614.7	897000	1331432
1939-11-04T19:00:03	614.7	978000	1351807
1939-11-04T19:30:03	604.7	1140000	1375557
1939-11-04T20:00:03	604.7	1090000	1398266
1939-11-04T20:30:03	604.7	1100000	1421179
1939-11-04T21:00:03	604.7	1090000	1443887
1939-11-04T21:30:03	604.7	1140000	1467637
1939-11-04T22:00:03	599.7	1155000	1491700
1939-11-04T22:30:03	614.7	1023000	1513012
1939-11-04T23:00:03	614.7	960000	1533012
1939-11-04T23:30:03	614.7	992000	1553679
1939-11-05T00:00:03	614.7	1055000	1575658
1939-11-05T00:30:03	614.7	1060000	1597741
1939-11-05T01:00:03	614.7	1070000	1620033
1939-11-05T01:30:03	614.7	1072000	1642366
1939-11-05T02:00:03	614.7	1060000	1664450
1939-11-05T02:30:03	614.7	1118000	1687741
1939-11-05T03:00:03	614.7	1057000	1709762
1939-11-05T03:30:03	614.7	1050000	1731637
1939-11-05T04:00:03	614.7	1050000	1753512
1939-11-05T04:30:03	614.7	1055000	1775491
1939-11-05T05:00:03	614.7	1055000	1797471

1939-11-05T05:30:03	614.7	1057000	1819491
1939-11-05T06:00:03	614.7	1055000	1841471
1939-11-05T06:30:03	614.7	1058000	1863512
1939-11-05T07:00:03	614.7	1022000	1884804
1939-11-05T07:30:03	614.7	1032000	1906304
1939-11-05T08:00:03	614.7	1010000	1927346
1939-11-05T08:30:03	614.7	1080000	1949846
1939-11-05T09:00:03	614.7	1043000	1971575
1939-11-05T09:30:03	614.7	1072000	1993908
1939-11-05T10:00:03	609.7	1065000	2016096
1939-11-05T10:30:03	609.7	1097000	2038950
1939-11-05T11:00:03	609.7	1107000	2062012
1939-11-05T11:30:03	609.7	1074000	2084387
1939-11-05T12:00:03	609.7	1057000	2106408
1939-11-05T12:30:03	609.7	1037000	2128012
1939-11-05T13:00:03	609.7	1040000	2149679
1939-11-05T13:30:03	609.7	1027000	2171075
1939-11-05T14:00:03	609.7	1046000	2192866
1939-11-05T14:30:03	614.7	620000	2205783
1939-11-05T16:55:03	-99999	0	2205783
1939-11-05T17:00:03	624.7	984000	2209200
1939-11-05T17:30:03	614.7	1066000	2231408
1939-11-05T18:00:03	614.7	977000	2251762
1939-11-05T18:30:03	609.7	1072000	2274096
1939-11-05T19:00:03	609.7	1072000	2296429
1939-11-05T19:30:03	614.7	968000	2316596
1939-11-05T20:00:03	614.7	1015000	2337741

1939-11-05T20:30:03	614.7	1064000	2359908
1939-11-05T21:00:03	609.7	1107000	2382971
1939-11-05T21:30:03	609.7	1050000	2404846
1939-11-05T22:00:03	609.7	1055000	2426825
1939-11-05T22:30:03	609.7	1096000	2449658
1939-11-05T23:00:03	609.7	1062000	2471783
1939-11-05T23:30:03	609.7	1096000	2494616
1939-11-06T00:00:03	609.7	1055000	2516596
1939-11-06T00:30:03	609.7	922000	2535804
1939-11-06T01:00:03	609.7	1092000	2558554
1939-11-06T01:30:03	609.7	1055000	2580533
1939-11-06T02:00:03	614.7	1004000	2601450
1939-11-06T02:30:03	614.7	1015000	2622596
1939-11-06T03:00:03	614.7	1035000	2644158
1939-11-06T03:30:03	614.7	1024000	2665491
1939-11-06T04:00:03	614.7	988000	2686075
1939-11-06T04:30:03	614.7	1015000	2707221
1939-11-06T05:00:03	614.7	1055000	2729200
1939-11-06T05:30:03	614.7	1043000	2750929
1939-11-06T06:00:03	614.7	1033000	2772450
1939-11-06T06:30:03	614.7	1055000	2794429
1939-11-06T07:00:03	614.7	1108000	2817512
1939-11-06T07:30:03	614.7	1043000	2839241
1939-11-06T08:00:03	614.7	1034000	2860783
1939-11-06T08:30:03	614.7	970000	2880991
1939-11-06T09:00:03	609.7	1040000	2902658
1939-11-06T09:30:03	-99999	0	2902658

1939-11-06T10:00:03	624.7	1035000	2924221
1939-11-06T10:30:03	614.7	1005000	2945158
1939-11-06T11:00:03	614.7	1068000	2967408
1939-11-06T11:30:03	614.7	1010000	2988450
1939-11-06T12:00:03	614.7	1010000	3009491
1939-11-06T12:30:03	614.7	1080000	3031991
1939-11-06T13:00:03	614.7	956000	3051908
1939-11-06T13:30:03	614.7	966000	3072033
1939-11-06T14:00:03	614.7	966000	3092158
1939-11-06T14:30:03	614.7	1005000	3113096
1939-11-06T15:00:03	614.7	1005000	3134033
1939-11-06T15:30:03	614.7	975000	3154346
1939-11-06T16:00:03	614.7	1005000	3175283
1939-11-06T16:30:03	614.7	1006000	3196241
1939-11-06T17:00:03	614.7	983000	3216721
1939-11-06T17:30:03	614.7	983000	3237200
1939-11-06T18:00:03	614.7	975000	3257512
1939-11-06T18:30:03	614.7	984000	3278012
1939-11-06T19:00:03	614.7	974000	3298304
1939-11-06T19:30:03	609.7	1048000	3320137
1939-11-06T20:00:03	609.7	1075000	3342533
1939-11-06T20:30:03	614.7	988000	3363116
1939-11-06T21:00:03	614.7	1025000	3384471
1939-11-06T21:30:03	609.7	1038000	3406096
1939-11-06T22:00:03	609.7	1027000	3427491
1939-11-06T22:30:03	609.7	1068000	3449741
1939-11-06T23:00:03	609.7	1040000	3471408

1939-11-06T23:30:03	614.7	992000	3492075
1939-11-07T00:00:03	614.7	1033000	3513596
1939-11-07T00:30:03	614.7	1052000	3535512
1939-11-07T01:00:03	614.7	1113000	3558700
1939-11-07T01:30:03	614.7	1077000	3581137
1939-11-07T02:00:03	614.7	1074000	3603512
1939-11-07T02:30:03	609.7	1105000	3626533
1939-11-07T03:00:03	609.7	1105000	3649554
1939-11-07T03:30:03	609.7	1046000	3671346
1939-11-07T04:00:03	609.7	1063000	3693491
1939-11-07T04:30:03	609.7	1042000	3715200
1939-11-07T05:00:03	609.7	1023000	3736512
1939-11-07T05:30:03	609.7	1018000	3757721
1939-11-07T06:00:03	609.7	1035000	3779283
1939-11-07T06:30:03	609.7	1032000	3800783
1939-11-07T07:00:03	614.7	1035000	3822346
1939-11-07T07:30:03	614.7	1016000	3843512
1939-11-07T08:00:03	609.7	1053000	3865450
1939-11-07T08:30:03	614.7	1058000	3887491
1939-11-07T09:00:03	609.7	1052000	3909408
1939-11-07T09:30:03	609.7	1060000	3931491
1939-11-07T10:00:03	609.7	1060000	3953575
1939-11-07T10:30:03	609.7	1025000	3974929
1939-11-07T11:00:03	609.7	1065000	3997116
1939-11-07T11:30:03	609.7	1025000	4018471
1939-11-07T12:00:03	609.7	1048000	4040304
1939-11-07T12:30:03	609.7	1046000	4062096

1939-11-07T13:00:03	609.7	1070000	4084387
1939-11-07T13:30:03	609.7	1070000	4106679
1939-11-07T14:00:03	604.7	1070000	4128971
1939-11-07T14:30:03	604.7	1083000	4151533
1939-11-07T15:00:03	604.7	1098000	4174408
1939-11-07T15:30:03	604.7	1098000	4197283
1939-11-07T16:00:03	604.7	1098000	4220158
1939-11-07T16:30:03	604.7	1086000	4242783
1939-11-07T17:00:03	604.7	1090000	4265491
1939-11-07T17:30:03	604.7	1084000	4288075
1939-11-07T18:00:03	604.7	1084000	4310658
1939-11-07T18:30:03	604.7	1085000	4333262
1939-11-07T19:00:03	604.7	1085000	4355866
1939-11-07T19:30:03	604.7	1065000	4378054
1939-11-07T20:00:03	604.7	1063000	4400200
1939-11-07T20:30:03	604.7	1090000	4422908
1939-11-07T21:00:03	604.7	1064000	4445075
1939-11-07T21:30:03	604.7	1062000	4467200
1939-11-07T22:00:03	604.7	1062000	4489325
1939-11-07T22:30:03	604.7	1056000	4511325
1939-11-07T23:00:03	604.7	1055000	4533304
1939-11-07T23:30:03	604.7	1058000	4555346
1939-11-08T00:00:03	604.7	1055000	4577325
1939-11-08T00:30:03	604.7	1060000	4599408
1939-11-08T01:00:03	604.7	1095000	4622221
1939-11-08T01:30:03	604.7	1056000	4644221
1939-11-08T02:00:03	604.7	1053000	4666158

1939-11-08T02:30:03	604.7	1060000	4688241
1939-11-08T03:00:03	604.7	1100000	4711158
1939-11-08T03:30:03	604.7	1095000	4733971
1939-11-08T04:00:03	604.7	1100000	4756887
1939-11-08T04:30:03	604.7	1080000	4779387
1939-11-08T05:00:03	604.7	1085000	4801991
1939-11-08T05:30:03	604.7	1050000	4823866
1939-11-08T06:00:03	604.7	1056000	4845866
1939-11-08T06:30:03	604.7	1100000	4868783
1939-11-08T07:00:03	604.7	1095000	4891596
1939-11-08T07:30:03	604.7	1056000	4913596
1939-11-08T08:00:03	604.7	1100000	4936512
1939-11-08T08:30:03	604.7	1096000	4959346
1939-11-08T09:00:03	604.7	1096000	4982179
1939-11-08T09:30:03	604.7	1120000	5005512
1939-11-08T10:00:03	604.7	1096000	5028346
1939-11-08T10:30:03	604.7	1120000	5051679
1939-11-08T11:00:03	604.7	1096000	5074512
1939-11-08T11:30:03	604.7	1004000	5095429
1939-11-08T12:00:03	604.7	990000	5116054
1939-11-08T12:30:03	604.7	990000	5136679
1939-11-08T13:00:03	609.7	1004000	5157596
1939-11-08T13:30:03	609.7	1000000	5178429
1939-11-08T14:00:03	609.7	972000	5198679
1939-11-08T14:30:03	609.7	958000	5218637
1939-11-08T15:00:03	609.7	958000	5238596
1939-11-08T15:30:03	609.7	959000	5258575

1939-11-08T16:00:03	612.7	971000	5278804
1939-11-08T16:30:03	604.7	996000	5299554
1939-11-08T17:00:03	609.7	983000	5320033
1939-11-08T17:30:03	609.7	1066000	5342241
1939-11-08T18:00:03	604.7	1068000	5364491
1939-11-08T18:30:03	604.7	1058000	5386533
1939-11-08T19:00:03	604.7	1058000	5408575
1939-11-08T19:30:03	604.7	1058000	5430616
1939-11-08T20:00:03	604.7	1003000	5451512
1939-11-08T20:30:03	604.7	996000	5472262
1939-11-08T21:00:03	604.7	1010000	5493304
1939-11-08T21:30:03	609.7	1018000	5514512
1939-11-08T22:00:03	609.7	1000000	5535346
1939-11-08T22:30:03	604.7	1010000	5556387
1939-11-08T23:00:03	604.7	1045000	5578158
1939-11-08T23:30:03	604.7	1058000	5600200
1939-11-09T00:00:03	604.7	1046000	5621991
1939-11-09T00:30:03	604.7	1008000	5642991
1939-11-09T01:00:03	609.7	1053000	5664929
1939-11-09T01:30:03	609.7	1063000	5687075
1939-11-09T02:00:03	609.7	1057000	5709096
1939-11-09T02:30:03	609.7	1052000	5731012
1939-11-09T03:00:03	609.7	1050000	5752887
1939-11-09T03:30:03	609.7	1013000	5773991
1939-11-09T04:00:03	609.7	1053000	5795929
1939-11-09T04:30:03	604.7	1015000	5817075
1939-11-09T05:00:03	604.7	1040000	5838741

1939-11-09T05:30:03	604.7	1042000	5860450
1939-11-09T06:00:03	604.7	1035000	5882012
1939-11-09T06:30:03	609.7	1042000	5903721
1939-11-09T07:00:03	609.7	1050000	5925596
1939-11-09T07:30:03	609.7	1042000	5947304
1939-11-09T08:00:03	609.7	1080000	5969804
1939-11-09T08:30:03	609.7	1058000	5991846
1939-11-09T09:00:03	609.7	1058000	6013887
1939-11-09T09:30:03	609.7	1054000	6035846
1939-11-09T10:00:03	609.7	1044000	6057596
1939-11-09T10:30:03	604.7	1064000	6079762
1939-11-09T11:00:03	604.7	1042000	6101471
1939-11-09T11:30:03	604.7	1048000	6123304
1939-11-09T12:00:03	604.7	1048000	6145137
1939-11-09T12:30:03	604.7	1056000	6167137
1939-11-09T13:00:03	604.7	1056000	6189137
1939-11-09T13:30:03	604.7	1044000	6210887
1939-11-09T14:00:03	604.7	1012000	6231971
1939-11-09T14:30:03	604.7	1046000	6253762
1939-11-09T15:00:03	604.7	1016000	6274929
1939-11-09T15:30:03	604.7	1064000	6297096
1939-11-09T16:00:03	604.7	1060000	6319179
1939-11-09T16:30:03	604.7	1044000	6340929
1939-11-09T17:00:03	604.7	1056000	6362929
1939-11-09T17:30:03	604.7	1010000	6383971
1939-11-09T18:00:03	604.7	1044000	6405721
1939-11-09T18:30:03	604.7	1028000	6427137

1939-11-09T19:00:03	604.7	1045000	6448908
1939-11-09T19:30:03	604.7	1052000	6470825
1939-11-09T20:00:03	604.7	1020000	6492075
1939-11-09T20:30:03	604.7	1032000	6513575
1939-11-09T21:00:03	604.7	1032000	6535075
1939-11-09T21:30:03	604.7	1040000	6556741
1939-11-09T22:00:03	604.7	1028000	6578158
1939-11-09T22:30:03	604.7	1025000	6599512
1939-11-09T23:00:03	604.7	1028000	6620929
1939-11-09T23:30:03	604.7	1030000	6642387
1939-11-10T00:00:03	604.7	1030000	6663846
1939-11-10T00:30:03	604.7	1030000	6685304
1939-11-10T01:00:03	604.7	1028000	6706721
1939-11-10T01:30:03	604.7	1030000	6728179
1939-11-10T02:00:03	604.7	1017000	6749366
1939-11-10T02:30:03	604.7	1014000	6770491
1939-11-10T03:00:03	604.7	1012000	6791575
1939-11-10T03:30:03	604.7	1014000	6812700
1939-11-10T04:00:03	604.7	1013000	6833804
1939-11-10T04:30:03	604.7	1016000	6854971
1939-11-10T05:00:03	604.7	1004000	6875887
1939-11-10T05:30:03	604.7	1020000	6897137
1939-11-10T06:00:03	604.7	1022000	6918429
1939-11-10T06:30:03	604.7	1026000	6939804
1939-11-10T07:00:03	604.7	1026000	6961179
1939-11-10T07:30:03	604.7	1018000	6982387
1939-11-10T08:00:03	604.7	1050000	7004262

1939-11-10T08:30:03	604.7	1032000	7025762
1939-11-10T09:00:03	604.7	1032000	7047262
1939-11-10T09:30:03	604.7	1052000	7069179
1939-11-10T10:00:03	-99999	0	7069179
1939-11-10T10:30:03	-99999	0	7069179
1939-11-10T11:00:03	-99999	0	7069179
1939-11-10T11:30:03	599.7	1110000	7092304
1939-11-10T12:00:03	599.7	1105000	7115325
1939-11-10T12:30:03	599.7	1104000	7138325
1939-11-10T13:00:03	599.7	1130000	7161866
1939-11-10T13:30:03	599.7	1120000	7185200
1939-11-10T14:00:03	599.7	1105000	7208221
1939-11-10T14:15:03	-99999	0	7208221
1939-11-10T16:30:03	614.7	1462000	7345283
1939-11-10T17:00:03	589.7	1606000	7378741
1939-11-10T17:30:03	589.7	1690000	7413950
1939-11-10T18:00:03	574.7	1704000	7449450
1939-11-10T18:30:03	574.7	1716000	7485200
1939-11-10T19:00:03	574.7	1715000	7520929
1939-11-10T19:30:03	574.7	1715000	7556658
1939-11-10T20:00:03	574.7	1732000	7592741
1939-11-10T20:30:03	574.7	1716000	7628491
1939-11-10T21:00:03	574.7	1720000	7664325
1939-11-10T21:30:03	574.7	1726000	7700283
1939-11-10T22:00:03	574.7	1746000	7736658
1939-11-10T22:30:03	574.7	1746000	7773033
1939-11-10T23:00:03	574.7	1746000	7809408

1939-11-10T23:30:03	574.7	1746000	7845783
1939-11-11T00:00:03	574.7	1746000	7882158
1939-11-11T00:30:01	574.7	1750000	7918576
1939-11-11T01:00:01	574.7	1750000	7955034
1939-11-11T01:30:01	574.7	1750000	7991493
1939-11-11T02:00:01	574.7	1750000	8027951
1939-11-11T02:30:01	574.7	1745000	8064305
1939-11-11T03:00:01	574.7	1745000	8100660
1939-11-11T03:30:01	574.7	1745000	8137014
1939-11-11T04:00:01	574.7	1745000	8173368
1939-11-11T04:30:01	569.7	1735000	8209514
1939-11-11T05:00:01	569.7	1742000	8245806
1939-11-11T05:30:01	569.7	1742000	8282098
1939-11-11T06:00:01	569.7	1742000	8318389
1939-11-11T06:30:01	569.7	1766000	8355181
1939-11-11T07:00:01	569.7	1760000	8391848
1939-11-11T07:30:01	569.7	1744000	8428181
1939-11-11T08:00:01	569.7	1744000	8464515
1939-11-11T08:30:01	564.7	1685000	8499619
1939-11-11T09:00:01	564.7	1720000	8499621
1939-11-11T09:30:01	564.7	1627000	8533517
1939-11-11T09:40:01	-99999	0	8533517
1939-11-11T10:40:01	-99999	0	8533517
1939-11-11T11:00:01	579.7	1510000	8554491
1939-11-11T11:30:01	579.7	1624000	8588324
1939-11-11T12:00:01	579.7	1618000	8622032
1939-11-11T12:30:01	579.7	1618000	8655741

1939-11-11T13:00:01	579.7	1625000	8689595
1939-11-11T13:30:01	579.7	1620000	8723345
1939-11-11T14:00:01	579.7	1625000	8757200
1939-11-11T14:30:01	579.7	1625000	8791054
1939-11-11T15:00:01	579.7	1620000	8824804
1939-11-11T15:30:01	569.7	1528000	8856637
1939-11-11T16:00:01	574.7	1528000	8888471
1939-11-11T16:30:01	574.7	1532000	8920387
1939-11-11T17:00:01	574.7	1525000	8952158
1939-11-11T17:30:01	574.7	1525000	8983929
1939-11-11T18:00:01	574.7	1525000	9015700
1939-11-11T18:30:01	574.7	1526000	9047492
1939-11-11T19:00:01	574.7	1526000	9079284
1939-11-11T19:30:01	574.7	1522000	9110992
1939-11-11T20:00:01	574.7	1532000	9142909
1939-11-11T20:30:01	574.7	1532000	9174826
1939-11-11T21:00:01	574.7	1535000	9206805
1939-11-11T21:30:01	574.7	1532000	9238722
1939-11-11T22:00:01	574.7	1533000	9270659
1939-11-11T22:30:01	574.7	1540000	9302743
1939-11-11T23:00:01	574.7	1536000	9334743
1939-11-11T23:30:01	574.7	1546000	9366951
1939-11-12T00:00:01	574.7	1540000	9399035
1939-11-12T00:30:01	574.7	1540000	9431118
1939-11-12T01:00:01	574.7	1540000	9463201
1939-11-12T01:30:01	574.7	1540000	9495285
1939-11-12T02:00:01	574.7	1544000	9527452

1939-11-12T02:30:01	574.7	1550000	9559743
1939-11-12T03:00:01	574.7	1544000	9591910
1939-11-12T03:30:01	574.7	1540000	9623994
1939-11-12T04:00:01	574.7	1540000	9656077
1939-11-12T04:30:01	574.7	1540000	9688160
1939-11-12T05:00:01	574.7	1540000	9720244
1939-11-12T05:30:01	574.7	1536000	9752244
1939-11-12T06:00:01	574.7	1540000	9784327
1939-11-12T06:30:01	574.7	1530000	9816202
1939-11-12T07:00:01	574.7	1535000	9848182
1939-11-12T07:30:01	574.7	1550000	9880473
1939-11-12T08:00:01	574.7	1532000	9912390
1939-11-12T08:30:01	574.7	1550000	9944682
1939-11-12T09:00:01	574.7	1556000	9977099
1939-11-12T09:30:01	574.7	1535000	10009078
1939-11-12T10:00:01	574.7	1550000	10041370
1939-11-12T10:30:01	574.7	1543000	10073516
1939-11-12T11:00:01	574.7	1545000	10105703
1939-11-12T11:30:01	574.7	1548000	10137953
1939-11-12T12:00:01	574.7	1552000	10170287
1939-11-12T12:30:01	574.7	1552000	10202620
1939-11-12T13:00:01	574.7	1536000	10234620
1939-11-12T13:30:01	574.7	1536000	10266620
1939-11-12T14:00:01	574.7	1536000	10298620
1939-11-12T14:30:01	574.7	1545000	10330808
1939-11-12T15:00:01	574.7	1536000	10362808
1939-11-12T15:30:01	574.7	1545000	10394996

1939-11-12T16:00:01	574.7	1518000	10426621
1939-11-12T16:30:01	574.7	1518000	10458246
1939-11-12T17:00:01	574.7	1520000	10489913
1939-11-12T17:30:01	574.7	1538000	10521954
1939-11-12T18:00:01	574.7	1522000	10553663
1939-11-12T18:30:01	574.7	1522000	10585371
1939-11-12T19:00:01	574.7	1522000	10617080
1939-11-12T19:30:01	574.7	1522000	10648788
1939-11-12T20:00:01	574.7	1522000	10680497
1939-11-12T20:30:01	574.7	1522000	10712205
1939-11-12T21:00:01	574.7	1522000	10743913
1939-11-12T21:30:01	574.7	1522000	10775622
1939-11-12T22:00:01	574.7	1520000	10807289
1939-11-12T22:30:01	574.7	1522000	10838997
1939-11-12T23:00:01	574.7	1520000	10870664
1939-11-12T23:30:01	574.7	1520000	10902330
1939-11-13T00:00:01	574.7	1520000	10933997
1939-11-13T00:30:01	574.7	1520000	10965664
1939-11-13T01:00:01	574.7	1520000	10997331
1939-11-13T01:30:01	574.7	1506000	11028706
1939-11-13T02:00:01	574.7	1524000	11060456
1939-11-13T02:30:01	574.7	1505000	11091810
1939-11-13T03:00:01	574.7	1505000	11123164
1939-11-13T03:30:02	574.7	1505000	11154519
1939-11-13T04:00:02	574.7	1505000	11185873
1939-11-13T04:30:02	574.7	1508000	11217290
1939-11-13T05:00:02	574.7	1508000	11248706

1939-11-13T05:30:02	574.7	1512000	11280207
1939-11-13T06:00:02	574.7	1496000	11311373
1939-11-13T06:30:02	574.7	1512000	11342873
1939-11-13T07:00:02	574.7	1506000	11374248
1939-11-13T07:30:02	574.7	1492000	11405332
1939-11-13T08:00:02	569.7	1508000	11436749
1939-11-13T08:30:02	569.7	1538000	11468790
1939-11-13T09:00:01	-99999	0	11468790
1939-11-13T09:00:02	569.7	1538000	11468800
1939-11-13T09:30:02	564.7	1532000	11500717
1939-11-13T10:00:02	-99999	0	11500717
1939-11-13T10:30:02	-99999	0	11500717
1939-11-13T11:00:02	-99999	0	11500717
1939-11-13T11:30:02	589.7	1584000	11533717
1939-11-13T12:00:02	564.7	1590000	11566842
1939-11-13T12:30:02	579.7	1620000	11600592
1939-11-13T13:00:02	579.7	1620000	11634342
1939-11-13T13:30:02	579.7	1620000	11668093
1939-11-13T14:00:02	579.7	1610000	11701634
1939-11-13T14:30:02	579.7	1612000	11735218
1939-11-13T15:00:02	579.7	1610000	11768760
1939-11-13T15:30:02	579.7	1624000	11802593
1939-11-13T16:00:02	579.7	1626000	11836468
1939-11-13T16:30:02	579.7	1618000	11870176
1939-11-13T17:00:02	579.7	1636000	11904260
1939-11-13T17:30:02	579.7	1630000	11938218
1939-11-13T18:00:02	579.7	1618000	11971927

1939-11-13T18:30:02	579.7	1618000	12005635
1939-11-13T19:00:02	579.7	1610000	12039177
1939-11-13T19:30:02	579.7	1628000	12073094
1939-11-13T20:00:02	579.7	1628000	12107010
1939-11-13T20:30:02	579.7	1610000	12140552
1939-11-13T21:00:02	579.7	1580000	12173469
1939-11-13T21:30:02	579.7	1585000	12206490
1939-11-13T22:00:02	579.7	1580000	12239407
1939-11-13T22:30:02	579.7	1585000	12272428
1939-11-13T23:00:02	579.7	1582000	12305386
1939-11-13T23:30:02	579.7	1582000	12338344
1939-11-14T00:00:02	579.7	1580000	12371261
1939-11-14T00:30:02	579.7	1596000	12404511
1939-11-14T01:00:02	579.7	1595000	12437741
1939-11-14T01:30:02	579.7	1588000	12470824
1939-11-14T02:00:02	579.7	1588000	12503907
1939-11-14T02:30:02	579.7	1590000	12537032
1939-11-14T03:00:02	579.7	1590000	12570158
1939-11-14T03:30:02	579.7	1580000	12603074
1939-11-14T04:00:02	579.7	1580000	12635991
1939-11-14T04:30:02	579.7	1580000	12668908
1939-11-14T05:00:02	579.7	1578000	12701783
1939-11-14T05:30:02	574.7	1580000	12734700
1939-11-14T06:00:02	569.7	1590000	12767825
1939-11-14T06:30:02	564.7	1576000	12800658
1939-11-14T07:00:02	559.7	1578000	12833533
1939-11-14T07:30:02	554.7	1566000	12866158

1939-11-14T08:00:02	554.7	1566000	12898783
1939-11-14T08:30:02	554.7	1574000	12931575
1939-11-14T09:00:01	-99999	0	12931575
1939-11-14T09:00:02	554.7	1574000	12931590
1939-11-14T09:30:02	549.7	1578000	12964465
1939-11-14T10:00:02	549.7	1580000	12997382
1939-11-14T10:30:02	549.7	1574000	13030173
1939-11-14T11:00:02	549.7	1570000	13062882
1939-11-14T11:30:02	549.7	1570000	13095590
1939-11-14T12:00:02	549.7	1570000	13128299
1939-11-14T12:30:02	549.7	1570000	13161007
1939-11-14T13:00:02	549.7	1565000	13193611
1939-11-14T13:30:02	549.7	1570000	13226320
1939-11-14T14:00:02	549.7	1570000	13259028
1939-11-14T14:30:02	549.7	1566000	13291653
1939-11-14T15:00:02	549.7	1566000	13324278
1939-11-14T15:30:02	549.7	1565000	13356883
1939-11-14T16:00:02	549.7	1565000	13389487
1939-11-14T16:30:02	544.7	1546000	13421695
1939-11-14T17:00:02	544.7	1546000	13453904
1939-11-14T17:30:02	544.7	1530000	13485779
1939-11-14T18:00:02	544.7	1530000	13517654
1939-11-14T18:30:02	544.7	1535000	13549633
1939-11-14T19:00:02	544.7	1535000	13581612
1939-11-14T19:30:02	544.7	1538000	13613654
1939-11-14T20:00:02	544.7	1538000	13645696
1939-11-14T20:30:02	544.7	1546000	13677904

1939-11-14T21:00:02	544.7	1546000	13710113
1939-11-14T21:30:02	544.7	1564000	13742696
1939-11-14T22:00:02	544.7	1558000	13775155
1939-11-14T22:30:02	544.7	1558000	13807613
1939-11-14T23:00:02	544.7	1558000	13840072
1939-11-14T23:30:02	544.7	1564000	13872655
1939-11-15T00:00:02	544.7	1564000	13905238
1939-11-15T00:30:02	544.7	1544000	13937405
1939-11-15T01:00:02	544.7	1545000	13969593
1939-11-15T01:30:02	539.7	1560000	14002093
1939-11-15T02:00:02	539.7	1540000	14034176
1939-11-15T02:30:02	539.7	1540000	14066260
1939-11-15T03:00:02	539.7	1544000	14098426
1939-11-15T03:30:02	539.7	1544000	14130593
1939-11-15T04:00:02	539.7	1544000	14162760
1939-11-15T04:30:02	539.7	1548000	14195010
1939-11-15T05:00:02	539.7	1550000	14227302
1939-11-15T05:30:02	539.7	1550000	14259594
1939-11-15T06:00:02	539.7	1546000	14291802
1939-11-15T06:30:02	539.7	1546000	14324010
1939-11-15T07:00:02	539.7	1546000	14356219
1939-11-15T07:30:02	539.7	1546000	14388427
1939-11-15T08:00:02	539.7	1550000	14420719
1939-11-15T08:30:02	534.7	1546000	14452927
1939-11-15T09:00:01	-99999	0	14452927
1939-11-15T09:00:02	534.7	1540000	14452946
1939-11-15T09:30:02	-99999	0	14452946

1939-11-15T09:45:02	-99999	0	14452946
1939-11-15T12:00:02	-99999	0	14452946
1939-11-15T12:45:02	-99999	0	14452946
1939-11-15T13:00:02	574.7	978000	14463134
1939-11-15T13:30:02	574.7	952000	14482968
1939-11-15T14:00:02	589.7	948000	14502718
1939-11-15T14:30:02	594.7	1115000	14525947
1939-11-15T15:00:02	594.7	970000	14546155
1939-11-15T15:30:02	594.7	876000	14564405
1939-11-15T16:00:02	599.7	828000	14581655
1939-11-15T16:30:02	594.7	1138000	14605364
1939-11-15T17:00:02	589.7	1036000	14626947
1939-11-15T17:30:02	594.7	1120000	14650281
1939-11-15T18:00:02	594.7	1076000	14672697
1939-11-15T18:30:02	594.7	1186000	14697406
1939-11-15T19:00:02	594.7	1162000	14721614
1939-11-15T19:30:02	594.7	1175000	14746093
1939-11-15T20:00:02	594.7	1175000	14770573
1939-11-15T20:30:02	594.7	1180000	14795156
1939-11-15T21:00:02	594.7	1213000	14820427
1939-11-15T21:30:02	594.7	1173000	14844865
1939-11-15T22:00:02	594.7	1167000	14869177
1939-11-15T22:30:02	594.7	1092000	14891927
1939-11-15T23:00:02	594.7	1098000	14914802
1939-11-15T23:30:02	594.7	1080000	14937302
1939-11-16T00:00:02	589.7	1082000	14959844
1939-11-16T00:30:02	589.7	1086000	14982469

1939-11-16T01:00:02	589.7	1085000	15005073
1939-11-16T01:30:02	589.7	1160000	15029240
1939-11-16T02:00:02	589.7	1168000	15053573
1939-11-16T02:30:02	589.7	1088000	15076240
1939-11-16T03:00:02	589.7	1108000	15099324
1939-11-16T03:30:02	589.7	1133000	15122928
1939-11-16T04:00:02	589.7	1183000	15147574
1939-11-16T04:30:02	589.7	1216000	15172907
1939-11-16T05:00:02	589.7	1130000	15196449
1939-11-16T05:30:02	589.7	1123000	15219845
1939-11-16T06:00:02	574.7	1130000	15243386
1939-11-16T06:30:02	554.7	1126000	15266845
1939-11-16T07:00:02	554.7	1102000	15289803
1939-11-16T07:30:02	554.7	1102000	15312762
1939-11-16T08:00:02	554.7	1042000	15334470
1939-11-16T08:30:02	554.7	1073000	15356824
1939-11-16T09:00:02	554.7	1087000	15379470
1939-11-16T10:00:02	-99999	0	15379470
1939-11-16T11:15:02	-99999	0	15379470
1939-11-16T11:30:02	599.7	948000	15389349
1939-11-16T12:00:02	599.7	984000	15409849
1939-11-16T12:30:02	599.7	982000	15430307
1939-11-16T13:00:02	599.7	974000	15450599
1939-11-16T13:30:02	599.7	1072000	15472932
1939-11-16T14:00:02	599.7	1105000	15495953
1939-11-16T14:30:02	594.7	1105000	15518974
1939-11-16T15:00:02	594.7	1085000	15541578

1939-11-16T15:30:02	594.7	1078000	15564037
1939-11-16T16:00:02	594.7	1005000	15584974
1939-11-16T16:30:02	594.7	1035000	15606537
1939-11-16T17:00:02	594.7	1045000	15628308
1939-11-16T17:30:02	594.7	1022000	15649599
1939-11-16T18:00:02	594.7	986000	15670141
1939-11-16T18:30:02	594.7	1036000	15691724
1939-11-16T19:00:02	594.7	1036000	15713308
1939-11-16T19:30:02	594.7	989000	15733912
1939-11-16T20:00:02	594.7	1036000	15755495
1939-11-16T20:30:02	594.7	1036000	15777079
1939-11-16T21:00:02	594.7	1050000	15798954
1939-11-16T21:30:02	594.7	1036000	15820537
1939-11-16T22:00:02	594.7	1006000	15841496
1939-11-16T22:30:02	594.7	1054000	15863454
1939-11-16T23:00:02	594.7	991000	15884100
1939-11-16T23:30:02	589.7	955000	15903996
1939-11-17T00:00:02	584.7	912000	15922996
1939-11-17T00:30:02	584.7	910000	15941954
1939-11-17T01:00:02	584.7	880000	15960288
1939-11-17T01:30:02	589.7	750000	15975913
1939-11-17T02:00:02	594.7	750000	15991538
1939-11-17T02:30:02	589.7	930000	16010913
1939-11-17T03:00:02	589.7	998000	16031704
1939-11-17T03:30:02	589.7	1018000	16052913
1939-11-17T04:00:02	589.7	970000	16073121
1939-11-17T04:30:02	579.7	1205000	16098226

1939-11-17T05:00:02	579.7	1048000	16120059
1939-11-17T05:30:02	579.7	1016000	16141226
1939-11-17T06:00:02	579.7	1000000	16162059
1939-11-17T06:30:02	579.7	1050000	16183934
1939-11-17T07:00:03	579.7	1055000	16205913
1939-11-17T07:30:03	584.7	1060000	16227997
1939-11-17T08:00:03	584.7	1060000	16250080
1939-11-17T08:30:03	584.7	1210000	16275289
1939-11-17T09:00:03	584.7	1190000	16300080
1939-11-17T09:30:03	584.7	1160000	16324247
1939-11-17T10:00:03	589.7	1045000	16346018
1939-11-17T10:30:03	589.7	1026000	16367393
1939-11-17T10:45:01	-99999	0	16367393
1939-11-17T11:00:01	614.7	0	16367393
1939-11-17T11:15:01	619.7	0	16367393
1939-11-17T11:30:01	619.7	0	16367393
1939-11-17T11:45:01	619.7	0	16367393
1939-11-17T12:00:01	619.7	0	16367393
1939-11-17T12:30:01	619.7	0	16367393
1939-11-17T13:30:01	619.7	0	16367393
1939-11-17T14:00:01	622.7	0	16367393
1939-11-17T15:00:01	622.7	0	16367393
1939-11-18T09:00:01	624.7	0	16367393
1939-11-18T09:30:01	624.7	0	16367393
1939-11-18T12:00:01	624.7	0	16367393
1939-11-18T12:15:00	624.7	0	16367393
1939-11-18T13:00:00	609.7	944000	16396893

1939-11-18T14:00:00	609.7	774000	16429143
1939-11-18T15:00:00	609.7	818000	16463226
1939-11-18T16:00:00	584.7	1190000	16512810
1939-11-18T17:00:00	594.7	956000	16552643
1939-11-18T18:00:00	594.7	852000	16588143
1939-11-18T19:00:00	594.7	826000	16622560
1939-11-18T20:00:00	594.7	795000	16655685
1939-11-18T21:00:00	599.7	724000	16685852
1939-11-18T22:00:00	604.7	830000	16720435
1939-11-18T23:00:00	604.7	772000	16752602
1939-11-19T00:00:00	604.7	830000	16787185
1939-11-19T01:00:00	604.7	700000	16816352
1939-11-19T02:00:00	604.7	768000	16848352
1939-11-19T03:00:00	604.7	890000	16885435
1939-11-19T04:00:00	604.7	814000	16919352
1939-11-19T05:00:00	604.7	740000	16950185
1939-11-19T06:00:00	604.7	662000	16977769
1939-11-19T07:00:00	604.7	758000	17009352
1939-11-19T08:00:00	604.7	734000	17039935
1939-11-19T09:00:00	604.7	780000	17072435
1939-11-19T10:00:00	604.7	724000	17102602
1939-11-19T11:00:00	584.7	1160000	17150936
1939-11-19T12:00:00	584.7	1187000	17200394
1939-11-19T13:00:00	584.7	1223000	17251352
1939-11-19T14:00:00	584.7	1173000	17300227
1939-11-19T15:00:00	584.7	1122000	17346978
1939-11-19T16:00:00	584.7	942000	17386228

1939-11-19T17:00:00	594.7	870000	17422478
1939-11-19T18:00:00	594.7	876000	17458978
1939-11-19T19:00:00	594.7	814000	17492894
1939-11-19T20:00:00	594.7	740000	17523728
1939-11-19T21:00:00	594.7	788000	17556561
1939-11-19T22:00:00	594.7	752000	17587895
1939-11-19T23:00:00	594.7	744000	17618895
1939-11-20T00:00:00	599.7	708000	17648395
1939-11-20T01:00:00	599.7	716000	17678228
1939-11-20T02:00:00	599.7	780000	17710728
1939-11-20T03:00:00	599.7	868000	17746895
1939-11-20T04:00:00	599.7	903000	17784520
1939-11-20T05:00:00	594.7	830000	17819103
1939-11-20T06:00:00	594.7	814000	17853020
1939-11-20T07:00:00	594.7	774000	17885270
1939-11-20T08:00:00	599.7	788000	17918103
1939-11-20T09:00:00	599.7	768000	17950103
1939-11-20T10:00:00	589.7	1023000	17992728
1939-11-20T11:00:00	584.7	1200000	18042729
1939-11-20T12:00:00	584.7	1254000	18094979
1939-11-20T13:00:00	579.7	1250000	18147062
1939-11-20T14:00:00	579.7	1298000	18201145
1939-11-20T15:00:00	579.7	1145000	18248854
1939-11-20T16:00:00	579.7	1156000	18297021
1939-11-20T17:00:00	584.7	1032000	18340021
1939-11-20T18:00:00	584.7	990000	18381271
1939-11-20T19:00:00	584.7	983000	18422229

1939-11-20T20:00:00	589.7	960000	18462229
1939-11-20T21:00:00	589.7	972000	18502729
1939-11-20T22:00:00	589.7	1012000	18544896
1939-11-20T23:00:00	589.7	1007000	18586854
1939-11-21T00:00:00	589.7	1030000	18629771
1939-11-21T01:00:00	589.7	1050000	18673521
1939-11-21T02:00:00	589.7	1090000	18718938
1939-11-21T03:00:00	589.7	1095000	18764563
1939-11-21T04:00:00	584.7	1095000	18810188
1939-11-21T05:00:00	584.7	1080000	18855188
1939-11-21T06:00:00	584.7	1056000	18899188
1939-11-21T07:00:00	584.7	1072000	18943855
1939-11-21T08:00:00	584.7	1025000	18986563
1939-11-21T09:00:00	584.7	1056000	19030563
1939-11-21T10:00:00	584.7	1000000	19072230
1939-11-21T11:00:00	584.7	1002000	19113980
1939-11-21T12:00:00	584.7	1000000	19155647
1939-11-21T13:00:00	584.7	1070000	19200230
1939-11-21T14:00:00	584.7	1063000	19244522
1939-11-21T15:00:00	584.7	1094000	19290105
1939-11-21T16:00:00	584.7	1064000	19334439
1939-11-21T17:00:00	584.7	1047000	19378064
1939-11-21T18:00:00	584.7	1052000	19421897
1939-11-21T19:00:00	584.7	1058000	19465980
1939-11-21T20:00:00	584.7	1070000	19510564
1939-11-21T21:00:00	584.7	1070000	19555147
1939-11-21T22:00:00	584.7	979000	19595939

1939-11-21T23:00:00	584.7	948000	19635439
1939-11-22T00:00:00	584.7	1022000	19678022
1939-11-22T01:00:00	584.7	1066000	19722439
1939-11-22T02:00:00	584.7	1070000	19767023
1939-11-22T03:00:00	584.7	1066000	19811439
1939-11-22T04:00:00	584.7	1065000	19855814
1939-11-22T05:00:00	584.7	1065000	19900189
1939-11-22T06:00:00	584.7	1060000	19944356
1939-11-22T07:00:00	584.7	1065000	19988731
1939-11-22T08:00:00	584.7	1098000	20034481
1939-11-22T09:00:00	579.7	1066000	20078898
1939-11-22T10:00:00	584.7	1092000	20124398
1939-11-22T11:00:00	584.7	1105000	20170440
1939-11-22T12:00:00	584.7	1082000	20215523
1939-11-22T13:00:00	579.7	1080000	20260523
1939-11-22T14:00:00	579.7	1086000	20305773
1939-11-22T15:00:00	579.7	1092000	20351273
1939-11-22T16:00:00	579.7	1080000	20396273
1939-11-22T17:00:00	579.7	1073000	20440982
1939-11-22T18:00:00	579.7	1073000	20485690
1939-11-22T19:00:01	579.7	1077000	20530565
1939-11-22T20:00:01	579.7	1078000	20575482
1939-11-22T21:00:01	579.7	1058000	20619565
1939-11-22T22:00:01	579.7	1135000	20666857
1939-11-22T23:00:01	579.7	1105000	20712899
1939-11-23T00:00:01	579.7	1082000	20757982
1939-11-23T01:00:01	579.7	1085000	20803191

1939-11-23T02:00:01	579.7	1080000	20848191
1939-11-23T03:00:01	579.7	1083000	20893316
1939-11-23T04:00:01	579.7	1080000	20938316
1939-11-23T05:00:01	579.7	1080000	20983316
1939-11-23T06:00:01	579.7	1092000	21028816
1939-11-23T07:00:01	579.7	1092000	21074316
1939-11-23T08:00:01	579.7	1071000	21118941
1939-11-23T09:00:01	584.7	978000	21159691
1939-11-23T10:00:01	584.7	1045000	21203233
1939-11-23T11:00:01	584.7	912000	21241233
1939-11-23T12:00:01	584.7	873000	21277608
1939-11-23T13:00:01	584.7	842000	21312691
1939-11-23T14:00:01	584.7	868000	21348858
1939-11-23T15:00:01	584.7	1015000	21391150
1939-11-23T16:00:01	584.7	1006000	21433067
1939-11-23T17:00:01	584.7	992000	21474400
1939-11-23T18:00:01	584.7	998000	21515983
1939-11-23T19:00:01	584.7	995000	21557442
1939-11-23T20:00:01	584.7	866000	21593525
1939-11-23T21:00:01	589.7	868000	21629692
1939-11-23T22:00:01	589.7	878000	21666275
1939-11-23T23:00:01	589.7	852000	21701775
1939-11-24T00:00:01	589.7	903000	21739400
1939-11-24T01:00:01	589.7	908000	21777234
1939-11-24T02:00:01	589.7	982000	21818150
1939-11-24T03:00:01	589.7	1015000	21860442
1939-11-24T04:00:01	589.7	1036000	21903609

1939-11-24T05:00:01	589.7	1056000	21947609
1939-11-24T06:00:01	589.7	1036000	21990776
1939-11-24T07:00:01	584.7	1015000	22033067
1939-11-24T08:00:01	584.7	1003000	22074859
1939-11-24T09:00:01	584.7	1017000	22117234
1939-11-24T10:00:01	584.7	923000	22155693
1939-11-24T11:00:01	584.7	916000	22193859
1939-11-24T12:00:01	584.7	993000	22235234
1939-11-24T13:00:01	584.7	1022000	22277818
1939-11-24T14:00:01	584.7	1043000	22321276
1939-11-24T15:00:01	584.7	1095000	22366901
1939-11-24T16:00:01	584.7	1098000	22412651
1939-11-24T17:00:01	579.7	1045000	22456193
1939-11-24T18:00:01	579.7	1085000	22501401
1939-11-24T19:00:01	579.7	1070000	22545985
1939-11-24T20:00:01	579.7	1092000	22591485
1939-11-24T21:00:01	579.7	1098000	22637235
1939-11-24T22:00:01	579.7	1072000	22681902
1939-11-24T23:00:01	579.7	1072000	22726568
1939-11-25T00:00:01	579.7	1094000	22772152
1939-11-25T01:00:00	579.7	1082000	22817225
1939-11-25T02:00:00	579.7	1030000	22860142
1939-11-25T03:00:00	579.7	1075000	22904934
1939-11-25T04:00:00	579.7	1116000	22951434
1939-11-25T05:00:00	584.7	1046000	22995017
1939-11-25T06:00:00	584.7	1080000	23040017
1939-11-25T07:00:00	584.7	1076000	23084851

1939-11-25T08:00:00	584.7	1068000	23129351
1939-11-25T09:00:00	579.7	1035000	23172476
1939-11-25T10:00:00	579.7	1054000	23216393
1939-11-25T11:00:00	579.7	1038000	23259643
1939-11-25T12:00:00	579.7	1044000	23303143
1939-11-25T13:00:00	579.7	1062000	23347393
1939-11-25T14:00:00	579.7	1054000	23391310
1939-11-25T15:00:00	579.7	1056000	23435310
1939-11-25T16:00:00	579.7	1100000	23481143
1939-11-25T17:00:00	579.7	1095000	23526768
1939-11-25T18:00:00	579.7	1125000	23573643
1939-11-25T19:00:00	579.7	1105000	23619685
1939-11-25T20:00:00	579.7	1110000	23665935
1939-11-25T21:00:00	579.7	1122000	23712685
1939-11-25T22:00:00	579.7	1155000	23760810
1939-11-25T23:00:00	579.7	1150000	23808727
1939-11-26T00:00:00	579.7	1164000	23857227
1939-11-26T01:00:00	579.7	1165000	23905769
1939-11-26T02:00:00	579.7	1165000	23954310
1939-11-26T03:00:00	574.7	1140000	24001810
1939-11-26T04:00:00	574.7	1113000	24048185
1939-11-26T05:00:00	574.7	1094000	24093769
1939-11-26T06:00:00	574.7	1067000	24138227
1939-11-26T07:00:00	574.7	1044000	24181727
1939-11-26T08:00:00	579.7	1015000	24224019
1939-11-26T09:00:00	574.7	1062000	24268269
1939-11-26T10:00:00	574.7	1048000	24311936

1939-11-26T11:00:00	574.7	1070000	24356519
1939-11-26T12:00:00	574.7	1088000	24401853
1939-11-26T13:00:00	574.7	1104000	24447853
1939-11-26T14:00:00	574.7	1105000	24493894
1939-11-26T15:00:00	574.7	1052000	24537728
1939-11-26T16:00:00	574.7	1078000	24582644
1939-11-26T17:00:00	579.7	988000	24623811
1939-11-26T18:00:00	579.7	982000	24664728
1939-11-26T19:00:00	579.7	990000	24705978
1939-11-26T20:00:00	579.7	1014000	24748228
1939-11-26T21:00:00	579.7	1048000	24791895
1939-11-26T22:00:00	579.7	972000	24832395
1939-11-26T23:00:00	579.7	1012000	24874562
1939-11-27T00:00:00	579.7	945000	24913937
1939-11-27T01:00:00	579.7	916000	24952103
1939-11-27T02:00:00	579.7	842000	24987187
1939-11-27T03:00:00	579.7	888000	25024187
1939-11-27T04:00:00	584.7	870000	25060437
1939-11-27T05:00:00	584.7	928000	25099104
1939-11-27T06:00:00	584.7	984000	25140104
1939-11-27T07:00:00	584.7	1018000	25182520
1939-11-27T08:00:00	584.7	1050000	25226270
1939-11-27T09:00:00	579.7	1045000	25269812
1939-11-27T10:00:00	574.7	962000	25309895
1939-11-27T11:00:00	579.7	934000	25348812
1939-11-27T12:00:00	579.7	924000	25387312
1939-11-27T13:00:00	579.7	887000	25424271

1939-11-27T14:00:00	584.7	830000	25458854
1939-11-27T15:00:00	584.7	832000	25493521
1939-11-27T16:00:00	584.7	958000	25533437
1939-11-27T17:00:00	584.7	1005000	25575313
1939-11-27T18:00:00	584.7	986000	25616396
1939-11-27T19:00:00	584.7	986000	25657479
1939-11-27T20:00:00	584.7	1010000	25699563
1939-11-27T21:00:00	584.7	1035000	25742688
1939-11-27T22:00:00	584.7	1042000	25786104
1939-11-27T23:00:00	584.7	1044000	25829605
1939-11-28T00:00:00	584.7	1054000	25873521
1939-11-28T01:00:00	584.7	1053000	25917396
1939-11-28T02:00:00	584.7	980000	25958230
1939-11-28T03:00:00	584.7	912000	25996230
1939-11-28T04:00:00	584.7	828000	26030730
1939-11-28T05:00:00	584.7	826000	26065147
1939-11-28T06:00:00	584.7	788000	26097980
1939-11-28T07:00:00	584.7	796000	26131147
1939-11-28T08:00:00	584.7	934000	26170063
1939-11-28T09:00:00	584.7	906000	26207813
1939-11-28T10:00:00	579.7	1080000	26252813
1939-11-28T11:00:00	579.7	1326000	26308064
1939-11-28T12:00:00	579.7	1266000	26360814
1939-11-28T13:00:00	579.7	1170000	26409564
1939-11-28T14:00:00	579.7	1148000	26457397
1939-11-28T15:00:00	579.7	1077000	26502272
1939-11-28T16:00:00	579.7	1043000	26545731

1939-11-28T17:00:00	579.7	1004000	26587564
1939-11-28T18:00:00	579.7	949000	26627106
1939-11-28T19:00:00	579.7	930000	26665856
1939-11-28T20:00:00	579.7	1002000	26707606
1939-11-28T21:00:00	579.7	1010000	26749689
1939-11-28T22:00:00	584.7	862000	26785606
1939-11-28T23:00:00	584.7	790000	26818523
1939-11-29T00:00:00	584.7	790000	26851439
1939-11-29T01:00:00	584.7	782000	26884023
1939-11-29T02:00:00	584.7	754000	26915439
1939-11-29T03:00:00	584.7	802000	26948856
1939-11-29T04:00:00	584.7	742000	26979773
1939-11-29T05:00:00	584.7	732000	27010273
1939-11-29T06:00:00	584.7	742000	27041190
1939-11-29T07:00:01	584.7	810000	27074940
1939-11-29T08:00:01	584.7	746000	27106023
1939-11-29T09:00:01	584.7	755000	27137481
1939-11-29T09:30:01	584.7	918000	27156612
1939-11-29T11:00:01	-99999	0	27156612
1939-11-29T12:00:01	-99999	0	27156612
1939-11-29T13:00:01	584.7	970000	27197028
1939-11-29T14:00:01	584.7	852000	27232528
1939-11-29T15:00:01	584.7	1180000	27281695
1939-11-29T16:00:01	584.7	1202000	27331778
1939-11-29T17:00:01	584.7	1205000	27381987
1939-11-29T18:00:01	584.7	1194000	27431737
1939-11-29T19:00:01	584.7	1193000	27481445

1939-11-29T20:00:01	584.7	1195000	27531237
1939-11-29T21:00:01	584.7	1228000	27582404
1939-11-29T22:00:01	584.7	1214000	27632987
1939-11-29T23:00:01	584.7	1226000	27684071
1939-11-30T00:00:01	584.7	1230000	27735321
1939-11-30T01:00:01	579.7	1222000	27786237
1939-11-30T02:00:01	579.7	1214000	27836821
1939-11-30T03:00:01	579.7	1216000	27887488
1939-11-30T04:00:01	579.7	1202000	27937571
1939-11-30T05:00:01	579.7	1212000	27988071
1939-11-30T06:00:01	579.7	1210000	28038488
1939-11-30T07:00:01	579.7	1212000	28088988
1939-11-30T08:00:01	579.7	1241000	28140696
1939-11-30T09:00:01	579.7	1240000	28192363
1939-11-30T10:00:01	579.7	1245000	28244238
1939-11-30T11:00:01	579.7	1185000	28293613
1939-11-30T12:00:01	579.7	1190000	28343197
1939-11-30T13:00:01	579.7	1172000	28392030
1939-11-30T14:00:01	579.7	1185000	28441405
1939-11-30T15:00:01	579.7	1120000	28488072
1939-11-30T16:00:01	579.7	1116000	28534572
1939-11-30T17:00:01	564.7	1115000	28581030
1939-11-30T18:00:01	569.7	1115000	28627489
1939-11-30T19:00:01	569.7	1154000	28675572
1939-11-30T20:00:01	569.7	1143000	28723197
1939-11-30T21:00:01	569.7	1134000	28770447
1939-11-30T22:00:01	569.7	1107000	28816572

1939-11-30T23:00:01	569.7	1096000	28862239
1939-12-01T00:00:01	569.7	1104000	28908239
1939-12-01T01:00:01	569.7	1103000	28954197
1939-12-01T02:00:01	569.7	1071000	28998822
1939-12-01T03:00:01	569.7	1043000	29042281
1939-12-01T04:00:01	569.7	1046000	29085864
1939-12-01T05:00:01	569.7	1068000	29130364
1939-12-01T06:00:01	569.7	1098000	29176114
1939-12-01T07:00:01	569.7	1077000	29220989
1939-12-01T08:00:01	569.7	1073000	29265698
1939-12-01T09:00:01	569.7	1078000	29310615
1939-12-01T10:00:01	569.7	1085000	29355823
1939-12-01T11:00:01	569.7	1085000	29401031
1939-12-01T12:00:01	569.7	1075000	29445823
1939-12-01T13:00:01	569.7	1050000	29489573
1939-12-01T14:00:01	569.7	1079000	29534531
1939-12-01T15:00:01	569.7	1068000	29579032
1939-12-01T16:00:01	569.7	1088000	29624365
1939-12-01T17:00:01	569.7	1040000	29667698
1939-12-01T18:00:01	569.7	1060000	29711865
1939-12-01T19:00:01	569.7	1055000	29755823
1939-12-01T20:00:01	569.7	1040000	29799157
1939-12-01T21:00:01	569.7	1050000	29842907
1939-12-01T22:00:01	569.7	1055000	29886865
1939-12-01T23:00:01	569.7	1085000	29932074
1939-12-02T00:00:01	569.7	1055000	29976032
1939-12-02T01:00:01	569.7	1057000	30020074

1939-12-02T02:00:01	569.7	1062000	30064324
1939-12-02T03:00:01	569.7	1060000	30108491
1939-12-02T04:00:01	569.7	1064000	30152824
1939-12-02T05:00:01	569.7	1060000	30196991
1939-12-02T06:00:01	569.7	1042000	30240407
1939-12-02T07:00:01	569.7	966000	30280658
1939-12-02T08:00:01	569.7	950000	30320241
1939-12-02T09:00:01	574.7	924000	30358741
1939-12-02T09:30:01	574.7	0	30358741
1939-12-11T00:00:00	604.6	0	30358741
1940-07-23T00:00:00	628.9	0	30358741
1943-06-22T00:00:00	629.7	0	30358741
1945-05-03T00:00:00	633	0	30358741
1947-06-04T00:00:00	636.1	0	30358741
1947-06-04T12:00:00	636.1	0	30358741
1956-11-10T15:00:00	636.1	0	30358741
1956-11-10T16:00:00	184.7	1920000	30518741
1956-11-10T18:00:00	-99999	2640000	30938741
1956-11-10T21:50:00	369.7	0	30938741
1956-11-10T22:00:00	624.7	0	30938741
1956-11-10T22:10:00	636.7	0	30938741
1956-11-11T12:43:00	636	118455	30950241
1956-11-11T15:03:00	636	120000	30951641
1956-11-11T15:15:00	632	205714	30966641
1956-11-11T17:05:00	-99999	0	30966641
1956-11-12T09:20:00	636.7	0	30966641
1956-11-12T09:32:00	617	701726	31024241

1956-11-12T11:30:00	585	1226667	31139241
1956-11-12T13:45:00	510	2016000	31286241
1956-11-12T15:30:00	452	2755200	31429741
1956-11-12T16:45:00	402	3244800	31598741
1956-11-12T18:00:00	377	3552000	31672741
1956-11-12T18:31:00	-99999	0	31672741
1956-11-12T18:57:00	626.7	0	31672741
1956-11-13T09:30:00	634.7	0	31672741
1958-01-01T00:00:00	634.7	-99999	33852741
1958-02-01T00:00:00	626.2	-99999	35951741
1958-03-01T00:00:00	623.2	-99999	38309741
1958-04-01T00:00:00	621.2	-99999	40570741
1958-05-01T00:00:00	620.2	-99999	42520741
1958-06-01T00:00:00	619.2	-99999	44252741
1958-07-01T00:00:00	618.7	-99999	45934741
1958-08-01T00:00:00	617.7	-99999	47660741
1958-09-01T00:00:00	615.7	-99999	49631741
1958-10-01T00:00:00	614.2	-99999	51912741
1958-11-01T00:00:00	611.7	-99999	54184741
1958-12-01T00:00:00	609.7	-99999	56620741
1959-01-01T00:00:00	607.7	-99999	59084741
1959-02-01T00:00:00	606.2	-99999	61410741
1959-03-01T00:00:00	604.7	-99999	64026741
1959-04-01T00:00:00	606.7	-99999	64312741
1959-05-01T00:00:00	606.2	-99999	65155741
1959-06-01T00:00:00	603.2	-99999	67315741
1959-07-01T00:00:00	601.7	-99999	69404741

1959-08-01T00:00:00	599.7	-99999	71636741
1959-09-01T00:00:00	598.2	-99999	73702741
1959-10-01T00:00:00	596.2	-99999	75945741
1959-11-01T00:00:00	594.7	-99999	78281741
1959-12-01T00:00:00	593.2	-99999	80645741
1960-01-01T00:00:00	592.2	-99999	82118741
1960-02-01T00:00:00	592.2	-99999	83443741
1960-03-01T00:00:00	589.2	-99999	85908741
1960-04-01T00:00:00	587.7	-99999	88364741
1960-05-01T00:00:00	585.7	-99999	90726741
1960-06-01T00:00:00	583.7	-99999	92612741
1960-07-01T00:00:00	582.7	-99999	94456741
1960-08-01T00:00:00	581.2	-99999	96441741
1960-09-01T00:00:00	579.7	-99999	99047741
1960-10-01T00:00:00	578.2	-99999	1.02E+08
1960-11-01T00:00:00	572.2	-99999	1.05E+08
1960-12-01T00:00:00	564.7	-99999	1.09E+08
1961-01-01T00:00:00	560.2	-99999	1.14E+08
1961-02-01T00:00:00	558.7	-99999	1.18E+08
1961-03-01T00:00:00	554.7	-99999	1.22E+08
1961-04-01T00:00:00	551.7	-99999	1.26E+08
1961-05-01T00:00:00	548.7	-99999	1.3E+08
1961-06-01T00:00:00	546.7	-99999	1.34E+08
1961-07-01T00:00:00	543.7	-99999	1.38E+08
1961-08-01T00:00:00	540.7	-99999	1.42E+08
1961-09-01T00:00:00	536.7	-99999	1.46E+08
1961-10-01T00:00:00	534.7	-99999	1.51E+08

1961-11-01T00:00:00	529.2	-99999	1.55E+08
1961-12-01T00:00:00	526.7	-99999	1.59E+08
1962-01-01T00:00:00	14.7	-99999	1.62E+08
1962-02-01T00:00:00	14.7	-99999	1.64E+08
1962-03-01T00:00:00	566.2	-99999	1.67E+08
1962-04-01T00:00:00	522.7	-99999	1.7E+08
1962-05-01T00:00:00	519.7	-99999	1.73E+08
1962-06-01T00:00:00	518.7	-99999	1.76E+08
1962-07-01T00:00:00	517.7	-99999	1.79E+08
1962-08-01T00:00:00	516.2	-99999	1.82E+08
1962-09-01T00:00:00	14.7	-99999	1.85E+08
1962-10-01T00:00:00	512.2	-99999	1.88E+08
1962-11-01T00:00:00	509.7	-99999	1.91E+08
1962-12-01T00:00:00	507.7	-99999	1.94E+08
1963-01-01T00:00:00	505.2	-99999	1.97E+08
1963-02-01T00:00:00	502.7	-99999	2E+08
1963-03-01T00:00:00	500.7	-99999	2.03E+08
1963-04-01T00:00:00	498.2	-99999	2.07E+08
1963-05-01T00:00:00	494.2	-99999	2.1E+08
1963-06-01T00:00:00	490.7	-99999	2.13E+08
1963-07-01T00:00:00	488.2	-99999	2.17E+08
1963-08-01T00:00:00	487.7	-99999	2.19E+08
1963-09-01T00:00:00	483.7	-99999	2.22E+08
1963-10-01T00:00:00	480.7	-99999	2.25E+08
1963-11-01T00:00:00	476.2	-99999	2.28E+08
1963-12-01T00:00:00	474.2	-99999	2.32E+08
1964-01-01T00:00:00	472.2	-99999	2.35E+08

1964-02-01T00:00:00	472.7	-99999	2.37E+08
1964-03-01T00:00:00	475.2	-99999	2.38E+08
1964-04-01T00:00:00	475.2	-99999	2.39E+08
1964-05-01T00:00:00	475.2	-99999	2.41E+08
1964-06-01T00:00:00	475.2	-99999	2.42E+08
1964-07-01T00:00:00	475.2	-99999	2.43E+08
1964-08-01T00:00:00	474.7	-99999	2.44E+08
1964-09-01T00:00:00	474.2	-99999	2.46E+08
1964-10-01T00:00:00	473.7	-99999	2.47E+08
1964-11-01T00:00:00	473.7	-99999	2.48E+08
1964-12-01T00:00:00	473.7	-99999	2.49E+08
1965-04-22T10:00:00	455.5	0	2.49E+08
1965-04-23T08:00:00	455.5	0	2.49E+08
1965-04-23T09:00:00	455.5	0	2.49E+08
1965-04-23T12:00:00	455.5	0	2.49E+08
1965-04-23T18:00:00	455.5	0	2.49E+08
1965-04-23T22:00:00	455.5	0	2.49E+08
1965-04-24T10:00:00	455.5	0	2.49E+08
1965-04-25T11:00:00	456	0	2.49E+08
1965-04-25T16:00:00	456.5	0	2.49E+08
1965-04-25T21:00:00	456.5	0	2.49E+08
1965-04-26T10:00:00	456.5	0	2.49E+08
1965-04-26T16:00:00	456.5	0	2.49E+08
1965-04-26T21:00:00	456.5	0	2.49E+08
1965-04-27T08:30:00	456.5	0	2.49E+08
1965-04-28T08:30:00	456.5	0	2.49E+08
1965-04-29T08:30:00	456.5	0	2.49E+08

1965-04-30T08:30:00	456.5	0	2.49E+08
1965-05-03T08:30:00	456.5	0	2.49E+08
1965-05-05T08:30:00	456.5	0	2.49E+08
1965-05-10T08:30:00	456.5	0	2.49E+08
1965-05-12T08:30:00	457	0	2.49E+08
1965-05-19T08:30:00	457.5	0	2.49E+08
1965-05-25T08:30:00	458	0	2.49E+08
1965-06-09T08:30:00	458.5	0	2.49E+08
1965-06-23T11:00:00	459.5	0	2.49E+08
1965-07-15T11:45:00	459.5	0	2.49E+08
1965-08-13T14:30:00	461	0	2.49E+08
1965-09-24T11:30:00	462	0	2.49E+08
1965-11-09T11:15:00	465	0	2.49E+08
1965-12-07T11:30:00	463	0	2.49E+08
1965-12-30T15:15:00	463	0	2.49E+08
1966-02-04T14:30:00	464	0	2.49E+08
1966-02-24T11:30:00	464	0	2.49E+08
1966-04-01T14:15:00	465	0	2.49E+08
1966-04-22T08:45:00	465	0	2.49E+08
1966-05-25T12:15:00	465.5	0	2.49E+08
1966-06-30T12:00:00	465.5	0	2.49E+08
1966-07-20T16:25:00	466	0	2.49E+08
1966-08-22T12:25:00	466	0	2.49E+08
1966-10-10T11:30:00	467	0	2.49E+08
1967-03-06T11:30:00	468.5	0	2.49E+08
1967-04-05T15:45:00	468.5	0	2.49E+08
1967-05-08T11:45:00	469	0	2.49E+08

1967-06-06T11:30:00	469	0	2.49E+08
1967-07-25T12:00:00	469.5	0	2.49E+08

8.4 Appendix 4 – Well log digitization

Well logs can be digitized using free online software that is designed to extract data from images of graphs. The tool used in this thesis was WebPlotDigitizer 4.5 (Rohatgi 2020) available at https://apps.automeris.io/wpd/ .

For the poorest quality graphs such as those for Cousland 1 (Figure 79 A), a bitmap tracer was run in inkscape first to remove background noise (Figure 79 B), then the colour was inverted to provide contrast (Figure 79 C), before the axes and log itself was traced in WebPlotDigitizer 4.5 (Figure 79 D). The resulting points were checked for outliers (Figure 79 E) which were subsequently removed (Figure 79 F). WebPlotDigitizer 4.5 then allows the download of the data as a csv file.

For better quality logs which were extracted from a pdf as an svg file (Figure 80 A), layers could simply be removed to isolate the log (Figure 80 B), before steps D to F in Figure 79 were performed.

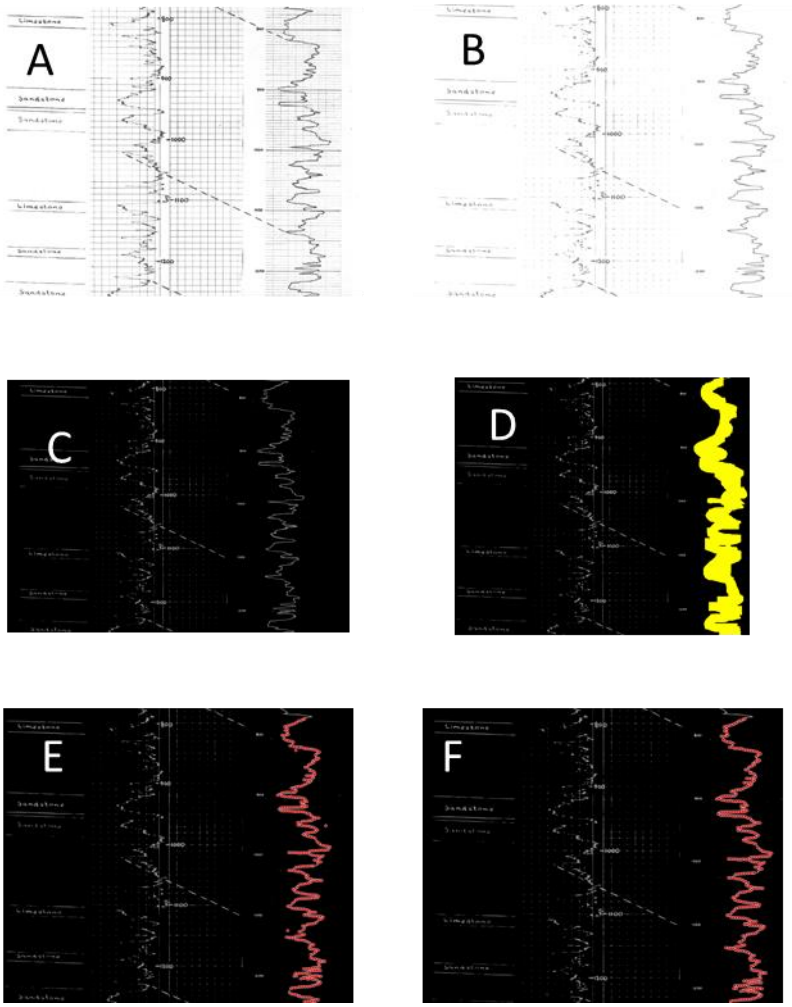

Figure 79: digitization steps for poor quality images of well logs

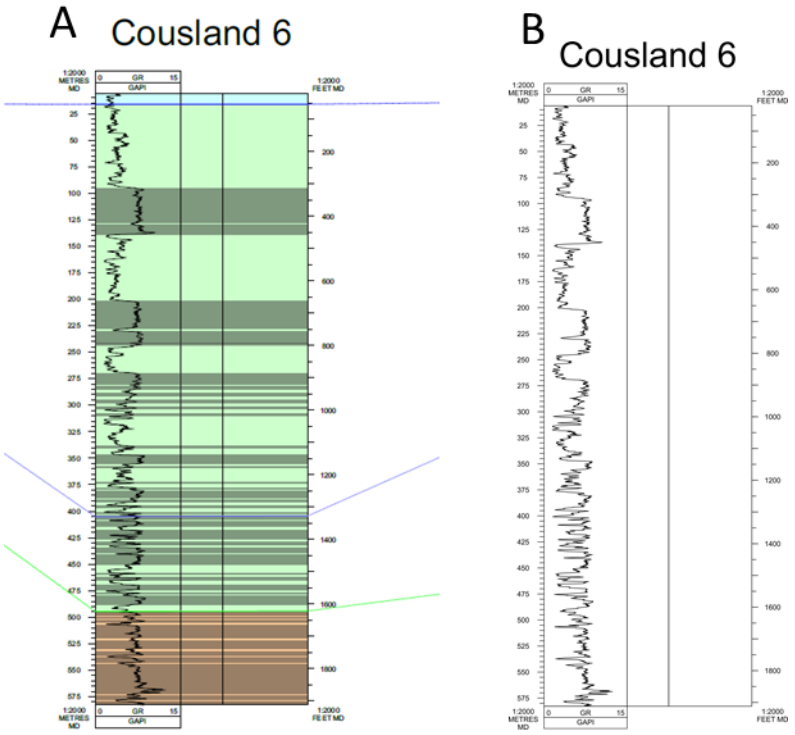

Figure 80: digitization steps for good quality svg images of well logs

8.5 Appendix 5 – Inflow/outflow program

8.5.1 Code and user guide

It is recommended to install Pycharm and use it to run the below programs. Also make sure to pip install the following python libraries: pandas, matplotlib, CoolProp, numpy, shapely.geometry, scipy.stats, playsound, and functools.

This code is not the most efficient, elegant, or well written – it could easily be self contained rather than in three chunks and the n_wells file could be incorporated into the data file – but it works (see https://c.tenor.com/fJAoBHWymY4AAAAC/do-not-touch-it-programmer.gif). However, please feel free to make it your own.

The workflow is as follows:

1. Format your data as TABLE X, save it as a csv named "gas_fields_props.csv"
2. Make well files for the number of wells to be studied in that particular run and save it as a csv – in the example code below the file is named "n_wells_single.csv"
3. Make folders in the working directory called "INPUT" and "OUTPUT"
4. Adjust all highlighted directory strings in the code to your own ones
5. Run the input file generator and save the output into the INPUT folder
6. Run the main program
7. Run the Results appender and extra calculations program

Given two simple files, the input file generator program will generate all the necessary input files and then the main program can be run to do the analysis.

Format your data like this and save it as a .csv file called gas_fields_props:

field_name	Pr_psia	k_mD	poro_frac	h_ft	L_ft	GIIP_MMSCF	Tres_R	plateau
Cousland	660	70	0.15	48	1582	870	527.67	90

Input file generator

```
import pandas as pd
import numpy as np
import os
from functools import reduce
```

```
# this code generates the input files needed for the inflow/outflow model
# change folder to working folder for your project
folder = r"C:\Users\s1669173\PycharmProjects\pythonProject1 - Copy"

# take original input data and add gas column
df = pd.read_csv('gas_fields_props.csv')
gas = pd.DataFrame(['H2', 'CH4'], columns = ['gas']) # change gases you want to
investigate here
dataframes = [df, gas]
df = reduce(lambda left, right: pd.merge(left, right, how='cross'), dataframes)
#print(df)
print(df.columns)

# take each row and make it a new df with a range of pressures
z = 1
for index, row in df.iterrows():
  x = str(z) + '_timesteps.csv'
  b = df.iloc[[index]]
  p = b['Pr_psia'].iloc[0]
  pressures = np.arange(100, p + 1, 100)
  pressures = pressures.tolist()
  b.drop(columns = ['Pr_psia'], inplace=True)
  print(pressures)
  c = pd.DataFrame(pressures,columns = ['Pr_psia'])
  dataframes = [b, c]
  a = reduce(lambda left, right: pd.merge(left, right, how='cross'), dataframes)
  a = a.sort_values(by = 'Pr_psia', ascending=False)
  a.to_csv(x)
  z = z + 1

# make a list of all the timesteps files to refer to
li = []
for root, dirs, files in os.walk(folder, topdown=False):
  for name in files:
```

```
    if "_timesteps" in name:
      print(os.path.join(root, name))
      x = os.path.join(root, name)
      li.append(x)

len(li)
li2 = []

wellbore_diams_inches = np.arange(2, 10 + 1, 2)
wellbore_diams_inches = wellbore_diams_inches.tolist()
for i in li:
  # reads file to get input data
  gas_fields_props = pd.read_csv(i)
  well_diam_variation = pd.DataFrame(wellbore_diams_inches, columns =
['D_wb_inches']) # diameter of the wellbore in inches pd.DataFrame(['H2', 'CH4'],
columns = ['gas'])
  dataframes = [gas_fields_props, well_diam_variation] # list the two dataframes
  df = reduce(lambda left, right: pd.merge(left, right, how='cross'), dataframes) #
combine them
  print(df)
  #exit()
  for i in wellbore_diams_inches:
    df2 = df[df['D_wb_inches'] == i].reset_index()
    df2['rw_ft'] = df2['D_wb_inches'] / 12 / 2
    y = str(df2['field_name'].iloc[0]) + '_' + df2['gas'].iloc[0] + '_timesteps_' + str(
      df2['D_wb_inches'].iloc[0]) + '_inches.csv'
    df2.to_csv(y)
```

Main program

```
import CoolProp.CoolProp
import pandas as pd
from CoolProp.CoolProp import PropsSI
import numpy as np
import matplotlib.pyplot as plt
from shapely.geometry import LineString
from scipy.stats import linregress
import math
import os
import playsound
import sys


sys.stdout = open('console_output.txt', 'w')

# INPUT DATA
##########################################################################
########################################
# well parameters
re = 4920 # effective radius [ft] - equiv to 1500 metres
# rw = 0.25 # wellbore radius [ft] 6" tubing
S = 1 # skin factor - assumed as 1
delta_P = 1 # change in pressure between each row of data [psi]
Area = np.pi * re ** 2 # effective area [ft^2]
# Area_wb = np.pi * rw ** 2 # wellbore cross-sectional area [ft^2]
well_angle = 0 # degrees inclination of the well (0 = vertical)
# D_wb = rw * 2 * 12 # diameter of tubing in inches
epsilon = 0.0006 # pipe roughness assumed 0.0006 inches
dd_factor = 0.5 # wellhead pressure [psi] assumed to be 0.3 times the reservoir
pressure - so drawdown factor is 0.3

# reservoir paraemters
```

```
rf = 0.9 # gas recovery factor
Ca = 31.62 # dietz shape factor

# standard conditions and surface temp
Tsc = 491.67 # temperature [Rankine]
Psc = 14.5038 # pressure [psia]
T_surface_C = 15 # surface temperature [celcius] - assumed to be 15 C (518.67 in rankine)
T_surface_R = T_surface_C * (
    9 / 5) + 491.67 # surface temperature [RANKINE] - assumed to be 15 C (518.67 in rankine)

# conversion factors
psi_to_pascal = 6894.76 # multiply for pascal / divide for psi
PaS_to_cP = 1000 # multiply for cP / divide for Pa S
kg_mol_to_lb_lbmol = 1000 # multiply for lb/lbmol / divide for kg/mol
kg_m3_to_lb_ft3 = 0.062428 # multiply for lb/ft3 / divide for kg/m3
secs_to_days = 86400 # multiply for days / divide for seconds
m3_to_ft3 = 35.3147 # multiply for feet / divide for metres
inches_to_metres = 0.0254
metres_to_feet = 3.28084 # multiply for feet / divide for metres
rankine_to_kelvin = 5 / 9 # multiply for kelvin / divide for rankine

# fluid parameters

HHV_H2 = 39.4 # kWh/kg
HHV_CH4 = 15.4 # kWh/kg
# function for specific gravity


def specific_gravity(gas):
  return CoolProp.CoolProp.PropsSI('D', 'T', 273.15, 'P', 100e5, gas) / CoolProp.CoolProp.PropsSI('D', 'T', 273.15, 'P', 100e5, 'AIR')

# Erosional velocity variables
```

```
# from API RP 14E (1984)
# c is a constant 100 for continuous service, 150 for intermittent service (assume
intermittent for this well)
c = 150

### FUNCTIONS
##########################################################################
########################################

# calculate Z factor and make function for later use
def zfactorSI(temp, pressure, gas):
  return CoolProp.CoolProp.PropsSI('Z', 'T', temp, 'P', pressure, gas)

def pressure_col(Pr):
  Pwf = 1
  li = []
  while Pwf <= Pr + 1:
    li.append(Pwf)
    Pwf += delta_P
  return li

# calculate viscosity [cP] and make function for later use
def VISCcP(temp, pressure, gas):
  return CoolProp.CoolProp.PropsSI('V', 'T', temp, 'P', pressure, gas) * 1000

# calculate density and make function for later use [lb/ft3]
def dens_field(temp, pressure, gas):
  return CoolProp.CoolProp.PropsSI('D', 'T', temp, 'P', pressure, gas) *
kg_m3_to_lb_ft3

# calculate density and make function for later use [kg/m3]
def dens_SI(temp, pressure, gas):
  return CoolProp.CoolProp.PropsSI('D', 'T', temp, 'P', pressure, gas)

# Pseduopressure - define function for 2(p/uz)
```

```
def two_puz(p, u, z):
  return 2 * (p / (u * z))

### FLOW RATE FUNCTIONS
##############################################################################
##############################
# define flow rate equation- from gas reservoir engineering Lee & Wattenbarger
# Ppr - Ppwf = A*qg + B*qg^2

# define function for A from flow rate equation. Parameters are:
# temp [Kelvin], perm, thickness, Area, Dietz shape factor, wellbore radius, Skin
def A_flow(T, k, h, Area, Ca, rw, S):
  return (1.422 * (10 ** 6) * T / (k * h)) * (1.151 * np.log(10.06 * Area / (Ca * rw * rw)) -
0.75 + S)

# define function for B from flow rate equation. Parameters are:
# temp [Kelvin], perm, thickness, D (from flow rate equation)
def B(T, k, h, D):
  return 1.422 * (10 ** 6) * T * D / (k * h)

# define D from flow rate equation. Parameters are:
# beta, perm, molecular weight of gas/gas mixture, pressure @ STP, thickness,
viscosity, wellbore radius, Temp@STP [Kelvin]
def D(beta, k, M, Psc, h, visc, rw, Tsc):
  return 2.715 * (10 ** -12) * beta * k * M * Psc / (h * visc * rw * Tsc)

# define beta from equation for D. Parameters are:
# perm, porosity
def beta(k, por):
  return 1.88 * (10 ** 10) * (k ** -1.47) * (por ** -0.53)

# define reaaranged flow rate equation to give qg. Parameters are:
# A, B, average reservoir pseudopressure, well flowing pseduopressure
def Forcheimer_qg(a, b, mr, mbh):
  return (-a + (((a ** 2) + 4 * b * (mr - mbh)) ** 0.5)) / (2 * b)
```

```
### TPR FUNCTIONS
#########################################################################
#####################################
# BHFP estimate : ptf is tubing head pressure, L is length of tubing, well_angle is
angle of tubing (vertical = 0 degrees)
def BHFP_estimate(ptf, L, well_angle):
  return ptf + 0.25 * (ptf / 100) * ((L * np.cos(well_angle)) / 100)


# Calculate the Reynold's number: qg is flow rate [MSCF/d] , sg is specific gravity, d
is diameter of the wellbore [inches], ug is viscosity in cP
def Nre(qg, sg, d, ug):
  nre = (20 * sg * qg) / (ug * d)
  if nre > 0:
    return nre
  else:
    return 100

# calculate the friction factor: Nre_tpr is the Reynold's number, epsilon is the pipe
roughness [inches], D_wb wellbore diameter [inches]
def ff(Nre_tpr, epsilon, D_wb):
  if Nre_tpr > 2000:
    return 4 * (2.28 - 4 * np.log(
      (epsilon / D_wb) + (21.25 / Nre_tpr ** 0.9))) ** -2 # Jain and Swamee ref 13 CH
4
  else:
    return 64 / Nre_tpr

# calculate the variable s for the Pwf equation

def s(sg, L, well_angle, Zav_tpr, Tav_tpr):
  return 0.0375 * sg * L * np.cos(well_angle) / (Zav_tpr * Tav_tpr)

# pwf equation
```

```
def pwf_tpr(Pwh, s, qg, f_tpr, Tav_tpr, Zav_tpr, D_wb, well_angle):
  return (Pwh ** 2 * math.exp(s) + ((6.67e-4 * qg**2 * f_tpr * Tav_tpr**2 * Zav_tpr**2)
/ (D_wb**5 * np.cos(well_angle))) * (math.exp(s) - 1))**(1/2)

def TPR(qg, Pwh, L, Tres_rankine, sg, gas, D_wb):
    x = 1 # to keep an eye on the number of interations the while loop does later
    Z_over_Z = 1 # arbitrary number to kick off the loop
    V_over_V = 1 # arbitrary number to kick off the loop

    # step 1. estimate BHFP to start
    BHFP_est = BHFP_estimate(Pwh, L, well_angle)

    # step 2. use estimate to calculate average wellbore temp and pressure
    Tav_tpr = (Tres_rankine + T_surface_R) / 2
    print(str(Tav_tpr) + ' Rankine')
    Pav_tpr = (BHFP_est + Pwh) / 2
    print(str(Pav_tpr) + ' psi')

    # step 3. use av temp and pressure to calculate gas average viscosity and
compressibility
    Zav_tpr = zfactorSI(Tav_tpr * rankine_to_kelvin, Pav_tpr * psi_to_pascal, gas)
    Viscav_tpr = VISCcP(Tav_tpr * rankine_to_kelvin, Pav_tpr * psi_to_pascal, gas)

    # step 4. calculate the Reynold's number
    Nre_tpr = Nre(qg, sg, D_wb, Viscav_tpr)
    print('Reynold number = ' + str(Nre_tpr))
    if Nre_tpr <= 2000:
      print('laminar flow')
    elif 2000 < Nre_tpr < 4000:
      print('unstable flow')
    else:
      print('turbulent flow')

    # step 5. calculate the friction factor
```

```
    f_tpr = ff(Nre_tpr, epsilon, D_wb)
    print('friction factor = ' + str(f_tpr))

    # set the tolerance of 0.5% for our z and viscosity and begin the loop
    while ((round(Z_over_Z, 3) > 0.005) and (round(V_over_V, 3) > 0.005)):
      print('interation ' + str(x)) # keep an eye on the number of iterations it takes
      print('BHFP est ' + str(x) + ': ' + str(BHFP_est) + ' psi')

      # step 6. calculate s
      s_tpr = s(sg, L, well_angle, Zav_tpr, Tav_tpr)
      #s_tpr = s_tpr.astype(float)

      # step 7. calculate Pwf
      pwf_tpr_2 = pwf_tpr(Pwh, s_tpr, qg, f_tpr, Tav_tpr * rankine_to_kelvin, Zav_tpr,
D_wb, well_angle)
      print('calculated BHFP est ' + str(x) + ': ' + str(pwf_tpr_2) + ' psi')

      # caculate z and visc new average pressure
      Pav_tpr_2 = (pwf_tpr_2 + Pwh) / 2

      Zav_tpr_2 = zfactorSI(Tav_tpr * rankine_to_kelvin, Pav_tpr_2 * psi_to_pascal,
gas)
      Viscav_tpr_2 = VISCcP(Tav_tpr * rankine_to_kelvin, Pav_tpr_2 * psi_to_pascal,
gas)

      # compare to original estimate
      Z_over_Z = (Zav_tpr_2 - Zav_tpr) / Zav_tpr_2
      V_over_V = (Viscav_tpr_2 - Viscav_tpr) / Viscav_tpr_2

      # reset variables
      Zav_tpr = Zav_tpr_2
      Viscav_tpr = Viscav_tpr_2
      x= x + 1
```

```
    return pwf_tpr_2


def TPR_Katz(sg, D, pwf, pwh, L, Tres_rankine, gas):

  Tav_tpr = (Tres_rankine + T_surface_R) / 2
  print(str(Tav_tpr) + ' Rankine')
  Pav_tpr = (pwf + pwh) / 2
  print(str(Pav_tpr) + ' psi')
  Zav_tpr = zfactorSI(Tav_tpr * rankine_to_kelvin, Pav_tpr * psi_to_pascal, gas)
  print(str(Zav_tpr) + ' Z factor')
  s_tpr = s(sg, L, well_angle, Zav_tpr, Tav_tpr)
  print(str(s_tpr) + ' s')
  f_tpr = (2*np.log(3.71/(epsilon/D)))**-2
  print('friction factor = ' + str(f_tpr))
  try:
    qg = (200000 *((s_tpr * D**5* (pwf**2 - math.exp(s_tpr) * pwh**2))/( sg * Tav_tpr *
Zav_tpr * L * f_tpr * (math.exp(s_tpr)-1)))**0.5)/1e6
    return qg
  except:
    return 0

### EROSIONAL VELOCITY CALCULATION
##########################################################################
##################

# define erosional velocity function from API RP 14E (1984)
# ve = c/(density)^0.5 where density will change with pwf and units are ft/s
# c is a constant 100 for continuous service, 150 for intermittent service
# ve * x-sectional area of wellbore = flow rate

# define function for ve - [m/s]. Parameters are:
# constant c, well flowing pressure, reservoir temperature
def ve(c, density):
  return 1.22 * c / (density ** 0.5)
```

```
# calculate the velocity of the gas flow as per equation in Chapter 6, p. 62 from:
# Standard Handbook of Petroleum and Natural Gas Engineering doi:
10.1016/B978-0-12-383846-9.00006-0.
# ft/s
def gas_velocity_field(Q, Pb, Tf, Z, D, Pm, Tb):
  return (127.3 * 10 ** 3 * Q * Pb * Tf * Z / (D ** 2 * Pm * Tb)) / 60

## OPERATING POINT FUNCTIONS

def op_point_psi(qg_in, qg_out, pwf):
  try:
    first_line = LineString(np.column_stack((qg_in, pwf)))
    second_line = LineString(np.column_stack((qg_out, pwf)))
    intersection = first_line.intersection(second_line)
    op_point = intersection.x
    return op_point
  except:
    return 0

def op_point_pwf(qg_in, qg_out, pwf):
  try:
    first_line = LineString(np.column_stack((qg_in, pwf)))
    second_line = LineString(np.column_stack((qg_out, pwf)))
    intersection = first_line.intersection(second_line)
    op_point_pwf = intersection.y
    return op_point_pwf
  except:
    return 0

## EXPANSION FACTOR
def e_factor(z, T, P):
  return 35.3 * P / (z * T)

## PLATEAU RATE CALCULATION
```

```
def Qp(Qi, Tp, GIIPl):
  return 1 / ((1 / Qi) + (Tp / GIIPl))

## WELL POWER RATING EQUATION
def well_power_MW(gas, intersection_x):
  if gas == 'H2':
    return HHV_H2 * (intersection_x / m3_to_ft3 * 1000000) / 24 * PropsSI('D', 'T',
Tsc * rankine_to_kelvin, 'P',
                                Psc * psi_to_pascal, gas) / 1000
  elif gas == 'CH4':
    return HHV_CH4 * (intersection_x / m3_to_ft3 * 1000000) / 24 * PropsSI('D', 'T',
Tsc * rankine_to_kelvin, 'P',
                                 Psc * psi_to_pascal, gas) / 1000
  else:
    return 0



#########################################################################
#########################################################
### MAIN CALCULATOR
#########################################################################
#####################################
def IPR_CALCULATOR(field_name, gas, Pr, k, poro, h, L, GIIP, Tres_rankine, Tp,
D_wb, rw):

  # file setup field_name = 'XXX' gas = 'CH4' # used to call fluid type from CoolProp -
list:
  # http://www.coolprop.org/fluid_properties/PurePseudoPure.html#list-of-fluids
  title = gas + ' IPR calculation' + ' for the ' + str(field_name) + ' gas field'
  print(title)

  # some internal variables
  Tres_kelvin = Tres_rankine * 5 / 9 # reservoir temperature [Kelvin]
  Pwh = Pr * dd_factor # wellhead pressure [psi] assumed to be 0.3 times the
```

```
reservoir pressure
  sg = specific_gravity(gas) # specific gravity of gas - air = 1
  print(str(gas) + ' SG = ' + str(round(sg, 5)))
  M = CoolProp.CoolProp.PropsSI('M', 'T', Tres_kelvin, 'P', (Psc * psi_to_pascal),
gas) * kg_mol_to_lb_lbmol
  print(str(gas) + ' M = ' + str(round(M, 5)) + ' lb/lbmol')

## CREATING AND POPULATING THE DATAFRAME
##########################################################################
############

  # create a dataframe. will be added to later
  header = ['Z']
  df = pd.DataFrame(columns=header)

  # define pressure in previously defined increments (variable delta_P) up to
reservoir pressure & add to dataframe
  df.insert(0, "pressure [psia]", pressure_col(Pr))
  print(df)

## COMPRESSIBILITY (Z), VISCOSITY, AND DENSITY CALCULATIONS
#################################################################
  # add z factor to df
  df['Z'] = df.apply(lambda x: zfactorSI(Tres_kelvin, x['pressure [psia]'] *
psi_to_pascal, gas), axis=1)

  # add viscosity to df
  df['VISC [cP]'] = df.apply(lambda x: VISCcP(Tres_kelvin, x['pressure [psia]'] *
psi_to_pascal, gas), axis=1)

  # add density to df
  df['density [lb/ft3]'] = df.apply(lambda x: dens_field(Tres_kelvin, x['pressure [psia]'] *
psi_to_pascal, gas), axis=1)

  # add density to df
```

```
  df['density [kg/m3]'] = df.apply(lambda x: dens_field(Tres_kelvin, x['pressure [psia]']
* psi_to_pascal, gas), axis=1)

  ## PSEUDOPRESSURE CALCULATION
##########################################################################
####################
  # how to calculate pseudopressure: do the following steps as per Al-Husseiny
trapezoid method
  # '2(p/uz)', 'delta P [psia]', '2(p/uz) * delta P', 'sum'

  # how to calculate pseudopressure: do the following steps as per Al-Husseiny
trapezoid method
  # '2(p/uz)', 'delta P [psia]', '2(p/uz) * delta P', 'sum'

  df['2(p/uz) * delta P'] = df.apply(lambda x: two_puz(x['pressure [psia]'], x['VISC
[cP]'], x['Z']),
                  axis=1) * delta_P

  df['pseudopressure'] = df['2(p/uz) * delta P'].cumsum()
  # define the average reservoir pseudopressure
  Pres_pseudo = df['pseudopressure'].iloc[-1]

  ## FLOW RATE EQUATION - RESERVOIR INTO WELLBORE
##########################################################################
###

  # make A a variable as it does not vary with pressure increments
  A = A_flow(Tres_rankine, k, h, Area, Ca, rw, S)

  # calculate the flow rate for each pressure increment and add it to dataframe
  df['qg [MMSCF/d]'] = df.apply(
    lambda x: Forcheimer_qg(A, B(Tres_rankine, k, h, D(beta(k, poro), k, M, Psc, h,
x['VISC [cP]'], rw, Tsc)),
              Pres_pseudo, x['pseudopressure']), axis=1)
```

```
  # define the AOFP/theoretical maximum rate qg @ pwf = 1 psi
  AOFP = df['qg [MMSCF/d]'].iloc[0]

  ## BHFP CALCULATION - FLOW RATE AT BOTTOM OF WELLBORE - KATZ
METHOD

  df['TP_Qg [MMSCF/d]'] = df.apply(lambda x: TPR_Katz(sg, D_wb, x['pressure
[psia]'], Pwh, L, Tres_rankine, gas), axis = 1)

  ## BHFP CALCULATION - PRESSURE AT BOTTOM OF WELLBORE


  df['TP_BHP [psia]'] = df.apply(lambda x: TPR(x['qg [MMSCF/d]'] * 1000, Pwh, L,
Tres_rankine, sg, gas, D_wb), axis=1)

  ## EROSIONAL VELOCITY
  df['Vg [ft/s]'] = gas_velocity_field(df['qg [MMSCF/d]'], Pwh, Tres_rankine, df['Z'],
D_wb, df['pressure [psia]'], T_surface_R)

  ## WELL DIAMETER
  df['Well diameter [inches]'] = D_wb

  # save df results
##########################################################################
#################################
  print(df)
  csv_name = field_name + '_' + str(Pr) + '_Pr_' + gas + '_' + str(D_wb) +
'_inches_IPR.csv'
  print(csv_name)
  df.to_csv(csv_name)

##########################################################################
#####################################################

  ## CHECK INTERSECTION OF IPR AND TPR - needs to have try statement
```

```
otherwise no intersect will throw errors

  first_line = LineString(np.column_stack((df['qg [MMSCF/d]'], df['pressure [psia]'])))
  #first_line = first_line.buffer(0)
  second_line = LineString(np.column_stack((df['qg [MMSCF/d]'], df['TP_BHP
[psia]'])))
  #second_line = second_line.buffer(0)
  #try:
  intersection = first_line.intersection(second_line)


  ## OPERATING POINT COORDINATES
  operating_point = op_point_psi(df['qg [MMSCF/d]'], df['pressure [psia]'],
df['TP_BHP [psia]'])
  operating_point_pwf = op_point_pwf(df['qg [MMSCF/d]'], df['pressure [psia]'],
df['TP_BHP [psia]'])
  #except:
    #operating_point = None
    #operating_point_pwf = None


  ## GAS PLATEAU RATE CALCULATION
##########################################################################
######################
  # lookup the number of wells in the field
  n_wells = wells_file.loc[(wells_file['field_name'] == field_name, 'n_wells')].iloc[0]


  # to calculate the GIIP for hydrogen we need to find the expansion factor ratio
between methane and hydrogen at res conditions
  # expansion factor function z is compressibility factor, T is temperature in degrees
rankine, P is pressure in psia
  CH4_e = e_factor(
    CoolProp.CoolProp.PropsSI('Z', 'T', Tres_kelvin, 'P',
gas_fields_props['Pr_psia'].iloc[0] * psi_to_pascal, 'CH4'), Tres_rankine,
```

```
gas_fields_props['Pr_psia'].iloc[0])
  H2_e = e_factor(
    CoolProp.CoolProp.PropsSI('Z', 'T', Tres_kelvin, 'P',
gas_fields_props['Pr_psia'].iloc[0] * psi_to_pascal, 'H2'), Tres_rankine,
gas_fields_props['Pr_psia'].iloc[0])
  e_ratio = H2_e / CH4_e
  # adjust giip for hydrogen
  if gas == 'H2':
    GIIP = GIIP * e_ratio
  # perform plateau rate calculation

  Q_plat = Qp((intersection.x * n_wells), Tp, GIIP)

## DRAWDOWN
##########################################################################
##########################################
  DD = Pr - intersection.y

## WORKING GAS AND CUSHION GAS VOLUMES
##########################################################################
###############
# assumes that there is 10% irrecoverable gas in the reservoir i.e. a recovery factor
of 90%
  WGV = Q_plat * Tp
  CGV = (GIIP * rf) - WGV
  WG_CG_ratio = WGV / CGV
  CG_percentage = (CGV / (WGV + CGV)) * 100

## WELL POWER CALCULATION - how much energy does the well deliver
  well_power = well_power_MW(gas, intersection.x)

## EROSIONAL VELOCITY LIMITS

  Pwf_int = intersection.y
  dens_int_SI = dens_SI(Tres_kelvin, Pwf_int * psi_to_pascal, gas)
```

```
  ve_int_ft_s = ve(100, dens_int_SI) * metres_to_feet
  # convert to equivalent flow rate in MMSCF/d - do all in SI units then convert at end
  # to flow rate by multiplying velocity by area of wellbore and conversion to
MMSCF/d
  V_limit_q = (ve_int_ft_s * (np.pi * D_wb ** 2) * secs_to_days) / 1000000
  # except:
  #   Q_plat = None
  #   DD = None
  #   WGV = 0
  #   CGV = (GIIP * rf) - WGV
  #   WG_CG_ratio = WGV / CGV
  #   CG_percentage = (CGV / (WGV + CGV)) * 100
  #   well_power = 0
  #   Pwf_int = None
  #   dens_int_SI = None
  #   ve_int_ft_s = 0
  #   # convert to equivalent flow rate in MMSCF/d - do all in SI units then convert at
end
  #   # to flow rate by multiplying velocity by area of wellbore and conversion to
MMSCF/d
  #   V_limit_q = None

  to_append = [field_name, n_wells, D_wb, gas, GIIP, Pr, DD, Tp, Q_plat, WGV,
CGV, WG_CG_ratio, CG_percentage, ve_int_ft_s,
         V_limit_q, well_power, operating_point, operating_point_pwf, AOFP]
  df_length = len(calc_df)
  calc_df.loc[df_length] = to_append
  calc_name = calc_df['field'].iloc[0] + '_' + calc_df['gas'].iloc[0] + '_' + str(
     calc_df['Well diameter [inches]'].iloc[0]) + '_inches'+
'_calculated_storage_props.csv'
  calc_df.to_csv(calc_name)

  # timesteps dataframe

  # add P/Z column for well forecasting
```

```
  p_over_z_init = gas_fields_props['Pr_psia'].iloc[0] /
zfactorSI(gas_fields_props['Tres_R'].iloc[0] * rankine_to_kelvin,
gas_fields_props['Pr_psia'].iloc[0] * psi_to_pascal, gas_fields_props['gas'].iloc[0])
  # p/z slope and intercept for Gp column
  x1 = 0
  x2 = GIIP # MMSCF
  y1 = p_over_z_init
  y2 = 0
  slope, intercept, r_value, p_value, std_err = linregress([x1, x2], [y1, y2])

  # p over z each timestep
  p_over_z_timestep = df['pressure [psia]'].iloc[-1] / df['Z'].iloc[-1]

  # gas produced [MMSCF]
  Gp = (p_over_z_timestep - intercept) / slope

  # rate
  Qg = operating_point
  Pwf_op = operating_point_pwf
  to_append = [field_name, n_wells, D_wb, gas, GIIP, Pr, p_over_z_timestep, Gp,
Qg, Pwf_op, e_ratio]
  df_length = len(df_steps)
  df_steps.loc[df_length] = to_append



  ## ## PLOT THE CURVES
##########################################################################
###################################
  # plot the output (IPR & TPR curves) on the same graph
  # tells plot to share the axis i.e. add to one graph gca = get current axis
  ax = plt.gca()

  # IPR curve with label for gas type
  ipr_label = 'IPR - ' + str(gas)
```

```
  df.plot(kind='line', x='qg [MMSCF/d]', y='pressure [psia]', ax=ax, label=ipr_label,
color='black')
  plt.xlim([0, df['qg [MMSCF/d]'].iloc[0] * 1.1])
  plt.ylim([0, Pr * 1.1])
  tpr_label = 'TPR ' + str(round(D_wb, 2)) + '" tubing ' + str(round(Pwh)) + ' psia'
  try:
    df.plot(x= 'qg [MMSCF/d]', y='TP_BHP [psia]', ax=ax, label=tpr_label,
color='black', linestyle='--')
  except:
    pass

  ## INTERSECTION (IF IT INTERSECTS)
  #try:
  # define and show the intersection
  intersect_label = 'qg = ' + str(round(intersection.x, 4)) + ' MMSCF/d \nPwf = ' +
str(round(intersection.y)) + ' psia'
  if intersection.geom_type == 'MultiPoint':
    plt.plot(*LineString(intersection).xy, 'o', label='intersect_label')
  elif intersection.geom_type == 'Point':
    plt.plot(*intersection.xy, 'o', label='operating rate')
    plt.annotate(intersect_label, (intersection.x, intersection.y * 1.1))
  #except:
   # pass
  # sort out axis labels
  plt.xlabel('qg [MMSCF/d]')
  plt.ylabel('Pwf [psia]')

  # erosional velocity for intersection Pwf
  try:
    Ve_label = 'Ve limit: ' + str(round(ve_int_ft_s, 1)) + ' ft/s'
    plt.axvline(x=V_limit_q, label=Ve_label, linestyle='dashed', c='black', lw=0.75)
  except:
    pass
```

```
  # title and legend
  plt.legend(loc='lower left')
  plt.title(title)
  png_name = 'IPR_plot_' + field_name + '_' + str(Pr) + '_Pr_' + gas + str(D_wb) +
'_inches.png'
  plt.savefig(png_name)
  plt.cla()
  plt.clf()



# import the wells file that contains the number of wells in each field
wells_file = pd.read_csv('INPUT/n_wells_single.csv')

# to automatically find all the input files
li = []
for root, dirs, files in
os.walk(r"C:\Users\s1669173\PycharmProjects\pythonProject1\INPUT",
topdown=False):
  for name in files:
    if "_timesteps" in name:
      print(os.path.join(root, name))
      x = os.path.join(root, name)
      li.append(x)
print(li)
list = pd.DataFrame(li)
list.to_csv('file_paths.csv')

for i in li:

## INPUT SETUP
################################################################################
########################################
```

```
  # create a df to store key data calculated by model
  calcs_col_names = ["field", "n_wells", "Well diameter [inches]", "gas", "GIIP
[MMSCF]", "initial reservoir pressure [psi]",
          "drawdown [psi]", "plateau time [days]", "plateau rate [MMSCF/D]",
          "WGV [MMSCF]", "CGV [MMSCF]", "WGV:CGV [ratio]", "Cushion gas
requirement [%]",
          "Ve limit [ft/s]", "Qg Ve limit [MMSCF/D]", "well power [MW]", "Qg Operating
point [MMSCF/D]", "Pwf Operating point [psi]", "AOFP [MMSCF/d]"]
  calc_df = pd.DataFrame(columns=calcs_col_names)

  steps_col_names = ['field_name', 'n_wells', 'Well diameter [inches]', 'gas', 'GIIP
[MMSCF]', 'Pr [psia]', 'p_over_z', 'Gp [MMSCF]',
          'Qg [MMSCF/D]', 'Pwf [psia]', 'expansion ratio']

  df_steps = pd.DataFrame(columns=steps_col_names)

  print(df_steps)
  # x is used later to loop the naming function function
  x = 1

  # reads file to get input data
  gas_fields_props = pd.read_csv(i)

  # make a new folder to save shizzle in
  parent_dir = r'C:\Users\s1669173\PycharmProjects\pythonProject1\OUTPUT'
  directory = str(gas_fields_props['field_name'].iloc[0]) + '_' +
str(gas_fields_props['gas'].iloc[0]) + '_' + str(
      gas_fields_props['D_wb_inches'].iloc[0]) + '_inches'
  path = os.path.join(parent_dir, directory)
  os.mkdir(path)
  os.chdir(path)

  y = 1
  for i,r in gas_fields_props.iterrows():
    #plt.figure(y)
```

```
    IPR_CALCULATOR(r['field_name'], r['gas'],
r['Pr_psia'],r['k_mD'],r['poro_frac'],r['h_ft'],r['L_ft'],r['GIIP_MMSCF'], r['Tres_R'],
r['plateau'], r['D_wb_inches'], r['rw_ft'])
    print(str(y) + ' IPR curves constructed')
    # plt.show(block=False)
    # plt.pause(0.5)
    # plt.close(fig=int(y))
    y = y + 1

  # timestep calculations
  # average gas produced
  df_steps['delta Gp [MMSCF]'] = df_steps['Gp [MMSCF]'].diff()

  # average rate
  df_steps['Qg_av [MMSCF/D]'] = df_steps['Qg
[MMSCF/D]'].rolling(window=2).mean()

  # number of days between each rate
  df_steps['delta_t [days]'] = df_steps['delta Gp [MMSCF]'] / df_steps['Qg_av
[MMSCF/D]']

  # cumulative days - production time
  df_steps['t [days]'] = df_steps['delta_t [days]'].cumsum()
  timesteps_name = df_steps['field_name'].iloc[0] + '_timesteps_' +
df_steps['gas'].iloc[0] + '_' + str(df_steps['Well diameter [inches]'].iloc[0]) +
'_inches.csv'
  df_steps.to_csv(timesteps_name)

  df_steps.plot(kind='line', x='t [days]', y='Qg_av [MMSCF/D]', marker='s',
legend=False, color='k', linewidth=1)
  plt.ylabel('Qg [MMSCF/D]')
  plt.xlim(0, )
  plt.ylim(0, )
  png_name = df_steps['field_name'].iloc[0] +'_forecast_' + df_steps['gas'].iloc[0] + '_'
+ str(df_steps['Well diameter [inches]'].iloc[0]) + '_inches.png'
```

```
  plt.savefig(png_name)
  plt.cla()
  plt.clf()


print('Finshed! ' + str(y) + ' IPR curves constructed')
sys.stdout.close()

# next lines play triumphant music when the code has finished. I chose the Rocky theme tune. Can also recommend Oh Yeah by Yello…
p = r'C:\\Users\s1669173\PycharmProjects\pythonProject1\INPUT\rocky.mp3'
playsound.playsound(p)
```

Results appender and extra calculations

```
import pandas as pd
import os
import CoolProp.CoolProp
from CoolProp.CoolProp import PropsSI

# well power for plateau rate

HHV_H2 = 39.4 # kWh/kg
HHV_CH4 = 15.4 # kWh/kg
Tsc = 491.67 # temperature [Rankine]
Psc = 14.5038 # pressure [psia]

psi_to_pascal = 6894.76 # multiply for pascal / divide for psi
PaS_to_cP = 1000 # multiply for cP / divide for Pa S
kg_mol_to_lb_lbmol = 1000 # multiply for lb/lbmol / divide for kg/mol
kg_m3_to_lb_ft3 = 0.062428 # multiply for lb/ft3 / divide for kg/m3
secs_to_days = 86400 # multiply for days / divide for seconds
m3_to_ft3 = 35.3147 # multiply for feet / divide for metres
inches_to_metres = 0.0254
metres_to_feet = 3.28084 # multiply for feet / divide for metres
rankine_to_kelvin = 5 / 9 # multiply for kelvin / divide for rankine

def well_power_MW(gas, q):
  if gas == 'H2':
    return HHV_H2 * (q / m3_to_ft3 * 1000000) / 24 * PropsSI('D', 'T', Tsc *
rankine_to_kelvin, 'P',
                                Psc * psi_to_pascal, gas) / 1000
  elif gas == 'CH4':
    return HHV_CH4 * (q / m3_to_ft3 * 1000000) / 24 * PropsSI('D', 'T', Tsc *
rankine_to_kelvin, 'P',
                                 Psc * psi_to_pascal, gas) / 1000
  else:
    return 0
```

```
li = []
for root, dirs, files in
os.walk(r"C:\Users\s1669173\PycharmProjects\pythonProject1\OUTPUT",
topdown=False):
  for name in files:
    if "storage_props" in name:
      print(os.path.join(root, name))
      x = os.path.join(root, name)
      li.append(x)
print(li)

aggregated_results = pd.DataFrame()

for i in li:
  df = pd.read_csv(i)
  df['root'] = i
  aggregated_results = aggregated_results.append(df.iloc[0])[df.columns.tolist()]

aggregated_results['well power plateau [MW]'] = aggregated_results.apply(lambda
x:well_power_MW(x['gas'], x['plateau rate [MMSCF/D]']), axis = 1)

aggregated_results['per well power plateau [MW]'] = aggregated_results['well power
plateau [MW]'] / aggregated_results['n_wells']

aggregated_results['per well plateau rate [MMSCF/D]'] =
aggregated_results['plateau rate [MMSCF/D]'] / aggregated_results['n_wells']

aggregated_results.to_csv('results_appended.csv')
print(aggregated_results)

# END OF CODE
```

8.5.2 Results

Results from the inflow/outflow performance program

Table 24: summarized test data results from the inflow/outflow program. More columns are outputted but they do not fit this appendix - full table will be available with thesis data package. Plateau time is 90 days for this run. GIIP is gas initially in place, WGV is working gas volume, and CGV is cushion gas volume. MMSCF is million standard cubic feet and MW is megawatt

field	number of wells	Well diameter [inches]	gas	GIIP [MMSCF]	plateau rate [MMSCF/D]	WGV [MMSCF]	CGV [MMSCF]	Cushion gas requirement [%]	well power plateau [MW]	per well power plateau [MW]	per well plateau rate [MMSCF/D]
Cousland	3	2	CH4	870	5.77848	520.0632	262.9368	33.58069	74.34218	24.78073	1.92616
Cousland	3	4	CH4	870	6.034857	543.1372	239.8628	30.63382	77.64056	25.88019	2.011619
Cousland	3	6	CH4	870	6.140025	552.6023	230.3977	29.425	78.99358	26.33119	2.046675
Cousland	3	8	CH4	870	6.21253	559.1277	223.8723	28.59161	79.92638	26.64213	2.070843
Cousland	3	2	H2	778.4975	5.929966	533.697	166.9508	23.82806	24.45367	8.151224	1.976655
Cousland	3	4	H2	778.4975	6.065038	545.8534	154.7943	22.09303	25.01068	8.336892	2.021679
Cousland	3	6	H2	778.4975	6.139062	552.5156	148.1321	21.14217	25.31593	8.438644	2.046354
Cousland	3	8	H2	778.4975	6.191993	557.2793	143.3684	20.46227	25.5342	8.511401	2.063998
Grijpskerk	20	2	CH4	381000	928.0014	83520.13	259379.9	75.64301	11939.06	596.9532	46.40007
Grijpskerk	20	4	CH4	381000	2322.118	208990.6	133909.4	39.05202	29874.86	1493.743	116.1059
Grijpskerk	20	6	CH4	381000	2803.1	252279	90620.98	26.42782	36062.87	1803.144	140.155
Grijpskerk	20	8	CH4	381000	2941.778	264760	78139.95	22.78797	37847.01	1892.351	147.0889
Grijpskerk	20	2	H2	346729.6	2029.542	182658.7	129397.9	41.46615	8369.314	418.4657	101.4771
Grijpskerk	20	4	H2	346729.6	3091.742	278256.8	33799.85	10.83132	12749.56	637.4779	154.5871
Grijpskerk	20	6	H2	346729.6	3264.383	293794.4	18262.18	5.852202	13461.48	673.0742	163.2191
Grijpskerk	20	8	H2	346729.6	3306.62	297595.8	14460.82	4.634039	13635.66	681.783	165.331
Hatfield Moors	4	2	CH4	6100	25.88293	2329.463	3160.537	57.56897	332.993	83.24824	6.470732

Hatfield Moors	4	4	CH4	6100	29.37197	2643.477	2846.523	51.84923	377.8807	94.47018	7.342992
Hatfield Moors	4	6	CH4	6100	30.13312	2711.981	2778.019	50.60144	387.6732	96.91829	7.53328
Hatfield Moors	4	8	CH4	6100	30.639	2757.51	2732.49	49.77214	394.1815	98.54537	7.659749
Hatfield Moors	4	2	H2	5467.545	29.90825	2691.743	2229.047	45.29857	123.334	30.83351	7.477063
Hatfield Moors	4	4	H2	5467.545	31.3027	2817.243	2103.547	42.74815	129.0844	32.2711	7.825675
Hatfield Moors	4	6	H2	5467.545	31.92026	2872.824	2047.966	41.61865	131.6311	32.90776	7.980066
Hatfield Moors	4	8	H2	5467.545	32.36494	2912.845	2007.945	40.80534	133.4648	33.3662	8.091236
Rough	45	2	CH4	366000	1468.513	132166.1	197233.9	59.87671	18892.93	419.8429	32.63361
Rough	45	4	CH4	366000	2500.885	225079.6	104320.4	31.66981	32174.76	714.9947	55.57522
Rough	45	6	CH4	366000	2694.145	242473	86926.95	26.38948	34661.12	770.2472	59.86989
Rough	45	8	CH4	366000	2762.542	248628.8	80771.22	24.52071	35541.08	789.8017	61.38982
Rough	45	2	H2	315659.2	2366.547	212989.3	71103.98	25.02839	9759.04	216.8676	52.58994
Rough	45	4	H2	315659.2	2860.731	257465.8	26627.43	9.372777	11796.93	262.154	63.57181
Rough	45	6	H2	315659.2	2921.343	262920.8	21172.39	7.45262	12046.88	267.7083	64.91873
Rough	45	8	H2	315659.2	2945.982	265138.4	18954.84	6.672049	12148.48	269.9663	65.46627
Cousland	1	2	CH4	870	3.202345	288.2111	494.7889	63.19143	41.1993	41.1993	3.202345
Cousland	1	4	CH4	870	3.445716	310.1144	472.8856	60.39407	44.33035	44.33035	3.445716
Cousland	1	6	CH4	870	3.549866	319.4879	463.5121	59.19694	45.67027	45.67027	3.549866
Cousland	1	8	CH4	870	3.623208	326.0887	456.9113	58.35393	46.61384	46.61384	3.623208
Cousland	1	2	H2	778.4975	3.640461	327.6415	373.0062	53.23734	15.01234	15.01234	3.640461
Cousland	1	4	H2	778.4975	3.796166	341.655	358.9928	51.23727	15.65443	15.65443	3.796166
Cousland	1	6	H2	778.4975	3.884108	349.5697	351.078	50.10763	16.01707	16.01707	3.884108
Cousland	1	8	H2	778.4975	3.948167	355.335	345.3127	49.28478	16.28124	16.28124	3.948167
Grijpskerk	5	2	CH4	381000	277.6485	24988.36	317911.6	92.71264	3572.045	714.409	55.52969
Grijpskerk	5	4	CH4	381000	986.2867	88765.8	254134.2	74.11321	12688.92	2537.785	197.2573
Grijpskerk	5	6	CH4	381000	1392.118	125290.6	217609.4	63.46147	17910.09	3582.017	278.4236
Grijpskerk	5	8	CH4	381000	1535.956	138236	204664	59.6862	19760.61	3952.123	307.1912

Grijpskerk	5	2	H2	346729.6	838.797	75491.73	236564.9	75.80832	3458.986	691.7971	167.7594
Grijpskerk	5	4	H2	346729.6	1941.505	174735.5	137321.1	44.0052	8006.275	1601.255	388.3011
Grijpskerk	5	6	H2	346729.6	2238.931	201503.8	110552.8	35.42717	9232.783	1846.557	447.7862
Grijpskerk	5	8	H2	346729.6	2320.241	208821.7	103234.9	33.08211	9568.085	1913.617	464.0482
Hatfield Moors	1	2	CH4	6100	9.067849	816.1064	4673.894	85.13467	116.6611	116.6611	9.067849
Hatfield Moors	1	4	CH4	6100	10.87879	979.0913	4510.909	82.16591	139.9595	139.9595	10.87879
Hatfield Moors	1	6	CH4	6100	11.30173	1017.156	4472.844	81.47257	145.4008	145.4008	11.30173
Hatfield Moors	1	8	CH4	6100	11.58879	1042.991	4447.009	81.00198	149.0939	149.0939	11.58879
Hatfield Moors	1	2	H2	5467.545	11.85395	1066.856	3853.934	78.31942	48.88269	48.88269	11.85395
Hatfield Moors	1	4	H2	5467.545	12.75475	1147.927	3772.863	76.67189	52.59733	52.59733	12.75475
Hatfield Moors	1	6	H2	5467.545	13.17004	1185.303	3735.487	75.91234	54.30989	54.30989	13.17004
Hatfield Moors	1	8	H2	5467.545	13.4756	1212.804	3707.986	75.35347	55.56995	55.56995	13.4756
Rough	15	2	CH4	366000	644.712	58024.08	271375.9	82.38492	8294.447	552.9631	42.9808
Rough	15	4	CH4	366000	1412.884	127159.6	202240.4	61.39661	18177.25	1211.817	94.19227
Rough	15	6	CH4	366000	1608.435	144759.1	184640.9	56.0537	20693.08	1379.538	107.229
Rough	15	8	CH4	366000	1683.068	151476.1	177923.9	54.01453	21653.26	1443.551	112.2045
Rough	15	2	H2	315659.2	1433.827	129044.4	155048.8	54.57673	5912.738	394.1825	95.58847
Rough	15	4	H2	315659.2	2090.093	188108.4	95984.86	33.78639	8619.013	574.6008	139.3395
Rough	15	6	H2	315659.2	2189.671	197070.4	87022.89	30.6318	9029.645	601.9763	145.978
Rough	15	8	H2	315659.2	2231.641	200847.7	83245.56	29.3022	9202.72	613.5147	148.7761
Cousland	2	2	CH4	870	4.810937	432.9844	350.0156	44.70187	61.8944	30.9472	2.405469
Cousland	2	4	CH4	870	5.080478	457.243	325.757	41.6037	65.36214	32.68107	2.540239
Cousland	2	6	CH4	870	5.192795	467.3515	315.6485	40.31271	66.80713	33.40356	2.596397
Cousland	2	8	CH4	870	5.270831	474.3748	308.6252	39.41573	67.8111	33.90555	2.635416
Cousland	2	2	H2	778.4975	5.124293	461.1863	239.4614	34.17715	21.13128	10.56564	2.562146
Cousland	2	4	H2	778.4975	5.276614	474.8952	225.7525	32.22054	21.75941	10.87971	2.638307
Cousland	2	6	H2	778.4975	5.360972	482.4875	218.1603	31.13694	22.10729	11.05364	2.680486

Cousland	2	8	H2	778.4975	5.421679	487.9511	212.6966	30.35714	22.35763	11.17881	2.71084
Grijpskerk	11	2	CH4	381000	566.26	50963.4	291936.6	85.13753	7285.134	662.2849	51.47818
Grijpskerk	11	4	CH4	381000	1695.74	152616.6	190283.4	55.49238	21816.29	1983.299	154.1582
Grijpskerk	11	6	CH4	381000	2196.059	197645.3	145254.7	42.36066	28253.07	2568.461	199.6417
Grijpskerk	11	8	CH4	381000	2354.137	211872.4	131027.6	38.21162	30286.8	2753.346	214.0125
Grijpskerk	11	2	H2	346729.6	1463.091	131678.2	180378.4	57.8031	6033.417	548.4924	133.0083
Grijpskerk	11	4	H2	346729.6	2661.678	239551	72505.57	23.23475	10976.08	997.8259	241.9708
Grijpskerk	11	6	H2	346729.6	2901.901	261171.1	50885.51	16.3065	11966.7	1087.882	263.8092
Grijpskerk	11	8	H2	346729.6	2963.076	266676.9	45379.76	14.54215	12218.97	1110.816	269.3706
Hatfield Moors	2	2	CH4	6100	15.99567	1439.61	4050.39	73.77759	205.7899	102.895	7.997835
Hatfield Moors	2	4	CH4	6100	18.74835	1687.351	3802.649	69.265	241.2041	120.602	9.374174
Hatfield Moors	2	6	CH4	6100	19.37307	1743.576	3746.424	68.24088	249.2413	124.6207	9.686533
Hatfield Moors	2	8	CH4	6100	19.79328	1781.395	3708.605	67.552	254.6475	127.3238	9.896641
Hatfield Moors	2	2	H2	5467.545	19.83717	1785.346	3135.444	63.71831	81.80347	40.90173	9.918587
Hatfield Moors	2	4	H2	5467.545	21.08305	1897.474	3023.316	61.43965	86.94112	43.47056	10.54152
Hatfield Moors	2	6	H2	5467.545	21.6472	1948.248	2972.542	60.40782	89.26755	44.63378	10.8236
Hatfield Moors	2	8	H2	5467.545	22.05826	1985.244	2935.546	59.656	90.96267	45.48134	11.02913
Rough	30	2	CH4	366000	1112.977	100168	229232	69.59078	14318.84	477.2948	37.09924
Rough	30	4	CH4	366000	2097.153	188743.8	140656.2	42.70073	26980.61	899.3538	69.90511
Rough	30	6	CH4	366000	2305.146	207463.1	121936.9	37.01788	29656.51	988.5503	76.83818
Rough	30	8	CH4	366000	2380.797	214271.8	115128.2	34.95089	30629.8	1020.993	79.35991
Rough	30	2	H2	315659.2	2035.516	183196.4	100896.8	35.51538	8393.95	279.7983	67.85053
Rough	30	4	H2	315659.2	2619.292	235736.2	48357	17.02152	10801.29	360.0431	87.30972
Rough	30	6	H2	315659.2	2696.118	242650.6	41442.64	14.58769	11118.1	370.6035	89.87059
Rough	30	8	H2	315659.2	2727.7	245493	38600.23	13.58717	11248.34	374.9447	90.92334
Cousland	1	2	CH4	870	3.202345	288.2111	494.7889	63.19143	41.1993	41.1993	3.202345
Cousland	1	4	CH4	870	3.445716	310.1144	472.8856	60.39407	44.33035	44.33035	3.445716

Cousland	1	6	CH4	870	3.549866	319.4879	463.5121	59.19694	45.67027	45.67027	3.549866
Cousland	1	8	CH4	870	3.623208	326.0887	456.9113	58.35393	46.61384	46.61384	3.623208
Cousland	1	2	H2	778.4975	3.640461	327.6415	373.0062	53.23734	15.01234	15.01234	3.640461
Cousland	1	4	H2	778.4975	3.796166	341.655	358.9928	51.23727	15.65443	15.65443	3.796166
Cousland	1	6	H2	778.4975	3.884108	349.5697	351.078	50.10763	16.01707	16.01707	3.884108
Cousland	1	8	H2	778.4975	3.948167	355.335	345.3127	49.28478	16.28124	16.28124	3.948167
Grijpskerk	1	2	CH4	381000	58.60462	5274.416	337625.6	98.46182	753.969	753.969	58.60462
Grijpskerk	1	4	CH4	381000	242.4455	21820.1	321079.9	93.6366	3119.147	3119.147	242.4455
Grijpskerk	1	6	CH4	381000	377.8193	34003.73	308896.3	90.08348	4860.778	4860.778	377.8193
Grijpskerk	1	8	CH4	381000	432.8218	38953.96	303946	88.63985	5568.404	5568.404	432.8218
Grijpskerk	1	2	H2	346729.6	203.1428	18282.85	293773.8	94.14117	837.7094	837.7094	203.1428
Grijpskerk	1	4	H2	346729.6	650.5978	58553.8	253502.8	81.23616	2682.9	2682.9	650.5978
Grijpskerk	1	6	H2	346729.6	836.8653	75317.88	236738.7	75.86404	3451.02	3451.02	836.8653
Grijpskerk	1	8	H2	346729.6	895.5155	80596.4	231460.2	74.17251	3692.878	3692.878	895.5155
Hatfield Moors	1	2	CH4	6100	9.067849	816.1064	4673.894	85.13467	116.6611	116.6611	9.067849
Hatfield Moors	1	4	CH4	6100	10.87879	979.0913	4510.909	82.16591	139.9595	139.9595	10.87879
Hatfield Moors	1	6	CH4	6100	11.30173	1017.156	4472.844	81.47257	145.4008	145.4008	11.30173
Hatfield Moors	1	8	CH4	6100	11.58879	1042.991	4447.009	81.00198	149.0939	149.0939	11.58879
Hatfield Moors	1	2	H2	5467.545	11.85395	1066.856	3853.934	78.31942	48.88269	48.88269	11.85395
Hatfield Moors	1	4	H2	5467.545	12.75475	1147.927	3772.863	76.67189	52.59733	52.59733	12.75475
Hatfield Moors	1	6	H2	5467.545	13.17004	1185.303	3735.487	75.91234	54.30989	54.30989	13.17004
Hatfield Moors	1	8	H2	5467.545	13.4756	1212.804	3707.986	75.35347	55.56995	55.56995	13.4756
Rough	1	2	CH4	366000	50.44498	4540.048	324860	98.62172	648.9924	648.9924	50.44498
Rough	1	4	CH4	366000	139.393	12545.37	316854.6	96.19145	1793.341	1793.341	139.393
Rough	1	6	CH4	366000	169.9751	15297.76	314102.2	95.35587	2186.789	2186.789	169.9751
Rough	1	8	CH4	366000	182.8263	16454.37	312945.6	95.00475	2352.125	2352.125	182.8263
Rough	1	2	H2	315659.2	154.5627	13910.64	270182.6	95.10349	637.3773	637.3773	154.5627

Rough	1	4	H2	315659.2	313.9652	28256.87	255836.4	90.05366	1294.713	1294.713	313.9652
Rough	1	6	H2	315659.2	349.8096	31482.86	252610.4	88.91812	1442.526	1442.526	349.8096
Rough	1	8	H2	315659.2	366.3186	32968.67	251124.6	88.39512	1510.605	1510.605	366.3186

8.6 Appendix 6 - Theoretical outline of GEM compositional simulator flow equations

The following is adapted from the GEM user guide.

Flow equations in GEM are discretised via the adaptive-implicit method which operates with different levels of implicitness in neighbouring grid blocks. Therefore in grid blocks with less changes over time, lower levels of implicitness can be used which reduces the computing time and storage requirements of the simulation. GEM uses a variation of the approach of Collins *et al.* (1992).

The material-balance finite-difference equations for the oil and gas phase components and the water component are:

Equation 11

$$\psi_i \equiv \Delta T_o^m y_{io}^m (\Delta p^{n+1} - \gamma_o^m \Delta D) + \Delta T_g^m y_{ig}^m \left(\Delta p^{n+1} + \Delta P_{cog}^m - \gamma_g^m \Delta D\right) + q_i^m - \frac{V}{\Delta t}\left[N_i^{n+1} - N_i^n\right] = 0 i = 1, \dots, n_c$$

Equation 12

$$\psi_{n_c+1} \equiv T_w^m (\Delta p^{n+1} - \Delta P_{cwo}^m - \gamma_w^m \Delta D) + q_{n_c+1}^m - \frac{V}{\Delta t}\left[N_{n_c+1}^{n+1} - N_{n_c+1}^n\right] = 0$$

where $N_i (i = 1, \dots, n_c)$ denote the moles of Component *i* per unit of gridblock volume, and where $N_{n_c+1}^n$ denotes the moles of water per unit of gridblock volume. Mass transfer between the hydrocarbon and water phases is assumed not to occur. Superscript *n* and *n+1* are the old and new timestep and superscript *m* refers to *n* for explicit gridblocks and *n+1* for fully-implicit gridblocks. Explicit in GEM refers to gridblocks with explicit transmissibilities in which only pressure is treated implicitly.

The N_i are related to the saturations, porosities, phase molar densities, and compositions:

Equation 13

$$N_{\mathrm{i}} = \phi\left(\rho_{\mathrm{o}} \mathrm{S}_{\mathrm{o}} \mathrm{y}_{\mathrm{io}} + \rho_{\mathrm{g}} \mathrm{S}_{\mathrm{g}} \mathrm{y}_{\mathrm{ig}}\right) i = 1, \dots, n_c$$

Equation 14

$$N_{n_c+1} = \phi \rho_w S_w$$

If the hydrocarbon system has two phases at a particular *p*, *T* and $N_i (i = 1, \dots, n_c)$, phase splits and compositions can be obtained through solving of the thermodynamic-equilibrium equation for N_{ig}, the moles of component *i* in the gas phase:

Equation 15

$$\mathbf{g}_i \equiv \ln f_{ig} - \ln f_{io} = 0 \; i = 1, \dots, n_c$$

For moles of component *i* in the oil phase, N_{io}:

Equation 16

$$N_{io} = N_i - N_{ig}\ i = 1, \ldots, n_c$$

The saturation equation

Saturations are related to N_i and ρ_m(m = o,g,w) via equations for water saturation, oil phase saturation, and gas phase saturation respectively:

Equation 17

$$S_w = N_{n_c+1}/(\phi\rho_w)$$

Equation 18

$$S_o = (1 - S_w)\frac{N_o/\rho_o}{N_o/\rho_o + N_g/\rho_g}$$

Equation 19

$$S_g = (1 - S_w)\frac{N_g/\rho_g}{N_o/\rho_o + N_g/\rho_g} = 1 - S_w - S_o$$

Mole or Volume Consistency Equations

From the definition of N_i(i = 1, . . . , n_c+1), the following forces consistency between the saturations, porosities, and densities and the N_i's:

Equation 20

$$\psi_p \equiv \sum_{i=1}^{n_c+1} N_i^{n+1} - \phi^{n+1}\left(\rho_o S_o + \rho_g S_g + \rho_w S_w\right)^{n+1} = 0$$

Rearranging gives:

Equation 21

$$\psi_p' \equiv V\frac{\sum_{i=1}^{n_c+1} N_i^{n+1}}{\left(\rho_o S_o + \rho_g S_g + \rho_w S_w\right)^{n+1}} - V\phi^{n+1} = 0$$

The first term gives the volume occupied by the fluids (oil, gas, water) and the second term is the pore volume, forcing consistency between fluid and pore volumes.

Decoupled Flash-Calculation Approach

a non -linear equation system of n_b(2n_c+2) formed of Equation 11,Equation *12*,Equation *15*, andEquation *21* can be solved thus:

Equation 22

$$\left(p, N_i, \ldots, N_{n_c}, N_{n_c+1}, N_{1g}, \ldots, N_{n_c g}\right)_k^{n+1}\ k = 1, \ldots, n_b$$

where n_b is the number of gridblocks. This is called the simultaneous-solution approach.

To alleviate the complexity associated with the simultaneous-solution of all governing equations,

Collins *et al.* (1992) solved the phase-equilibrium equations in an inner loop by decoupling them and it is a variation of this approach that is used in GEM. For gridblock k:

Equation 23

$$\mathbf{F}_k = \left(\psi_p', \psi_1, \ldots, \psi_{n_c+1}\right)_k^T \; k = 1, \ldots, n_b$$

Equation 24

$$\mathbf{X}_k = \left(p^{n+1}, N_1^{n+1}, \ldots, N_{n_c+1}^{n+1}\right)_k^T \; k = 1, \ldots, n_b$$

The phase-equilibrium equation is solved to convergence after every Newtonian iteration of **X.**

The separates the of solving flow and consistency equations from the phase-equilibrium equations, which allows flash calculations to be localized and developed separately, while allowing for different calculation techniques to be used. This approach can sometimes be less efficient than simultaneous solution, but is more flexible and robust when dealing with complex systems while allowing the repetition of calculations with unrealistic convergence occurs instead of repeating the timestep.

References

Collins, D.A., Nghlem, L.X., Li, V. ·k and Grabenstetter, J.E. 1992. An Efficient Approach to Adaptive-Implicit Compositional Simulation With an Equation of State.

Nomenclature

D	depth
f_{ij}	fugacity of component *i* in phase *j*
F	function
	phase-equilibrium function
n_b	number of gridblocks
n_c	number of components
N_i	moles of component *i* per unit block volume
p	pressure
P_{cog}	oil-gas capillary pressure

P_{cwo}	water-oil capillary pressure
q	injection/production rate
t	time
T_j	transmissibility of phase j
	gridblock volume
y_{ij}	mole fraction of component i in phase j
γ	specific gravity or gravity term in flow equation
Δt	timestep
ρ_m	molar density of phase m
ϕ	porosity
ψ	function
Superscripts	
(k)	iteration level
n	old time level
n+1	new time level
Subscripts	
i	component
j	phase
o	oil
g	gas
w	water